Propagation of rotational rifts across rheological heterogeneities: Insights from 3D analogue models

by

Nicolás E. Molnar

PhD Thesis
Submitted in fulfilment of the requirement for the degree of
Doctor of Philosophy

Supervisors:

Alexander R. Cruden

Peter G. Betts

School of Earth, Atmosphere and Environment

Monash University, Clayton, Victoria, Australia

2018

∞

General declaration

I hereby declare that this thesis contains no material which has been accepted for the award of any other degree or diploma at any university or equivalent institution and that, to the best of my knowledge and belief, this thesis contains no material previously published or written by another person, except where due reference is made in the text of the thesis.

This thesis includes 2 original papers published in peer reviewed journals and 2 unpublished publications. The core theme of the thesis is the deformation evolution of continental rifts. The ideas, development and writing up of all the papers in the thesis were the principal responsibility of myself, the candidate, working within the School of Earth, Atmosphere and Environment under the supervision of Alexander Cruden and Peter Betts.

In the case of chapters 2, 3, 4 and 5 my contribution to the work involved the following:

Thesis chapter	Publication title	Publication status	Nature and extent of candidate contribution	Co-author name(s) and extent of contribution
2	Interactions between propagating rotational rifts and linear rheological heterogeneities: insights from three-dimensional laboratory experiments	Published	**85%** - Majority of data generation, processing, interpretation and manuscript preparation	A.R. Cruden, 10% - Supervisory role P.G. Betts, 5% - Supervisory role
3	Unzipping continents and the birth of microcontinents	Published	**85%** - Majority of data generation, processing, interpretation and manuscript preparation	A.R. Cruden, 10% - Supervisory role P.G. Betts, 5% - Supervisory role
4	Rift propagation across pre-existing crustal heterogeneities: three-dimensional analogue models of rotational extension	In preparation	**85%** - Majority of data generation, processing, interpretation and manuscript preparation	A.R. Cruden, 10% - Supervisory role P.G. Betts, 5% - Supervisory role
5	The Red Sea revisited: inferences from 3D analogue modelling of propagating rifts	In preparation	**85%** - Majority of data generation, processing, interpretation and manuscript preparation	A.R. Cruden, 10% - Supervisory role P.G. Betts, 5% - Supervisory role

Candidate's signature   **Date**   05/07/2018

The undersigned hereby certify that the above declaration correctly reflects the nature and extent of the candidate's and co-authors' contributions to this work.

Main Supervisor signature   **Date**

To the names behind the initials in M. Tharp, M. Withjack, C. Ruppel, L. Royden, C. Ebinger, A. Clifton, G. Peron-Pinvidic, J. Autin, M. Zuber, S. Prosser, S. Hansen, T. Atwater.

Before reading their brilliant papers, I assumed they were men. I was wrong. I was biased.

To Marie, Martha, Carolyn, Leigh, Cinthia, Amy, Gwenn, Julia, Maria, Sarah, Samantha, Tanya, and many others who, like them, had to overcome implicit bias, had to fight stronger and stand firmer in an unequal world.
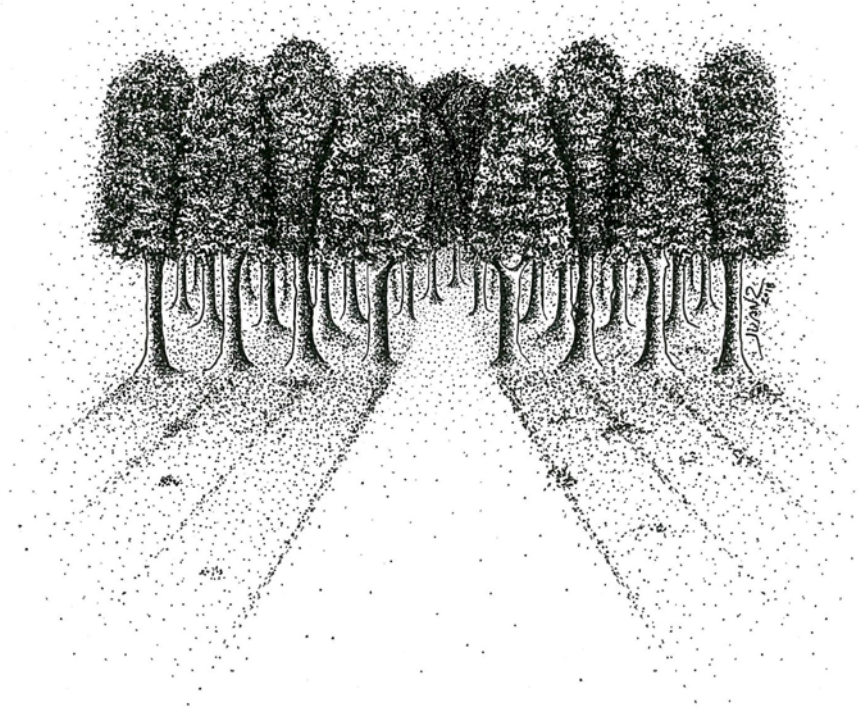
To all women in science.

"Much as I admired the elegance of physical theories, which at that time geology wholly lacked, I preferred a life in the woods to one in the laboratory"

- John Tuzo Wilson -

Table of contents

Chapter 1

Chapter 2

Chapter 3

Chapter 4

Chapter 5

Chapter 6

List of figures

Chapter 4

Chapter 5

Extended Data

List of tables

Chapter 2

Chapter 4

Acknowledgements

I once read that good things, when short, are twice as good. So, I tried to keep this short.

In March 2014, I sent an email to a researcher in each of the Group of Eight universities in Australia. My thought was to aim high, but I got six unsuccessful outcomes: three no-replies, two "I'm retired, try someone else" and one "Sorry bud, you've got no chances, don't even bother".

For some reason, one of these researchers received the same email - which I practically copied, slightly modified, and pasted - but he felt something different. He gave me a chance. I couldn't be more thankful to you, Sandy, because whatever you felt when you read my email, it changed my life. I jumped onto a plane in September that year with a lot of doubts, insecurities and sadness for leaving what I loved most back home, but there was something stronger that made me come all the way to Melbourne. What I have learnt in the last 4 years is immeasurable. Thank you, Sandy. Thank you for giving me this opportunity. And thank you for always pushing forward and giving me your total support for my ideas. Just a few weeks after I got to Monash you told me you were going to provide me with all the resources I needed, and that I should come up with something brilliant. We can discuss the brilliant aspect later, but you were true to your words and you have always given me your time, your advice and your guidance. You are a legend.

Pete, you completed the legendary team that supervised me in this crazy adventure that a PhD is. If I had to start all over again and I could choose my co-supervisor, I would choose you again. Many people know how hard it is to fight against one's ghosts, against the classic impostor syndrome, against the frustrations involved in being new to research. On those days when I was a bit down, I just wanted someone to look at me and tell me that what I was doing was fantastic. You were that 'someone' every time I needed it, Pete. You always sounded excited about what I was doing and that gave me strength to keep working. Thank you, Pete.

It's been a long and winding road, but I finally finished my PhD and I learned not only about geology but even more about life. Nothing would have been possible without the help of many people.

Thank you Stefan, David and Nasim for your kindness, you made me feel very welcome when I was the new guy. Thanks to all the amazing students and staff who I shared offices, labs, lunches and beers with. You made me feel part of the family. Everyone at the general office; Katie, Silvana, Christine, Emily. You run the show. Rob, Yuzhou, you are rad. Thank you. Caz, you are the number one and a role model. Thanks Roberto for giving me the chance of demonstrating in your unit. I learned a lot, from the teaching and from you. Thanks Fab to you as well. I enjoyed very much sharing pracs with you, but I enjoyed even more the very sincere and upfront conversations we have had, almost all of them centred on not knowing what I wanted to do after my PhD. And to you and Laurent, since your role as part of my panel for my milestones helped me stay on track and rethink certain concepts when I needed it.

I am also very thankful to Brett, Michael and the whole team at Monash Instrumentation Facility for their spectacular work on the apparatus I have used for my research. I have spent countless hours working with it in the laboratory, and without the help, advice and guidance of Santanu, Joao, Vincent, Zhihao, Catherine, Anung and Uchi, I would not have gotten so far. Every lab user like us also knows how important Rachelle, Junnel and Massimo are. Thank you, guys, you have been very helpful.

Jim and Julie and the outreach gang. You are responsible for one of the nicest things I have discovered while undertaking my PhD. I love to teach. I want to share what I know with a broad audience. I want to see those amazed faces when you talk about a remote moon of a faraway planet. I want to do outreach and science communication. And thank you, Pru, my first officemate. Partner of countless rock garden tours. Keep rocking it.

There is life outside campus, as some of you may know. I only made it thanks to all the people that gave me company throughout this stage. When you spend three and a half years in a city like Melbourne, you see many people arriving and many more leaving, looking for new adventures around the world. I am so lucky that these persons came to my life and, even if they are now a few thousand kilometres away, they will never go, they are part of my life. We shared road trips, nights out, *fulbo*, we watched movies, played chess or we just kept talking about parallel universes until 5 am, you all made me happy and complete; Consu, Pedro, Agus, Mages, Josh, Panchito, Mariano, Ale, Santi, Cori, Vicky, Franco, Nacho, Sofi, Magui, Camo, Feli, Zurdo, Barba, Rodri, Flor, Rodri, Pao, Feno, Jackie, Mencho, Juli, Baca, Lucy, Melbourne wouldn't have been the same without you.

My friends from Argentina deserve their words of gratitude as well. Australia is far away from everything on this planet, but friendship knows no distance and you have proven this to me. Thank you ❤.

Consu, nothing would have been the same without you. I knew nothing about love before, but I am now learning with you. You are a roller coaster that I don't want to get off from. Thank you for all your efforts to shorten the distance and to hold me together when I needed. I made it thanks to you. Te amo.

I am who I am thanks to my family. Every action I take and every decision I make is directly connected to the way how I have been raised. I couldn't be more grateful.

To everyone, thank you from my heart.

In Kerouac's words:

"What is that feeling when you're driving away from people and they recede on the plain till you see their specks dispersing? – it's the too-huge world vaulting us, and it's good-bye. But we lean forward to the next crazy venture beneath the skies"

Good bye, Australia.

Thank you.

Abstract

The continuous process of continental lithosphere stretching and breakup represents an integral part of the theory of plate tectonics. However, many first order questions still remain unanswered. Modern and ancient examples of rifts are known to overprint pre-existing linear mechanical heterogeneities in the crust and lithosphere. In turn, these pre-existing features are known to exert a significant control on the structural evolution of continental rifts. However, the influence of such features when the extension direction progressively changes over time remains uncertain.

This thesis focuses in both kinematic and mechanical aspects of the rifting process by exploring how rifts propagate into lithosphere containing variably oriented linear weak zones, using three-dimensional lithospheric-scale laboratory experiments of continental extension. The results of four series of experiments that provide key insights into the temporal evolution of propagating rifts are presented.

Experiments were initially performed to investigate the role of a weak linear zone in the lithospheric mantle, showing that when linear weaknesses are oriented at low angles to the rift axis, continental breakup develops by unzipping. Strong strain partitioning is observed when the linear heterogeneity is oriented at high angles with respect to the rift axis. These laboratory experiments also demonstrate that microcontinent formation at passive margins results from a combination of pre-existing linear weaknesses in the lithosphere and rotational extension, suggesting that microcontinent formation may be restricted to localized regions along passive margins associated with mechanical heterogeneities.

Results of experiments exploring how rifts propagate and interact with linear crustal rheological heterogeneities show that approximately rift-parallel pre-existing heterogeneities favour the formation of long, linear rift faults that reach their near-final length at early stages. Low angles between the heterogeneities and the propagating rift axis may result in strong strike-slip reactivation of the pre-existing structures. When the linear heterogeneities are oriented at high angles, rift branches become laterally offset as they propagate, resulting in complex fault patterns. Rift-perpendicular crustal heterogeneities do not affect fault trends during rift propagation, but they do cause stalling of the laterally growing faults.

A final series of laboratory experiments was performed to investigate the effect of pre-existing rheological heterogeneities in both the crust and lithospheric mantle. A comparison of the results from these experiments was used to define a hierarchy of influence, whereby crustal heterogeneities are outranked by lithospheric mantle heterogeneities. However, certain features observed in nature can only be explained by the combined effects of both types of heterogeneities. This series of experiments reproduces the geological history of the Red Sea and provides key insights on its deformation history in space and time.

The findings of this thesis provide significant new insights on the role of crustal and lithospheric heterogeneities during continental rifting. Comparison of the experiments to ancient and modern examples in nature contributes to explaining several common but still poorly understood processes of how propagating rifts interact with lithospheric heterogeneities. Similarities between the analogue experimental results and selected natural examples provide insights on how nature finds preferential pathways to breakup in heterogeneous continental lithosphere.

Chapter 1

Introduction

Chapter 1

1.1 Project rationale

When continents are pulled by moving lithospheric plates they break into pieces that drift apart to form new oceans. Continental rifts are thought to develop and propagate along the easiest path to continental break-up. Although these processes are recorded throughout Earth's history, many aspects that control the final three-dimensional shape of continental rifts and passive margins are still poorly understood. Continental lithosphere typically contains vertical and lateral variations in the mechanical properties of rocks, often regarded as linear zones of weakness. They are difficult to characterise in nature since geological events are continuously superimposed. It remains a challenge to understand how rifts interact with these zones of weakness, but it is essential for explaining the shape of modern rifted margins.

Tectonic processes occur over millions of years in nature. Modelling, whether numerical or physical, is therefore the best approach to investigate them and gain insights into the evolution of rift systems in time and space. In this thesis, I employ a laboratory setup that allows me to scale down time, dimensions and mechanical properties of rocks to approximately simulate geological processes in a more convenient timeframe and length scale. New modelling will lead to a better comprehension of how continents break up, providing a key to understanding Earth's past, which may even help to predict our planet's future tectonic evolution.

1.2 Aims and motivation

The overarching aim of this work is to better understand how rifts propagate prior to continental break up and how they interact with different kinds of linear lithospheric weaknesses. Understanding of deformation localisation and strain partitioning within propagating rifts, and their interaction with pre-existing linear structures or rheological heterogeneities, remains incomplete.

Many first-order questions about rifting and continental breakup remain unanswered, some of which are addressed in this thesis:

- What is the overall temporal and spatial evolution of deformation in large-scale propagating rifts?

- Do rifts always propagate towards a pole of rotation during rotational rifting?

- How is extension accommodated in the presence of a linear weak zone in the lithospheric mantle? And how do linear crustal heterogeneities influence rift morphology?

- Do lithospheric weaknesses contribute to the development of microcontinents during rifting?

These questions are addressed using analogue modelling. Three-dimensional, isostatically supported, brittle-ductile multilayer analogue models of rotational rifting are undertaken. Deformation is monitored at high spatio-temporal resolution. The experimental results are compared to selected natural examples of continental rifts with analogous kinematic and mechanical initial conditions. Based on these comparisons, differences and similarities, limitations and implications of the modelling for rifting evolution are discussed.

1.3 Thesis structure

This thesis is organised into an introductory chapter, followed by four research chapters, and a final discussion and conclusions chapter. The main findings of this work have been formatted as stand-alone journal articles (Chapters 2-5), which unavoidably results in partial repetition of the background material and method descriptions. The content of Chapters 2 and 3 is identical to the published versions. However, minor amendments were made in referencing and grammatical styles to maintain a constant format throughout the thesis. Chapters 4 and 5 will be ready for submission after minor modifications.

Chapter 1 is an introduction to the research topics and presents key background information for the thesis, including a literature review on continental rifting and geodynamic modelling, a comprehensive description of the laboratory modelling methodologies used and a summary of the current state of knowledge on propagating rifts.

Chapter 2 presents the first series of modelling results in which I investigate the role linear weak zones in the mantle play in the evolution of continental rifts. This section includes a complete description of the modelling setup and initial conditions, which are used as a reference for the following chapters. A characterisation of the evolution of deformation as a function of the linear weakness obliquity is presented, broken down into three categories: **(1)** homogeneous lithosphere, **(2)** low obliquity, and **(3)** moderate to high obliquity. This work represents the first comprehensive description and characterisation of modes of continental rotational extension as a function of the location and orientation of linear mantle heterogeneities.

Chapter 3 expands upon significant implications that arise from the experiments presented in Chapter 2, paying special attention to the poorly understood geodynamic process of microcontinent formation. This chapter describes the mechanism of formation and detachment of continental fragments from rifted margins. Results are supported by repeated observations under variable initial conditions in the experiments. The outcomes from this work demonstrate that microcontinent formation may occur during the latest stages of continental rifting rather than when oceanisation takes place, which is a significant advance in understanding microcontinent formation. This chapter specifies a geological framework in which to explain the location and distribution of many microcontinents preserved within the Earth's crust.

Chapter 4 investigates how rifts propagate and interact with linear rheological heterogeneities within the crust adopting a similar approach as in Chapter 2. The modelling results show a range of rift architecture styles that depend on the position and orientation of the linear heterogeneities. Outcomes of this chapter are significant for modern and ancient rifts and may help to better understand how nature finds the preferential pathway to breakup in heterogeneous continental lithosphere.

Chapter 5 reports on experiments that combine the mantle and crustal rheological heterogeneities investigated in the previous chapters, with direct application and comparison to the Red Sea rift system. Results of the experiments with combined presence of linear heterogeneities are compared to the previous modelling results. A hierarchy of controlling factors is established and implications for the evolution of the Red Sea rift system and other selected natural examples are discussed.

Chapter 6 summarises and links the main findings of the previous chapters and discusses their implications in a broader context. A hierarchy in the variables that control rift evolution under rotational kinematics is presented. Research questions that require further investigation are identified.

∞

The following appendices are included at the end of the thesis:

Appendix A – Evolutionary diagrams of all experiments performed.

Appendix B – Extensional apparatus design plans, 3D pdfs and animation files.

Appendix C – Extended Data movie files from Chapter 2.

Appendices B and C have been uploaded into Figshare for readers to access the information remotely.

All the references cited in this work are listed at the end of this document.

1.4 Context of the research

Continental rifting occurs in response to lithospheric stretching, which is in turn triggered by far-field extension, mantle plume activity, or a combination or both (e.g., Buiter and Torsvik, 2014 and references therein). A wide number of factors control how rifts evolve in time and space. The intrinsic complexity and three-dimensionality of natural systems make these processes very challenging to understand. After several decades of field observations and geophysical surveys, complemented with 2D and 3D analogue and numerical models with ever increasing resolution, many questions remain unanswered. Since it is impossible to test and characterise all the controlling parameters in a single study, my approach is to focus on two main aspects: rotational kinematics and pre-existing lithospheric rheological heterogeneities. The literature review presented below summarises the most significant advances made in continental rifting research in the past 50 years, in the context of the two aforementioned aspects.

1.4.1 Continental rifting and break-up

1.4.1.1 Early views

The concept of rifting was introduced in the scientific community in the 19th century when prominent researchers like Jean-Baptiste Élie de Beaumont (1827, 1841) described a doming and faulting mechanism for the formation of the Rhine Graben (Central Europe), or Charles Johnston (1844) who inferred that two separate plateaux in Ethiopia used to be contiguous before they split. However, it wasn't until the end of the century that the term "rift" was popularised worldwide by John W. Gregory, who in 1894 – probably inspired by Suess' (1891) ideas – defined a rift valley as "*a linear valley with parallel and almost vertical slides, which has fallen owing to a series of parallel faults*" (Fig. 1.1). Gregory recognised continental doming and symmetrical faulting and attributed their formation to extensional forces. Since then, the term and concept has prevailed in the literature, capturing increasing attention in the geoscience community over time. Substantial progress was made during the first notable European scientific expeditions to the East African Rift System (EARS) in the early 1900s. Petrological (e.g., Finckh, 1912), sedimentological (e.g., Behrend, 1918), volcanological (e.g., Reck, 1914) and paleontological (e.g., Hennig, 1916) studies contributed to the comprehension of the rifting process. However, it was structural and tectonic studies, such as those presented by Uhligh (1909, 1912) or the more detailed reviews of Krenkel (1913, 1924), along with Gregory's classic book (1921), that contributed the most to elucidating how rifts form and develop.
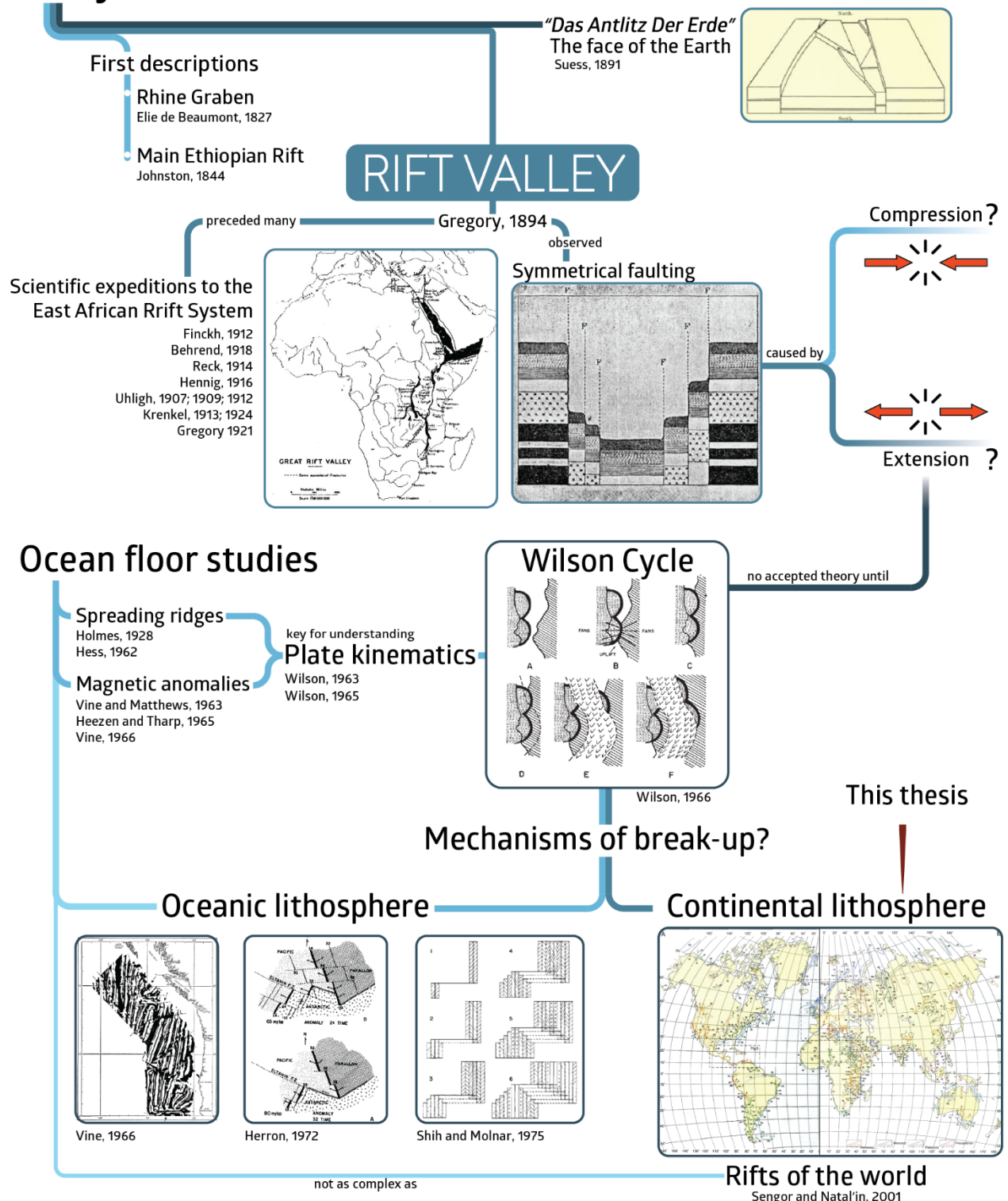
Figure 1.1 - Flow chart summarising key advances in the understanding of rifts as a result of extending lithosphere.

The following decades were characterised by a dispute between two different visions, one supporting the origin of the EARS as a result of extension, while others attributed it to compression

(Kumpunzu and Lubala, 1991 and references therein, Fig. 1.1). These disjunctive views had a simple explanation: natural systems are overly complex and difficult to interpret. Moreover, a consensus was then unconceivable due to the lack of an accepted paradigm for continental fragmentation and reassembly within the scientific community. The establishment of plate tectonics after Wilson's (1966) theory on the periodic cycle of ocean opening and closure, along with later developments (e.g., Burke and Dewey, 1974), defined a turning point in science that provided important contributions on continental rifting that became the 'building blocks' for more recent work (Fig. 1.1).

Advances in paleomagnetic research revealed how the entire geological history of ocean basins was 'printed' in the ocean floor (e.g., Bullard, 1965; Heezen and Tharp 1964; Vine 1966; Vine and Matthews 1963). The study and interpretation of magnetic anomalies in the oceanic crust led to the first quantitative and accurate analysis of relative plate motions and their respective velocities (e.g., Fisher et al 1971; McKenzie and Sclater, 1971; Pitman and Talwani 1972; Weissel and Hayes, 1972), which had significant implications for understanding of global plate kinematics. Direct evidence supported the theory of spreading ridges in the oceans, originally coined by Holmes (1928) and later reformulated by Hess (1962). Shih and Molnar (1975) proposed that spreading ridges do not form instantaneously, but instead develop by along-axis propagation of spreading centres. This idea supported what previous studies (e.g., Burke and Dewey, 1973; Maasha and Molnar, 1972; Scholz et al., 1975) had also inferred for the continental lithosphere; continental break-up must take place as a result of rifts that propagate laterally through the continents. Nonetheless, most of the advances at this time were focussed on the temporal and spatial evolution of the oceanic lithosphere. As eloquently expressed by McKenzie (1978):

> "*The general acceptance of plate tectonics and of the associated thermal models of plate creation has successfully accounted for the major horizontal and vertical motions of the ocean floor. No comparable progress has occurred in our understanding vertical movements in continental regions*".

In the 1970s and 1980s, increasing efforts were subsequently made to define and classify modes of continental extension, as summarised below.

1.4.1.2 Modes of lithospheric extension

Active vs. passive rifting

The leading causes of continental rifting have been a matter of considerable debate. The initiation of lithospheric extension has generally been attributed to two different mechanisms: one supported the idea of extension stretching the lithosphere until it fails, with associated mantle activity as a consequence of the process (e.g., McKenzie 1978; McKenzie and Weiss, 1975; Molnar and Tapponnier 1975; Sengör, 1976; Turcotte, 1974); the other proposed that impingement of mantle plumes at the base of the lithosphere causes crustal doming and extension that eventually leads to rifting (e.g., Bott and Kusznir, 1979; Burke and Dewey, 1973; Burke and Whiteman, 1973). This chicken-and-egg issue was addressed by Sengör and Burke (1978), who made the first generic distinction between these mechanisms, defining the former as **passive** rifting and the latter as **active** rifting (Fig. 1.2). Nevertheless, Sengör and Burke (1978) recognised that the end products of all rift processes are likely to look similar and evolved rifts are particularly difficult to interpret.
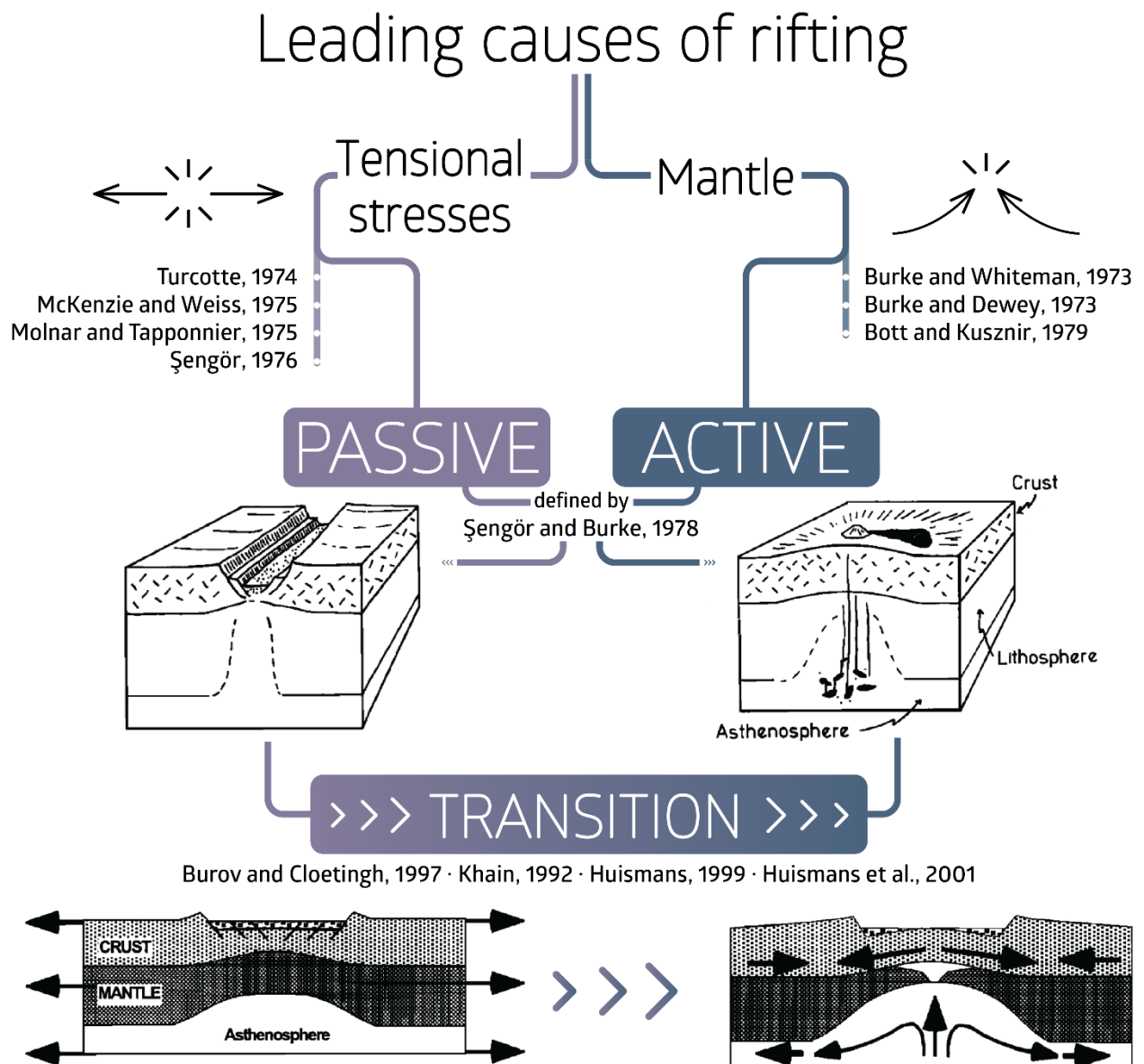
Figure 1.2 - **Flow chart summarising important steps made towards the classification of rifts as a function of the leading cause of their formation.**

Despite significant advances in understanding continental rifting over the last four decades, the classification of both ancient and modern rifts as passive or active is still contentious. More recent studies have suggested that a transition from a passive to active modes is more likely in most rift systems (e.g., Burov and Cloetingh, 1997; Huismans et al., 2001; Khain, 1992) and that only purely non-volcanic rifts can be undoubtedly considered as passive (Ziegler and Cloetingh, 2004). An extensive review by Buiter and Torsvik (2014) concluded that many cases of continental break-up are associated with large igneous provinces (LIP), but in most of them rifting was initiated first by tectonic forces and plume material flowed through the rifted lithosphere to help trigger continental break-up. The fact that there is still no complete consensus on the leading causes of continental rifting makes Sengör and Burke's statement from 1978, timeless:

"Rift studies are now at a very exciting stage"

Narrow, wide and core complex modes

Similar structural patterns have been described for various natural examples. Narrow regions of intense normal faulting characterise rifts such as the Rhine Graben (e.g., Ilies and Greiner, 1978), the Rio Grande Rift (e.g., Morgan et al., 1986), the Baikal Rift (e.g., Artemjev and Artyushkov, 1971; Zorin, 1981), the Gulf of Suez and northern Red Sea (e.g., Bonatti, 1985; Steckler et al., 1988) and the East African Rift System (e.g., Ebinger et al., 1989; Rosendahl, 1987). Conversely, highly extended terrains with a wider distribution of deformation characterise other examples such as the Basin and Range Province or southern Tibet (e.g., Armijo et al., 1986; Hamilton, 1987). These observations led to an alternative structure-based classification of continental rifts.
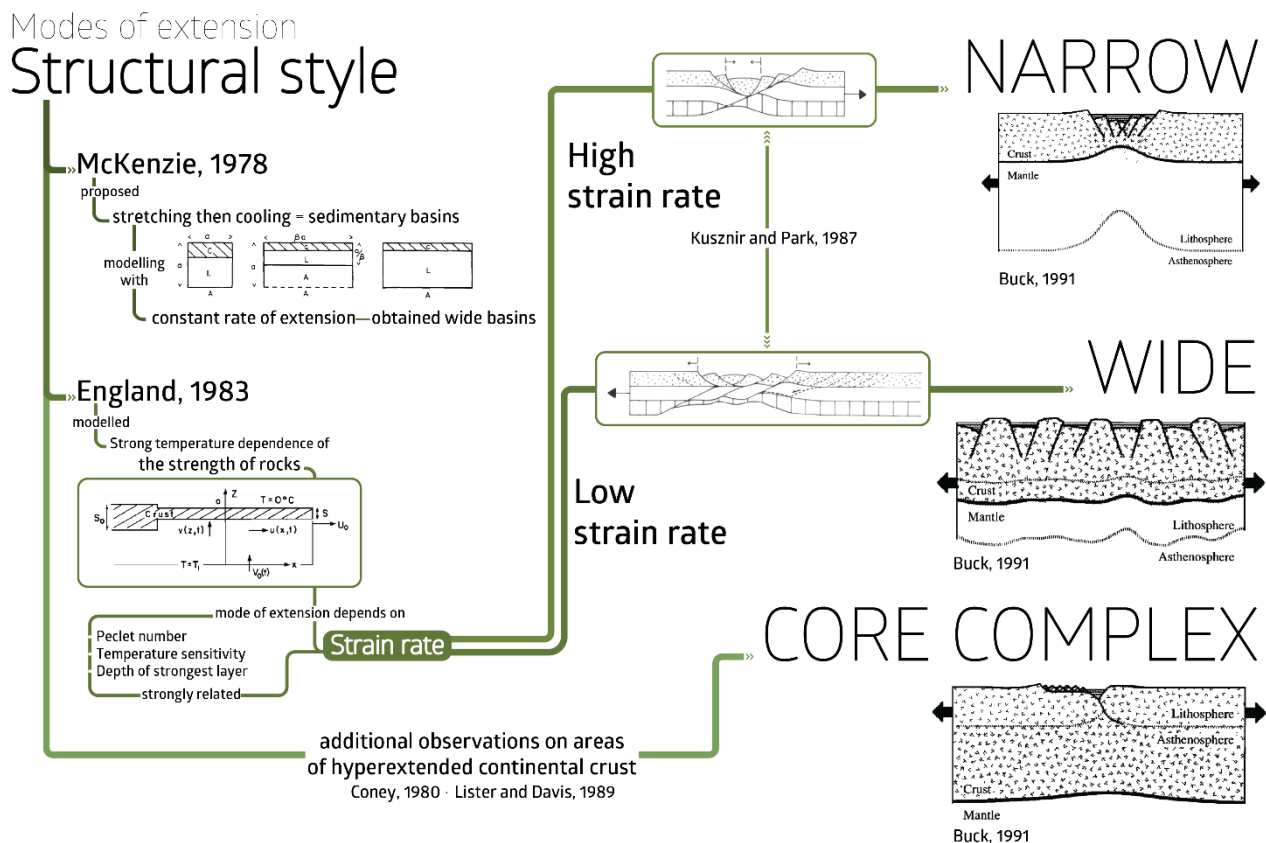
Figure 1.3 - **Flow chart summarising the classification of rifts from a structural point of view.**

McKenzie (1978) proposed a pioneering model for the development of sedimentary basins that considered early, effectively instantaneous stretching, followed by slow cooling of the lower section of the lithosphere and associated thermal subsidence. However, this model did not account for variations in the rate of extension. It is therefore only applicable to particular scenarios and for that reason applied to rifts that display wide areas of extensional faulting (e.g., Basin and Range, Aegean, North Sea [McKenzie, 1978]). England (1983) added a degree of complexity to this model by calculating the behaviour of the lithosphere under variable rates of extension, concluding that continental rifts can become either **narrow** or **wide** (Fig. 1.3). This difference arises due to the temperature-dependence strength of the lithosphere, and the close relation between strain rate and thermal diffusion (England, 1983). Kusznir and Park (1987) expanded upon this model, showing that lithospheric extension causes

both the thinning of the crust – which has a strain hardening effect - and an increase in the geothermal gradient – which has a strain softening effect. The rate of extension is therefore a critical parameter in defining which process dominates and determines the mode of continental extension.

A third mode of extension, termed **core complex mode**, was later proposed for regions of hyperextended continental crust in which middle to lower crustal high-grade metamorphic rocks are exhumed below lower-grade metamorphic rocks (e.g., Coney, 1980; Lister and Davis, 1989). Building on the aforementioned studies, Buck (1991) summarised these findings in three main modes of continental extension: narrow, wide, and core complex modes (Fig. 1.3).

Lithospheric shear models

An additional classification of continental extension was made based on the kinematics of progressive lithospheric stretching. McKenzie (1978) presented numerical simulations of lithospheric extension assuming homogeneous ductile stretching, termed **uniform pure shear** (Ruppel, 1995) (Fig. 1.4). Royden and Keen (1980) suggested a variation on this model, termed **non-uniform pure shear**, based on the fact that the crust and mantle lithosphere should be treated as mechanically distinct layers, which will thin by different amounts above and below a horizontal boundary (Fig. 1.4).
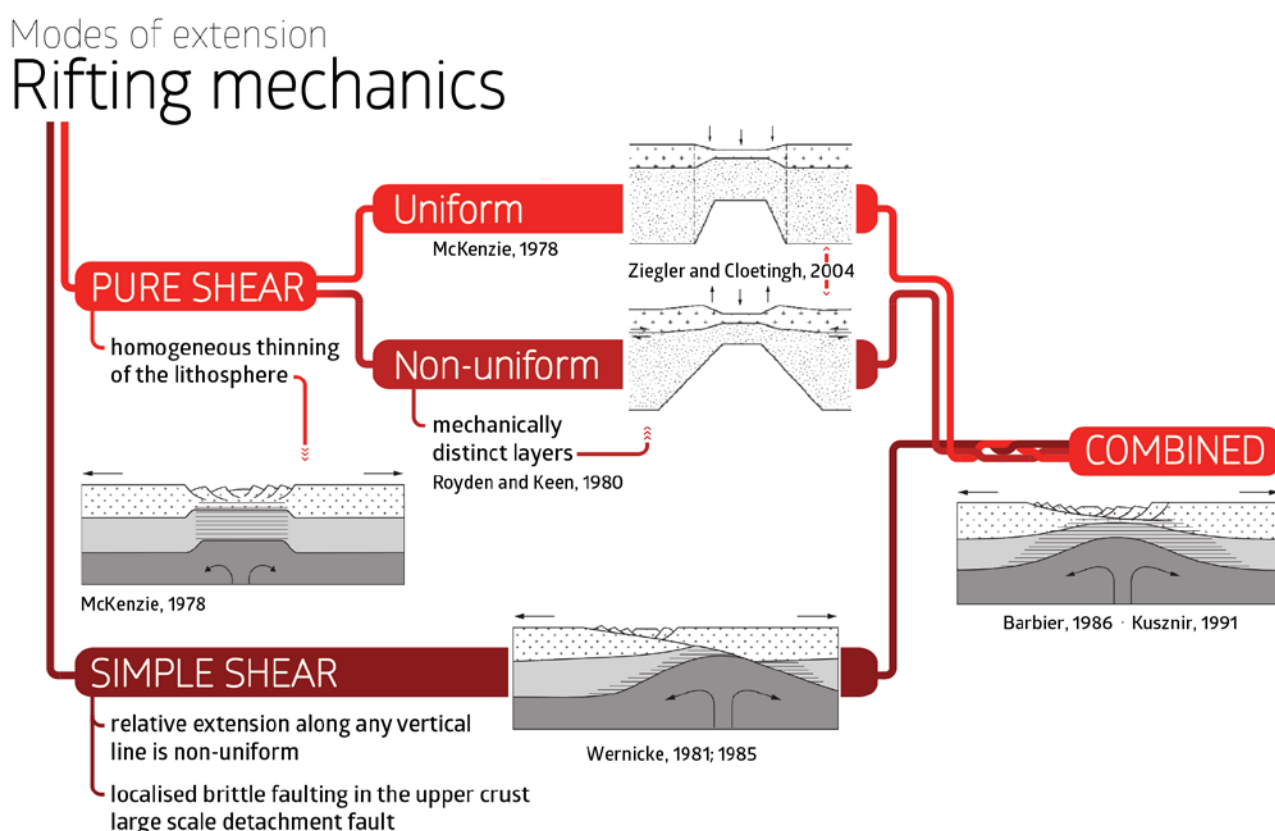
Figure 1.4 - **Flow chart summarising the classification of rifts as a function of the dominating mechanical process.**

Wernicke (1981; 1985) defined an alternate **simple shear** model in which the relative extension of crust and mantle lithosphere along any given vertical line is non-uniform (Fig. 1.4). This results in brittle faulting and localised strain in the upper crust, expressed as low-angle normal fault systems, above a

crustal-scale detachment fault. Finally, a superposition of both shear modes was proposed by Barbier (1986) to describe observations in the Bay of Biscay, termed the **combined shear** model (Barbier, 1986, Kusznir, 1991) (Fig. 1.4).

In a comprehensive review, Ruppel (1995) noted that rifts had traditionally been viewed as two-dimensional features and concluded that future research on rifting should focus on understanding tectonic style, evolutionary history and deep structure in three-dimensions.

1.4.1.3 New insights

Geological and geophysical observations

How continental lithosphere responds to regional extension (*passive* rifting), the upwelling of hot mantle material (*active* rifting), or to a combination of both is relatively well constrained. Cross-disciplinary efforts have been made to characterise, classify and elucidate the spatio-temporal evolution of continental rifts. However, the most significant insights for understanding geological features on Earth initially have been historically derived from direct observations in the field (e.g., de Beaumont, 1827; Gregory, 1894; Hall, 1812). The progress summarised above on classifying rifts from theoretical and conceptual points of view (e.g., Buck, 1991; Kusznir and Park, 1987; McKenzie, 1978; Royden and Keen, 1980; Sengör and Burke, 1978; Wernicke, 1985) was also accompanied by intense field- and geophysics-based work aimed at obtaining direct evidence for rifting processes from the geological record.

Much of this work focussed on characterising three-dimensional **structural** features and their significance for the geometrical evolution of normal fault systems (Jackson and McKenzie, 1983), oblique and strike-slip motion on normal faults (Burchfield and Steward, 1966; Rosendahl et al., 1986; Sharp et al., 2000), detachment faults and metamorphic core complexes (Davis, 1983; Fletcher et al., 1995; Lister and Davis, 1989; Malavielle and Taboada, 1991; Scott and Lister, 1992), oblique rift zones (Applegate and Shor, 1994; Chorowicz and Sorlein, 1992; Umhoefer and Stone, 1996), rotation of normal faults (Brun and Choukroune, 1983; Buck 1988; Nur et al. 1986), transfer/accommodation zones (Bosworth 1985, 1987; Gawthorpe and Hurst, 1993; Morley, 1990; Rosendahl et al., 1986), fault linkage and relay ramp structures (Crider and Pollard, 1998; Fossen and Rotevatn, 2016; Goguel, 1952; Larsen, 1988; Peacock and Sanderson, 1991; Willemse, 1997), and domino fault systems (Nur, 1986). With such structural variety and complexity, many publications attempted to provide more general descriptions of rifts (e.g., Angelier, 1985; Gibbs, 1984; Roberts and Yielding, 1994), modes of extensional tectonics (e.g., Wernicke and Burchfield, 1982) or the geometry and growth of normal faults (Childs et al., 2017). Additionally, the push for a unified terminology for classifying extensional features lead to the publication of several glossaries (e.g., Angelier, 1994; Biddle and Christie-Blick, 1985; Peacock et al., 2000; Peacock et al., 2016; Schultz and Fossen, 2008) and textbooks that include sections on extensional structures and rifting (Fossen, 2010; Price and Cosgrove, 1990; Ramsay and Huber, 1987; Twiss and Moores, 1992).

Sedimentological investigations identified depositional sequences that characterise each stage of rifting (pre-, syn- and post-rift). Building on fundamental contributions on sequence stratigraphy (Sloss, 1963; Vail et al., 1977), several authors studied small-scale characteristics of sedimentation in response

to normal faulting (e.g., Hooke, 1972; Watterson, 1986), as well as large-scale patterns of sediment infill and dispersal in rift basins (e.g., Crossley, 1984; Hooke, 1968; Leeder and Gawthorpe, 1987; Pitman and Andrews, 1985; Schlische and Olsen, 1990; Scholz et al., 1990; Vail, 1987). Reviews on this topic are provided by Allen and Allen (2005), Martins-Neto and Cateneau, (2009), Prosser (1991; 1993). Likewise, **petrological** and **geochemical** studies also contributed to understanding the geological history of rifts and constraining the timing of events that lead to their formation. Since many rifts are associated with igneous activity at some point during their evolution, numerous investigations have been carried out to understand the petrology and geochemistry of rift-related igneous rocks (e.g., Coleman et al., 1979; Neuman and Ramberg, 1977), the extrusion of flood basalts (e.g., Courtillot and Cisowski, 1987; Hinz 1981; Mutter et al., 1988; White and McKenzie, 1989), magma underplating (e.g., Furlong and Fountain, 1986; Herzberg et al., 1983) and strain localisation caused by the presence of magma (e.g., Arzi, 1978; Chery et al., 1989). Advances have also been made in the field of **geodesy** by accurately measuring plate movements and calculating global, regional and local strain rate maps (e.g., Kreemer et al., 2014; Global Strain Rate Map project). Together with improved **satellite** and **remote sensing** data (e.g., van der Meer, 2012) and expanding **earthquake** and **focal mechanism** databases (e.g., Global Centroid Moment Tensor database), the current state of knowledge of ancient and modern rifts has improved immensely thanks to direct geological evidence.

Seismic reflection and **refraction** data have become a standard tool for understanding the structures of sedimentary basins and passive margins (e.g., Cochran, 1981; Healy, 1982; Le Pichon et al., 1973, 1982; Mooney, 1985; Phillips and Ross, 1970) and the acquisition of new data continues to contribute to improve knowledge on the nature of lithospheric extension (e.g., McDermott and Reston, 2015; Ranero and Perez-Gussinyé, 2010). The use of **potential field data** has similarly become invaluable for capturing the three-dimensional architecture of buried terranes from a local to global scale (e.g., Chakravarthi et al., 2013; Lillie, 1999; Lowrie et al., 1997; Nabighian et al., 2005). **Gravity** (e.g., Allen and Allen, 2005; Bake and Wohlenberg, 1971; Blakeley et al., 1999; Ramberg, 1978) and **magnetic field** (e.g., Campbell, 1997; Haggerty, 1979; Lillie, 1999; Milsom, 2003; Nabighian, 2005) are used to quantifying sediment thicknesses and crustal thinning, map fault geometries at depth and produce consistent geological models with decreasing ambiguity over time. Processing of seismic and potential field data provides essential information such as **subsidence patterns** (e.g., Ebinger et al., 1989; Gupta, 1998; McKenzie, 1978; Morley, 1988; Xie and Heller, 2009;) and helps to derive spatial and temporal variations in **strain rate** (e.g., Walsh and Watterson, 1991; White, 1993, 1994).

The three-dimensional characterisation of mantle structure and the lithosphere-asthenosphere boundary was greatly improved by the integration of previous approaches with **seismic tomographic imaging** (e.g., Amato et al., 1993; Green et al., 1991). The increasingly high-resolution of this methodology (e.g., Begg et al., 2009; Bastow, 2005, 2008; Goes 2000; Karato, 1993; Montelli, 2004; 2006; Tillman, 2001;) has resulted in a better understanding of asthenospheric structure from global (e.g., Ritsema and Allen, 2003; Simmons et al., 2011) to regional tomographic models (Bastow, 2005; 2008; Benoit, 2006). Combining these studies with **heat flow** measurements (e.g., Allen and Allen, 2013; Birch, 1954; Chapman and Rybach, 1985; Courthey and White, 1986; Detrick et al. 1986; Hersen et al., 1982; Pollack, 1993; Rolandone et al., 2013) has contributed to understanding crustal composition, radiogenic heat generation (e.g., Jaupart and Mareschal, 1999; Rolandone et al. 2002) and the thermal behaviour of the Earth's interior. These geophysical methods are used to constrain the pre-existing

structural and thermal state of the asthenosphere and lithosphere, which is a fundamental parameter for the evolution of continental rifts. Progress made in geophysical data acquisition and processing applied to rift studies has grown exponentially over the last 40 years and several comprehensive reviews are available on this topic (e.g., Almakli et al., 2014; Engdahl et al., 1998; Hansen 2012; Hansen and Nyblade, 2013; Lillie 1999; Nabighian, 2005;).

1.4.1.4 Microcontinent formation

The occurrence of microcontinents outboard of passive margins and stranded in ocean basins is genetically linked to the process of continental rifting and the subsequent transition to oceanisation. Although the concept of microcontinents from a morphological point of view has been discussed extensively and is now generally accepted (e.g., Heezen and Tharp, 1965; Nemčok et al., 2016 Peron-Pinvidic and Manatschal, 2010; Scrutton, 1976; Vink et al., 1984), the leading causes for their formation are still debated.
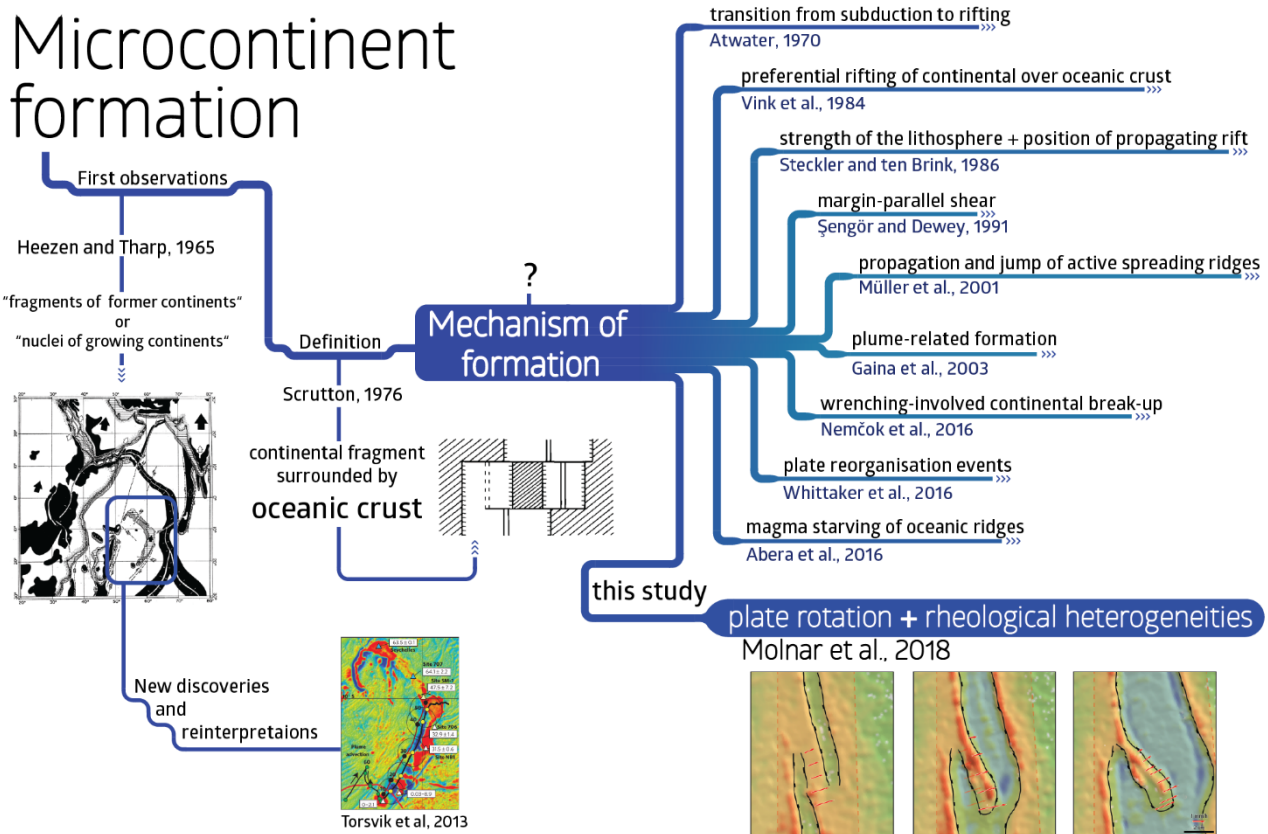
Figure 1.5 - **Flow chart summarizing the current state of knowledge on microcontinent formation.**

Heezen and Tharp (1965) originally described microcontinents as blocky, flat-topped features that ought to have crustal thicknesses of continental proportions and inferred they were either fragments of former continents or nuclei of growing continents (Fig. 1.5). Scrutton (1976) later refined the concept and concluded that microcontinents must be surrounded by oceanic crust (Fig. 1.5). Vink et al. (1984) proposed that microcontinents form due to the relative weakness of continental lithosphere in comparison to oceanic lithosphere. The onset of rifting near a diverging plate boundary should localise in the weaker continental lithosphere, potentially resulting in displaced terranes such as Baja in the Gulf

of California or the Lomonosov Ridge in the Arctic Ocean (Vink et al., 1984) (Fig. 1.5). Steckler and ten Brink (1986) similarly proposed that the strength of the lithosphere, in addition to the relative position of a propagating rift with respect to the hinge zone of the rifted margin, are the two main controlling factors in the development of new continental fragments (Fig. 1.5).

A number of investigations have focussed on microcontinents, such as the continental fragments of northwestern Australia (e.g., Pigram and Davies, 1987), southeast Asia (e.g., Metcalfe, 1988) and the Jan Mayen microcontinent in the Norwegian Greenland Sea (e.g., Gudlaugsson et al., 1988). More recent studies have explored the tectonic history of examples such as the Mauritian continental fragments in the Indian Ocean (Torsvik et al., 2013) (Fig. 1.5), the Limpopia and Beira highs in the southern Indian Ocean (Reeves et al., 2016) and Sri Lanka (Ana Desa et al., 2018). Furthermore, microcontinents have been recognised to play a significant role in the evolution of orogenic systems, as inferred from ancient examples preserved in the Precordillera of South America (Thomas and Astini, 1996), and in the Altaids in Eurasia (Sengör et al., 1993).

Pushcharovsky (2013), Nemčok (2016), Peron-Pinvidic and Manatschal (2010) have identified and classified different types of continental fragments that are partially or completely surrounded by oceanic lithosphere. However, a common classification of microcontinents in terms of mechanisms and timing of formation has not yet been proposed. Nevertheless, most studies concur that the degree of isolation of the preserved continental fragment (i.e. either still attached to the passive margin or a microcontinent *sensu stricto*) depends on how effective and continuous in time the processes leading to their formation are. Proposed separation mechanisms for microcontinent formation include: transitions from subduction to rifting (Atwater 1970), margin-parallel shear (Sengör and Dewey, 1991), propagation and jump of active spreading ridges (Müller et al., 2001), plume-related formation (Gaina et al., 2003), wrenching-involving continental break-up (Nemčock et al., 2016), plate reorganisation events (Whittaker et al., 2016) or magma starving of oceanic ridges (Abera et al., 2016) (Fig. 1.5). Overall, most of these concepts and arguments have been circumstantial and lacking support from numerical or analogue dynamic modelling. Chapter 3 of this thesis expands upon this matter and discusses the implications of my modelling results for the mechanism of microcontinent formation.

1.5 Methodology

1.5.1 Introduction

All of the experimental results presented in this thesis are based on laboratory simulations of extending lithosphere. The definition of experimental tectonics, commonly referred to as analogue modelling, has been elegantly expressed by Ranalli (2001):

> *"The term experimental tectonics is nowadays generally used to denote the study of tectonic processes in nature by means of scale models in the laboratory. The purpose of scale models is not simply to reproduce natural observation, but to test by controlled experiments hypotheses as to the driving mechanisms of tectonic processes."*

The principles behind this technique are based on achieving geometrical, kinematic and dynamic similarity between laboratory experiments and the natural prototypes. Ramberg's (1967) famously stated:

> *"The significance of scale-model work in tectonic studies lies in the fact that a correctly constructed dynamic scale model passes through an evolution which simulates exactly that of the original (the prototype), though on a more convenient geometric scale (smaller) and with a conveniently changed rate (faster)"*

Similarly, numerical models have been fundamental to improve the understanding of complex thermo-mechanical processes in extensional settings in both 2D and 3D. A review of the most significant advances carried out by both numerical and analogue modelling is summarised below.

1.5.1.1 Numerical modelling

The main advantage of computational geodynamics is that it simulates complex rock properties such as temperature- and stress-dependent viscosity, composite rheology, heat flow and radiogenic heating (Brune et al., 2016). Pioneering work on numerical modelling of rifting by England (1983), Kusznir and Park (1987) and Buck (1991), among others, became the foundation for later, more sophisticated models. Dunbar and Sawyer (1996) extended 2D models to 3D for the first time in order to study rift propagation across a heterogeneous continental lithosphere. In this study, relationships were established between rift propagation rate and the mechanical and geometrical characteristics of the lithosphere (i.e. strength and length of the stronger region). However, they indicated that "*the process of continental break-up is far more complex than the treatment it is given in this study*".

Many numerical studies of rifting are limited to 2D simulations in order to successfully incorporate realistic temperature-dependant and elasto-visco-plastic rheologies. Some of the key parameters tested in these models include:

- **Pre-rift conditions**: Armitage et al. (2010), Ben-Avraham and Katsman (2015), Corti et al. (2003), Gueydan et al. (2008), Jammes et al. (2010), Petersen et al. (2015).

- **Pre-existing heterogeneities**: Beaumont and Ings (2012), Chenin and Beaumont (2013), Huet et al. (2011).

- **Coupled versus decoupled rheology and lithospheric strength:** Brune et al. (2016), Gueydan et al. (2008), Huismans and Beaumont (2011; 2014), Lavier and Manatschal (2006), Wu et al. (2015), Svartman Dias et al. (2015).

- **Pure shear versus simple shear modes**: Chen et al. (2013).

- **Styles of rifting**: Gueydan and Précigout (2013), Jeanniot et al. (2016), Nagel and Buck (2004), Sharples et al. (2015).

- **Extension rate**: van Wijk and Cloetingh (2002).

- **Rift reactivation and migration and multiphase deformation**: Naliboff and Buiter (2015), Naliboff et al. (2017).

- **Rift to drift transition**: Perez-Gussinye et al. (2006), Marotta et al. (2016).

- **Causes of rift initialisation and localisation**: Brune and Autin (2013), Gueydan and Précigout (2013), Huismans and Beaumont (2003), Tommasi and Vauchez (2001), Watremez et al. (2013).

With increasing computational efficiency, a variety of three-dimensional codes have been developed in the last ~10 years (e.g., Braun et al., 2008; Gerya and Yuen, 2007; Moresi et al., 2007; Petrunin and Sobolev, 2008; Popov and Sobolev, 2010) and applied to the geodynamics of continental rifting and break-up. Some of the main aspects addressed by 3D numerical models of rifting are:

- **Pre-rift conditions and pre-existing rheological heterogeneities**: Allken et al. (2011), Beniest et al. (2017), Brune et al. (2017), Feng et al. (2015), Gac and Geoffroy (2009), Heine and Brune (2014), Le Pourhiet et al. (2012, 2014), van Wijk (2005).

- **Coupled versus decoupled rheology and layer strength:** Allken et al. (2012).

- **Obliquity and rotation**: Brune et al. (2012), Brune (2014), Brune and Autin, (2013).

- **Rift propagation**: Koopman et al. (2014), van Wijk and Blackman (2005).

- **Growth and interaction of normal faults**: Feng et al. (2015), Finch and Gawthorpe (2017).

- **Mantle plumes and mantle flow**: Brune et al. (2013); Burov and Gerya (2014); Farrington et al. (2010), Koptev et al. (2015).

- **Ocean initiation**: Le Pourhiet (2017), Liao and Gerya (2014).

- **Transform faults**: Behn et al. (2002), Choi et al. (2008), Gerya (2010; 2012; 2013), Gregg et al. (2009), Hieronymus (2004).

Buck (1991) specified that "*completely different model results are due to the way thermal boundary conditions are handled*", providing a simple explanation to the wide variety of previous modelling results. The dependency on pre-existing and/or boundary conditions is valid not only for numerical models, but also for ancient and modern natural examples. It is therefore challenging to establish a

classification scheme for continental rifts and the parameters that control their initiation and spatio-temporal evolution.

Efforts have also been made in computational geodynamics to simulate propagating rifts (e.g., Dunbar and Sawyer, 1996; Koopman et al., 2014; Mondy et al., 2018; van Wijk and Blackman; 2005) (Fig. 1.6). However, simulating the rotational kinematic boundary conditions observed in nature – which in turn produces a propagating rift - remains a challenge due to the computationally expensive calculations required.

1.5.1.2 Analogue modelling

The use of different materials to simulate the behaviour of rocks in the laboratory is an essential tool for understanding the deformation of the lithosphere at multiple scales. So-called experimental tectonics has been successfully applied to model natural examples since the 19th century (e.g., Hall, 1812, 1815; Willis, 1893). A series of landmark papers using laboratory modelling in the first half of the 20th century investigated dome formation (Escher and Kuenen (1929), the fluid mechanics of salt domes (Nettleton 1934; 1943), the mechanics of geological structures (Hubbert, 1951) and extensional faults (Cloos, 1930). Buckingham (1914) and Hubbert's (1937) work on the theory of scale models, and its application to structural geology, established analogue modelling as an accepted methodology in the geoscientific community. In the following decades, efforts were made to discover additional model materials in order to recreate a wider variety of natural phenomena (e.g., Ramberg's 1967). Modelling of subsiding 'sheets', orogenic belts and mantle convection (Ramberg, 1967) became a reality, and in parallel with the establishment of plate tectonics theory in the 1970s, setting the scene for a period of significant advances in the understanding of continental rifts by means of analogue modelling.

Initial analogue modelling studies of divergent settings were focussed on investigating the formation of transform faults in the oceanic lithosphere (Oldenburg and Brune 1972; 1975). Employing a thermomechanical setup with paraffin waxes, orthogonal ridge-transform patterns were successfully reproduced (Oldenburg and Brune, 1972; 1975). Subsequent investigations by Freund and Merzer (1976) concluded that the orthogonal pattern was only formed due to the inherent anisotropy of the type of waxes used. Rather than concluding that the experiments were not valid, they proposed that the transform pattern of oceanic plate separation was similarly related to seismic anisotropies of the upper mantle (Freund and Merzer, 1976).

The first analogue models on continental extension were presented in the late 1980s. Withjack and Jamison (1986) investigated oblique rifting, Vendeville et al. (1987) explored the formation and propagation of normal faults in orthogonal extension, and Allemand et al. (1989) investigated the symmetry and asymmetry of rifts using 3- and 4-layer model lithospheres. Davy and Cobbold (1991), although investigating compressional processes, expanded upon these studies and discussed in detail an experimental method for modelling deformation of the lithosphere and potential future applications. This approach has since been adopted by the analogue modelling community, resulting in significant progress in rift modelling studying key parameters such as:

- **Pre-rift conditions, crustal layering and modes of continental extension**: Benes and Davy (1996), Brun (1999)

- **Control of rift obliquity** Autin et al. (2010), Corti (2008), McClay and White (1995), Tron and Brun (1991), Withjack and Jamison (1986).

- **Polyphase rifting:** Bonini et al. (1997), Keep and McClay (1997).

- **Rift propagation and rheological heterogeneities:** Benes (1995), Benes and Scott (1996), Mart and Dauteuil (2000), Molnar et al. (2017).

- **Control of lithospheric mechanical structure and rheological heterogeneities** Corti (2012; 2013), Corti et al. (2011); Sokoutis et al. (2007).

- **Combined rift obliquity and pre-existing rheological heterogeneities** Agostini et al. (2009), Autin et al. (2013), Cappelleti et al. (2013), Corti (2012).

- **Lithospheric necking**: Nestola et al. (2013; 2015).

- **Reactivation of extensional basins**: Dooley and Schreurs (2012), Panien et al. (2005).

- **Fault interaction:** Le Calvez and Vendeville, (1996), Le Calvez and Vendeville (2002), Sims et al. (1999).

- **Far field stresses and external forces**: Bellahsen et al. (2003), Marques et al. (2007).

- **Origin and interaction between oceanic ridge segments**: Dauteuil et al. (2002), Oldenburg and Brune (1972, 1975), Tentler and Acocella (2010).

- **Reproducibility of analogue models**: Schreurs et al. (2006).

Furthermore, novel laboratory techniques and new materials have been introduced, resulting in major improvements in modelling both extensional and compressional processes. The incorporation of temperature sensitive materials began in the 70s (e.g., O'Bryan et al., 1975; Oldenburg and Brune, 1972; 1975; Ragnarsson et al., 1996; Shemenda and Grocholsky, 1994), but precise control of the imposed thermal gradients was lacking. Advances in model setup and materials allowed for improved simulations of sea-floor spreading (Katz et al., 2005), thermal plumes (Davaille et al., 1999; 2002) and a more realistic geothermal gradients (e.g., Boutelier et al., 2002; Boutelier and Oncken, 2011; Boutelier and Cruden, 2013; Wosnitza et al., 2001). However, mimicking normal faults and the general behaviour of the brittle upper crust still represents a limitation in such thermo-mechanical model setups.

The integration of analogue modelling with new deformation monitoring techniques improved the understanding of lithospheric deformation significantly. Laser measuring devices were used to quantify dynamic topography, surface patterns and subsidence in great detail (e.g., Autin et al., 2010; Corti et al., 2012; Cruden et al., 2006; Pysklywec et al., 2004; Schlagenhauf et al., 2008). In the last ~10 years, analogue modelling has greatly benefited from new high-resolution optical image correlation techniques (e.g., Adam et al., 2005; Galland et al., 2016; Herbert et al., 2015; Riller et al., 2012; Schrank et al., 2010), allowing for quasi-continuous monitoring of surface topography, strain partitioning and localisation. Internal deformation has also become quantifiable by running computed tomography (CT) scans of analogue experiments (e.g., Adam et al., 2013; Schreurs, 1994; Zwaan et al., 2017a; 2017b). These techniques have special interest for the study of smaller scale fault development of continental rifts in time and space.

In addition to the aforementioned contributions, further details of modelling investigations of rifting can be found in extensive reviews by Acocella (2014), Brun (1999), Brune et al. (2016), Corti et al. (2003), Gerya (2012), Ranalli (2001) and Ziegler and Cloetingh (2004).

1.5.1.3 The research problem

Most modelling studies have focussed on isolating and testing a specific variable; all the parameters except one are usually fixed, in order to understand its particular role in the style of continental rifting. It is generally agreed that three main parameters control the first-order modes of rifting (Corti et al., 2003): **(1)** strain rate and rate of extension, **(2)** pre-rift conditions, mainly associated with the lithospheric layers strength and their degree of coupling or decoupling, and **(3)** pre-existing (or inherited) mechanical heterogeneities. In this thesis, I pay special attention to the latter parameter in cases where the mechanical heterogeneity is related to linear weak areas in the lithosphere.

A significant amount of work has been done on the rheological properties of the lithosphere (e.g., Artyushkov 1973; Kirby 1983; Ranalli, 1982; Ranalli and Murphy, 1987) in order to understand its behaviour when submitted to tectonic forces. Several studies have also evaluated the role of chemical composition, pressure and temperature in laboratory experiments of rock deformation (e.g., Goetze and Evans, 1979; Kohlstedt et al., 1995), and the concept of variable rheological profiles (or strength envelopes) in the lithosphere was established by the end of the 20th century (Goetze and Evans, 1979; Ranalli, 1995). These advances were fundamental for quantifying and constraining the role of mechanical heterogeneities in the lithosphere during continental extension.

The concept of inherited features from previous tectonic phases, which can act as pre-existing weaknesses, and influence the evolution of rifts, has been the topic of debate for more than 50 years (e.g., Corti et al., 2013; Korme et al., 2004; Milani and Davison, 1988; Morley, 1999; Sleep, 1971; Theunissen et al., 1996; Wilson, 1966). Weaknesses in the lithospheric mantle can be associated with the activity of mantle plumes (e.g., Corti, 2008; Hill, 1991), hot spots tracks (Morgan, 1981), mantle penetrating shear zones with reduced grain size (Bercovici and Ricard, 2008; Heron et al., 2016), or inherited mechanical anisotropies with lattice preferred orientation of olivine crystals (Tommasi and Vauchez, 2001). Heterogeneities in the crust are commonly associated with pre-existing basement faults (e.g., Holdsworth et al., 1997; Wilson et al., 2010), suture zones (Bosworth et al., 2005 and references therein; Stern and Johnson, 2010;) and orogenic belts (Vauchez et al, 1997), which often juxtapose different lithospheric blocks with different ages and mechanical properties. Both mantle and crustal heterogeneities potentially localise strain, and consequently influence where and how the lithosphere deforms. The recognition of these pre-existing structures or rheological heterogeneities is common in the geological record, but how they influence the localisation and partitioning of deformation during continental breakup remains poorly understood.

Propagating rifts

Tectonic chart of the world

Plate kinematics

important implications for

Wilson, 1963

Heezen and Tharp, 1965

Vine and Matthews, 1963

Holmes, 1928
Hess, 1962
defined

Propagating rifts in mid-ocean ridges

in

OCEANS

magnetic anomalies

Spreading ridges

Herron, 1972

Shih and Molnar, 1975

Hey, 1977

Hey et al., 1980

Bonini, 2005
Zwaan et al., 2017
Lyakhovsksy et al., 2012
Koehn et al., 2008
Franke et al., 2000
Ford et al., 2016
Keranen and Klemperer, 2008

in

CONTINENTS

first
observations

Burke and Dewey, 1973
Maasha and Molnar, 1972
Scholz et al., 1975

still poorly
understood

Conceptual models

V-shaped propagating rifts
against 'locked' zones
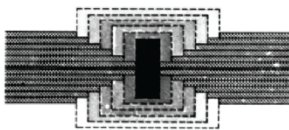
Crustal thinning in rift tip,
sea-floor spreading behind

Propagating rifts as a consequence
of motion about a pole of rotation

Courtillot, 1982

Vink et al., 1982
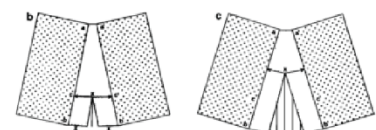
Martin et al., 1984

Numerical models
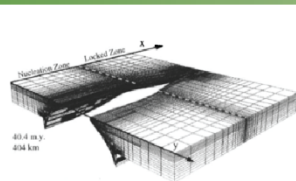
Dunbar and Sawyer, 1996
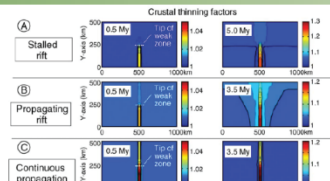
van Wijk and Blackman, 2005
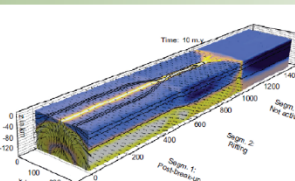
Koopman et al., 2014
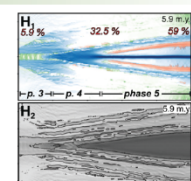
Mondy et al., 2014

Analogue models
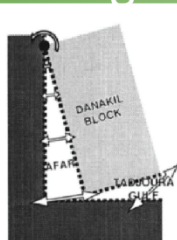
Souriot and Brun, 1992
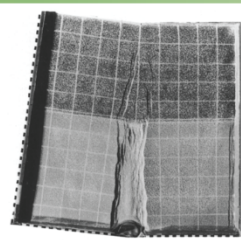
Benes and Scott, 1996
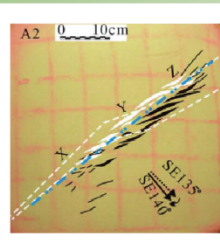
Sun et al., 2009
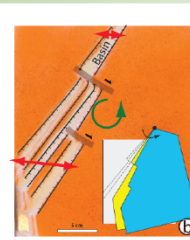
Philippon et al., 2014
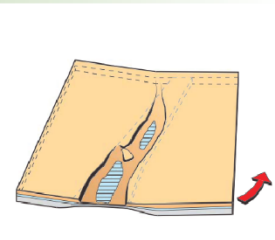
Molnar et al. 2017 (this thesis)

Figure 1.6 - Flow chart summarising important steps and current state of knowledge in understanding propagating rifts in oceanic and continental lithosphere.

How rifts propagate along-axis as a result of the relative rotational motion of two diverging lithospheric plates is an additional variable that hasn't been widely evaluated. Due to the availability of geophysical and paleomagnetic data in the ocean floor, rift propagation was initially investigated in the oceanic realm (e.g., Benes et al., 1994; Heezen and Tharp, 1965, Hey 1980, Hey et al., 2010; Mondy et al, 2018; Shih and Molnar 1975; Vine, 1966). Conversely, the propagation of continental rifts is complex and poorly understood. Courtillot (1980) studied propagating rifts and defined the concept of "*progressive tearing*", with application to the Gulf of Aden. He later proposed the conceptual model of V-shaped propagating rifts that advance, nucleate and become locked against 'asperities' (i.e. heterogeneities) (Courtillot, 1982) (Fig. 1.6). However, the relative rotation of plates was not discussed in detail. Vink (1982) proposed a model for continental break-up with "distortion", in which the author established that rifts propagating through a continent extend by crustal thinning and normal faulting near the propagating tip, while the region behind expands by sea-floor spreading (Fig. 1.6). Martin (1984) later defined the propagation of a rift as a natural consequence of the relative motion of rigid plates about a pole of rotation (Fig. 1.6).

Although many major continental breakup events in Earth's history are known to have involved relative rotation between plates, most geodynamic modelling has focused on rifting in which the relative plate motion is orthogonal or oblique and constant over time (e.g., Agostini et al., 2009; Autin et al., 2013; Benes and Davy, 1996; Brune, 2014; Clifton et al., 2000; Corti et al., 2003; Dauteuil and Brun, 1993; van Wijk, 2005). The simulation of large-scale rotations on Earth has been scarcely investigated. Few models have focused on investigating rotational kinematics with variable rheological heterogeneities and most of these were restricted to direct comparisons with selected natural examples, such as the Afar triangle (Souriot and Brun, 1992), the Havre Trough (Benes and Scott, 1996), the Kuril arc (Schellart et al., 2003), the South China Sea (Sun et al., 2009) or the Gofa Province (Philippon et al., 2014), rather than characterising the first-order role of pre-existing rheological heterogeneities in controlling the evolution of propagating rifts (Fig. 1.6).

Since natural rift systems are integrally three-dimensional, there is a need to further increase modelling capabilities in order to simulate realistic rotational kinematic boundary conditions and test different hypothesis. Due to the inherent difficulty of achieving this with numerical models, in addition to the high-resolution benefits obtained through physical simulations, I opt for a novel analogue approach, which can successfully simulate large-scale rotations on Earth. My laboratory experiments are innovative in that they incorporate three-dimensional relative motion of lithospheric plates containing linear heterogeneities around a pole of rotation to simulate complex extensional settings. This work aims to provide the hitherto lacking support for some of the remaining first-order questions on continental rifting and break-up. The details on scaling, experimental setup and modelling materials are outlined below.

1.5.2 Experimental design

To address the problem of rotational rifting or continental lithosphere containing linear heterogeneities, I employ a multipurpose experimental apparatus that can impose pure, oblique and rotational rifting boundary conditions on analogue model lithospheres over a range of strain rates. Surface strain and dynamic topography in the experiments is quantified using a high-resolution particle

imaging velocimetry (PIV) and digital photogrammetry monitoring system. Analysis of the resulting fault patterns, dynamic topography, velocity fields and strain localisation allows me to compare the experimental outcomes with previous analogue and numerical models, as well as with available structural and geophysical data from worldwide examples of ancient and modern rift systems.
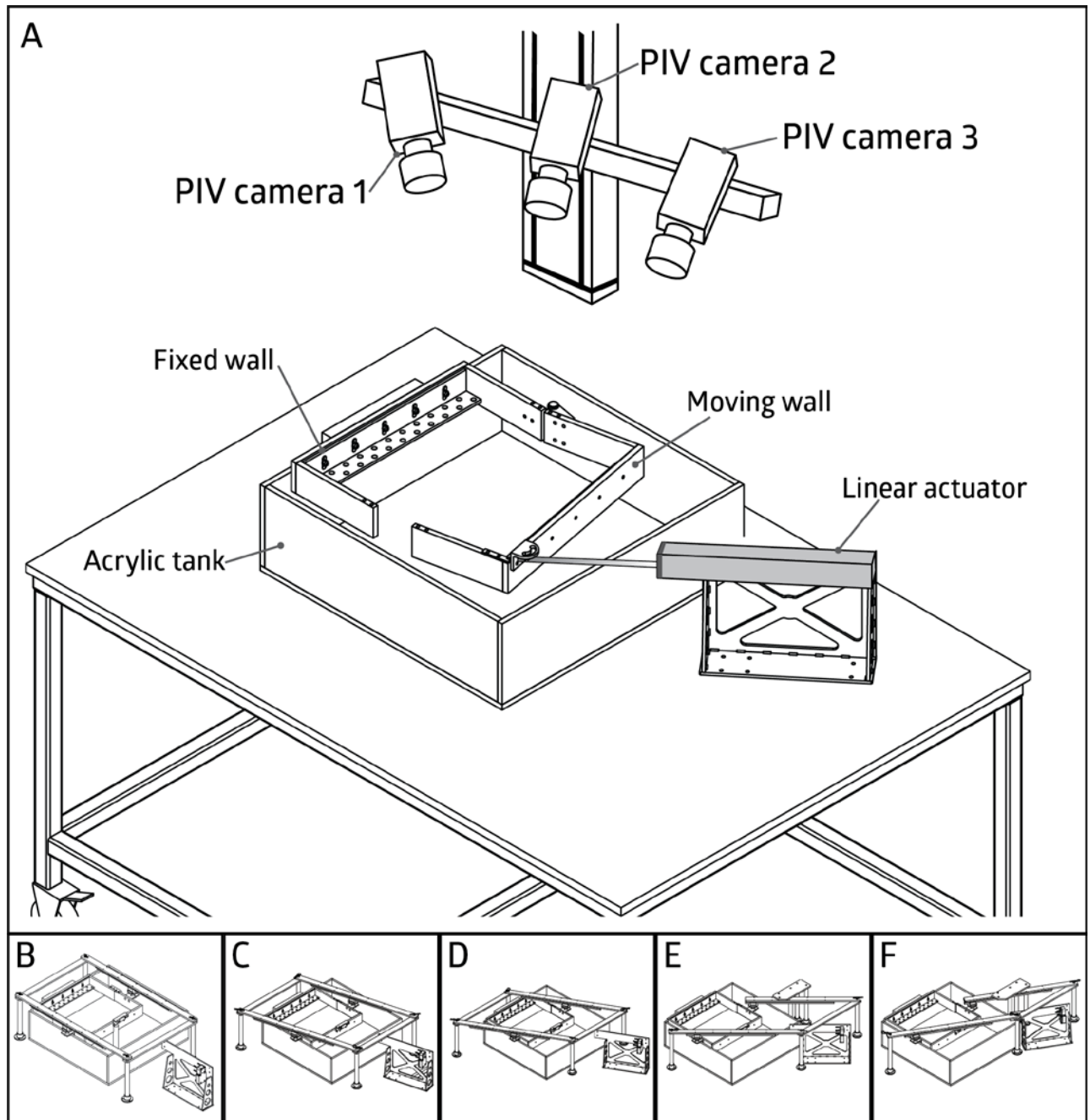
Figure 1.7 - **Experimental apparatus set up: A. Rotational extension; B. Pure extension; C. 15° oblique extension; D. 30° oblique extension; E. 45° oblique extension; F. 60° oblique extension.**

The experimental apparatus consists of a 65 x 65 x 20 cm acrylic tank resting on a table (Fig. 1.7). The apparatus was designed so that all experiments can be run starting from the same initial state. The model lithosphere is attached to "U" shaped walls, one being fixed and the other is pulled by a linear actuator at a controlled, constant rate, which can vary from 0.000151 mm/s to 40 mm/s. Considering

the velocity scaling factor used in the experiments (See Materials and Scaling), this range covers the equivalent range of estimates for rates of extension of ancient rifts and GPS measurements from modern rifts. A rail system ensures purely horizontal displacement of the U-shaped walls. The arrangement of the rail system can be modified to achieve orthogonal and oblique (15°, 30°, 45°, 60°) geometries of extension. Additionally, a rotational extension boundary condition can be simulated by fixing a pivot on one side of the U-shaped walls and pulling the moving wall from the opposite side with the linear actuator in an anticlockwise fashion (Fig. 1.7).

1.5.3 Materials and scaling

The experimental approach is based on modelling Earth's lithosphere submitted to extensional forces under different boundary conditions. The general construction of the experiments and the scaling for the materials employed follows the approach for analogue modelling described in previous studies such as Ramberg, (1967), Davy and Cobbold (1991) and Benes and Davy (1996). Lengths, time and forces are scaled down in order to have a suitable sized model that behaves mechanically like the prototype (nature). The scaling is only approximate since uncertainties or complexities that occur in nature are not reproducible in the laboratory. With the objective of simulating a variety of lithospheric strength profiles and lateral strength changes, different values for of the ductile materials can be achieved by employing different proportions of the component mixtures. All the experiments reported here comprise a simplified three-layer lithosphere with a brittle upper crust, a ductile lower crust and a ductile lithospheric mantle, overlying a fluid model asthenosphere. The rheological properties of the ductile and fluid materials described below were measured over the relevant range of experimental strain rates (1×10^{-5} to 5×10^{-4} s^{-1}) using an Anton Paar Physica MCR-301 parallel plate rheometer, following methodologies described in previous analogue modelling studies (e.g., Boutelier et al., 2008; 2016, Duarte et al., 2014; Schellart 2011; ten Grotenhuis et al., 2002). Flow tests were carried out to investigate the dependency of the rheology on shear strain and stress-ramp tests were done to investigate yield stress and post-yielding flow (Boutelier et al., 2008; Duarte et al., 2014) (Fig. 1.8). The density of the model asthenosphere was measured using an Anton Paar DMA4500 density meter, while the density of the PDMS-based mixtures was obtained by measuring the volume of displaced water by samples of known weight (Schopfer and Zulauf, 2002). Numerous tests have been carried out in order to quantify the main rheological parameters for each model material, as specified next.

Rheology tests workflow
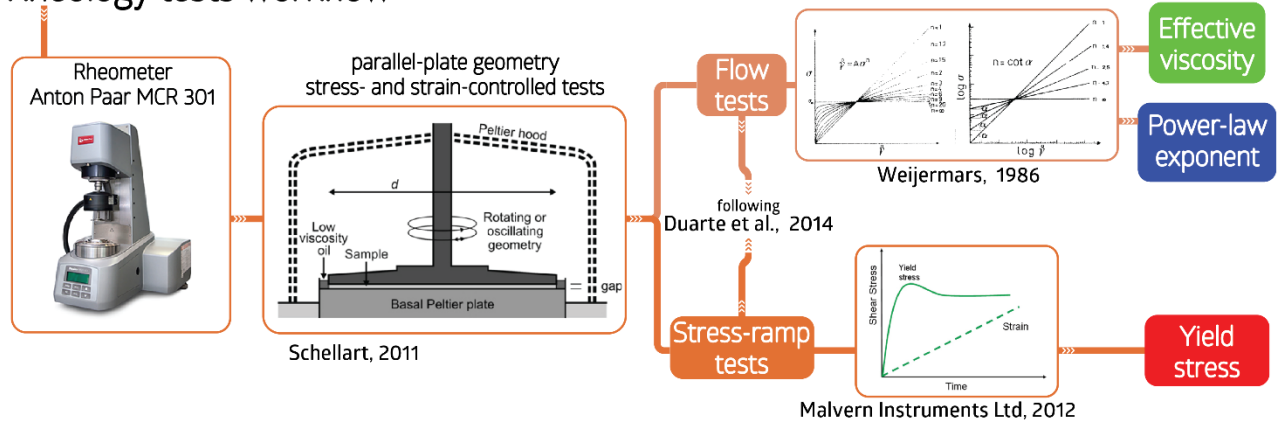
Figure 1.8 - Rheology tests workflow used for the measuring of the rheological properties of the materials used in this study.

Lower crust

For practical purposes, I used the physical properties of the ductile lower crust material as the main constraint to subsequently define the viscosity and density for the remaining model materials. I use Wacker Elastomer NA polydimethylsiloxane (PDMS) as the material to model the ductile lower crust. PDMS is an optically clear, high viscosity, high molecular weight silicone polymer frequently used in analogue modelling (e.g., Cruden et al., 2006; Marques et al., 2007; Pysklywec and Cruden, 2004) (Fig. 1.9). It has a density of $\rho_m \approx 980$ kg/m^3, which for a lower crust density of $\rho_n \approx 2760$ kg/m^3 sets a density scaling factor $\rho^* = \rho_m/\rho_n = 0.355$ km (subscripts m and n refer to model and nature, respectively). I performed a series of controlled shear rate tests (e.g., Schellart, 2011; Duarte et al., 2014) to measure the viscosity at different shear rates, which indicated that the employed PDMS has an effective viscosity of $\eta_m \approx 4 \times 10^4$ Pa s under experimental conditions (Fig. 1.9). Considering a lower crust viscosity of $\eta_n \approx 2 \times 10^{21}$ Pa s for scaling purposes, this defines a viscosity scaling factor $\eta^* = \eta_m/\eta_n = 2 \times 10^{17}$. PDMS and PDMS mixtures with granular materials have a slightly non-Newtonian rheology defined by the power law:

$$\sigma^n = \eta\dot{\varepsilon} \qquad (1.1)$$

Where σ is stress, $\dot{\varepsilon}$ is strain rate, η is viscosity, and n is the power law exponent of the material. The power law exponent of the material can be determined from equation (1.1) from stress - strain-rate measurements (Weijemars, 1986) (Fig. 1.9). Calculation of the yield stress of PDMS was done using a stress ramp test (Malvern Instruments Ltd., 2012) giving a value PDMS$_{ys}$ = 5 Pa.
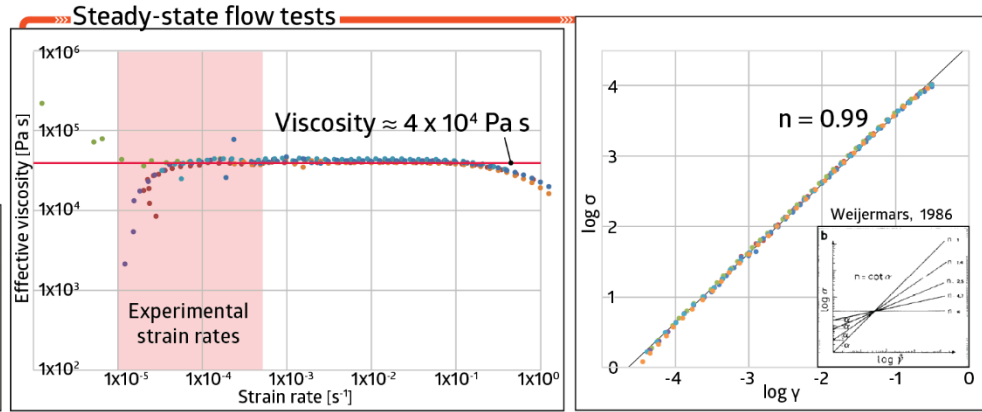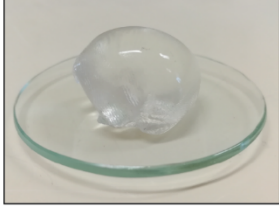
Figure 1.9 - **Characteristics and rheological properties of the model lower crust.**

An initial model crustal thickness value of L_m = 14 mm was used to represent a crustal thickness in nature L_p = 35 km. The scaling factor for length, L^*, is therefore fixed by the equation $L^* = L_m/L_p = 4 \times 10^{-7}$. Following Pysklywec and Cruden (2004), the time scaling factor is set by the ductile material, calculated from:

$$t^* = \eta^* / \rho^* \cdot g^* \cdot L^* \qquad (1.2)$$

All the experiments are carried out at the normal field of gravity (1 g), therefore the gravity scale ratio is $g^* = g_m/g_n = 1$. A time scaling factor $t^* = 1.41 \times 10^{-10}$ is obtained from equation (1.2), meaning that 1 hour in the experiment corresponds to ~0.8 Ma in nature. The scaling parameters between the experiments and nature are summarised in table format in each chapter accordingly.

Lithospheric mantle

The appropriate rheology of the model lithospheric mantle is achieved by adding appropriate amounts of black Colorific Plasticene® and 3M® hollow glass microspheres to PDMS (Fig. 1.10). Plasticene is a modelling material with Reiner-Rivlin fluid characteristics, namely a complex rheological behaviour (McClay, 1976, Zulauf and Zulauf, 2004). Mixtures of Plasticene with PDMS are commonly used in laboratory experiments (Zulauf et al., 2003, Cruden et al., 2006, Boutelier et al., 2008). K-1 class 3M® microspheres are hollow glass fine particles with very high strength with a true density of 0.125 g/cm^3 and a particle size of 120 µm also frequently used as solid fillers in PDMS-based mixtures (e.g., Cruden et al., 2006; Boutelier et al., 2008). While blending Plasticine with PDMS increases both the density and effective viscosity, adding microspheres decreases the density and increases the effective viscosity. The variations of these physical properties are then controlled by the proportions of Plasticene and solid fillers used (e.g., Boutelier et al., 2008). A volume percentage mixture of 57% PDMS + 29% black Colorific Plasticene® + 14% 3M® hollow glass microspheres (class K-1) resulted in a model lithospheric mantle density of $\rho_m \approx 1080$ kg/m^3, which scales up to a natural lithospheric mantle density of $\rho_p \approx 3050$ kg/m^3. Following a similar procedure as with the PDMS, the rheological parameters of the mixtures were measured with identical tests by the parallel plate rheometer. The model lithospheric mantle has a power law exponent n = 1.25, an effective viscosity of $\eta_m \approx 2 \times 10^5$ Pa s under experimental conditions, equivalent to $\eta_p \approx 1 \times 10^{22}$ Pa s in nature, and a yield strength LM_{ys} = 25 Pa (Fig. 1.10).
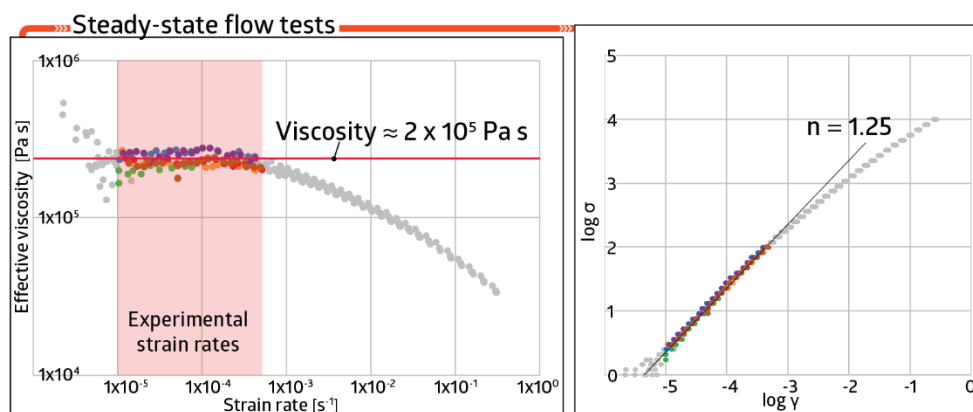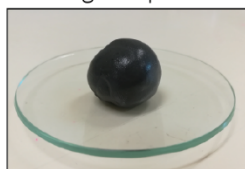
Figure 1.10 - **Characteristics and rheological properties of the model lithospheric mantle.**

I excluded the 3M® hollow glass microspheres and varied the proportions of PDMS and Plasticine to prepare a mixture that mimics a model weak lithospheric mantle, with similar density to the 'normal' lithosphere but with a smaller effective viscosity. A density of $\rho_m \approx 1075$ kg/m^3, which scales up to a natural lithospheric mantle density of $\rho_p \approx 3030$ kg/m^3, was achieved with a volume percentage mixture of 81.5% + 18.5% black Colorific Plasticine. Additional rheometric tests were carried out on the mixture and an effective viscosity $\eta_m \approx 1 \times 10^5$ Pa s under experimental conditions was obtained, equivalent to $\eta_m \approx 5 \times 10^{21}$ Pa s in nature.

Asthenospheric mantle

The required physical properties of the model asthenospheric mantle were achieved using a solution of Natrosol® 250 HH and sodium chloride in deionised water, which allows for precise control of its viscosity and density. Natrosol® is a cellulose polymer employed to increase the viscosity of aqueous fluids, without significantly affecting their density. Handling and preparation of Natrosol solutions was done following Boutelier et al. (2016). As an aqueous solution, it behaves as a Newtonian viscous fluid under conditions typically employed in experimental tectonics (Boutelier et al., 2016) (Fig. 1.11). Flow tests indicate that my model asthenosphere has a Newtonian viscosity of $\eta_m \approx 380$ Pa s, which represents $\eta_n \approx 1.9 \times 10^{19}$ in nature, which is a reasonable approximation for the upper mantle viscosity (~10^{19} – 10^{20} Pa s [Artyushkov, 1983]; ~10^{19} – 10^{21} Pa s [Ranalli, 1995]) (Fig. 1.11). I control the solution density by adding sodium chloride to water, following previous analogue modelling experiments (Davaille 1999; Davaille et al., 2002). The proportions were varied until I achieved a density of $\rho_m \approx 1100$ kg/m^3, equivalent to a natural asthenosphere density of $\rho_n \approx 3100$ kg/m^3 (e.g., Pysklywec and Cruden, 2004).
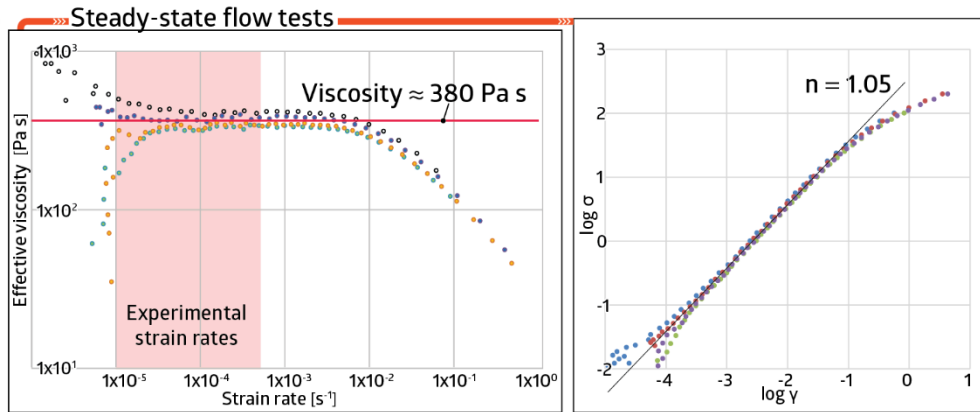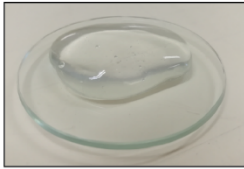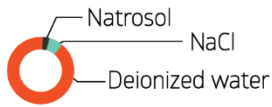
Figure 1.11 - Characteristics and rheological properties of the model asthenosphere.

Upper crust

The brittle upper crust is modelled using granular materials, combining appropriate proportions of fine quartz sand and Envirospheres® hollow ceramic spheres, with bulk densities of 1550 kg/m^3 and 390 kg/m^3, respectively. The graded quartz sand has a homogeneous grain size distribution with 75% of the grains falling between 435 and 500 μm, and the hollow ceramic Envirospheres have a very homogeneous grain size distribution, with 90% of the grains in the 100-150 μm range. These two materials were combined in the ratio 3.11:1 (quartz sand:Envirospheres) to achieve a density $\rho_m \approx 928$ kg/m^3, which scales to a natural upper crustal density of $\rho_p \approx 2650$ kg/m^3. Hubbert-type (Hubbert, 1937) shear box tests were conducted to determine the peak and stable sliding cohesion and angle of internal friction values (Fig. 1.12) of the mix. A peak strength angle of internal friction $\phi = 38°$ and cohesion value of $\sigma_0 \approx 9$ Pa were determined, indicating that hollow ceramic spheres and sand mixtures are appropriate analogues for modelling the brittle upper crust with a Mohr-Coulomb behaviour (e.g., Byerlee, 1978, Davy and Cobbold, 1991).
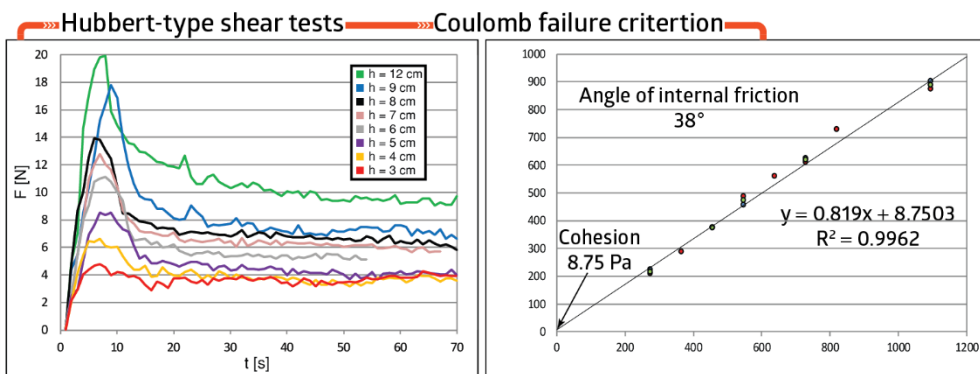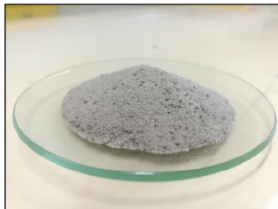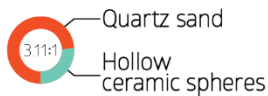
Figure 1.12 - Characteristics and rheological properties of the model upper crust.

1.5.4 Monitoring of deformation

The model surfaces were monitored using a stereoscopic 3D Particle Imagery Velocimetry (PIV) system, which provides precise spatio-temporal measurements of deformation and dynamic

topography. The PIV system is equipped with two 4-megapixel high-speed cameras that provide a spatial resolution of ~0.1 mm and a temporal resolution of ~0.1 s. However, due to the length of the experiments carried out for this work (~37 hours), successive PIV images are taken at a time interval of 120 seconds, well within limit to monitor slow model deformation (<0.002 mm s^{-1}). The deforming surface must contain a random pattern of particles, which allows the PIV system to capture successive images for subsequent optical cross correlation and displacement field calculation. This pattern is obtained by including dark-coloured particles in the sifted granular material mix. Stereo cross correlation of sequential images (Adam et al., 2005) was employed to compute high-resolution displacement fields using LaVision Davis imaging software.

Surface topography: stereoscopic images are used to create digital elevation models of dynamic topography with an accuracy of <0.1 mm. Integrating the original rectified images with the resulting DEMs and the surface incremental and cumulative strain data provides detailed insights on the structural evolution and on subsidence/uplift patterns.

Displacement: particle velocity measurements are directly analogous to GPS vectors in nature. Quantitative results can be therefore correlated with available GPS data in regions of interest. Displacement fields additionally indicate sense of motion of extensional structures with oblique- or strike-slip components in the experiments.

Differential strain: strain in different directions can be derived from the displacement gradients, which allows us to characterize strain localization and deformation partitioning during the modelled continental break-up in great detail. The quasi-continuous monitoring of deformation allows the detection of structures or series of structures that become active/inactive at any point during the experiment.

Cumulative strain: incremental data field maps are sequentially added in order to obtain cumulative data values at a given experimental time. This procedure allows the visualisation and identification of areas that accommodated most extensional deformation.

Figure 1.13 - Synthesis of the four main parameters that are used throughout the thesis to describe the first-order evolution of deformation in the laboratory experiments.

During the processing stage, a series of parameters are manually set in order to compute either incremental data or cumulative data (calculated as the sum of the incremental data). In this way, the

model evolution in four dimensions (x, y, z, time) can be characterised for both the whole experiment or for a selected time range. Figure 1.13 shows the four main parameters that are used throughout the thesis to describe the first-order evolution of deformation in the laboratory experiments.

1.5.5 Model limitations

The versatility of analogue modelling has provided important insights in understanding of the surface and internal deformation of extending lithosphere with complex three-dimensional setups. Additionally, they been successfully combined with high-resolution monitoring techniques to elucidate patterns of strain partitioning and localisation. Nonetheless, the lack of more complex elasto-visco-plastic rheologies and realistic temperature-dependent materials remains a limitation for laboratory scale models. Since the apparatus is isothermal, the presence of linear thermal anomalies (Chapters 2 and 3) can be simulated by varying the viscosity of the model lithospheric mantle. I alternatively recreate crustal heterogeneities by adding linear segments of the model lower crust material in the lower crust-upper crust interface, therefore reducing the overall integrated strength of the crust along those segments (Chapter 4). Although weak zones may not be linear in nature, the modelled weaknesses are analogous to strain corridors, a thermal anomaly with a roughly linear trend, previously thinned sections of the lithosphere, suture zones and/or shear zones.

In the experiments, the focus is mainly on rotational extension. Although the apparatus is unable to recreate multi-phase rift systems (e.g., Bonini 1997, Keep and McClay 1997), the role of such kinematic conditions on continental break-up is beyond of the scope of this study. On the other hand, the construction of laboratory experiments is always subject to the introduction of heterogeneities or discontinuities produced by the lab user during the handling of the materials and set up of the layers. In order to reduce this to a minimum, the ductile layers are first made separately by allowing them to spread to the desired area and thickness within a rigid frame. Specially designed 4 cm wide horizontal grips are also incorporated along two sides of the lithospheric mantle layer, which is then placed on top of the model asthenospheric mantle, within the U-shaped walls. The ductile crust layer is then placed on top and the model is left to sit to allow sufficient time to achieve isostatic equilibrium and for air bubbles to dissipate (~12 h). The model upper crust layer is then deposited by sifting granular materials from a height of ~15 cm. No manual off scraping is done to prevent alterations in the mechanical properties of the upper crustal layer due to unwanted compaction. Once all model lithosphere layers are in place and in isostatic equilibrium with the asthenosphere, the grips are fastened to the extension-perpendicular sides of the U-shaped walls.

The opening of the U-shaped walls creates a free edge in which granular material from the upper crust collapses by gravity (Fig. 1.14). Similarly, the pull exerted by the linear actuator on the U-shaped walls creates unwanted differential thinning of the model lithosphere in the vicinity of the horizontal grips (Fig. 1.14). These unwanted boundary conditions of the experimental setup affects a small area that is outside the region of interest (i.e. the surface area selected for deformation monitoring) and is therefore not considered to be detrimental to the results. An 80:20 wt % paraffin oil in petrolatum jelly mixture (Duarte et al., 2014) is used as a lubricant between the model lateral boundaries and the confining U-shaped walls to minimise other boundary effects. The lateral side boundary effect caused

by the grip between the model lithosphere and the side walls is therefore significantly reduced and is considered negligible for the experiment results.
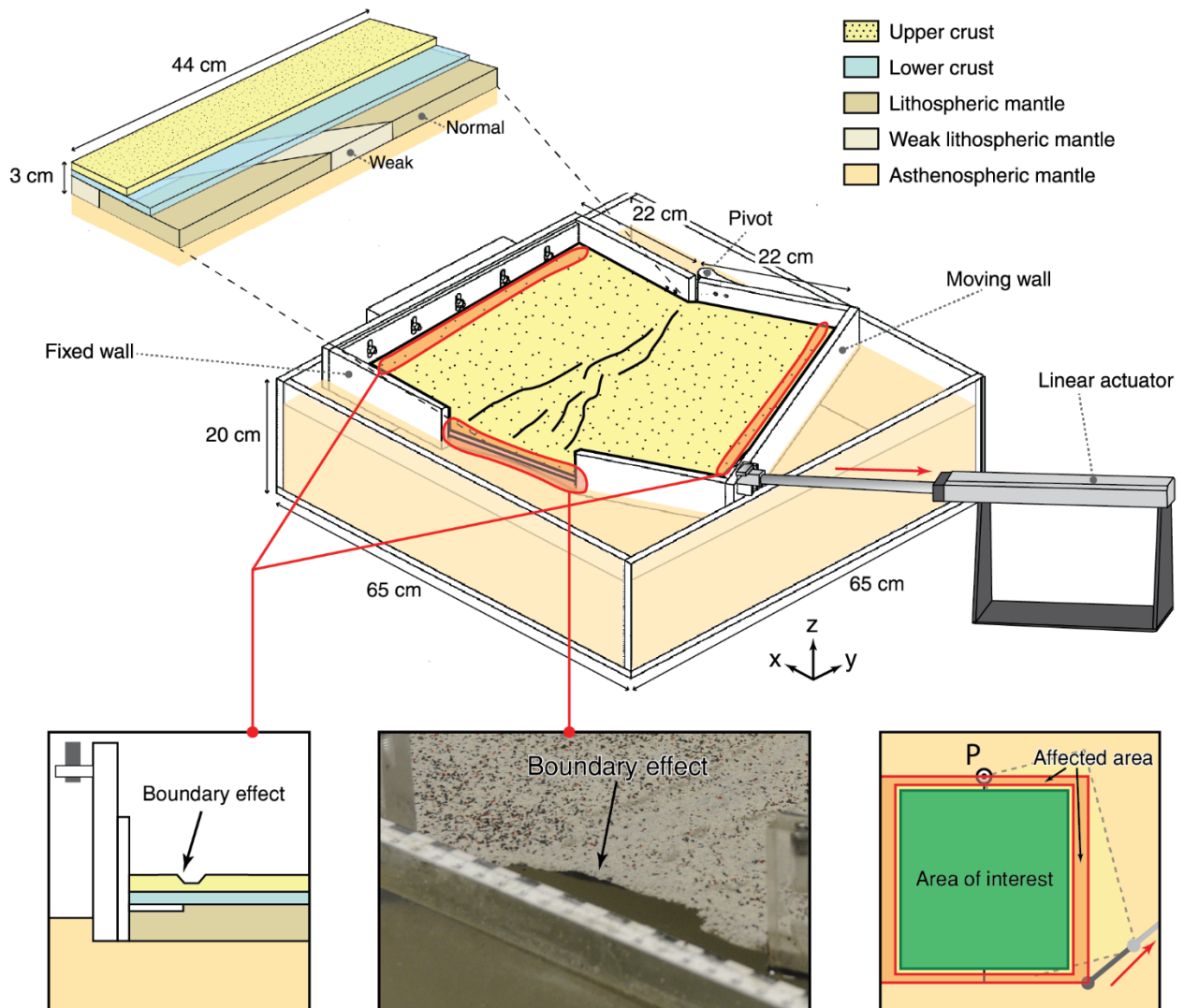
Figure 1.14 - **Model setup and initial configuration of the rotational experiments, showing the extent of the unwanted boundary effect and the area affected.**

Experiments with the same initial conditions and parameters were replicated to test for reproducibility. Although minor differences have been observed between repeated experiments, all analogue models displayed similar behaviour in terms of their first-order geometric and kinematic evolution. Exceptional cases with larger discrepancies (e.g., compare Experiments 3, 5, 6 and 8 or Experiments 24, 25 and 26 in Appendix A) occurred when there were technical and/or handling errors during the preparation and subsequent setup of the model layers. Top-view topographic evolution for all experiments are presented in Appendix A.

Chapter 2

Interactions between propagating rifts and linear weaknesses in the lithospheric mantle

Abstract

The lateral propagation of rifts is a consequence of the relative divergence of lithospheric plates about a pole of rotation. Modern and ancient examples of rifts are known to overprint pre-existing linear anisotropies in the crust and lithosphere, such as lithospheric boundaries, crustal sutures, and thermal anomalies. Here I investigate how propagating rifts interact with pre-existing structures by using three-dimensional analogue experiments with rotational extensional boundary conditions and variably oriented linear weak zones in the lithospheric mantle. When linear weaknesses are oriented at low angles to the rift axis, early strain localization occurs in narrow domains, which merge at later stages, resulting in continental break up by unzipping. Strong strain partitioning is observed when the linear heterogeneity is oriented at high angles with respect to the rift axis. In these experiments, early sub-parallel V-shaped basins propagate toward the pole of rotation until they are abandoned and strain is transferred entirely to structures developed in the vicinity of the strongly oblique weak lithosphere zone boundary. The experimental results are characterised in terms of their evolution, patterns of strain localization, and surface topography as a function of the lithospheric heterogeneity obliquity angle. Comparison of the experiments to ancient and modern examples in nature may help to elucidate the common but still poorly understood process of propagating rift-lithospheric heterogeneity interaction.

2.1 Introduction

The orientation of newly formed ocean basin systems often occurs at oblique angles to pre-existing continental lithospheric structures such as suture zones, thermal weaknesses, and steps in the base of the lithospheric and Moho. Consequently, ancient orogenic systems and associated boundaries are preserved within the continental lithosphere on opposite sides of oceans. In modern rift systems such as those developed in the East African Rift and the juvenile Red Sea ocean basin, the axis of extension is oriented along the Mozambique Ocean suture zone (Kazmin et al., 1978), oblique to ancient Neoproterozoic sutures (e.g., Dixon et al., 1987) and thermal anomalies associated with mantle convection (e.g., Chang et al., 2011). Consequently, early held views of the Wilson cycle where continental break-up follows former sutures (Wilson, 1966) are not always valid; other compositional and/or thermal weaknesses play an important role in the localization of strain and rifting (e.g., Brune, 2014; Corti et al., 2003; Huismans and Beaumont, 2014; Manatschal et al., 2015; van Wijk, 2005). Despite their importance for continental rifting and ocean initiation, how pre-existing structures or rheological heterogeneities influence the localization and partitioning of deformation during continental break up remains poorly understood.

The kinematic history of divergent tectonic boundaries is likely to be characterised by multiple phases of successive orthogonal, oblique and rotational relative motions (e.g., Bonini et al., 1997; Keep and McClay, 1997; Müller et al., 2016; Seton et al., 2012). When lithospheric extension is governed by a rotational component, rift propagation is driven by relative plate motion about a pole of rotation (Hey et al., 1980; Martin, 1984). Simple crustal scale analogue experiments of rotational extension with a homogeneous crust have shown a characteristic triangular fault pattern and rotated blocks comparable to features observed in the Afar triangle (Souriot and Brun, 1992). This paper builds on this research by using analogue experiments to explore how linear lithospheric scale weak zones interact with propagating rifts during rotational extension, and how this interaction influences deformation and surface topography along the rift axis. Examples of mantle heterogeneities that may be represented in the experiments include active mantle plumes or hot spots (e.g., Hill, 1991), mantle penetrating shear zones characterised by reduced grain size (Bercovici and Ricard, 2014; Heron et al., 2016), or inherited mechanical anisotropies with lattice preferred orientation of olivine crystals (Tommasi and Vauchez, 2001). Our experiments also assess the roles propagating rift and lithospheric heterogeneity interactions may have during the transition from continental break up to ocean initiation, the onset of mantle exhumation, and as precursors to transform faults and ridge jumps.

Rift propagation has been the focus of many studies (e.g., Courtillot, 1982; Hey, 1977; Hey et al., 2010; Mart and Dauteuil, 2000; Martin, 1984; Shih and Molnar, 1975), but few have adopted a quantitative approach to address how continental break up is affected by heterogeneities in the continental lithosphere under rotational boundary conditions (e.g., Courtillot, 1982; Martin, 1984). Previous analogue models of oblique rifting (e.g., Ding and Li, 2016; Mart and Dauteuil, 2000; Tron and Brun, 1991) and thermo-mechanical numerical experiments (Dunbar and Sawyer, 1996; Van Wijk and Blackman, 2005) successfully investigated the dynamics and mechanics of propagating rifts in three-dimensions under a constant extension direction. Earlier analogue models with an imposed rotational boundary condition focused on specific cases, including the sinistral rotation of the Danakil Block (Souriot and Brun, 1992), propagation of rifting from oceanic to continental lithosphere with application

to the Havre Trough (Benes and Scott, 1996), anticlockwise rollback of the subducting Pacific plate in the Kuril Basin (Schellart et al., 2003) and the opening of the South China Sea (Sun et al., 2009). In this study I report the first series of three-dimensional, isostatically supported, brittle-ductile multilayer analogue experiments of rotational rifting in order to explore the effect of linear heterogeneities on divergent tectonic boundaries with a rotational component. Specifically, I characterize in detail how deformation propagates and how surface topography evolves within the model lithosphere as a function of the orientation of linear weak zones.
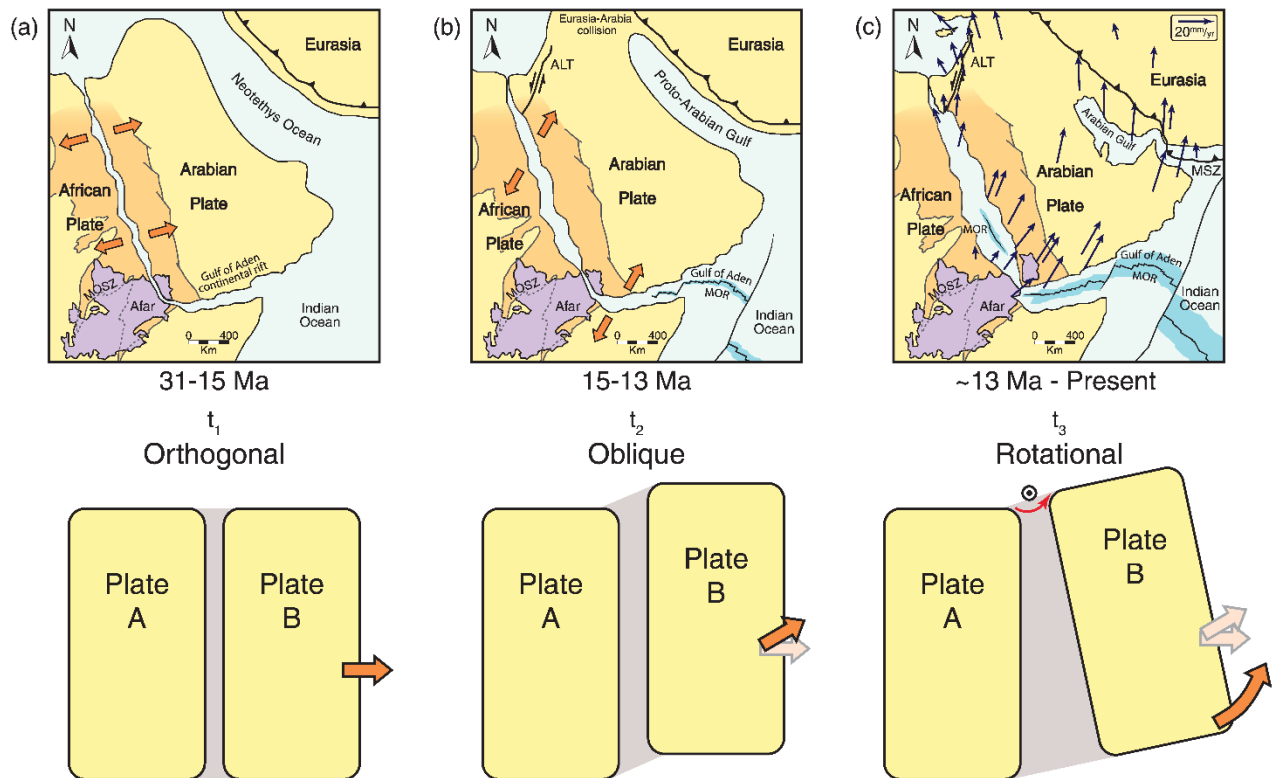
Figure 2.1 - **Cartoon reconstruction of the Red Sea – Gulf of Aden rift system Cenozoic evolution summarised in three stages, after Bosworth et al. (2005) A. Early Oligocene – Middle Miocene: Afar plume initiation and coeval opening of the Red Sea with extension direction normal to the rift axis (N60°E) driven by the closure of the Neotethys Ocean. Mozambique Ocean suture zone (MOSZ) mapped in orange after Kazmin et al. (1978) B. Middle Miocene – Late Miocene: collision of Arabia with Eurasia led to the formation of the Aqaba-Levant transform (ALT) boundary and the extension direction switched to highly oblique (N15°E) with respect to the Red Sea rift axis. Mid-ocean ridge (MOR) propagated west in the Gulf of Aden. C. Late Miocene – Present: continent-continent collision to the NW in contrast with the Makran subduction zone (MSZ) in the SE caused a slab pull gradient that resulted in a rotational anticlockwise motion of Arabia with respect to Eurasia. Sea-floor spreading in southern Red Sea initiated ~5 Ma. Dark blue arrows represent present-day GPS vectors for Arabia with respect to Eurasia (ArRajehi et al., 2010). Bottom cartoons illustrate a simplified analogous relative motion of plates. Our laboratory experiments aim to simulate similar boundary conditions to C.**

I compare our lithospheric-scale experimental results with natural examples from the Tyrrhenian Sea and the Red Sea – Gulf of Aden rift system, as it represents the best modern example of continental lithosphere that has undergone a transition from rifting to sea-floor spreading (Bosworth et al., 2005;

Almalki et al., 2015). Not only is the system underlain by a narrow zone of warm upper mantle related to the northward channelling of the Afar plume (Ritsema et al., 1999; Chang et al., 2011; Hansen and Nyblade, 2013), but it is also undergoing a strong rotational relative motion (ArRajehi et al., 2010; Bellahsen et al., 2003; Bosworth et al., 2005) (Fig. 2.1).

2.2 Experimental methods and materials

2.2.1 Experimental design

Our experiments focus on the kinematics and mechanics of rifting by attaching a model lithospheric plate to a moving wall pulled by a linear actuator (see Experimental Setup and Construction). In this way, I impose a rotational extensional boundary condition (Fig. 2.2a) that simulates progressive anticlockwise rotation similar to that of natural examples (e.g., Arabian Plate with respect to the African Plate over the last ~13 Ma; [ArRajehi et al., 2010; Bosworth et al., 2005]). Since our apparatus is isothermal, I simulate the presence of linear thermal anomalies by varying the viscosity of the model lithospheric mantle. Although weak zones may not be linear in nature, the model weak zone is analogous to a strain corridor or thermal anomaly with a roughly linear trend. Using this approach, rift-related deformation in the experiments propagates toward a fixed pole of rotation over time, and the propagation path and pattern of strain localization is influenced by the presence and orientation of a linear weakness zone in the mantle lithosphere (e.g., Agostini et al., 2009).
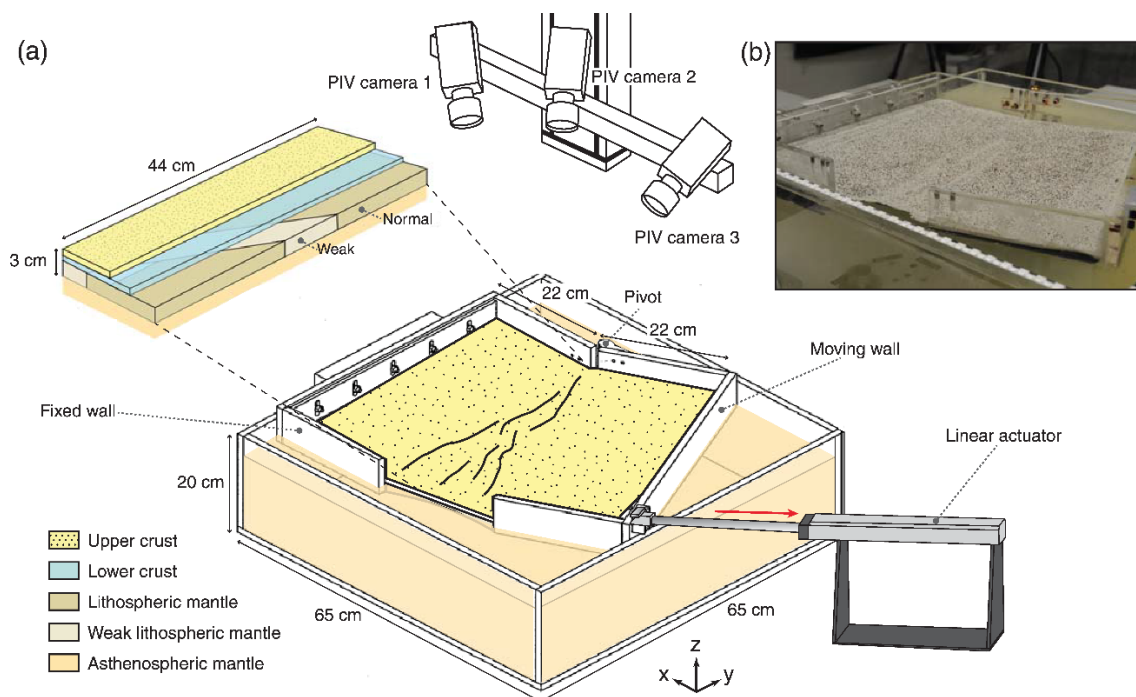
Figure 2.2 - **Experimental set up. A. 3D sketch of how the laboratory experiments were constructed. Particle-Imaging Velocimetry (PIV) cameras 1 and 3 were fixed in a stereoscopic set up to monitor deformation of the model surface. PIV camera 2 captured top-view images with oblique lightening to improve visualization of deformation patterns. B. Oblique view photo of the analogue model (Experiment 8 after 30% extension).**

All experiments described here consist of a 44 x 44 x 3 cm three-layer, brittle–ductile model lithospheric plate that floats isostatically on a fluid model asthenosphere contained within a 65 x 65 x 20 cm acrylic tank (Fig. 2.2). Below, I first describe the materials and scaling principles used for the experiments. I then provide details on the experimental apparatus and model construction, and finally discuss how deformation and surface topography are monitored during the experiments.

2.2.2 Materials and scaling

Lengths, time and forces are scaled down in analogue experiments in order to produce an appropriately sized model that behaves in a mechanically similar way to nature, over an appropriate period of time (Benes and Davy, 1996; Davy and Cobbold, 1991; Ramberg, 1967). The experiments reported here comprise a simplified 3-layer lithosphere with a brittle upper crust, a ductile lower crust and a ductile lithospheric mantle, overlying the model asthenosphere (Fig. 2.3a).

The length scale ratio, L^*, for all experiments was fixed by setting the model crustal thickness, $L_m = 14$ mm to represent a crustal thickness in nature $L_p = 35$ km, such that $L^* = L_m/L_p = 4 \times 10^{-7}$, where subscripts m and p refer to the model and natural prototype, respectively. This length scale ratio was suitable for the simulation of large areas on Earth (1100 km x 1100 km) undergoing rotational extension within the confines of our acrylic tank.

Polydimethylsiloxane (PDMS) was used to model the ductile lower crust (Fig 3). PDMS is an optically clear, high viscosity, high molecular weight silicone polymer frequently used in analogue modelling (e.g., Cruden et al., 2006; Marques et al., 2007; Pysklywec and Cruden, 2004). It has density $\rho_m \approx 970$ kg/m^3, which for a natural lower crust density of $\rho_p \approx 2760$ kg/m^3 sets a density scaling factor $\rho^* = \rho_m/\rho_p = 0.355$. PDMS and PDMS mixtures with granular materials have a slightly non-Newtonian rheology defined by the power law:

$$\sigma^n = \eta\dot{\varepsilon} \quad (2.1)$$

where σ is stress, $\dot{\varepsilon}$ is strain rate, η is viscosity and n is the power-law exponent of the material.

Our PDMS (Wacker Elastomer NA) is a Newtonian viscous fluid with a power-law exponent of n ~ 1 at our experimental strain rates (1 x 10^{-5} to 5 x 10^{-4} s^{-1}). This PDMS has a viscosity of $\eta_m \approx 4 \times 10^4$ Pa s and if I assume, for scaling purposes, a natural lower crust viscosity of $\eta_n \approx 2 \times 10^{21}$ Pa s, I set a viscosity scaling factor of $\eta^* = \eta_m/\eta_p = 2 \times 10^{-17}$. All experiments were carried out in the normal field of gravity (1 g), so the scale ratio for gravitational acceleration is $g^* = g_m/g_p = 1$. The time scaling factor for the experiments can then be defined as $t^* = \eta^* / \rho^* g^* L^* = t_m/t_p = 1.41 \times 10^{-10}$, meaning that 1 hour in the experiment corresponds to ~0.8 Ma in nature. The scaling parameters and experimental and natural material properties and dimensions are summarised in Table 2.1.
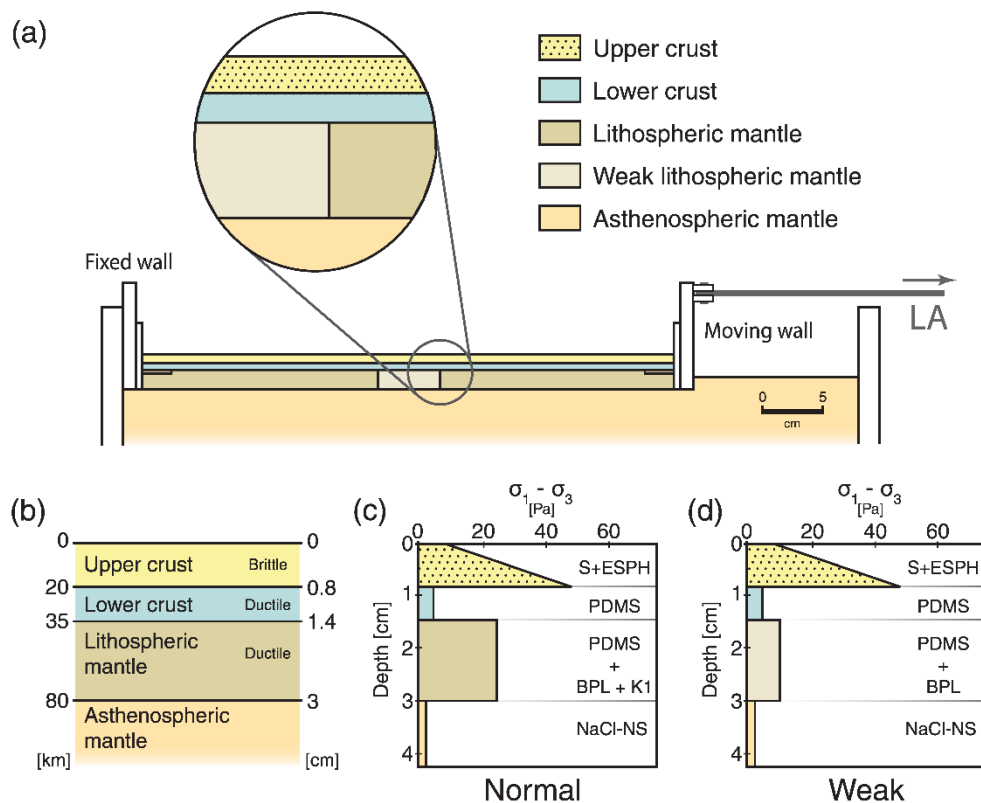
Figure 2.3 - Schematic illustration of the rheological layering of the analogue models and strength profiles of the normal and weak lithospheres. A. Cross section along the centre of the model showing how models are constructed, rheological layering and approximate location of the weak lithospheric mantle prior to deformation. B. Natural prototype and scaled down thicknesses for all models (See Table 2.1 for details). (c and d) Representative strength profiles of the model normal and weak lithospheres. Abbreviations: S – Fine quartz sand, ESPH - Envirospheres® hollow ceramic spheres, PDMS – Polydimethylsiloxane, BPL - Colorific® black plasticine, K1 - 3M® hollow glass microspheres, NaCl-N – Sodium chloride-Natrosol solution.

A solution of Natrosol® 250 HH and sodium chloride in deionised water was used to model the asthenospheric mantle (Boutelier et al., 2016) (Fig. 2.3). Natrosol® is a cellulose-based polymer designed to increase the viscosity of aqueous fluids without significantly affecting their density. As an aqueous solution, it behaves as a Newtonian viscous fluid under conditions typically employed in experimental tectonics (Boutelier et al., 2016).

Considering our scaling factors and the range of values that have been estimated for the viscosity of the asthenosphere in nature ($\sim 10^{19} - 10^{20}$ Pa s [Artyushkov, 1983]; $\sim 10^{19} - 10^{21}$ Pa s [Ranalli, 1995]), I varied the concentrations of Natrosol® 250 HH (e.g., Boutelier et al., 2016) and sodium chloride (e.g., Davaille, 1999; Davaille et al., 2002) to achieve appropriate values for our experiments. The final model asthenosphere has a viscosity of $\eta_m \approx 380$ Pa s, which represents $\eta_p \approx 1.9 \times 10^{19}$ in nature, and has a density of $\rho_m \approx 1100$ kg/m^3, equivalent to a natural asthenosphere density of $\rho_p \approx 3100$ kg/m^3 (e.g., Pysklywec and Cruden, 2004).

The model lithospheric mantle is composed of a mixture of black Colorific Plasticine®, 3M® hollow glass microspheres and PDMS (e.g., Cruden et al., 2006; Riller et al., 2012) (Fig. 2.3). Blending plasticine with PDMS increases the density and effective viscosity and adding microspheres decreases the density

while also increasing the effective viscosity of the mixture. I also varied the proportions of these components to achieve suitable upscaled values for the lithospheric mantle viscosity and density. A volume percentage mixture of 57% PDMS + 29% black Colorific Plasticene® + 14% 3M® hollow glass microspheres (class K-1) resulted in a model lithospheric mantle density of $\rho_m \approx 1080$ kg/m^3, which scales up to a natural lithospheric mantle density of $\rho_p \approx 3050$ kg/m^3. The rheological properties of the mixture were measured over the relevant experimental strain rate range (1 x 10^{-5} to 5 x 10^{-4}) using an Anton Paar Physica MCR-301 parallel plate rheometer. Results show that the PDMS-based lithospheric mantle analogue material is slightly non-Newtonian, with a power-law exponent n=1.25 and an effective viscosity of $\eta_m \approx 2$ x 10^5 Pa s, equivalent to $\eta_p \approx 1$ x 10^{22} Pa s in nature. This gives a viscosity ratio of ~520 with respect to the Natrosol-NaCl solution, falling in the upper limit for the range of natural viscosity contrasts between the lithospheric and sub-lithospheric mantle (~100-500 [Funiciello et al., 2008; Schellart, 2008; Wu et al., 2008]).

To model a weak lithospheric mantle I varied the proportions of PDMS and black Colorific Plasticene® to obtain a similar density to the surrounding normal lithospheric mantle but a smaller effective viscosity (Fig. 2.3). The weak lithospheric mantle analogue material comprising a volume percentage mixture of 81.5% PDMS + 18.5% black Colorific Plasticene® has a density of $\rho_m \approx 1075$ kg/m^3 and an effective viscosity of $\eta_m \approx 1$ x 10^5 Pa s, equivalent to $\eta_p \approx 5$ x 10^{21} Pa s (Table 2.1).

Table 2.1 - Scaling and Experimental Parameters for the Analogue Models

		Thickness		Density		Viscosity		
		Model (mm)	Nature (km)	Model (kg/m^3)	Nature (kg/m^3)	Model (Pa s)	Nature (Pa s)	Material
Normal Lithosphere								
Upper crust	Brittle	8	20	928	2600	-	-	S + ESPH
Lower crust	Ductile	6	15	982	2760	4×10^4	2×10^{21}	PDMS
Lithospheric mantle	Ductile	16	45	1090	3050	2×10^5	1×10^{22}	PDMS + BPL + K1
Weak Lithosphere								
Upper crust	Brittle	8	20	928	2600	-	-	S + ESPH
Lower crust	Ductile	6	15	982	2760	4×10^4	2×10^{21}	PDMS
Weak lithospheric mantle	Ductile	16	45	1075	3030	1×10^5	5×20^{21}	PDMS + BPL
Asthenosphere		-	-	1100	3100	380	1.9×10^{19}	NaCl-NS
Scaling factors: model/prototype		$L^* = 4 \times 10^{-7}$		$\rho^* = 0.355$		$\mu^* = 2 \times 10^{-17}$		
Time scaling factor		$t^* = \eta^*/(\rho^* \cdot g^* \cdot L^*)$		$t^* = 1.41 \times 10^{10}$		1 h in model ~ 0.8 Ma in nature		
Velocity scaling factor		$v^* = l^*/t^*$		$v^* = 2.84 \times 10^3$		6 mm/h in model ~ 20 mm/yr in nature		
Gravity scaling factor		$g^* = g_m/g_p = 1$						

[a]S = sand; ESPH = hollow ceramic spheres; PDMS = polydimethylsiloxane; BPL = black plasticine; K1 = hollow glass microspheres; NaCl-NS = sodium chloride + Natrosol solution. All layers have dimensions of 440 × 440 mm. Model asthenosphere area is 626 × 626 mm.

The brittle upper crust is modelled using granular materials (Fig. 2.3). To achieve a scaled natural upper crustal density of $\rho_p \approx 2650$ kg/m^3, I mixed quartz sand and hollow ceramic Envirospheres® with bulk densities of 1550 kg/m^3 and 390 kg/m^3, respectively, in the ratio 3.11:1 to obtain a scaled down model upper crustal density of 940 kg/m^3. The graded quartz sand has a homogeneous grain size distribution with 75% of the grains falling between 435 and 500 μm and the hollow ceramic Envirospheres® have a very homogenous grain size distribution, with 90% of the grains in the 100-150 μm range. Hubbert-type shear box tests for the mixture determined an internal friction angle φ < 38° and a cohesion value of ~ 9 Pa. The internal friction angle and the negligible cohesion of the mixture makes it an appropriate analogue to model brittle upper crust with a Mohr-Coulomb behaviour (e.g., Byerlee, 1978; Davy and Cobbold, 1991; Schellart, 2000).

2.2.3 Experimental setup and construction

All experiments start from the same initial state, in which the model lithosphere is attached to two U-shaped walls with internal dimensions of 44 x 44 x 3 cm. One wall is fixed to the side of the acrylic tank wall and the other is pulled by a linear actuator at a controlled divergence rate (Figs. 2.2a and 2.3). A pivot is fixed on one side of the U-shaped walls and the linear actuator rod pulls the moving wall from the opposite side in an anticlockwise fashion, creating a rotational extensional boundary condition (Fig. 2.2a). The opening of the U-shaped walls creates a free edge in which granular material from the upper crust collapses by gravity (Fig. 2.2b). This unwanted boundary condition of the experimental setup affects a small area that is outside the region of interest (i.e. the surface area selected for deformation monitoring processing) and is therefore not considered to be detrimental to the results. I use an 80:20 wt % paraffin oil in petrolatum jelly mixture (Duarte et al., 2014) as a lubricant between the model lateral boundaries and the confining U-shaped walls to minimize other boundary effects. The lateral side boundary effect caused by the grip between the model lithosphere and the side walls is therefore significantly reduced and is considered negligible for the experiment results.

The model mantle lithosphere and ductile crust layers are constructed to sit within the pair of U-shaped walls, to which they are attached on the sides perpendicular to the extension direction (Fig. 2.3a). The ductile layers are first made separately by allowing them to spread to the desired area and thickness within a rigid frame. Lithospheric mantle linear weak zones are prepared individually using the same technique and are incorporated into the normal lithospheric mantle layer by inserting them into a space created by cutting and removing material. This procedure is done ~48 hours before the experiment to allow the normal-weak combined lithospheric mantle material to settle within the rigid frame. Specially designed 4 cm wide horizontal grips are also incorporated along two sides of the lithospheric mantle layer, which is then placed on top of the model asthenospheric mantle, within the U-shaped walls (Figs. 2.2 and 2.3). The ductile crust layer is then placed on top and the model is left to sit to allow sufficient time to achieve isostatic equilibrium and for air bubbles to dissipate (~7 hours). The model upper crust layer is then deposited by sifting granular materials (See Materials and Scaling) from a height of ~15 cm. No manual off scraping is done to prevent alterations in the mechanical properties of the upper crustal layer due to unwanted compaction. Once all model lithosphere layers are in place and in isostatic equilibrium with the asthenosphere, the grips are fastened to the extension perpendicular sides of the U-shaped walls.

Linear weak zones are incorporated into the model lithospheric mantle with orientations defined by the angle, α, between the trend of the weakness and the orthogonal to the initial extension direction. All linear weak zones had constant width of 5 cm and α was varied in 15° increments from 0° to 60° (Fig. 2.4). The oblique linear zones were positioned in such way that they cross the centre of the model lithospheric plate in map view (defined by the intersection of the two diagonals of the square lithospheric plate; see Fig. 2.4). The final shape and location of the weak zone at the end of each experiment is inferred using control points. Granular material is removed using a vacuum cleaner and the ductile layers are then gradually removed by cutting them approximately perpendicular to the rift axis. After each section is removed the boundaries of the weak zone are observed in side view, marked on the surface and photographed from above. This is repeated 4 times and the final shape of the weak zone is deduced using 8 control points.
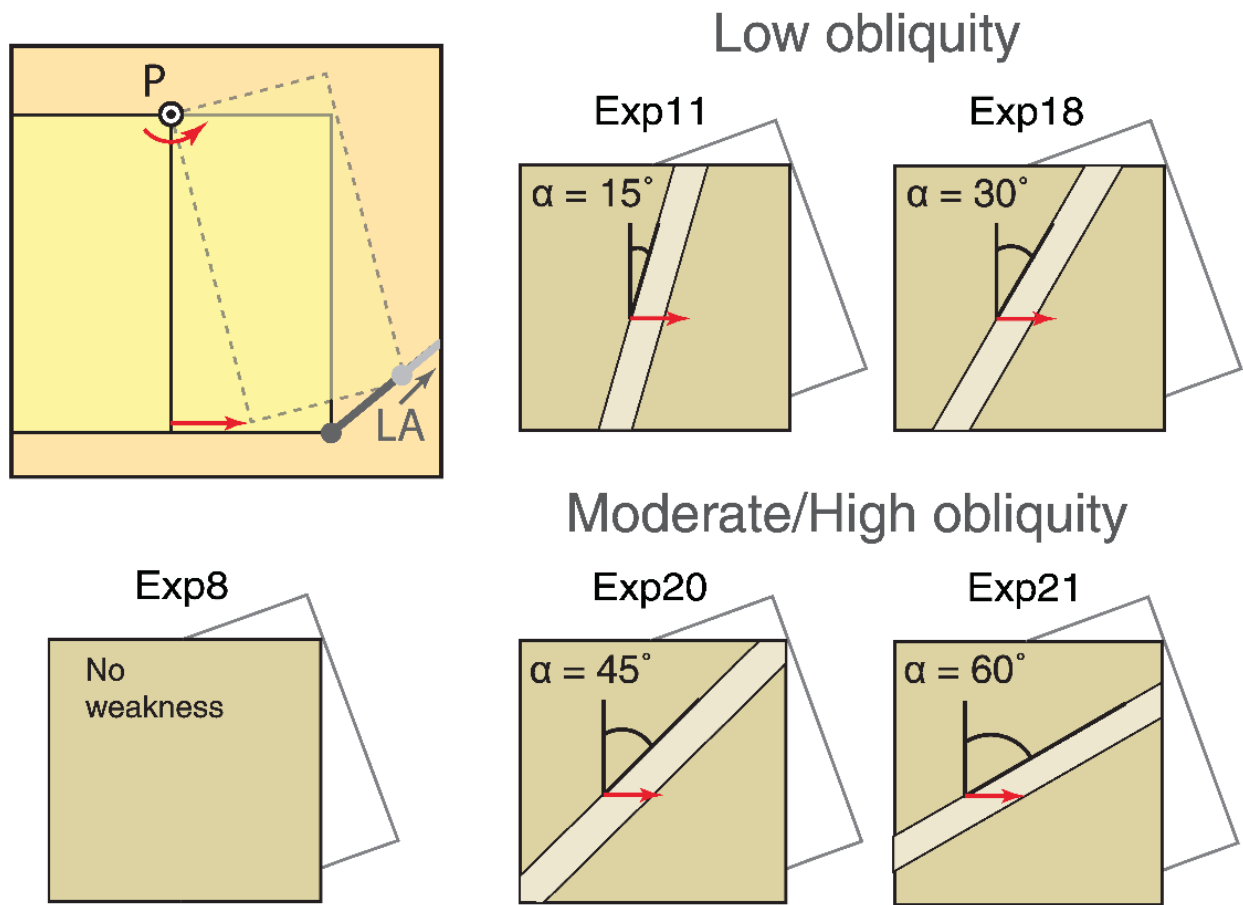
Figure 2.4 - Graphical summary of the boundary conditions for the laboratory experiments presented in this article. Top left: plan view sketch of the rotational boundary condition, imposed by fixing a pivot (P) at one side of a moveable U-shaped wall and pulling from the opposite side with a linear actuator (LA). Centre and right: lithospheric mantle linear weakness orientation (α) in plan view of the experiments discussed in this work.

2.2.4 Deformation monitoring and analysis

Stereoscopic particle image velocimetry (PIV) was used to monitor deformation of the model surface. The PIV system is equipped with three high-speed cameras that provide a spatial resolution of ≥0.1 mm and a temporal resolution of ≥0.1 s. Successive PIV images were taken at 2-minute intervals during each experimental run. Dark-coloured sand grains sifted on top of the model served as passive markers (Fig. 2.2b). Stereo cross-correlation (Adam et al., 2005) was used to obtain precise spatio-temporal measurements of incremental and cumulative deformation (e.g., Boutelier and Cruden, 2013; Riller et al., 2012; Schrank et al., 2008). Cumulative data is calculated as the sum of the incremental data. I computed high-resolution displacement fields, and based on the strain tensor,

$$E_{ij} = \frac{\partial v_i}{\partial_j} \text{ with } i \in \{x, y, z\} \text{ and } j \in \{x, y, z\} \quad (2.2)$$

I calculate the gradient in the vector component i along the j axis. In order to calculate total normal strain on the surface, instead of determining the horizontal normal strain along a single Cartesian coordinate direction (e.g., Boutelier and Cruden, 2013; Chen et al., 2016), I consider the 2D strain matrix

$$\begin{vmatrix} E_{xx} & E_{xy} \\ E_{yx} & E_{yy} \end{vmatrix} \qquad (2.3)$$

and define the normal strain, E_{surf}, on the surface as the largest eigenvalue of the matrix:

$$E_{surf} = \frac{(E_{xx} + E_{yy})}{2} + \sqrt{\left| \frac{(E_{xx} - E_{yy})^2}{4} + \frac{(E_{xy} - E_{yx})^2}{4} \right|} \qquad (2.4)$$

Detailed analysis of the models shows that the initial rupture of the model brittle crust occurs approximately when the incremental $E_{surf} > 1\%$ (e.g., Fig. 2.5a, 5% extension). I therefore define this value as a useful threshold to detect when a structure becomes active or inactive during the experiments, in order to track the migration of the rift tip. Digital elevation models (DEMs) created from the stereoscopic images are compared with top-view digital photographs taken with oblique lightening to improve visualization of fault segments.

2.3 Results

Fifteen experiments were carried out with initial conditions summarised in Table 2.2. Five experiments were repeated to test for reproducibility and resulted in similar first-order deformation patterns and evolution (see Movies 1 to 10 in the Extended Data). I focus on the results from five representative experiments (Fig. 2.4), which are subdivided into groups based on the obliquity angle of the linear zone of weakness, α, including one homogeneous reference experiment.

Table 2.2 - List of the Performed Analogue Experiments

Experiment	Weakness Obliquity Angle	Length Scaling Factor	Comment
3	No weakness	6.00E-07	First successful rotational experiment
5	No weakness		Failed due to initial setup
6	No weakness		Failed due to initial setup
8[a]	No weakness	4.00E-07	Similar evolution to Experiment 3
9	0°		Single propagating rift
10	−15°		Rift develops as compartments
11[a]	15°		Development of intrarift block
12	60°		Partitioned deformation
16	15°		15° repetition
17	30°		No development of intrarift block
18[a]	30°		30° repetition; development of intrarift block
19	45°		Partitioned deformation
20[a]	45°		45° repetition
21[a]	60°		60° repetition
22	No weakness		Similar evolution to Experiments 3 and 8

[a]Experiments discussed in this work.

As the apparatus is designed to impose rotational extension, I characterize the different rifting stages according to the maximum imposed percentage of stretching (i.e. displacement of the linear actuator), which occurs at the free side of the model, opposite the fixed pole of rotation (Figs. 2.2a and 2.3). For practical purposes, I define north as toward the pole of rotation, hence rift propagation takes place from south to north. The southern margin of the model is hereafter referred as the opening side.

Experimental results are presented in Figures 2.5 to 2.9 and are subdivided into three sections: structural evolution (Figs. 2.5a-2.9a), incremental strain (Figs. 2.5b-2.9b) and evolutionary topographic cross sections (Figs. 2.5c-2.9c). Structural evolution is presented in top view as line drawings of structures on colour digital-elevation models, together with the corresponding fault distribution for each stage illustrated as rose diagrams of fault azimuths. Incremental strain is also presented as top views as maps of incremental normal strain (E_{surf}) on the model surface draped over a shaded-relief DEM for each stage. The linear weakness boundaries, when present, are marked as dashed lines in all top view figures. I plot two profiles of the surface elevation and normal strain on the model surface (E_{surf}) for each stage, along sections indicated as dashed lines A and B in Figures 2.5b-2.9b. Incremental strain values that exceed the previously defined threshold ($E_{surf} > 1\%$) are indicated by orange shading to highlight areas where deformation is active at each stage.
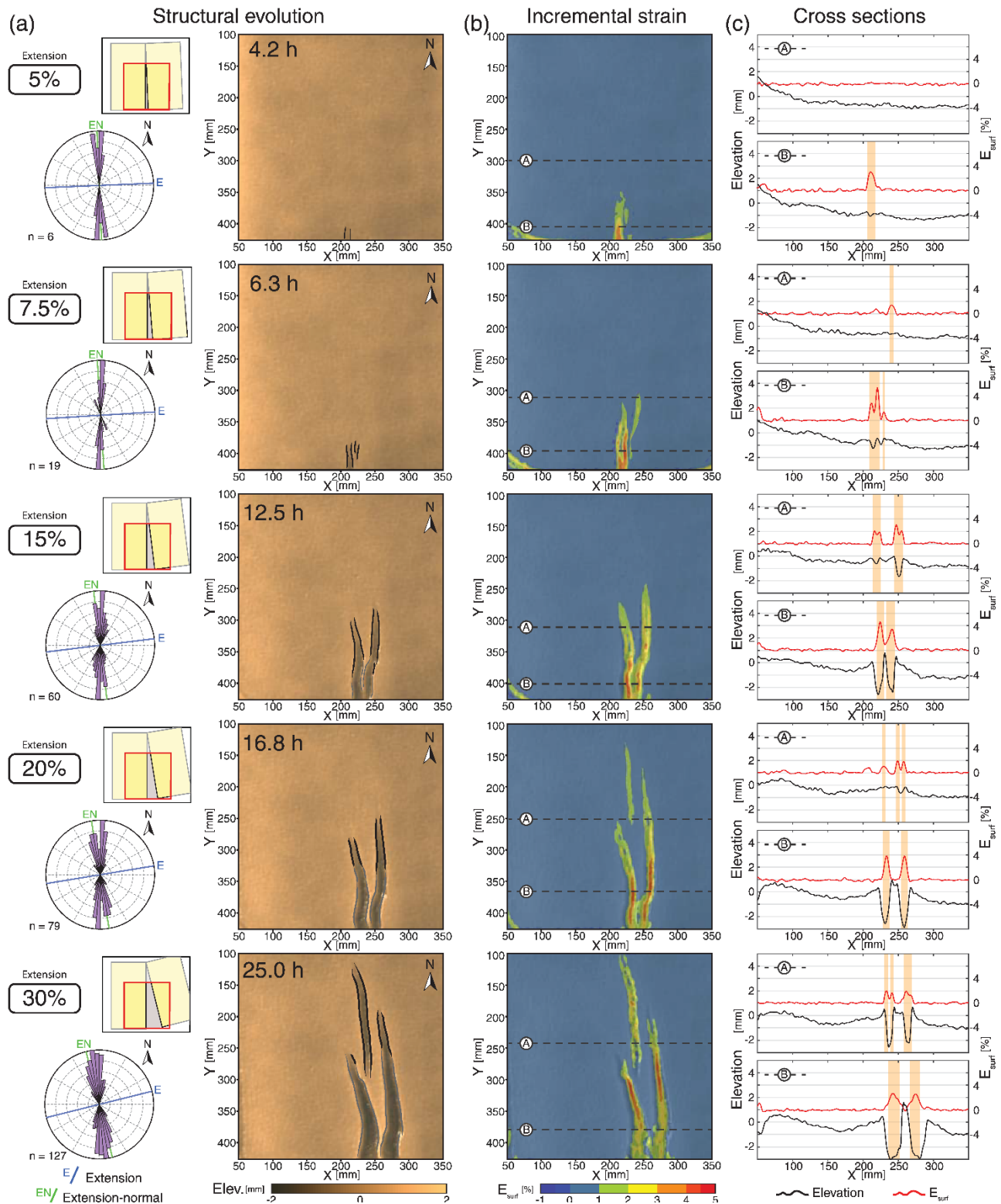
Figure 2.5 - Evolution of deformation for reference experiment 8 with homogeneous lithosphere (i.e. no lithospheric mantle weakness). A. Structural interpretation presented in top view DEMs. Black lines are active normal faults and grey lines are inactive normal faults at each stage. Rose diagrams at bottom left show normalised fault distribution with 36 bins (i.e. each bar represents a 5° azimuth range) weighted for the fault length. Coloured lines are the extension direction (E), extension-normal direction (EN) and the initial orientation of the linear weakness (W), when present. Schematic drawing in the top left illustrates the amount of rotation of the model in plan view. Red squares in small insets

indicate the area analysed. B. Maps of incremental normal strain on surface (E_{surf}) for each stage. Location of profiles A and B shown in panel C are indicated by black dotted lines. C. Surface elevation (black) and incremental normal strain on surface (red) profiles. Shaded areas indicate sections that are actively accommodating extension at each stage (i.e. $E_{surf} > 1$ %, see text for details). For detailed model evolution, see Extended Data Movie 1.

2.3.1 Reference experiment – Homogeneous lithosphere (Experiment 8)

Early stages

After 5% extension, short, normal faults formed perpendicular to the extension direction as strain localised at the south central end of model (Fig. 2.5a, b: 5% extension). During this stage, extension was accommodated on these major boundary faults as they propagated northward. At 7.5% extension, incremental strain measurements show the initiation of a second, subparallel rift segment that propagated toward the pole of rotation (Fig. 2.5b: 7.5% extension). Increasing stretching activated linear normal linear faults that bound both segments and led to the development of two V-shaped graben with northward propagating tips. Although the eastern graben developed later, its propagation was faster than the western graben (cf. Fig. 2.5a, b: 7.5-15% extension). Cross sections of surface elevation and incremental strain in the southern half of the model at 15% extension (Fig. 2.5c) indicate that the two rift depressions have similar geometry in the southern end, with the western graben recording higher incremental strain. However, toward the centre of the model the eastern graben accommodates more extension and is bound by faults with greater throws compared to the western graben. Orientation analysis indicates that the boundary faults of the V-shaped basins strike approximately perpendicular to the stretching direction as they propagate (Fig. 2.5a).

Advanced stages

The main boundary faults opposite the pole of rotation were active until ~15% extension, when strain gradually localised in the floors of the southern parts of the two early-formed rift depressions as they became wider (Fig. 2.5a, b: 15-20% extension). With increasing extension, the bounding faults of the two graben structures propagated northward and the separation between the rift segments increased. Northward propagation of the western graben terminated when it reached the centre of the model after ~20% extension (Fig. 2.5a, b). Subsequent extensional deformation in the model was transferred to the eastern graben and to a newly formed central graben located between the eastern and western graben (Fig. 2.5a, b: 20-30% extension). As extension continued, the rift-subparallel bounding faults of the central graben propagated to the north and south. Ongoing deformation was entirely accommodated by the central graben as it propagated toward the pole of rotation. At very advanced stages (>30% extension) the main rift boundary faults in the southern-half of the model became inactive as strain became localised in the rift depressions (Fig. 2.5b, c: 30% extension). These areas of lithospheric thinning also became wider to the south. This trend continued until maximum extension of the experiment was reached (~45%), at which point no further evidence of fault nucleation between rift zone compartments was observed.
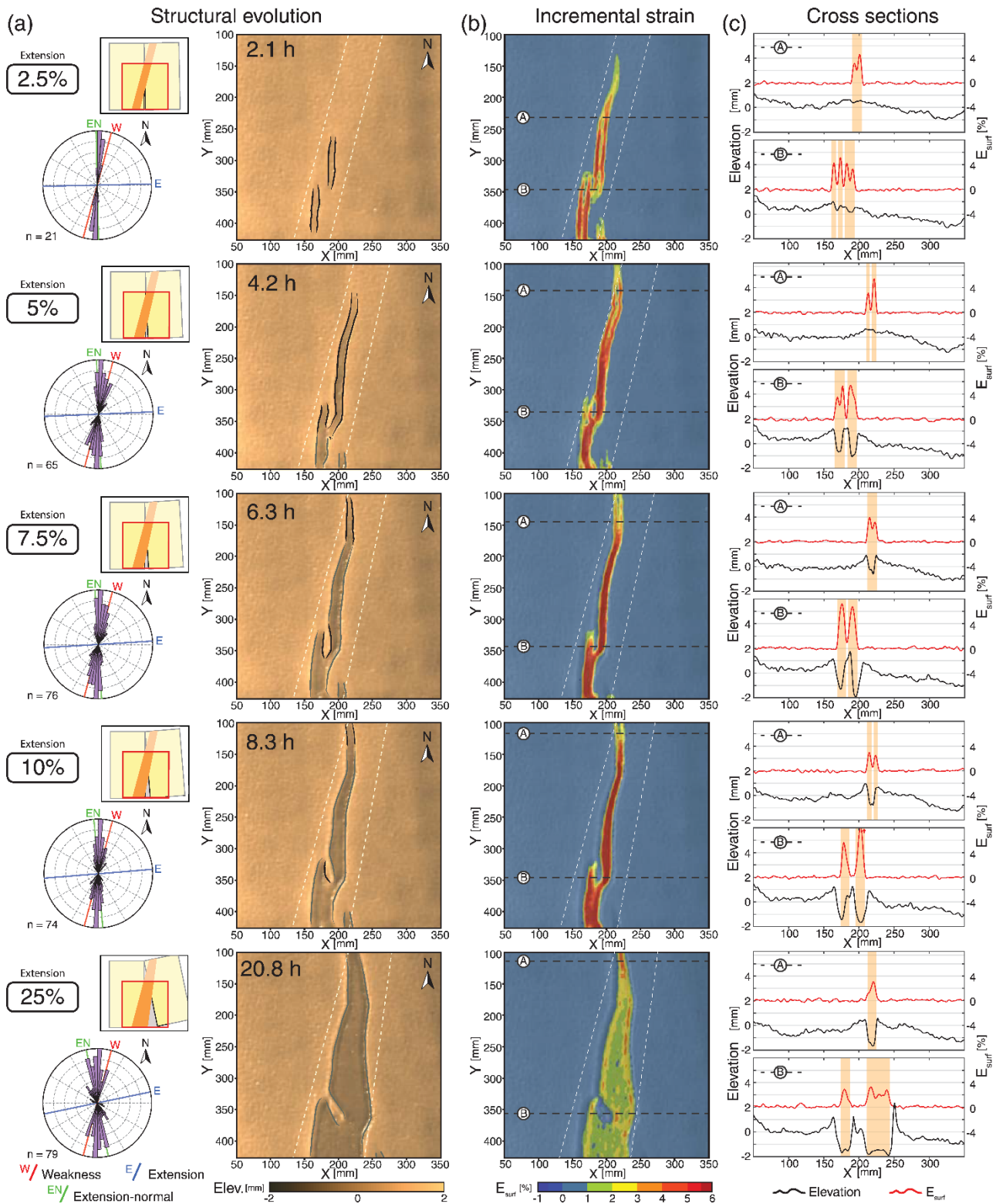
Figure 2.6 - Evolution of deformation with a low obliquity (α = 15°) linear weakness zone (Exp. 11), illustrated as in figure 2.5. A. Schematic drawing in the top left illustrates the amount of rotation of the model and approximate location of the lithospheric mantle linear weakness. Red squares in small insets indicate area analysed. Boundaries of the linear weakness are shown as white dotted lines in panels A and B. For detailed model evolution, see Extended Data Movie 2.
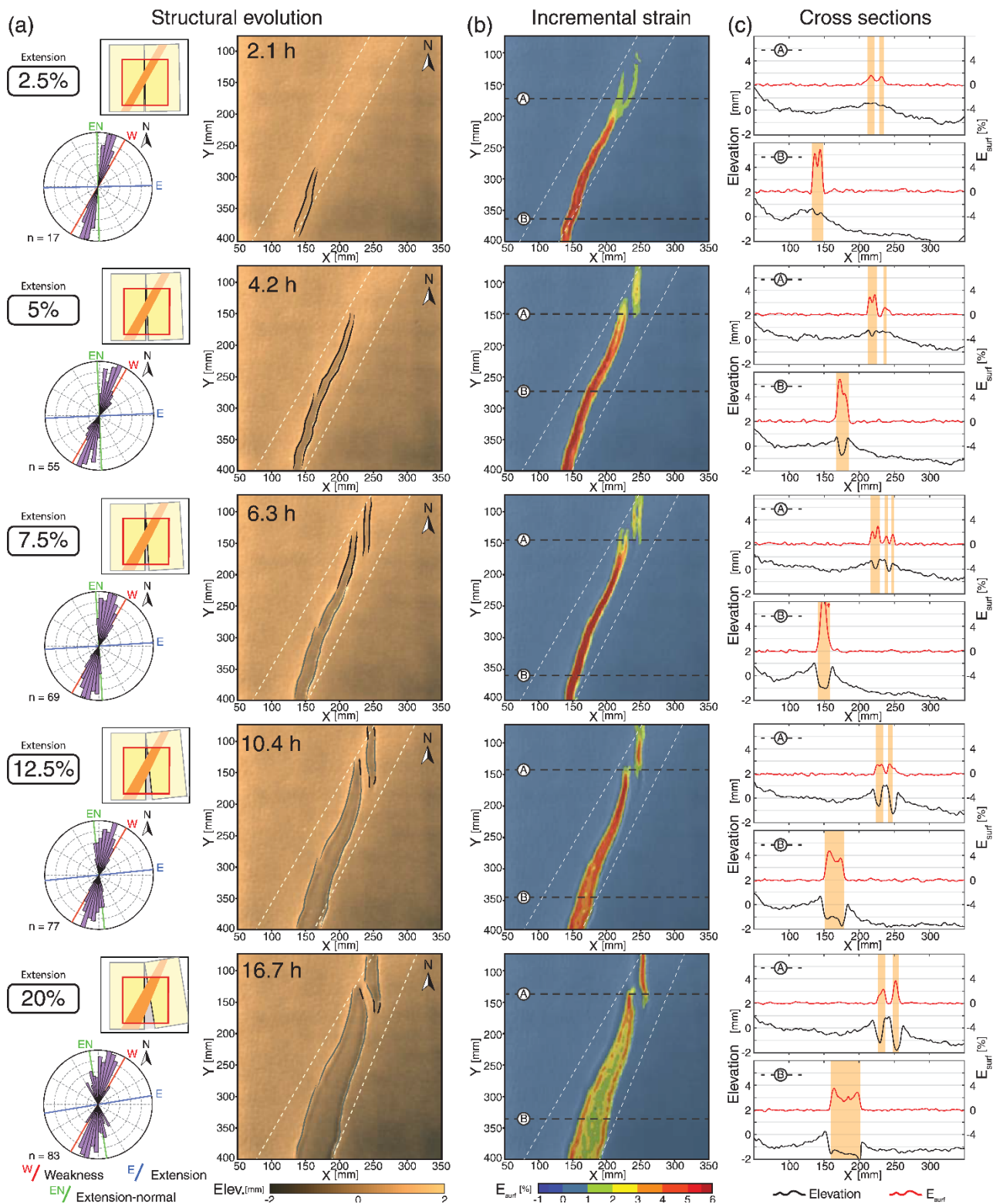
Figure 2.7 - Evolution of deformation with a low obliquity ($\alpha = 30°$) linear weakness zone (Exp. 18), illustrated as in figures 2.5 and 2.6. A. Schematic drawing in the top left illustrates the amount of rotation of the model and approximate location of the lithospheric mantle linear weakness. Red squares in small insets indicate area analysed. Boundaries of the linear weakness are shown as white dotted lines in panels A and B. For detailed model evolution, see Extended Data Movie 3.
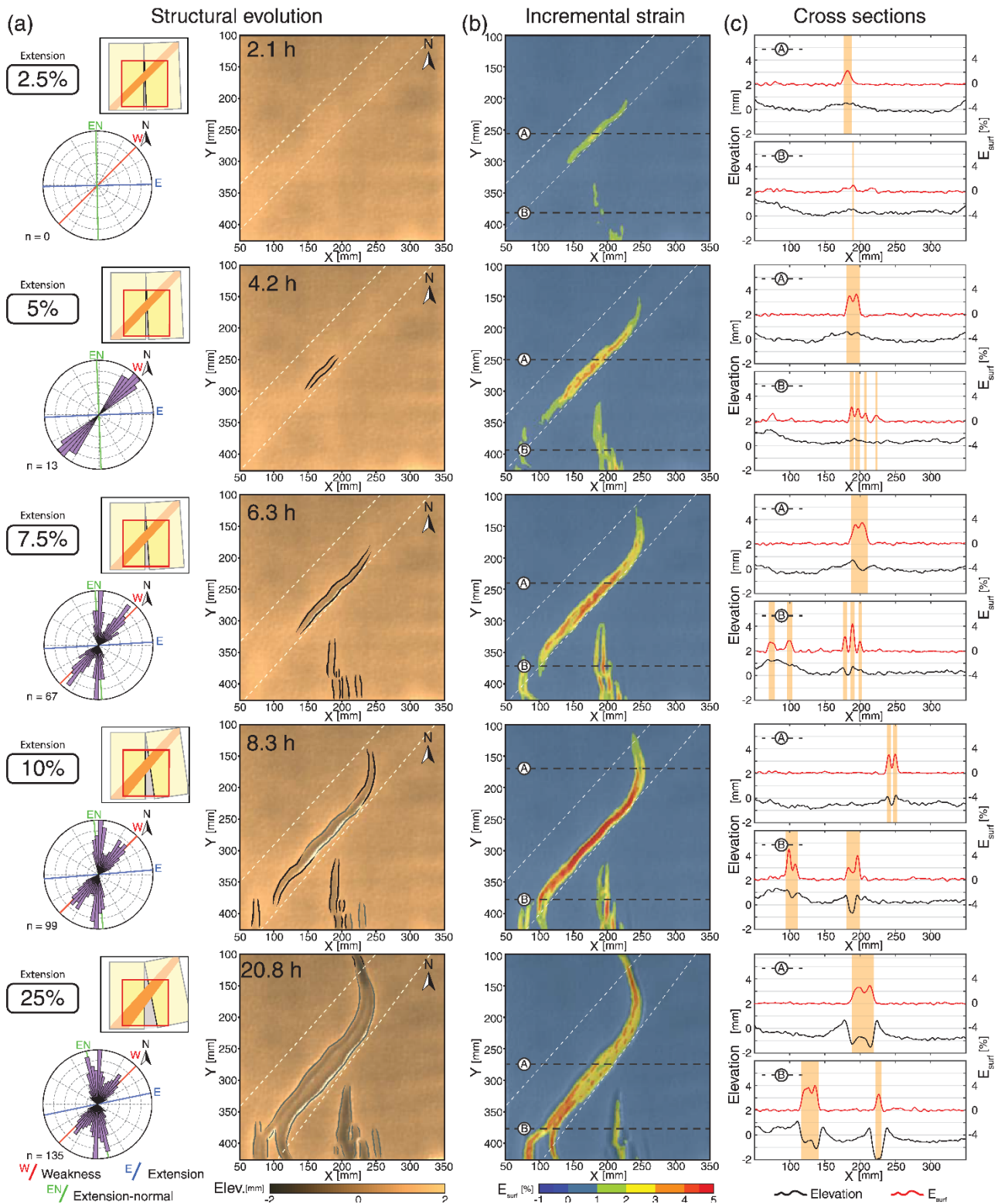
Figure 2.8 - Evolution of deformation with a moderate obliquity ($\alpha = 45°$) linear weakness zone (Exp. 20), illustrated as in figures 2.5 and 2.6. A. Schematic drawing in the top left illustrates the amount of rotation of the model and approximate location of the lithospheric mantle linear weakness. Red squares in small insets indicate area analysed. Boundaries of the linear weakness are shown as white dotted lines in panels A and B. For detailed model evolution, see Extended Data Movie 4.
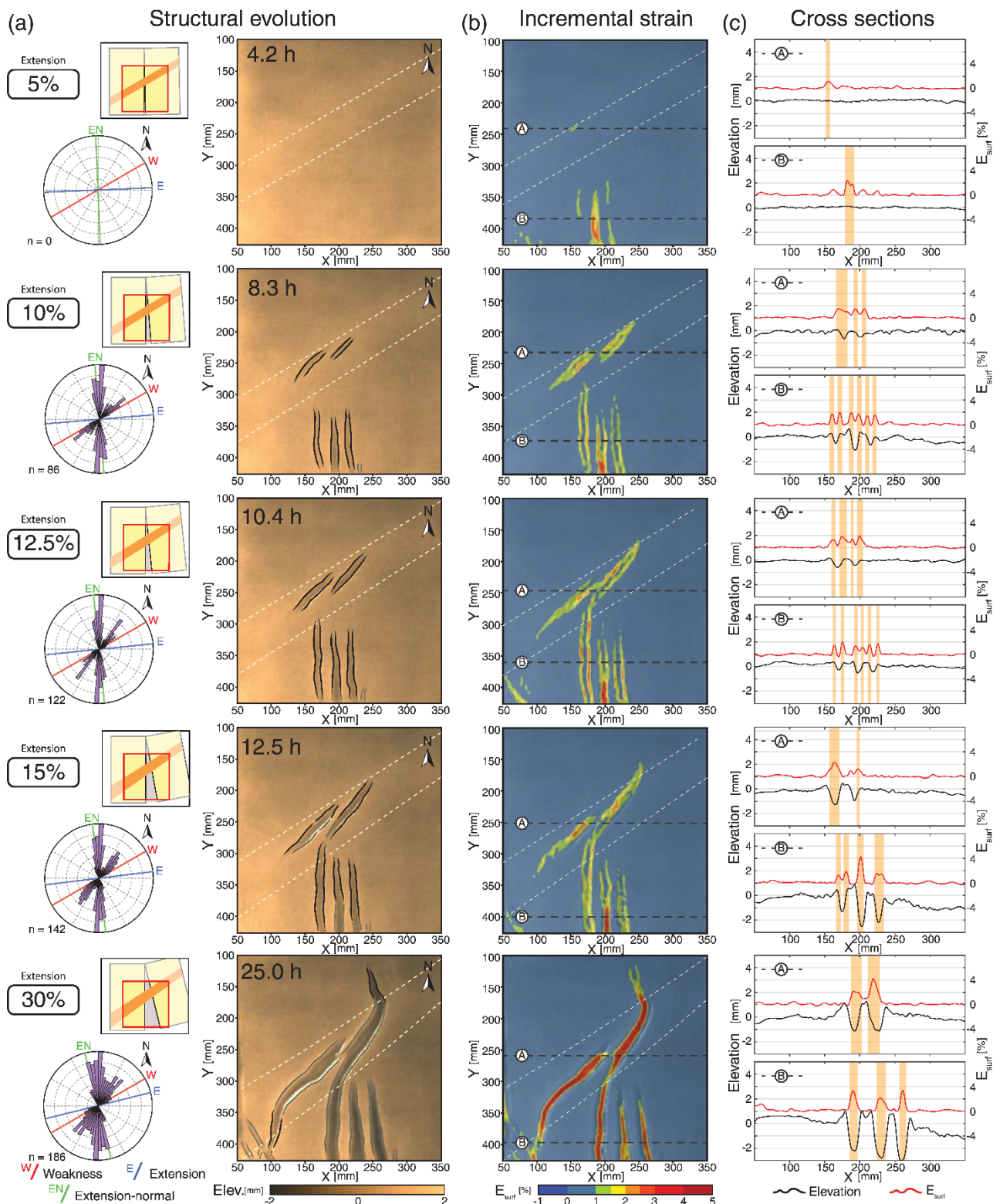
Figure 2.9 - Evolution of deformation with a high obliquity (α = 60°) linear weakness zone (Exp. 21), illustrated as in figures 2.5 and 2.6. A. Schematic drawing in the top left illustrates the amount of rotation of the model and approximate location of the lithospheric mantle linear weakness. Red squares in small insets indicate area analysed. Boundaries of the linear weakness are shown as white dotted lines in panels A and B. For detailed model evolution, see Extended Data Movie 5.

2.3.2 Low obliquity weakness zone (Experiments 11 and 18)

2.3.2.1 Experiment 11

Early stages

Experiments with a low obliquity ($\alpha = 15°$) linear weakness zone are characterised by early development (2.5% extension) of two north-south oriented rift segments, delineated by linear normal faults that strike at intermediate angles between the trend of the linear weakness zone and the direction perpendicular to the initial extension direction (Fig. 2.6a: 2.5% extension). Elongated domains of incremental strain illustrate how these normal faults formed approximately in the centre of the linear weakness zone and delimited a southwest and a central graben (Fig. 2.6a, b: 2.5% extension). Extension was progressively accommodated by these structures as their throw increased and as they propagated both north and south. After 5% extension the northern tip of the southwest graben reached its maximum propagation point (Fig. 2.6a). Comparison between incremental strain measurements at 2.5% and 5% extension show that the two en-echelon oriented rift segments within the weak zone propagate sideways and start to overlap (Fig. 2.6a: 5% extension). The deflection in the strike of the faults as they overlap is probably due to rift interaction, which is a consequence of the close proximity of the two rift segments (compare Zwaan et al., 2016). With further extension, the main boundary faults in the centre of the model propagated northward with an orientation that gradually became aligned with the trend of the weakness zone (Fig. 2.6a, b). By 7.5% extension, surface elevation and strain profiles (Fig. 2.6c: 7.5% extension) indicate that the only active fault segments at 7.5% extension were those formed due to this northward migration of the central V-shaped basin. At this stage strain progressively localised in the narrow rift depressions to the south of the model.

Advanced stages

The activity of the boundary faults diminished with progressive deformation, showing no substantial variations in vertical throw after 7.5% extension (Fig. 2.6c). At this stage, strain became highly localised in the centre of the rift depression and extension was consequently accommodated by lower crustal and lithospheric mantle stretching within the linear weakness zone. This resulted in a different amount of thinning between the normal and weak lithosphere. The boundary faults were oriented perpendicular to the direction of extension as they grew toward the model pivot point (proxy for pole of rotation). Observations on the overall evolution of deformation show that strain is focused in the linear weakness zone for the majority of the experiment. No substantial change in deformation style was observed with progressive stretching after 10% extension. However, a rotating intra-rift block developed with increasing extension (Fig. 2.6a: 10-25% extension). The rift segments that nucleated at early stages (<5% extension) delimit a horst that rotated anticlockwise about an independent pole of rotation located on the west margin of the rift. The final stages of the experiment show a wide distribution of strain in the thinned-lithosphere of the rift floors, and their margins are characterised by progressive upward flexure due to local isostasy associated with the rift flanks (Fig. 2.6b, c). Extensional structures only developed outside the weak zone at late stages and resulted in the anastomosing geometry of the main rift boundary faults (see Extended Data Movie 2).

2.3.2.2 Experiment 18

Experiment 18 (α = 30°) developed a very similar deformation evolution to Experiment 11 in terms of compartmentalization and strain partitioning, with slight differences in the timing (i.e. percent of extension) at which each step in the evolution took place. Comparison between Experiment 11 (α = 15°) and Experiment 18 (α = 30°) shows that the southernmost end of the weak zone is closer to the point of maximum extension in experiments with a lower obliquity linear weakness (Fig. 2.4). This results in an earlier widening of the weak zone and causes deformation to stay localised within it (cf. Figs. 2.6 and 2.7). In Experiment 18, an elongated rift segment that formed subparallel to the linear weak zone accommodated most of the extension at early stages (Fig. 2.7a, b: 2.5-5% extension). Strain localised along the linear weakness zone and progressive deformation led to the development of a second, north-south oriented graben. This resulted in the formation of an intra-rift block in the northern part of the model (Fig. 2.7a, c: 7.5% extension). The main difference between Experiments 11 and 18 was in the location of the anticlockwise rotating intra-rift block, which formed closer to the pole of rotation in Experiment 18. The geometry of a 30° oriented weakness zone results in a greater distance along the centre of the model between the opening side of the model and the linear weak zone boundary. The southernmost section of the weak zone in Experiment 18 is farther away from the point of maximum extension than in Experiment 11 (Fig. 2.4). As a result, strain partitioning and compartmentalization occurred at later stages and closer to the pole of rotation (Fig. 2.7a: 12.5-20% extension), indicating that the position of the weak zone influences the resulting structural pattern in addition to the angle of obliquity. The higher rotation rate of the intra-rift block in Experiment 18 is due to its proximity to the model pivot point.

2.3.3 Moderate obliquity weakness zone (Experiment 20)

Early stages

Incremental strain measurements at early stages of the α = 45° experiment (Fig. 2.8b: 2.5% extension) show two domains of incipient rift formation and propagation. Deformation was localised along the south eastern margin of the linear weak zone during this stage, as illustrated by the 45° striking oriented domain of incremental strain in the centre of the model (Fig. 2.8a, b). Minor domains oriented perpendicular to the extension direction accommodated deformation in the southern part of the model. As extension increased, the central rift zone propagated toward both the southwest and northeast, parallel to the linear weak zone, along which normal faults initiated after 5% extension, accommodating most of the deformation (Fig. 2.8a, b). At this stage, the extension-perpendicular domains of incremental strain increased steadily, but no rupture of the brittle upper crust was observed in the southern end of the model until 7.5% extension, when ongoing deformation in the area resulted in the development of a series of short, displacement-perpendicular rift segments (Fig. 2.8a). The activity of the boundary faults associated with these rift segments is greatest between ~7.5% and ~12.5% extension. The normal faults of the central graben also propagated in both directions during this stage and the tips of the central rift began to rotate progressively into alignment with the extension-perpendicular direction (Fig. 2.8a, b: 7.5-10% extension), producing a sigmoidal rift segment that remained within the weak zone until advanced stages of the experiment.

Advanced stages

After 10% extension, strain continued to be largely accommodated by the central rift segment, with increased vertical throw on its boundary faults and subsequent deepening of the rift floor (Fig. 2.8a, b). However, the activity of the delineated normal faults decreased after ~15% extension. This resulted in the progressive localization of strain toward the rift depression, resulting in differential thinning of the lithosphere. The earlier formed north-south graben structures in the south were aborted as extension continued, suggesting that deformation was entirely transferred to the boundary of the linear weak zone (Fig. 2.8b: 25% extension). No new rift segments were created between 25% and the maximum extension (~45%). Upward flexure of the thinned lithosphere was observed at late stages, as in the low obliquity experiments.

2.3.4 High obliquity linear weakness (Experiment 21)

The experiment with a highly oblique linear weakness zone ($\alpha = 60°$) showed similar behaviour to the moderate obliquity experiment ($\alpha = 45°$). Two domains of rift formation were also observed in the model, with some variations in the timing of the development of rift-related faults. The most relevant differences are described below.

Early stages

Deformation was initially localised parallel to the northern boundary of the weak zone (Fig. 2.9b, c: 5% extension) and in several sub-parallel rift segments that developed perpendicular to the extension direction in the southern part of the model, which then propagated with increasing stretching toward the pole of rotation (Fig. 2.9a, b: 5-10% extension). At 10% extension, the weak zone in the centre of the model is associated with the development of two deformation compartments with orientations that are intermediate between the trend of the discontinuity and the extension-perpendicular direction (Fig. 2.9a: 10-12.5% extension). Comparison with Experiment 20 ($\alpha = 45°$) shows that these rift segments formed in the centre of the model but are shorter in length in Experiment 21. However, the overall sigmoidal shape of the rift is maintained at advanced stages (cf. Figs. 2.8 and 2.9). These central structures propagated both southwest and northeast after 10% extension and, together with the displacement-perpendicular segments in the south, actively accommodate deformation until ~15% extension (Fig. 2.9a, b).

Advanced stages

After 15% extension, the propagation rate of the V-shaped basins in the southern part of the model diminished and deformation was progressively transferred to the central oblique graben structures (Fig. 2.9a, b). The length of the normal faults that delimit these graben increased steadily and their orientation gradually changed. As in the moderate obliquity experiments, these boundary faults eventually became aligned with the displacement-perpendicular direction (Fig. 2.9a, b: 15-30% extension). With ongoing deformation, the easternmost central graben merged with the main V-shaped basin as they propagated in opposite directions (Fig. 2.9a: 30% extension). The number of rift

segments stabilised during the advanced stages (+30% extension) when basin widening and strain localization in rift interiors was observed.

2.4 Synthesis and discussion

The experimental results described above demonstrate that the structural evolution and partitioning of strain in extending continental lithosphere is strongly influenced by the presence of linear rheological discontinuities. Since the external boundary conditions in each experiment were the same I can compare the different model results to gain insights on how the orientation of linear lithospheric weaknesses influences rift propagation. Figure 2.10 compares cumulative strain over time in the experiments as a function of linear weak zone orientation. It is observed that the presence of a linear zone of weakness in the lithosphere has a profound effect on the resultant architecture and strongly controls strain partitioning in propagating rifts. The strength of the normal lithospheric mantle in our models is approximately two times greater than that of the weak lithospheric mantle (Fig. 2.3 and Table 2.1), suggesting that even a relatively small difference (i.e. values within the same order of magnitude) in the strength of the layers will induce strong strain partitioning as observed in the experiments. When present, the boundary of the weak zone always localised deformation at some stage during the experiments. Previous analogue experiments with different experimental setups have also studied the effect of mechanical discontinuities during oblique rifting (Tron and Brun, 1991) and in rift basins with a rotational component (Philippon et al., 2014). Consistent with our results, these studies have similarly concluded that the resulting structural pattern can only be explained by considering the presence of inherited structures or rheological heterogeneities in addition to the geodynamic setting.

In terms of deformation evolution, I define three end-members: homogeneous lithosphere, low obliquity and moderate/high obliquity linear weaknesses. The key differences and observations between the experiments, broken down by these three categories, are summarised in Figure 2.11.

The change in the extension direction over time strongly controls the evolution of deformation and needs to be investigated jointly with the presence of a weak zone to understand how rifts propagate. Previous analogue modelling with a comparable linear weak lithospheric mantle (e.g., Agostini et al., 2009; Autin et al., 2010; Corti, 2008) but with a translational rather than a rotational boundary condition provided detailed analysis of fault patterns but did not characterize how faults propagate along the rift axis over time at large scales.
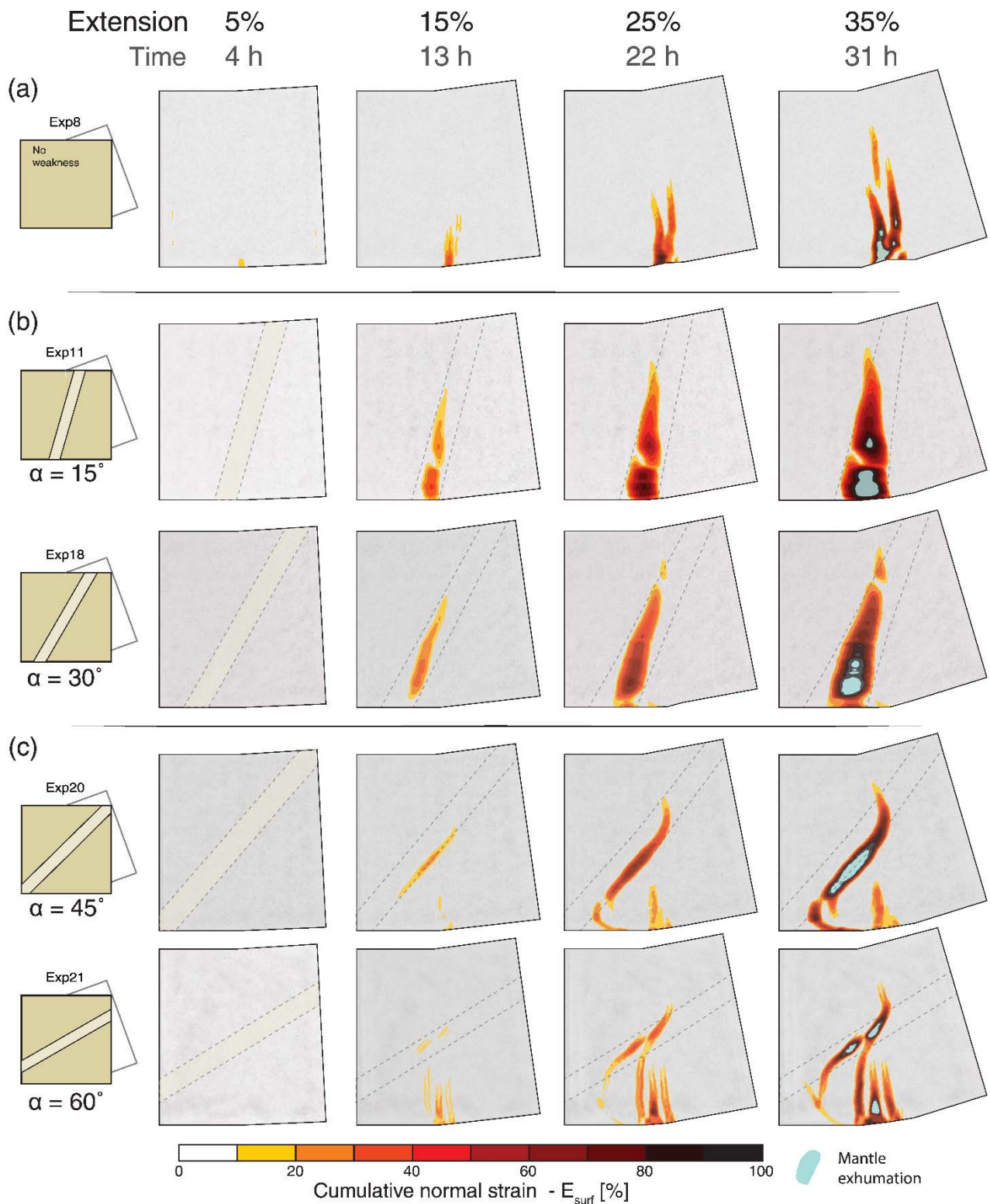
Figure 2.10 - Cumulative strain maps for each experiment after 5%, 15%, 25% and 35% extension. Strain values are normalised such that the maximum reached strain in each experiment is 100%. Three end-members are defined based on the overall deformation evolution of the models: A. homogeneous lithosphere, B. low obliquity and C. moderate/high obliquity. Colour scale indicates cumulative normal strain on surface (E_{surf}). For cumulative strain evolution, see Extended Data Movies 1-5.

In the reference experiment (Experiment 8, no weakness), extension was progressively accommodated in narrow segments as deformation propagated toward the pole of rotation while ongoing rotation resulted in highly extended areas at the opening side of the model, where early rupture and mantle exhumation occurred. However, when a lithospheric mantle weakness was present, the overall evolution of deformation became more complex and crustal stretching did not necessarily increase with progressive propagation of a rift. This is in agreement with Martin (1984) who proposed that continents should react differently in the rifting process when rifts cross older geotectonic features.
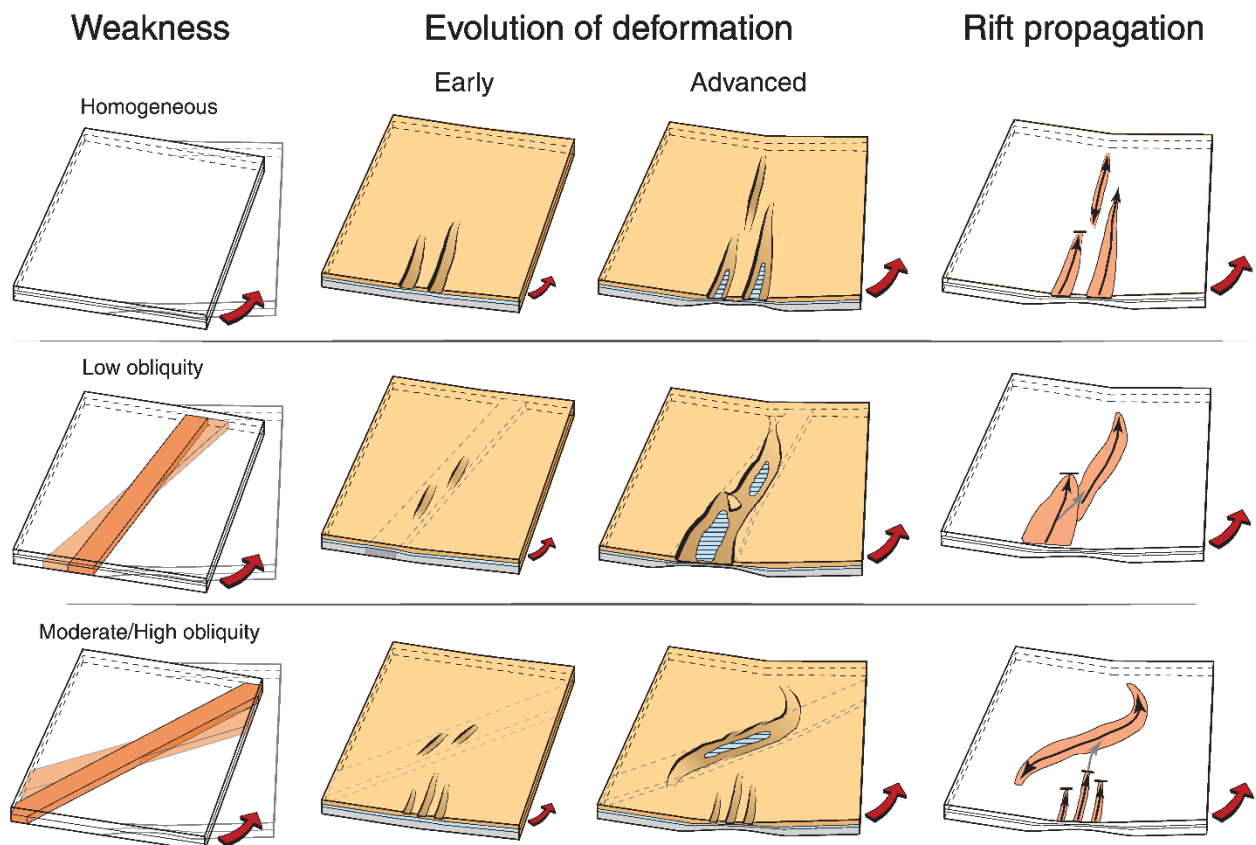
Figure 2.11 - **Summary of experimental findings in terms of evolution of deformation and rift propagation as a function of linear weakness obliquity.**

A homogeneous model lithosphere (i.e. no lithospheric mantle weakness) accommodated extension by forming V-shaped extensional basins with tips that propagated at constant rates toward the pole of rotation. Boundary faults delimiting these V-shaped basins that formed at early stages were progressively aborted and strain subsequently localised closer to the moving U-shaped wall and toward the pole of rotation. Normal faults that formed in the centre of the model propagated both toward and away from the pole of rotation. Although the asymmetric setup of the apparatus may tend to favour eastward migration of active structures, the final structural pattern of the homogeneous model lithosphere experiment is essentially symmetric. Therefore, I consider this model limitation to have a second-order influence on the experimental outcomes, and that our setup is an effective means to simulate rift propagation toward a pole of rotation. Furthermore, having a fixed plate and a moving plate is analogous to the natural cases discussed below (See Comparison with natural examples).

Models with low obliquity lithospheric weaknesses localised deformation more effectively along the rift axis (i.e. perpendicular to the extension direction) in comparison to the homogeneous and moderate/high obliquity models. Extension was accommodated in short, narrow domains at early stages by bounding faults with trends that are in between those of the linear weakness zone and the extension direction. This is consistent with observations based on strain and stress field analysis in natural examples of slow spreading ridges (e.g., Fournier et al., 2004; Fournier and Petit, 2007). The bounding faults nucleated and propagated at regular rates until strain was transferred to rift depressions. This consequently produced areas of hyper-extended lithosphere and, as a result, these experiments developed considerably wider rifts and showed larger isostatic adjustments during deformation. The rotational boundary condition prevented the nucleation of early rift compartments over time and promoted the formation of an independently rotating intra-rift segment. The location of this segment will depend not only on the orientation of the linear weakness zone and the geometry of the model, but also on the position of the oblique weak zone within the system. In the experiments presented here the linear weak zone always crosses the central point of the model lithosphere. Thus, when the linear weak zone is highly oblique, the southernmost point of the weak layer is farther away from the point of maximum extension (i.e. at the opening side and opposite the fixed pole of rotation). In comparison to low obliquity cases, this will favour considerably more strain partitioning between structures in the southern end of the model compared to those proximal to the weak zone.

Partitioning of deformation in moderate/high obliquity weakness experiments was more complex. Extension was initially accommodated by two different features. As in the homogeneous reference lithosphere model, sub-parallel V-shaped basins propagated toward the pole of rotation, while extension in the model centre was accommodated by weakness zone sub-parallel graben structures. Progressive stretching led to the abandonment of the early V-shaped basins and transfer of strain to structures developed in the vicinity of the weak lithosphere zone boundary. However, structures in high obliquity models would be different if the weak zone was placed closer to the opening side of the model. The relative position of the weak layer with respect to the point of maximum extension also plays an important role in the resulting structural patterns but is beyond the scope of this study.

2.4.1 Comparison with natural examples

I compare our experimental results with selected natural examples in which divergence rates or rheological boundary conditions are in good agreement with the general evolution of deformation in our models, despite some differences in their tectonic settings.

2.4.1.1 Vavilov Basin, Tyrrhenian Sea

The Vavilov Basin is located in the southern domain of the Central Mediterranean Tyrrhenian Sea, where south-eastward rollback of the Ionian plate beneath the Calabrian Arc (Fig. 2.12a) formed a Neogene-Quaternary back-arc basin (Faccenna et al., 1996; Malinverno and Ryan, 1986). The fault pattern in the Vavilov Basin is characterised by a series of linear normal faults with strikes that change gradually from NE-SW in the west to NW-SE in the east (Fig. 2.12a), defining a radial distribution about a pole of rotation to the north in the vicinity of Rome (Milia et al., 2016). This fault pattern is comparable to the results of Exp. 8 (Figs. 2.5 and 2.12b). The triangular shape of the Vavilov Basin resulted from

different rates of extension since the middle Miocene, which increased from ~20 mm/yr in the northern Tyrrhenian Sea to ~60 mm/yr in the southern Tyrrhenian Sea (Malinverno and Ryan, 1986; Patacca et al., 1990), causing the migration and rotation of the finite extensional axis (Mattei et al., 1996). The strong asymmetry of the basin is related to the curvature of the retreating trench and to an along strike variation in subduction regime, being deeper and steeper to the south (Faccenna et al., 1997; Finetti, 1982)

Although the general evolution of the Vavilov basin is well constrained, the fault pattern within the basin is difficult to interpret due to its complex kinematic history. Therefore, the timing and mechanical relationship between the major faults is matter of debate. Analysis of geophysical and geological data from the Vavilov Basin (Milia et al., 2016) indicates an eastward migration of deformation, where the oldest normal faults in the west of the basin were active until displacement was relayed to the central basin and finally to faults that bound the eastern margin of the basin. This interpretation is consistent with the deformation evolution observed in Experiment 8 (Figs. 2.5 and 2.12a), in which after 20% extension the delimiting boundary faults of the western graben became inactive and deformation was transferred to the eastern graben and to a newly developed central basin (Figs. 2.5 and 2.12a). This initial west to east gradient is analogous to the history of the Vavilov Basin (Milia et al., 2016), but at later stages in Experiment 8 fault activity switches to a central graben (Fig. 2.5a), which differs from the natural example. However, when this experiment was repeated, a west to east gradient was also observed and two new graben formed at late stages to the east of the main rift (Experiment 22; see Extended Data Movie 6).

Highly stretched fragments of continental crust that characterize the southern domain of the Tyrrhenian Sea (Rosenbaum and Lister, 2004) show a close match with the advanced stages (>30% extension) of Experiment 8, in which ongoing deformation led to a complete rupture of the upper crust in the southern-half of the model. As shown in the cumulative strain diagram for Experiment 8 (Fig. 2.10a), two triangular-shaped sections in this area of the model correspond to sections of hyper-extended crust that gave rise to mantle exhumation, favoured by localization of strain in the lithosphere-thinned rift depressions after ~30% extension (Fig. 2.5b). This is consistent with the observation of exhumed serpentinised upper mantle peridotites (Bonatti et al., 1990; Kastens et al., 1987; Milia et al., 2013) and mid-ocean ridge basalts (Kastens et al., 1988; Robin et al., 1987) in the southern Vavilov basin, which are attributed to relatively large bulk extension in this area. Overall, the eastward migration of hyper-extended crust sections documented in the experiments (Fig. 2.10a) is also similar to the evolution of the Vavilov Basin, in which mantle exhumation started in the Lower Pliocene and subsequently migrated eastwards (Milia and Torrente, 2015). A similar stepwise eastward migration of extension has been interpreted for the Latium offshore basin, in the Northern Tyrrhenian Sea (Buttinelli et al., 2014).
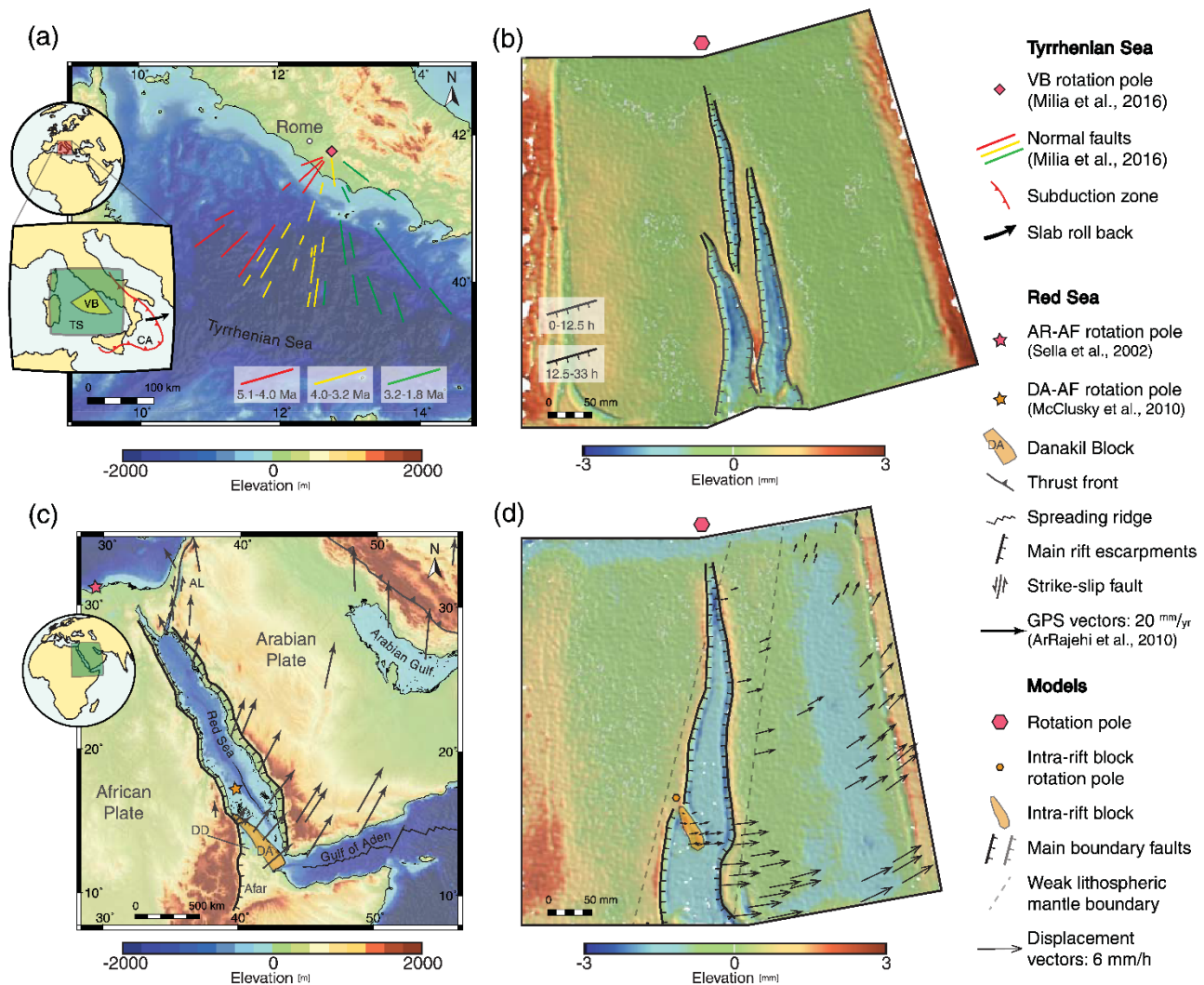
Figure 2.12 - Comparison between model results of experiments 8 and 11 and selected natural examples of rifting with a rotational component. A. Bathymetric and topographic map of the Vavilov Basin, Tyrrhenian Sea. Rollback associated to the subduction beneath the curved Calabrian Arc (CA) caused a strong anticlockwise motion that gave rise to the fan-shaped Vavilov Basin. Normal faults, coloured as a function of age as interpreted by Milia et al. (2016), indicate an eastward time migration of extension. B. Elevation map of experiment 8 at 40% extension. Delimiting boundary faults are coloured as a function of experimental time in which they were actively accommodating extension. The early developed western graben propagated northward until they became inactive after 20%. Deformation was progressively transferred to the eastern and central grabens. C. Bathymetric and topographic map of the Red Sea-Gulf of Aden rift system. GPS vectors (ArRajehi et al., 2010) indicate an anticlockwise rotation of Arabia with respect to Africa. Rotation pole is located in the northern coast of Egypt (Sella et al., 2002). The Danakil Block (DA) has an anticlockwise rotation motion about an independent rotation pole, located in the southern Red Sea (McClusky et al., 2010). D. Elevation map of experiment 11 at 20% extension. Displacement vectors of the model shows close similarity with GPS vectors of Arabia with respect to Africa (C). Deflections in the main boundary faults related to the weak lithospheric mantle also resemble the observed morphology of the main rift escarpments in the southern Red Sea (C). VB = Vavilov Basin; TS = Tyrrhenian Sea; CA = Calabrian Arc; AL = Aqaba-Levant transform boundary; DD = Danakil Depression.

2.4.1.2 Red Sea – Gulf of Aden rift system

Based on sea-floor magnetic anomaly patterns, McQuarrie et al. (2003) established that convergence between the Arabian and Eurasian plates has been effectively constant at 20-30 mm/yr over the last 56 Ma. The convergence rate between the African and Eurasian plates decreased to <10 mm/yr in the period 25-30 Ma, coeval with the initiation of the Afar Triple Junction and opening of the Red Sea (ArRajehi et al., 2010). These studies also indicate that the relative motion of Africa and Arabia increased by 70% (i.e. ~17 mm/yr) at ~13 Ma, and has remained approximately constant since then (Fig. 2.1).

Active rifting in the Gulf of Suez was abandoned in the Middle Miocene (~14 Ma) after Arabia collided with Eurasia, when plate motion was transferred to the Aqaba-Levant transform boundary (Fig. 2.1b). At this time, the Red Sea switched from rift-normal movement (N60°E) to highly oblique extension, parallel to the N15°E oriented Aqaba-Levant transform fault (Bosworth et al., 2005). The closure of the Neotethys Ocean played a substantial role in the kinematic evolution of this region, as continent-continent collision to the NW contrasted with the Makran subduction zone in the SE (Fig. 2.1b,c). The resulting gradient in the slab pull force exerted on the Arabian plate resulted in rotational anticlockwise motion of Arabia with respect to Africa, which is considered to be the main driver for the opening of the Red Sea (Bellahsen et al., 2003; Bosworth et al., 2005). Estimated Cenozoic extension/compression rates, based on sea floor magnetic data, and current extension rates measured using GPS (ArRajehi et al., 2010; Chu and Gordon, 1998; McClusky et al., 2010; McQuarrie et al., 2003) indicate that the rotational component of the Arabian Plate has been sustained over the last 13-14 Ma, with extension rates varying from ~7 mm/yr in the Northern Red Sea to ~16 mm/yr in the Southern Red Sea.

The effect of Afar Plume on the evolution of the Red Sea is not well understood, but it is commonly accepted that it acted as a trigger for the opening of the Red Sea-Gulf of Aden system at ~20-30 Ma (ArRajehi et al., 2010; Bellahsen et al., 2003; Bosworth et al., 2005; Zeyen et al., 1997). Ebinger and Sleep (1998) suggested a model comprising a single deep mantle plume that has been channelled along pre-existing zones of thin lithosphere. Several seismic tomographic studies have also suggested that channelling of Afar Plume material to the north may have been caused by the northward motion of the Arabia Plate (e.g., Chang et al., 2011; Hansen and Nyblade, 2013; Rolandone et al., 2013). The resulting thermal anomaly in the lithospheric mantle is hypothesised to cause significant localised weakening of the lithosphere in the Red Sea region (e.g., Bastow et al., 2005; Corti, 2008; Hill, 1991; Keranen and Klemperer, 2008).

Despite the simplifications in our analogue models, the scenario of an Afar Plume-related linear thermal anomaly is analogous to Experiments 11 and 18 with a low-obliquity linear weakness in the lithospheric mantle (Figs. 2.11 and 2.12d). Although the obliquity in nature is actually closer to 30° than to 15°, based on the position of the linear weakness (i.e. southern end of the weakness closer to the point of maximum extension) and on constraints from structural and geophysical data, I selected Experiment 11 (α =15°) for comparison. The rotational component imposed in the models is comparable to the last extensional phase in the Red Sea-Gulf of Aden system (Fig. 2.1c; 13 Ma - Present). South to north rift propagation in these experiments was initially controlled by the underlying weakness zone. The rift propagation direction eventually changed toward the pole of rotation at later stages. This

behaviour resulted in a characteristic structural pattern that is similar to observations in the Red Sea-Gulf of Aden rift system. The main rift escarpments in the Ethiopian Plateau and in western Yemen are oriented approximately N-S and the trend changes to roughly NW-SE north of latitude 16-18°N (Fig. 2.12c). Since continental rift initiation took place under an orthogonal extension regime for the entire southern Red Sea (Bosworth et al., 2005), this irregular pattern may be explained by the presence of pre-rift lithospheric structures or weaknesses that localised deformation (Lyakhovsky et al., 2012; Bosworth, 2015), which is consistent with the presence of the linear weak zones imposed in our models (Fig. 2.12d).

The subsequent deformation evolution in the southern Red Sea is strikingly similar to Experiment 11 (Figs. 2.6 and 2.12d). The early stages in this experiment (Fig. 2.6, 2.5% extension) show a compartmentalization of deformation in the vicinity of the weak lithosphere boundary zone. These compartments are analogous to the two rift branches in the southern Red Sea, namely a continuation of the main Red Sea Rift to the south and a western bifurcation known as the Danakil Depression (Fig. 2.12c). Progressive stretching of the model led to the development of an intra-rift block that rotates anticlockwise about an independent pole of rotation (Fig. 2.6, >10% extension), located in the western rift boundary. This resembles the proposed "crank-arm" model evolution for the Danakil Block (Sichler, 1980; Souriot and Brun, 1992) and it is supported by recent geodetic measurements (e.g., McClusky et al., 2010). Comparison between nature and analogue models suggest that differences in the rheological layering in the lithosphere, potentially caused by a channelling of the Afar Plume underneath the Arabian Plate, may have caused the formation of the Danakil Block (Fig. 2.12 c, d). Our models also suggest that extremely thinned sections of the lithosphere gave rise to mantle exhumation, which occurs in the centre of the model and then extends north and south at later stages (Fig. 2.10b). Although our models cannot reproduce the full transition from continental break up to ocean initiation and sea-floor spreading, the results are comparable with nature as crustal rupture is the final stage before the accretion of new oceanic crust, as has been occurring in the southern Red Sea since the Miocene-Pliocene transition (~5 Ma) (Bosworth et al., 2005).

2.5 Conclusions

Three-dimensional analogue models of rotational extension provide insights on how continental rifts interact with linear heterogeneities contained in the lithospheric mantle as they propagate toward a pole of rotation. The models allowed me to characterize the evolution of deformation as a function of the orientation of linear weaknesses with respect to the initial direction of extension. The results suggest that a weakness that is close in orientation to the rift axis (i.e. low obliquity) produces strain localization in short, narrow compartments at early stages which then merge and propagate at regular rates by a process of unzipping. In these scenarios, the displacement gradient along the rift axis caused by the rotational boundary condition may contribute to the formation of rotating intra-rift horsts. Models with a weakness that is unfavourably oriented to the rift axis (i.e. moderate/high obliquity) show strong partitioning of deformation. Large-scale V-shaped extensional basins that are synchronously abandoned can be explained by conditions similar to those replicated in these experiments.

By incorporating a rotating stretching vector in our analogue models I conclude that even short periods (model: ~12 h; nature: <10 Ma) of continuous change in the extension direction can produce

first-order structures that will govern the overall rift architecture. These changes in plate kinematics may also impact directly on the time and location of ocean initiation. When a linear lithospheric mantle weakness is present, it exerts a first-order control on the onset of mantle exhumation and potentially on the location of subsequent sea-floor spreading centres.

2.6 Acknowledgments

2.7 Extended Data

Video files showing the deformation evolution of the experiments discussed in this chapter are shown in Extended Data Movies 1 to 5. Extended Data Movies 6 to 10 show repeated experiments with the same boundary conditions. See Appendix C for more details and links to access the files.

Chapter 3

Unzipping continents and the birth of microcontinents

Abstract

Microcontinents occur outboard of passive margins and stranded in ocean basins. Three-dimensional analogue laboratory experiments of continental rifting demonstrate that microcontinent formation at passive margins requires a combination of pre-existing linear weaknesses in the lithosphere and rotational extension. Our results suggest that separation of microcontinents from passive margins occurs during the latest stages of continental break-up, before the onset of sea-floor spreading, and that pre-existing lithospheric weaknesses are a first order control on where they form. These findings suggest that microcontinent formation may be restricted to localised regions along passive margins associated with zones of lithospheric weakness, providing a new structural and tectonic framework for the interpretation of microcontinents in the geological record.

3.1 Introduction

The Earth's continents are a jigsaw assemblage of pre-existing continental fragments that had previously belonged to one or more pre-cursor continents and have been assembled, disassembled and reassembled, often multiple times, throughout our planet's history. Thus, knowing the timing, location, and mechanisms of continent fragmentation is a key component for unravelling Earth's geological history. Microcontinents are defined as isolated pieces of continental crust surrounded by oceanic crust (Scrutton, 1976) formed by this dispersion process. Understanding of microcontinents is improving with our increasing ability to probe and map the seafloor at higher spatial and temporal resolution. Such progress has led to the recent discovery of new microcontinents (e.g., Torsvik et al., 2013) and suggests that there are likely many more yet to be found. Research on present-day microcontinents provides important insights on continental breakup history (e.g., Nemčok et al., 2016). Three dimensional (3D) numerical models have revealed that large-scale reorganization of subduction systems occurs when microcontinents collide with continental or oceanic arcs, hence they play an extremely disruptive role in convergent margin geodynamics (Moresi et al., 2014). However, little is known about the mechanical processes that lead to microcontinent formation. It is generally agreed that most known microcontinents formed in divergent tectonic settings and that their initiation was particularly active during breakup of supercontinents (Torsvik et al., 2013; Whittaker et al., 2016). This is consistent with several modern examples, which are found adjacent to the conjugate margins of the Atlantic, Indian and Southern oceans and in the South China, Tasman and Red Seas (Fig. 3.1, Extended Data Fig. 3.1), as well as older examples preserved in orogenic systems such as the Precordillera in South America and the continental fragments of the Central Asian Orogenic Belt (Sengör et al., 1993; Thomas and Astini, 1996). Although previous research has proposed a range of separation mechanisms of microcontinents from continental margins (Abera et al., 2016; Müller et al., 2001; Nemčok et al., 2013, 2016; Peron-Pinvidic and Manatschal, 2010), significant gaps remain in determining the general kinematics and dynamics of their formation. Previous attempts to explain microcontinent formation have suggested that they form after continental rifting and breakup, requiring either the impingement of a mantle plume (Müller et al., 2001) or a plate reorganization event (Whittaker et al., 2016). These processes provide valid explanations for the development of certain examples, but fail to explain the location and distribution of other microcontinents preserved within the Earth's oceanic lithosphere. Our 3D scaled laboratory experiments show for the first time that microcontinents form during the last phases of continental rifting, when propagating rifts intersect vertical and lateral variations in the mechanical properties of the lithosphere and provide a plausible explanation of why they become stranded at the edges of continents.
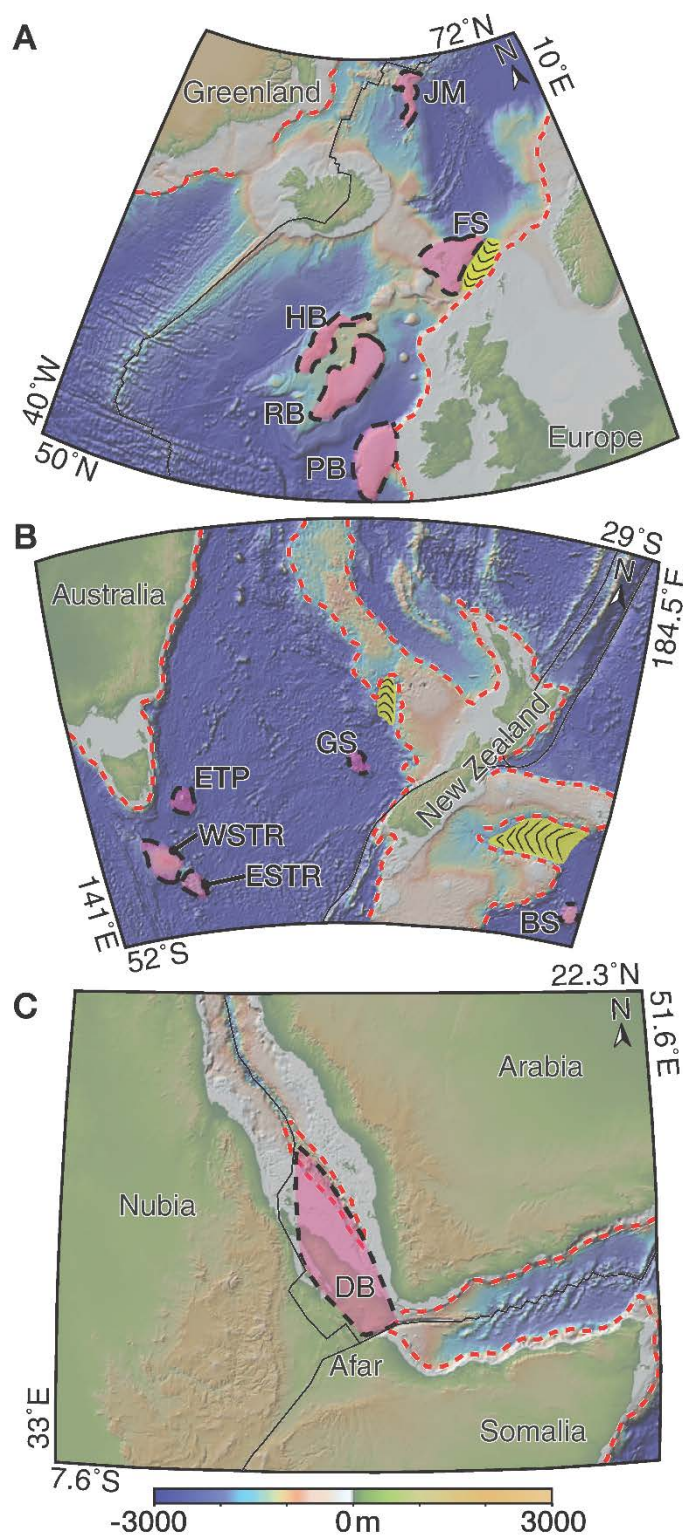
Figure 3.1 - Bathymetric and topographic maps of microcontinents and isolated continental fragments. Location of selected end-members (pink) and failed break-up basins (yellow). A: North Atlantic Ocean: Porcupine Bank (PB), Rockall Bank (RB), Hatton Bank (HB), Faroe-Shetland basin (FS) and Jan Mayen microcontinent (JM). B: Tasman Sea: East Tasman Plateau (ETP), West South Tasman Rise (WSTR), East South Tasman Rise (ESTR), Gilbert Seamount (GS) and Ballons Seamount (BS). C: Southern Red Sea microcontinent: Danakil block (DB). Ocean-continent boundary is represented by a dashed red line.

The development and propagation of rifts is a consequence of the relative motion of diverging plates around a pole of rotation (Martin, 1984). Major pre-existing weakness zones, such as ancient sutures, faults or shear zones (Corti, 2008; Heron et al., 2016; Tommasi and Vauchez, 2001), control the abandonment and jumping of rift branches as they propagate (Ziegler and Cloetingh, 2004), a process that can lead to the development of intra-rift blocks. While branching of propagating rifts may result in blocks of attenuated continental crust that remain attached to the passive margin (Fletcher et al., 2013), other intra-rift blocks may successfully isolate and evolve as microcontinents, a process that was previously thought to require either a spreading ridge jump following continent separation (Müller et al., 2001) or the presence of transform fault zones (Nemčok et al., 2016). Laboratory experimental methods are well suited for modelling lithospheric extension with rotational boundary conditions because such kinematic behavior cannot currently be simulated using numerical methods. I therefore address the intrinsically 3D problem of interaction between rotational extension and variably oriented, linear rheological heterogeneities in the lithosphere by carrying out scaled laboratory experiments of continental breakup. I then compare our modelling results with the only modern example of an actively forming microcontinent – the Danakil Block in the southern Red Sea (Eagles et al., 2002). The Danakil Block can be regarded as a natural laboratory, from which its tectonic and stratigraphic record of can be compared with other modern or ancient examples and contribute to understanding the nature and behavior of microcontinents in the geological record.

3.2 Model setup and results

Our scaled 3D laboratory modelling approach (Molnar et al., 2017) uses granular and viscous materials to simulate a three-layer continental lithosphere comprising a brittle upper crust, and a ductile lower crust and lithospheric mantle (Fig. 3.2). The model lithosphere floats isostatically on a lower viscosity, higher density model asthenosphere contained within an acrylic tank (Fig. 3.2). The experiments incorporate a linear weak zone in the lithospheric mantle representing a lithospheric-scale heterogeneity (Fig. 3.2), and its orientation with respect to the initial direction of extension (α) is varied between experiments. Rotational extension is imposed on the model lithosphere at a constant rate about a pivot fixed on the "north" side of the tank (Fig. 3.2). Surface strain and topography are quantified by high-resolution particle imaging velocimetry (PIV) and digital photogrammetry (Adam et al., 2005). See GSA Data Repository 2018146 for a complete description of the experimental design, materials, scaling and deformation monitoring technique.
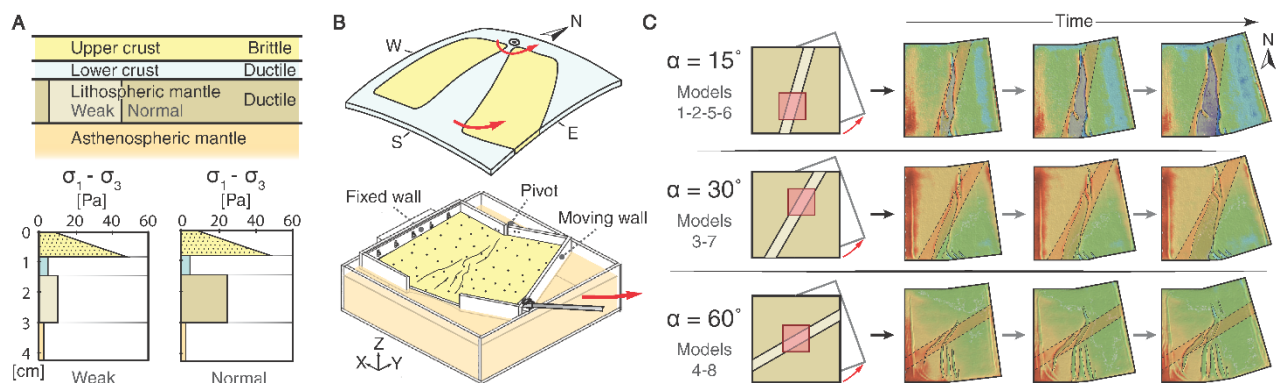
Figure 3.2 - Analogue model setup. A: Initial layering and rheological boundary conditions. B: Cartoon illustrating the rotational extension geometry (top) and 3D sketch of the experimental apparatus (bottom). For reference, geographic coordinates in the system are defined with north being toward the pole of rotation. C: Top-view illustration of the position and obliquity of the linear weak lithospheric mantle and summary evolutionary diagram. Red squares indicate location of the areas illustrated in Figure 3.3.

I present the results of four experiments out of an eleven-experiment series with three different linear weakness obliquity angles (σ = 15°, 30° and 60°) to highlight variations in deformation patterns and structural evolution (Fig. 3.3, Extended Data Figs. 3.2 and 3.3). Rotation of the moving plate creates a gradient in extensional strain that causes propagation of a rupture zone northwards toward the pivot point (Fig. 3.2), manifested by normal faults that define rift depression boundaries. All four experiments show three stages of evolution that lead to microcontinent formation: (1) an early stage in which extensional domains form, delimited by boundary faults oriented with trends that are intermediate to the extension-normal direction and the linear weak zone orientation (Fig. 3.3); (2) an intermediate stage characterised by the lateral propagation of the main boundary faults and subsequent formation of an intra-rift crustal block; and (3) an advanced stage where the crustal block breaks off by one of two different behaviors; the continental fragment bounded by the two extensional domains either rotates independently in an anticlockwise manner (Fig. 3.3), or the crustal block does not rotate and detaches completely from the western margin of the main rift (Model 3, Fig. 3.3). When this separation mechanism is not successful, a crustal block does not form, and the northward propagation of the westernmost rift branch is limited, resulting in a V-shaped region of thinned lithosphere that fails to rupture (Model 7, Extended Data Fig. 3.2).
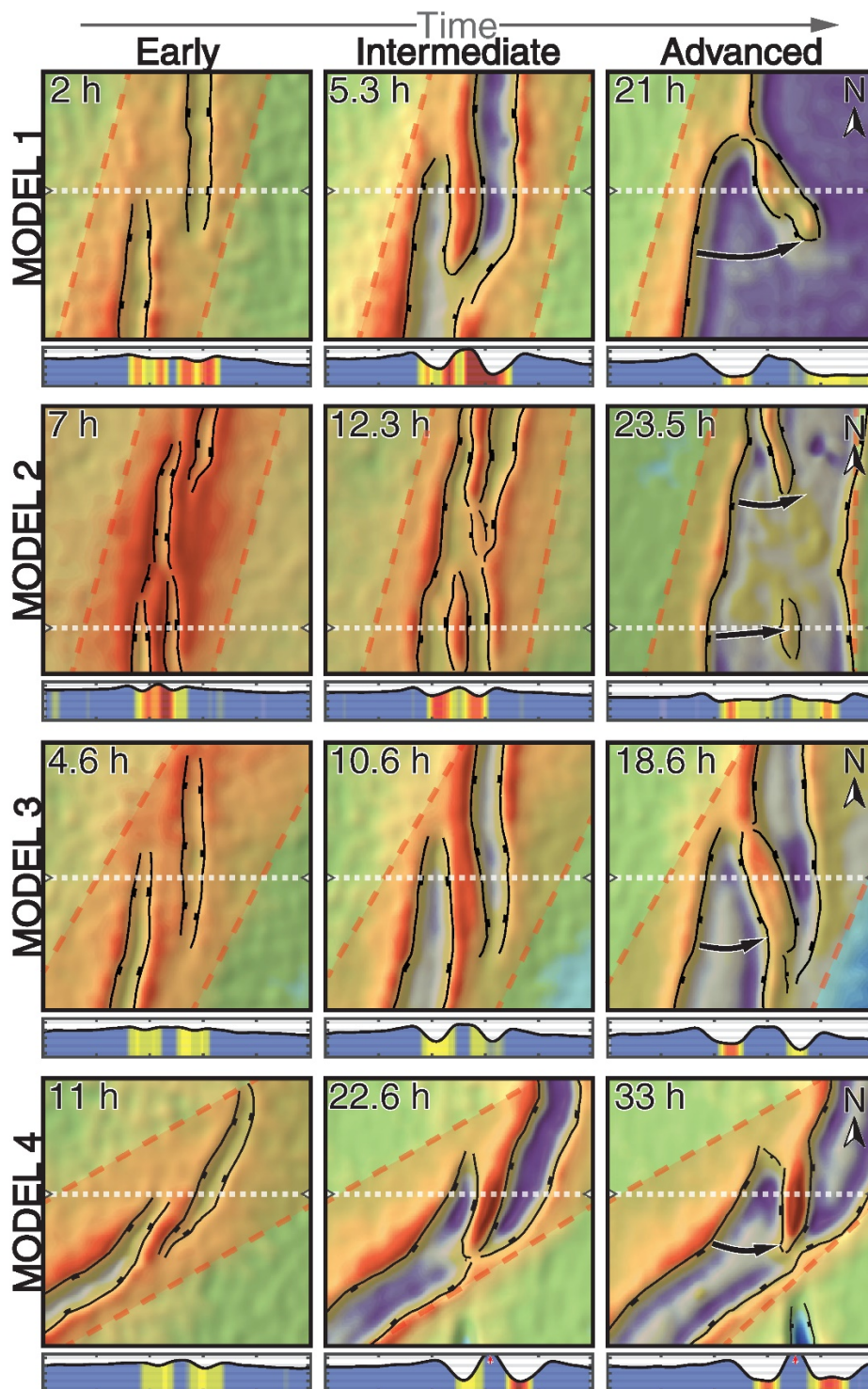
Figure 3.3 - Structural and topographic evolution of analogue models. Digital elevation models of the experiment surface and schematic evolution of experiments 1–4. Line drawings of structures show how the localization of main boundary faults within the weak lithospheric mantle (shaded orange) determines the localization of the microcontinental block that develops later. Arrows in advanced stages indicate the kinematic evolution of the microcontinental block. All diagrams represent a model area of 10 × 10 cm. Experimental time is indicated on each frame. Horizontal white dashed lines indicate the position of the topographic cross sections shown below each frame; colors represent differential normal strain on the model surface (see GSA Data Repository 2018146). Cross sections have a 3x vertical exaggeration.

A number of first-order structural similarities between isolated continental fragments in rifted margins have been recognised and characterised (e.g., Peron-Pinvidic and Manatschal, 2010). The different crustal configurations of these fragments range from failed V-shaped breakup basins (Fletcher et al., 2013) to enigmatic bathymetric highs (Williams et al., 2013), continental ribbons (Peron-Pinvidic and Manatschal, 2010) and microcontinents (Nemčok et al., 2016), depending on how successful the margin separation mechanism was, and as replicated in our experiments. I propose below a simple mechanical solution that explains the first-order evolution of microcontinental fragments and other intermediate structural features within rifted margins.

The presence of a linear weak region localizes deformation within rift depressions at early stages, which propagate both north and south, delimiting an intra-rift crustal block. Since the orientation of the weak zone boundary is oblique to the propagation direction of the rift depressions, the northern rift-tips migrate from weak toward strong lithospheric regions (Fig. 3.3). Ongoing deformation results in the progressive abandonment of the westernmost rift branches as they approach stronger regions because extension is preferentially accommodated in weaker areas of the lithosphere. The size and shape of the resulting rift-bounded microcontinent will therefore depend on the obliquity and position of the linear weakness with respect to the propagating rift axis, as similarly reported in recent analogue models by Dubinin et al. (2018). At later stages the final opening and spreading of the westernmost rift causes the crustal block to break off. A low-obliquity linear heterogeneity favors the formation of a detached continental fragment in only one of the margins (Fig. 3.3), whereas a highly oblique linear weakness may result in independently rotating intra-rift blocks at both conjugate margins (Model 8, Extended Data Fig. 3.2). The modelling results are compared to the Danakil Block, but have important implications for other natural examples such as the Jan Mayen microcontinent, the Chukchi Borderlands, the Limpopia and Beira fragments, Sri Lanka or Mauritia.

3.3 The Danakil Block

The Danakil Block, in the southern Red Sea, is the only known place on Earth where a microcontinent is actively forming on land (Eagles et al., 2002). I propose that it represents a modern analogue for the initial stages of our experiments. The kinematic evolution of the Red Sea - Gulf of Aden rift system is well constrained; the Arabian Plate has been rotating anticlockwise with respect to the Nubian Plate at a constant rate over the last 13–15 Myr (Bosworth et al., 2005) (Extended Data Fig. 3.4). Geophysical data also suggest that a NNE-trending narrow zone of warm upper mantle associated with northward channeling of the Afar Plume (Chang et al., 2011; Ebinger and Sleep, 1998) may have caused a roughly linear, thermally weakened lithospheric-scale heterogeneity (Extended Data Fig. 3.4). The early stages of deformation in our experiments are characterised by the development of two rift sub-parallel domains that delimit an undeformed intra-rift block in the vicinity of the weak lithosphere boundary (Fig. 3.3). These structures are analogous to the two rift branches that delimit the Danakil Block in the southern Red Sea (Fig. 3.4). The imposed rotational boundary condition creates a displacement gradient along the intra-rift block, which prevents the propagation of the early rift domains into the region north of the block, resulting in an independently rotating intra-rift segment (Fig. 3.4). At advanced stages of the experiments, a northward propagating rupture zone connects both extensional domains at the southern end of the intra-rift block. Differences in the timing of appearance of the

isolated block between our experiments and nature may be attributed to the polyphase rifting history of the Red Sea; namely that the orthogonal and oblique rifting phases that preceded the onset of current rotational kinematics (Bosworth et al., 2005) are not represented in the experiments. Despite the simplicity of our isothermal experiments, the general evolution of Model 1 closely resembles reconstructions proposed for the Danakil Block (Collet et al., 2000; McClusky et al., 2010). It also shows quantitative similarities, namely that the up-scaled duration of intra-rift block formation and rotation took ~11.6 Myr in the experiment, with a computed up-scaled rotation rate of 1.8°/Myr, which is in agreement with an estimated age of formation of the Danakil Block at 9 ± 4 Ma and its GPS-determined rotation rate of 1.9°/Myr (McClusky et al., 2010) (Fig. 3.4). Based on the modelling results, I hypothesize that the Danakil block formed due to the interaction between a north-westward propagating rift and a north-trending linear mantle weakness zone caused by the channeling of the Afar Plume, which are both associated with anticlockwise rotation of the Arabian Plate (Bosworth et al., 2005; Chang et al., 2011).
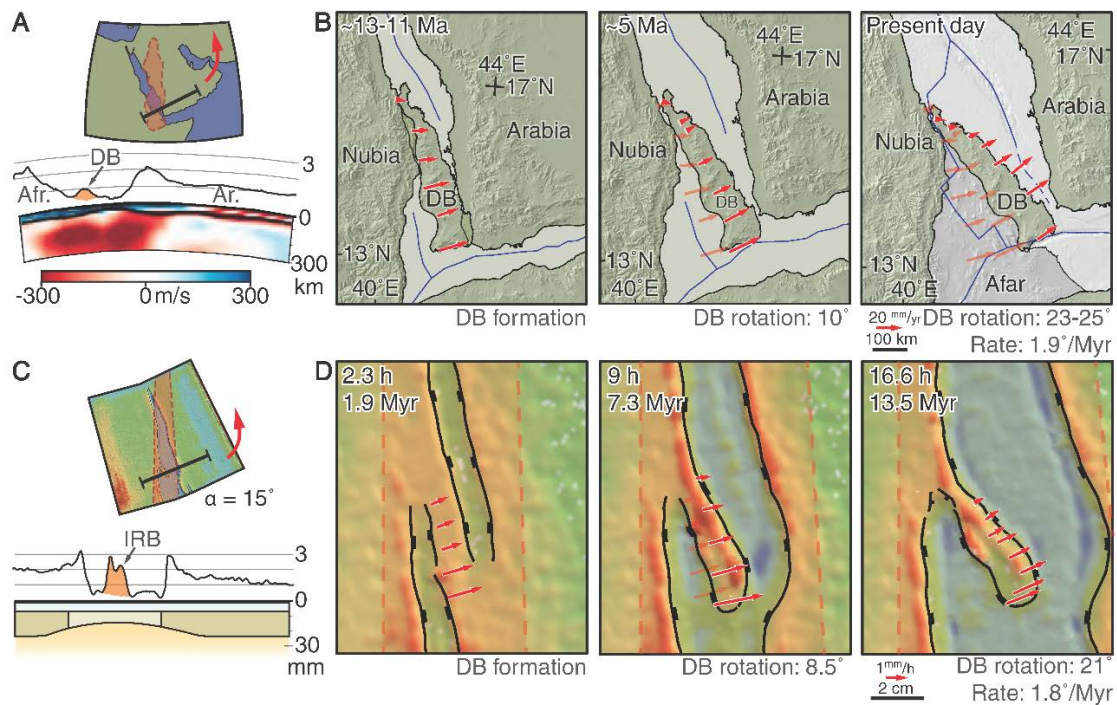
Figure 3.4 - Danakil Block evolution and comparison with analogue models. A: Bathymetry and topography with a 10x vertical exaggeration and shear wave velocities derived by joint inversion (from Chang et al., 2011), showing the location of the velocity perturbations below the southern Red Sea and its correlation with the position of the Danakil Block (DB). Position of the cross-section is indicated in a schematic regional map. B: Rotation model and reconstruction of the Danakil Block (DB), redrawn after (Collet et al., 2000) and (McClusky et al., 2010). Red arrows show inferred motion vectors (left and centre panels) and present day GPS vectors (right panel). Text indicates timing of the reconstruction stages and estimated amount of rotation of the Danakil Block (McClusky et al., 2010). C: Model 1 elevation profile with a 10x vertical exaggeration and location of the rheological weakness in the lithospheric mantle and its correlation with the position of the intra rift block (IRB). Position of the cross-section is indicated in the model drawing. D: Digital elevation models and structural evolution of Model 1. Velocity vectors are presented as red arrows and lithospheric mantle weakness is shaded orange. Results are rotated 15° anticlockwise for comparison. Text indicates experimental run-time, equivalent up-scaled time and the calculated rotation of the intra-rift block at each stage.

3.4 Conclusions

It has been suggested that lateral variations in the strength of extending lithosphere may influence the isolation of continental fragments from neighboring plates (Steckler and ten Brink, 1986; Vink et al., 1984). Such rheological heterogeneities can either be associated with processes linked to continental breakup itself (Kusznir and Karner, 2007) or to weak pre-existing lithospheric structures (Corti, 2008; Heron et al., 2016; Tommasi and Vauchez, 2001). Temporal changes in the extension direction, here recreated by incorporating a rotational boundary condition, represents a fundamental factor that causes rift-tips to propagate across these mechanical boundaries in the lithosphere. Incipient microcontinents can form as a consequence of this interaction, and this occurs during the late stages of continental rifting, before oceanisation begins. I also infer from our model results that the localization of an incipient microcontinent is controlled by pre-existing lithospheric architecture (e.g., Ghebreab, 1998). I therefore conclude that rotational extensional kinematics in the presence of a linear, lithospheric-scale weakness are the two key conditions required to form microcontinent fragments at continental margins. This finding provides a four-dimensional tectonic framework for microcontinent formation and may eventually contribute to paleo-tectonic reconstructions of their amalgamation at convergent plate margins where they are re-incorporated into new continents.

3.5 Acknowledgments

3.6 Additional remarks: types of lithospheric weaknesses

Many divergent tectonic settings occur in the presence of pre-existing structures in the lithosphere. These structures include lateral variations in lithospheric thickness that perturb mantle flow (e.g., Ebinger and Sleep, 1998), weaknesses within the lithospheric mantle or crust caused by activity of mantle plumes or hot spots (Corti, 2008), mantle penetrating shear zones characterised by reduced grain size (Heron et al., 2016), or inherited mechanical anisotropies with lattice preferred orientation of olivine crystals (Tommasi and Vauchez, 2001). Because these features lead to linear zones of anomalously weak or strong material within the lithosphere I refer to them as "rheological heterogeneities". For the specific case addressed in the main body of this manuscript, the roughly linear geometry may be related to the migration of plume material through thinned sections of lithosphere which, in turn, are associated with roughly linear ancient rifts or areas of intense extensional deformation (Ebinger and Sleep, 1998) (Extended Data Fig. 3.4).

Crustal heterogeneities are commonly associated with pre-existing basement faults (Wilson et al., 2010), suture zones (Stern and Johnson, 2010) and orogenic belts (Vauchez et al., 1997), which often juxtapose different lithospheric blocks with different ages and mechanical properties. These heterogeneities localize strain and consequently influence where and how the lithosphere deforms, ultimately affecting tectonic plate kinematics and strain distribution (Molnar et al., 2017).

3.7 Materials and Methods

All models were constructed using a length scale ratio of 4×10^{-7}, meaning that 1 cm in the models represents 25 km in nature. The initial 44 x 44 x 3 cm dimension of all models allowed to simulate the deformation of large lithospheric domains on Earth (~1100 x ~1100 km x ~80 km) submitted to rotational extensional kinematics. During assembly, the three-layer, brittle-ductile, model lithospheric plates were confined by two bottomless U-shaped acrylic walls that allowed the model lithosphere to float isostatically on a fluid model asthenosphere, contained within a 65 x 65 x 20 cm acrylic tank (Fig. 3.2). The brittle upper crust was modelled using a mixture of quartz sand and hollow ceramic microspheres and the ductile lower crust was replicated using silicone gum (polydimethylsiloxane). The model lithospheric mantle was prepared by mixing the same silicone gum with black modelling clay and hollow glass microspheres in appropriate proportions so as to obtain suitable up-scaled values for viscosity and density (Molnar et al., 2017). Similarly, a mixture of silicone and black modelling clay was used to model a weaker lithospheric mantle, which was prepared separately and incorporated into the reference lithospheric mantle during model construction. A solution of Natrosol® 250 HH and sodium chloride in water was used to model the low viscosity asthenospheric mantle. Complete scaling and physical property information of all the materials can be found in Molnar et al. (2017). Densities of the model ductile mixtures were calculated through the water displacement method, while the density of the model asthenospheric mantle was calculated using an Anton Paar DMA 4500 M density meter. The rheological properties of all materials and mixtures were tested and measured in the laboratory using an Anton Paar Physica MCR-301 parallel plate rheometer to ensure a suitable similarity with the natural prototype (Molnar et al., 2017).

A 5 cm wide linear weak zone was incorporated in the lithospheric mantle to investigate the mechanics of rifting in a heterogeneous lithosphere. The orientation of the linear weakness with respect to the initial extension direction was varied between experiments to analyze the influence of its obliquity. A rotational extensional boundary condition was imposed to study the interaction of rifts propagating towards a fixed pole of rotation in the presence of linear rheological heterogeneities. The progressive anticlockwise rotation was created by fixing one U-shaped wall to the side of the acrylic tank and pulling the other with a linear actuator at a constant divergence rate of $\sim 1.4^{-4}$ m s^{-1}, which scales to natural velocities of ~16 mm yr^{-1}, as estimated for the Southern Red Sea (Bosworth et al., 2005; McClusky et al., 2010). The properties of the analogue materials set dimensionless viscosity and density ratios which, in turn, define a time scale factor such that 1 h in the experiment corresponds to ~0.8 Ma in nature (Molnar et al., 2017). All models were run for 38 h, which corresponds to ~30 Ma and ~45% extension in nature.

The experiments were monitored using a particle image velocimetry (PIV) system. Sequential stereoscopic and top-view images were taken at 2 min intervals and processed using a stereo cross correlation technique (Adam et al., 2005) to obtain digital elevation models (DEMs) and high-resolution (≥0.1 mm) displacement fields. Color scheme chosen to illustrate topography as yellow and maroon for topographic highs and blue for low elevations and/or topographic depressions. Precise spatiotemporal measurements of differential and cumulative strain were subsequently computed and used to plot differential normal surface strain (Molnar et al., 2017), which are overlaid on the evolutionary cross-sections in Figure 3.3 and Extended Data Figures 3.2 and 3.3.

3.8 Extended Data
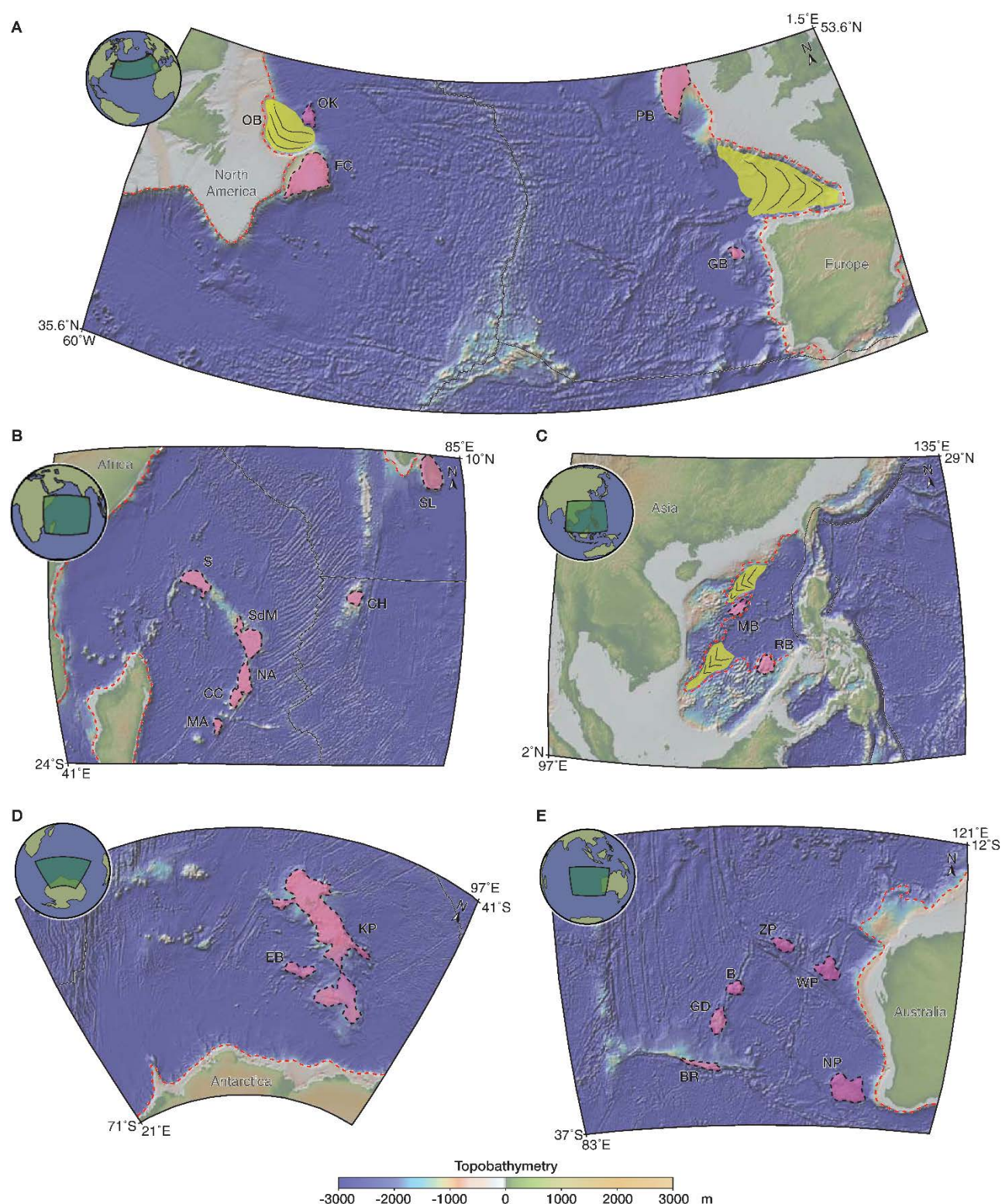
ED Figure 3.1 - Additional examples of microcontinents and isolated continental segments. Bathymetric and topographic maps with locations of selected end-members (pink) and failed break-up basins (yellow). A: Continental ribbons (Peron-Pinvidic and Manatschal, 2010) at both conjugate margins of the North Atlantic Ocean: Orphan basin (OB), Orphan Knoll (OK) and Flamish Cap (FC) at the Newfoundland margin and Porcupine Bank (PB) and Galicia Bank (GB) at the Iberian margin. B: Sri

Lanka (SL) and Mauritian continental fragments in the Indian Ocean: Seychelles (S), Saya de Malha (SdM), Nazaret (NA), Cargados-Carajos (CC), Mauritius (MA) and Chagos (CH). C: Failed break-up basins (yellow), Macclesfield Bank (MB) and Reed Bank (RB) in the South China Sea. D: Southern Ocean continental fragments: Elan Bank (EB) and Kerguelen Plateau (KP). E: South Indian Ocean continental fragments and ridges: Broken Ridge (BR), Gulden Draak microcontinent (GD), Batavia microcontinent (B), Zenith Plateau (ZP), Wallaby Plateau (WP) and Naturaliste Plateau (NP). Ocean-continent boundary is represented by a dashed red line.
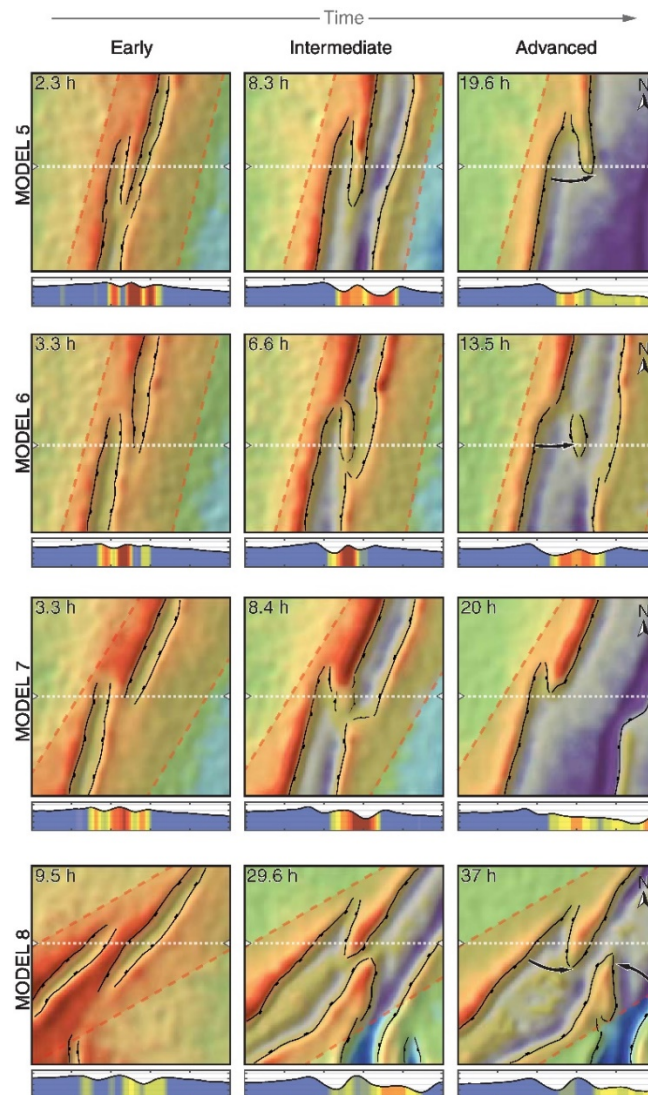
ED Figure 3.2 - Structural and topographic evolution of analogue models. Digital elevation models of the experiment surface and schematic evolution of experiments 5-8, illustrated as in Fig. 3.3. Line drawings of structures show localization of main boundary faults within the weak lithospheric mantle (shaded orange) at early stages, which subsequently determines the localization of the microcontinental block that develops at later stages. Arrows in advanced stages indicate the overall kinematic evolution of the microcontinental block. All diagrams represent a model area of 10 x 10 cm. Experimental time is indicated on each frame. Horizontal white dashed lines indicate the position of the topographic cross sections shown below each frame; colors representing differential normal strain on the model surface (Molnar et al., 2017) show how main boundary faults become inactive at advanced stages in the experiments and extension is accommodated within rift depressions. Cross sections have a 3x vertical exaggeration.

ED Figure 3.3 - Structural and topographic evolution of analogue models. Digital elevation models of the experiment surface and schematic evolution of experiments 9-10-11, illustrated as in Fig. 3.3 and Extended Data 3.2. Line drawings of structures show localization of main boundary faults within the weak lithospheric mantle (shaded orange) at early stages, which subsequently determines the localization of the microcontinental block that develops at later stages. Arrows in advanced stages indicate the overall kinematic evolution of the microcontinental block. All diagrams represent a model area of 10 x 10 cm. Experimental time is indicated on each frame. Horizontal white dashed lines indicate the position of the topographic cross sections shown below each frame; colors representing differential normal strain on the model surface (Molnar et al., 2017) show how main boundary faults become inactive at advanced stages in the experiments and extension is accommodated within rift depressions. Cross sections have a 3x vertical exaggeration.

ED Figure 3.4 - Red Sea-Gulf of Aden rift system comparison with analogue model. A. Topographic and bathymetric map of the Red Sea-Gulf of Aden rift system. Yellow arrows show GPS-derived velocities of Arabia with respect to Eurasia (McClusky et al., 2010), demonstrating the anticlockwise rotation of Arabia. Danakil Block (DB) highlighted in purple. Area shaded in red represents the region affected by the northward channeling of Afar hotspot (Chang et al., 2011), possibly causing thermal weakening of the lithosphere. Solid black line indicates the location of the cross section shown in (B). B. Bathymetry and topography with a 10x vertical exaggeration and shear wave velocity cross-sections across the Red Sea and Danakil Block, showing the approximate location of the velocity perturbations below the southern Red Sea and its correlation with the position of the Danakil Block (DB). Position of the cross-section in a schematic regional setting is indicated in the left panel. C. Model 1 elevation profile with a 10x vertical exaggeration and approximate location of the rheological weakness in the lithospheric mantle and its correlation with the position of the intra rift block (IRB). Position of the cross-section in the model was chosen for direct comparison with the prototype and is indicated in the left panel.

Chapter 4

Interactions between propagating rifts and linear weaknesses in the lower crust

Abstract

Pre-existing structures in the crust such as shear zones, faults and mobile belts are known to exert a significant control on the structural evolution of continental rifts. However, the influence of such features when the extension direction progressively changes over time remains uncertain. Here I present new results from three-dimensional (3D) lithospheric-scale laboratory experiments of rotational extension that provide key insights into the temporal evolution of propagating rifts. I specifically test and characterise how rifts propagate and interact with linear crustal rheological heterogeneities oriented at variable angles with respect to the extension direction. Results show that approximately rift-parallel pre-existing heterogeneities favour the formation of long, linear faults that reach near-final lengths at early stages. Low angles between the heterogeneities and the propagating rift axis may result in strong strike-slip reactivation of the pre-existing structures if they are suitably oriented with respect to the stretching direction. When the linear heterogeneities are oriented at intermediate to high angles rift branches become laterally offset as they propagate, resulting in complex rhombic fault patterns. Rift-perpendicular crustal heterogeneities do not affect fault trends during rift propagation, but cause the stalling and deepening of the laterally growing rift basins. Similarities between the analogue experimental results and selected natural examples provide insights on how nature finds the preferential pathway to breakup in heterogeneous continental lithosphere.

4.1 Introduction

The continental lithosphere is characterised by rheological heterogeneities and mechanical anisotropies inherited from previous tectonic events (e.g., Audet and Bürgmann, 2011). Rheological heterogeneities are commonly associated to past orogenic or intraplate processes (i.e. collisional belts, shear zones, rifts, thermal weakening) that result in areas of the lithosphere with a reduced strength. Mechanical anisotropies arise as a consequence of tectonic fabrics (i.e. foliations, lineations, crystallographic preferred orientations, reduced grain size) that define a mechanically weaker region than the surrounding lithosphere. It has long been recognised that they control the pattern, propagation and overall structural and sedimentological evolution of continental rifts (e.g., Rosendahl, 1987; Smith and Mosley, 1993; Vauchez et al., 1998; Will and Frimmel, 2017). The nature of the rheological heterogeneities and/or mechanical anisotropies, whether discrete or pervasive, has a first-order influence on the distribution of deformation (Morley, 1999). Many of these pre-existing features lead to linear zones of anomalously weak material within the lithosphere, heterogeneities and anisotropies can therefore be treated as equivalents and are referred to as weak seeds that are incorporated in the analogue models (see Section 4.2.2).
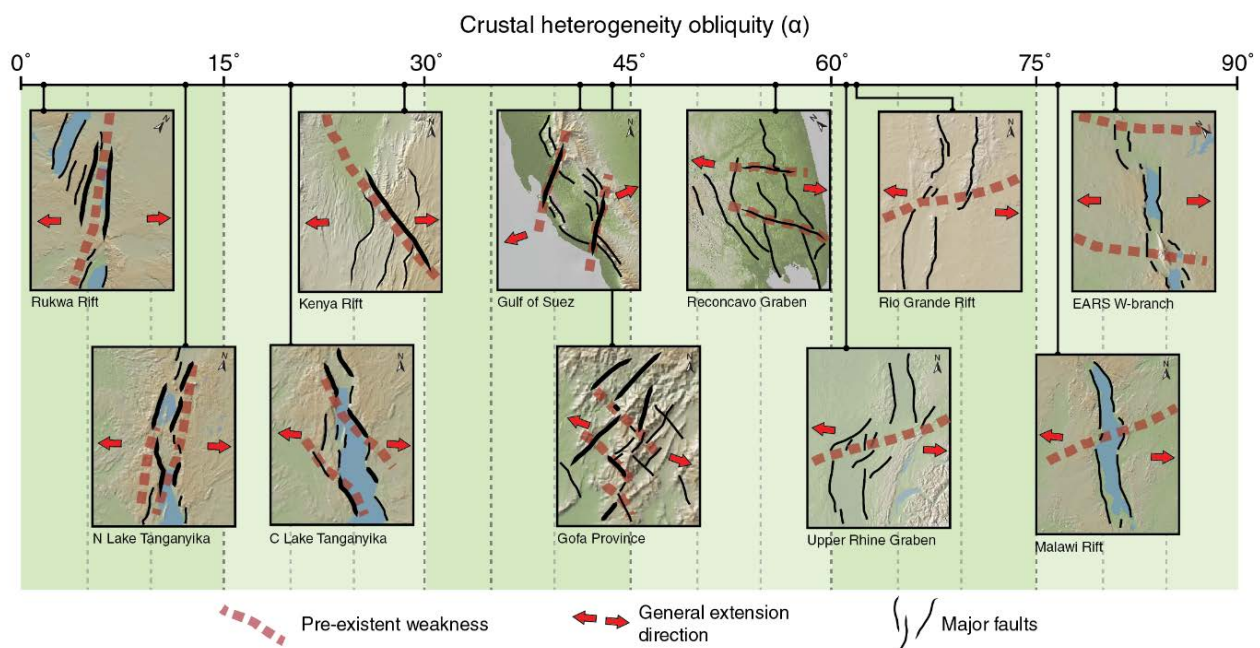
Figure 4.1 - Natural examples of continental rifts classified by the approximate angle of obliquity between the direction of extension and the controlling pre-existing crustal heterogeneities. Digital elevation maps (GeoMapApp, Ryan et al., 2009) and simplified line drawings of major extensional structures. Note that red arrows indicate the extension direction at the moment of rift formation, which may differ from present-day kinematics.

It is widely accepted that factors such as the location and obliquity of pre-existing structures with respect to the direction of extension (e.g., Acocella et al., 1999; Agostini et al., 2009; Ebinger et al., 2000) or temporal variations of the regional stress field (e.g., Ebinger et al., 2000; Morley, 2010) play a major role on rift evolution. Observations from many continental rifts have greatly improved our understanding of rift evolution as a function of the obliquity of pre-existing weaknesses (e.g., Autin et al., 2010; Corti et al., 2003; Morley, 1999; Ring, 1994). Natural examples show a wide variety of geometric

relationships, covering the entire range between rift-parallel weaknesses (e.g., Rukwa Rift [Morley et al., 1992]), to approximately rift-perpendicular weaknesses (e.g., Main Ethiopian Rift [Bonini et al., 2005]) (Fig. 4.1). Understanding the temporal evolution of rifts relies on timing and/or kinematic constraints preserved within the geological record. When such evidence is lacking or when it is obscured by the superimposition of tectonic events, deciphering the temporal evolution of rifts can become a challenge.

Complementary analogue (e.g., Acocella et al., 1999; Agostini et al., 2009; Corti, 2008; McClay and White, 1995) and numerical experiments (e.g., Brune, 2014; Naliboff et al., 2017) have provided important insights on the development and interaction of extensional faults, which help to constrain the overall temporal evolution of rifts. While it is recognised that temporal changes in the extension direction are a common feature of rifts in nature (e.g., Morley, 2010; Nemčok et al., 2016; Whittaker et al., 2016), such changes have typically not been included in geodynamic models of continental extension. Previous modelling studies that focused on the role of multi-phase rifts have successfully recreated different extension directions through time (e.g., Bonini et al., 1997; Duffy et al., 2017; Henza et al., 2010; Keep and McClay, 1997), but did so by imposing laterally homogeneous extensional boundary conditions during each phase. Conversely, the inclusion of a rotational kinematic boundary condition in experiments (e.g., Benes and Scott, 1996; Molnar et al., 2017; Tron and Brun, 1991) has effectively simulated progressive changes in extension direction over time. Such changes may induce a laterally heterogeneous strain field that results in a gradient in the amount of extension along the rift axis (e.g., Gofa Province, [Philippon et al., 2014]). When these conditions are met, rift branches usually propagate laterally towards a pole of rotation. How they propagate across transversal pre-existing crustal heterogeneities remains poorly understood.

Although both pre-existing heterogeneities and rotational extension are often identified as important factors in ancient and modern rifts, their combined influence has rarely been tested by means of analogue or numerical modelling (e.g., Benes and Scott, 1996; Molnar et al., 2017). In this study, I present a series of three-dimensional laboratory experiments addressing this topic. By measuring surface deformation in the experiments at high spatio-temporal resolution, I characterise the detailed structural evolution of continental rifts as a function of the obliquity of crustal heterogeneities. I compare our results to selected natural examples in order to provide new insights on rift migration and propagation across discrete pre-existing crustal heterogeneities.

4.2 Experimental procedure

4.2.1 Model setup

All laboratory experiments presented here comprise a three-layer, brittle-ductile model lithosphere that floats isostatically on a low-viscosity model asthenosphere, contained within an acrylic tank (Fig. 4.2). All models have initial dimensions of 44 x 44 x 3 cm and are constructed to sit within two U-shaped confining walls (Fig. 4.2a). The experimental setup was designed to simulate continental rifts that propagate and interact with variably oriented crustal anisotropies. I therefore mimic propagating rifts by imposing a rotational kinematic boundary condition on the models following the approach used in Molnar et al. (2017). The model lithospheric plate is attached to a moving U-shaped wall and

pulled by a linear actuator at a constant divergence rate (Fig. 4.2a). A hinge between the two confining walls acts as a fixed vertical pivot, creating a horizontal gradient in the imposed extensional strain field (Fig. 4.2a). The amount of extension in the models increases away from the pivot (Fig. 4.2c), which is analogous to creating an along-rift axis gradient in the amount of extension, as inferred from modern examples (e.g., Gofa Province (Philippon et al., 2014; Woodlark Basin [Mondy et al., 2018]).
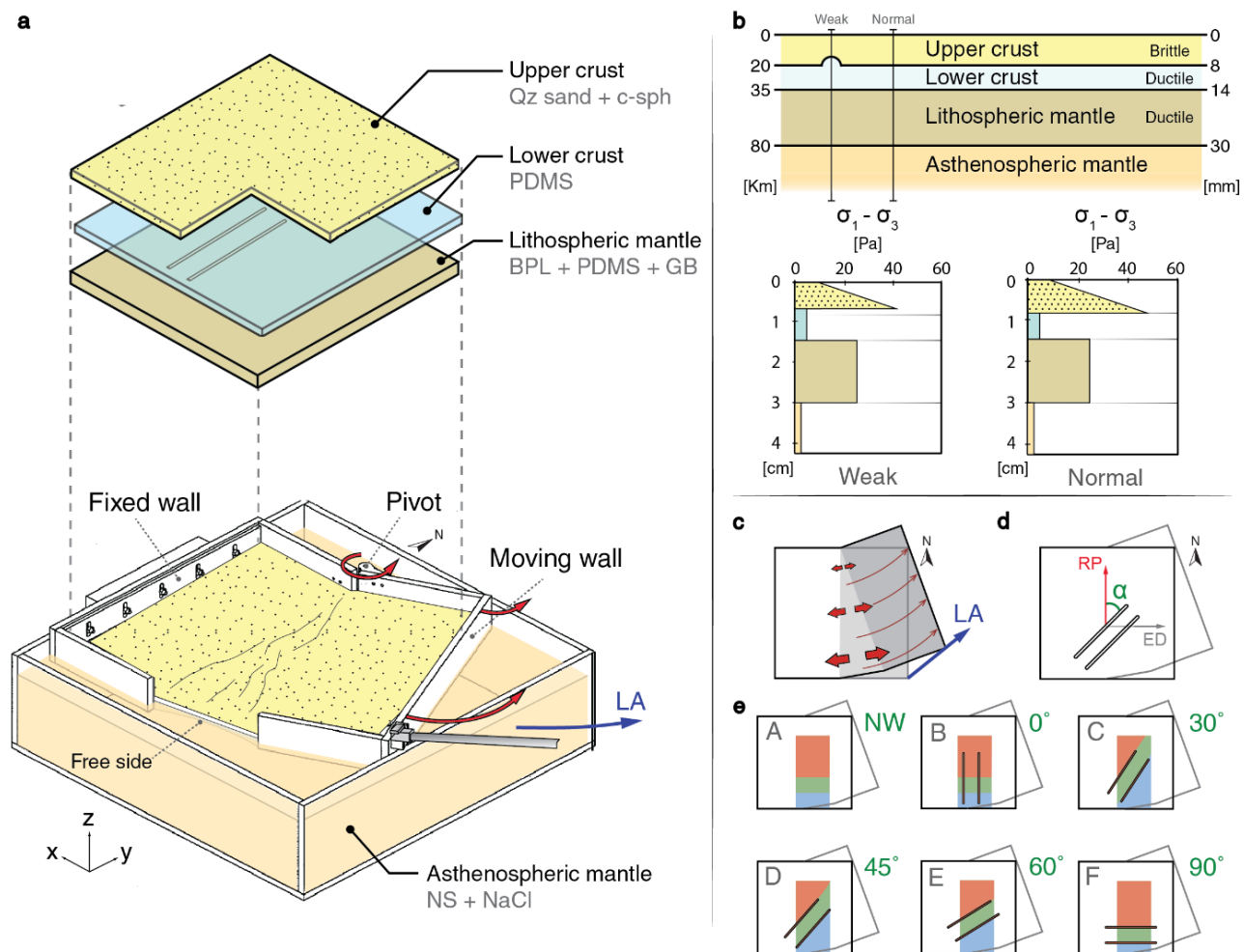
Figure 4.2 - Experimental setup and boundary conditions. A. Top: 3D sketch illustrating how the brittle-ductile multilayer lithosphere is constructed and positioned within two U-shaped containing walls. A side-cut of the model upper crust drawing shows how the weak seeds are incorporated to the model lithosphere. Bottom: cartoon drawing of the rotational extensional apparatus. Blue arrow indicates the direction in which the linear actuator (LA) pulls the moving wall at a constant velocity. A hinge between the U-shaped walls, on the opposite side of the linear actuator rod, acts as a fixed vertical pivot, creating a horizontal gradient in the imposed strain field (red arrows). Fixed pivot is designated as the north for reference. Abbreviations: c-sph = Ceramic spheres, PDMS = polydimethylsiloxane, BPL = Black plasticine, GB = Glass bubbles, NS = Natrosol, NaCl = Sodium Chloride. B. Cross section showing the rheological layering of the model lithosphere and representative strength profiles corresponding to the normal and weak sections of the crust (see text and Table 4.1 for details). C. Schematic top view drawing showing the motion described by the opening plate (in grey) and the subsequent gradient in extension produced along the rift axis (red arrows). LA = Linear actuator. D. Schematic top view drawing indicating the initial location of the

heterogeneities and the definition of the angle of obliquity (α). Model D (α = 45°) boundary conditions are used as an example. Abbreviations: ED = Extension direction, RP = General rift propagation direction. E. Graphical summary of the boundary conditions for all models discussed in this study. Coloured rectangles show the area analysed and presented in figures 4.3 to 4.8. Each colour indicates the location of the proximal (red), central (green) and distal (blue) domains for each model, delimited by the distance to the pole of rotation (Models A and B) or by the position of the linear heterogeneities (Models C to F). Abbreviation: NW = No weakness.

4.2.2 Materials, scaling and rheological layering

I scale down forces, length and time using dimensional scaling theory (Davy and Cobbold, 1991; Hubbert, 1937; Ramberg, 1967) in order to achieve an appropriately sized model that is kinematically and dynamically similar to the natural system. The scaling ratios (Table 4.1) for the experiments were set so that 1 cm in the models corresponds to 25 km in nature and 1 hr in the experiment represents ~0.8 Ma in nature. Since all experiments were carried out under the normal field of gravity (1 g), the gravitational scaling ratio is 1:1. The velocity scaling ratio is derived from the time, length and gravity scales, such that the divergence rate of ~5 mm/hr used in the experiments corresponds to ~16 mm/yr in nature. Scaling factors and experimental parameters are detailed in Table 4.1.

The model lithosphere is composed of a mixture of quartz sand and hollow ceramic microspheres to replicate the brittle upper crust, polydimethylsiloxane (PDMS) to model the ductile lower crust, and a mixture of black Colorific Plasticine®, 3M® hollow glass microspheres and PDMS to replicate the lithospheric mantle (Figs. 4.2a and 4.2b). The upper crustal granular material mixture obeys the Mohr-Coulomb failure criterion, with an angle of internal friction φ< 38° and cohesion ~ 9 Pa (Molnar et al., 2017). PDMS and the PDMS-based mixture used for the ductile layers are quasi-Newtonian fluids frequently used in analogue modelling studies (e.g., Cruden et al., 2006; Molnar et al., 2017; Riller et al., 2012; Weijermars, 1986). The model lithosphere overlies a model asthenosphere that comprises a solution of Natrosol® 250 HH plus sodium chloride in deionised water (Boutelier et al., 2016; Davaille, 1999). A complete description of the experimental setup, materials, scaling and model construction can be found in Molnar et al. (2017).

Table 4.1 - Scaling parameters for the analogue models

		Thickness		Density		Viscosity		Material
		Model [mm]	Nature [km]	Model [kg/m³]	Nature [kg/m³]	Model [Pa s]	Nature [Pa s]	
Upper Crust	Brittle	8	20	928	2600	-	-	S + ESPH
Lower Crust	Ductile	6	15	982	2760	4×10^4	2×10^{21}	PDMS
Linear weakness								
Upper Crust	Brittle	~7	~17.5	928	2600	-	-	S + ESPH
Lower Crust	Ductile	~7	~17.5	982	2760	4×10^4	2×10^{21}	PDMS
Lithospheric Mantle	Ductile	16	45	1090	3050	2×10^5	1×10^{22}	PDMS + BPL + K1
Asthenosphere		-	-	1100	3100	380	1.9×10^{19}	NaCl-NS

Scaling factors: model/prototype				
	$L^* = 4 \times 10^{-7}$	$\rho^* = 0.355$	$\mu^* = 2 \times 10^{-17}$	
Time scaling factor	$\eta^* = \rho^* \cdot g^* \cdot L^* \cdot t^*$	$> t^* = 1.41 \times 10^{10}$	$>$ 1 hr in model ~ 0.8 Ma in nature	
Velocity scaling factor	$v^* = l^*/t^*$	$> v^* = 2.84 \times 10^3$	$>$ 6 mm/hr in model ~ 20 mm/yr in nature	
Gravity scaling factor	$g^* = gm/gp = 1$			

All layers have dimensions of 440 x 440 mm. Model asthenosphere area is 626 x 626 mm.

S=Sand; ESPH=Hollow ceramic spheres; PDMS=Polydimethylsiloxane; BPL=Black Plasticine; K1=Hollow glass microspheres; NaCl-NS= Sodium chloride+Natrosol solution

I introduced discrete pre-existing crustal anisotropies (Morley, 1999) into the experiments following previous analogue modelling approaches (e.g., Le Calvez and Vendeville, 2002; Zwaan et al., 2015). Two ~3 mm wide and ~1 mm high linear semi-cylindrical seeds of PDMS were positioned on top of the homogenous lower crust prior to sifting the brittle upper crustal granular mixture. Since the brittle upper crust determines the maximum strength of the model lithosphere (Fig. 4.2b), the inclusion of these linear seeds locally reduces its thickness and hence the integrated resistance of the lithosphere to deformation. This effectively simulates planar zones of weakness such as fault planes, shear zones or areas of previously thinned crust (Morley, 1999; Zwaan et al., 2015).

Rather than trying to reproduce a specific natural scenario, our aim is to characterise how rifts propagate across crustal weaknesses as a function of their obliquity (α) with respect to the initial extension-normal direction (Fig. 4.2d). I set a distance of 5 cm between the two discrete linear anisotropies in order to allow enough space for rift branches to develop freely between them and to study their propagation and temporal evolution. For ease of analysis and discussion, I subdivide the resulting fault pattern into proximal, central and distal domains, which are delimited by the position of the linear anisotropies (Fig. 4.2e).

4.2.3 Deformation monitoring

I employ a particle image velocimetry (PIV) system to monitor deformation and surface topography during the experiments. The PIV system consists of two stereoscopic cameras and one top camera that are set to capture digital images of the experiments at 2-minute intervals, which provides quasi-continuous monitoring of deformation throughout the entire 36-hour duration of the experiments. The digital images are processed using a cross-correlation algorithm (Adam et al., 2005), which allows me to extract high-resolution topography, differential and cumulative strain, and velocity data from the models. See Extended Data for details on the methods used for PIV data calculations.

4.3 Results

A total of 12 experiments were carried out. Each experiment had identical rheological layering and kinematic boundary conditions. The angle of obliquity of the crustal anisotropies by 15° steps between each experiment. This chapter presents and describes the detailed results of 6 experiments in which the linear anisotropies were progressively rotated clockwise between experiments. Additional experiments with anticlockwise-rotated weak seeds were carried out for comparison and showed similar patterns and timing of deformation. Figure 4.2e and Table 4.2 summarise the initial conditions of the experiments discussed here. Results are divided into three stages in terms of the running time and the corresponding amount of displacement imposed at the free side of the model. The pole of rotation is designated as the north side for reference; hence, the amount of extension increases from north to south (Fig. 4.2c). Surface topography and differential strain for each time-step are used to display the general evolution of propagating rifts in each experiment. Rose diagrams of fault distributions and fault activity graphs are presented to depict the temporal evolution of the main rift faults for each of the previously defined proximal, central and distal domains.

Table 4.2 - List of the performed analogue models

| Model	Obliquity angle (α)	Weakness orientation
A*	No weakness	
B*	0°	-
C*	30°	Clockwise
C2	30°	Anticlockwise
D*	45°	Clockwise
D2	45°	Anticlockwise
E*	60°	Clockwise
E2	60°	Anticlockwise
F*	90°	-
G	15°	Clockwise
G2	15°	Anticlockwise
H	75°	Clockwise
H2	75°	Anticlockwise

Experiment evolution described in this work.

4.3.1 Model A (Homogeneous reference lithosphere)

Strain initially localised in the distal domain as extension was accommodated by linear, normal faults that formed perpendicular to the extension direction (Fig. 4.3a). Increasing stretching resulted in the propagation of these major boundary faults toward the pole of rotation, forming northward pointing V-shaped basins (Figs. 4.3a-4.3b). Differential strain measurements indicate the incipient formation of new rift graben in the central domain, bounded by linear normal faults that also strike approximately perpendicular to the stretching direction (Fig. 4.3b). After 18-19 hours, activity on the distal domain progressively decreased, rift tip propagation slowed down and central domain rift graben started to accommodate most of the extension (Fig. 4.3d). The bounding normal faults in the central domain formed V-shaped graben that propagated both north and south, with the eastern graben developing more rapidly and deeper (Figs. 4.3b-4.3c).

The overall deformation was gradually transferred towards the east and to the proximal domain, with faults that grew towards the pole of rotation due to the anticlockwise opening of the moving plate (Figs. 4.3a-4.3c). The main boundary faults in the distal domain were active for 26 hours (i.e. 21.1 My) (Fig. 4.3e), after which strain was transferred to the rift depressions (Fig. 4.3c). Normal faults in the central domain accommodated most of extension between 18 and 27 hours (i.e. 14.6 – 21.9 My (Fig. 4.3e). Finally, extension was predominantly accommodated in the proximal domain after 27 hours (i.e. 21.9 My). Comparison between fault orientations over the different time steps indicate that the boundary faults were oriented perpendicular to the extension direction during the entire experiment, and rift graben propagated both away from and towards the pole of rotation without being laterally offset as they grew in length (Figs. 4.3a-4.3c).
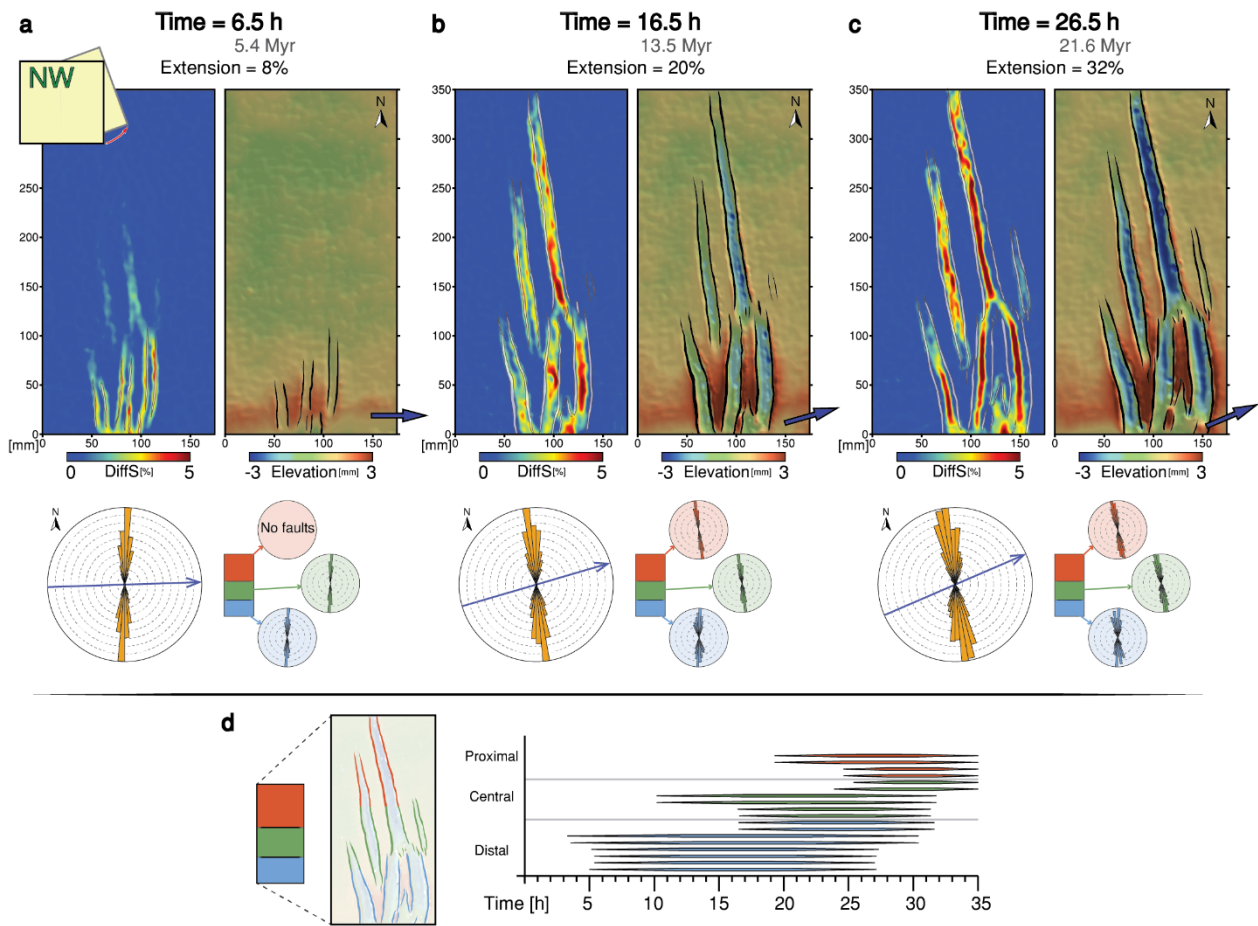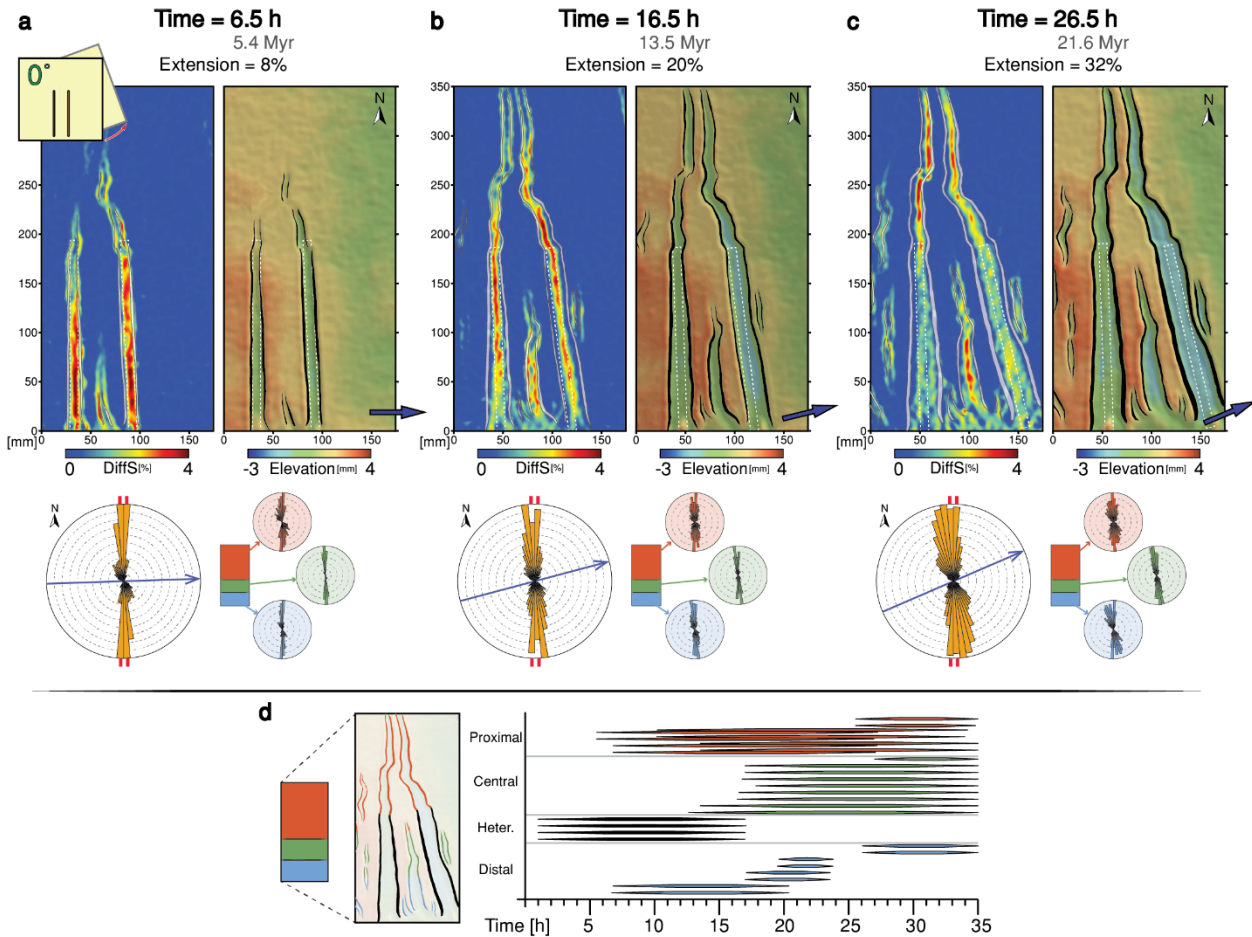
Figure 4.3 - Evolution of deformation for Model A with homogeneous lithosphere (i.e. no crustal anisotropy). Panels A, B and C display top view model deformation at early, intermediate and late stages respectively. Top-view differential strain on surface and structural interpretation in white lines are shown in the left part of each panel. Top-view DEMs and structural interpretation in black lines are shown in the right part of each panel. Blue arrow indicates the general extension direction at each stage. White dashed lines indicate approximate location of the crustal heterogeneities. Rose diagrams at the bottom of each panel illustrate normalised fault distribution weighted for the fault length for the whole model (orange) and subdivided for each domain (red, green and blue). Blue line in the rose diagrams indicate the general extension direction at each stage and the double red lines show the orientation of the crustal heterogeneities when present. D. Left: Top view line drawing of structures interpreted at late stages of the experiment, coloured according to the domain in which they formed. Right: Fault activity graph illustrating the timing of activity/inactivity for the main extensional faults.

4.3.2 Model B (α = 0°)

Deformation became highly localised at early stages, forming two elongated rifts aligned parallel to the crustal anisotropies. The presence of a linear weak seed produced anomalously long and straight bounding normal faults that reach their near-final lengths early in the experiments (Fig. 4.4a). Differential strain measurements showed a more evolved stage in the eastern rift graben, associated with its proximity to the moving plate (Fig. 4.4a). An incipient N-S oriented V-shaped central rift branch,

located between the two main rift compartments, was detected by differential strain measurements before developing on the surface (Fig. 4.4a). Rift branches that propagated northward beyond the crustal anisotropies showed a more irregular pattern, but orientation analysis indicates that the fault trends remained perpendicular to the extension direction (Fig. 4.4a).
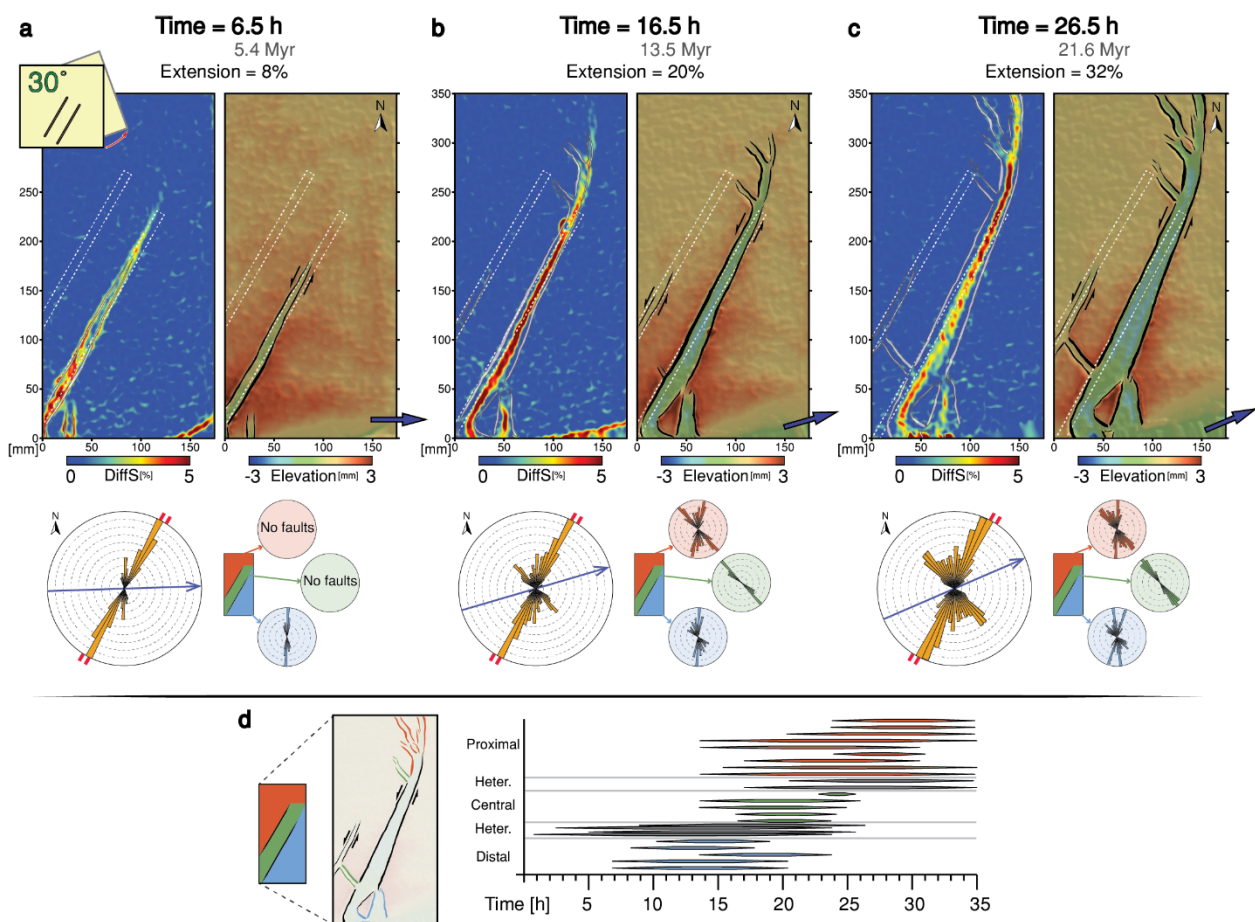

Figure 4.4 - Evolution of deformation for Model B with obliquity angle α = 0°, illustrated as in figure 4.3. Location of the crustal heterogeneities is illustrated as a dashed white line in panels A, B and C.

Deformation evolution followed the behaviour observed at early stages, with the widening of the two main rift branches accommodating most of the extension (Fig. 4.4b). In comparison to the early stages, the differential strain field map shows maximum strain values closer to the pole, indicating a progressive northward migration of deformation (cf. Figs. 4.4a and 4.4b). Rifts beyond the northern tips of the linear anisotropies continued their northward propagation as short arcuate segments but with an overall N-S trend. Fault development in the proximal domain was not controlled by pre-existing anisotropies, resulting in smaller, slightly laterally offset rift basins that subsequently merged into a single graben (Figs. 4.4a-4.4c). Although deformation in the eastern main branch initially propagated further north, higher values of differential strain were recorded in the western main branch at advanced stages (cf. Figs. 4.4a and 4.4c). Secondary rift branches with faults trending perpendicular to the extension direction developed on both sides of the linear anisotropy (Fig. 4.4c). During the final stages, maximum values of strain were observed in the proximal domain, near the pole of rotation, while deformation was more distributed and limited to the basin floors in the distal domain (Fig. 4.4c).

4.3.3 Model C (α = 30°)

Deformation became strongly localised early in the experiment due to the presence of the N30°E oriented crustal anisotropies, as observed in Model B (α = 0°) (Fig. 4.5a). Extension was accommodated almost entirely by elongated, N30°E oriented sinistral oblique normal faults that dislocated the distal and central domains (Fig. 4.5a). The only structural features that developed outside the linear weak area were two short, N-S oriented faults that delimited a rift depression in the distal domain of the model (Fig. 4.5a). With increasing deformation, this rift branch propagated northward and interacted with the southernmost anisotropy, creating minor disturbances in the local differential strain field (Fig. 4.5a). When deformation propagated beyond the anisotropy and into the central domain, the new rift bounding normal faults developed at high angles with respect to the stretching direction (Figs. 4.5b-4.5c).

Figure 4.5 - Evolution of deformation for Model C with obliquity angle α = 30°, illustrated as in figures 4.3 and 4.4.

Differential strain measurements indicate a progressive north-eastward propagation of strain along the southernmost anisotropy (Figs. 4.5a-4.5c). Deformation northeast of this anisotropy developed with a horsetail geometry (Fig. 4.5b), in which extension was accommodated by three curved splays that propagated towards the pole of rotation (Figs.4.5b-4.5c). The westernmost rift branches of the horsetail splay were bounded by normal faults trending approximately parallel to the central domain rift branch

(Fig. 4.5c). Strain was mainly localised along the southernmost crustal anisotropy throughout the entire experiment (cf. Figs. 4.5a-4.5c). Consequently, only minor sinistral oblique-slip extensional motion developed along the northern crustal anisotropy and faults were completely absent in the proximal domain (Fig. 4.5c). This indicates that the low obliquity angle of the crustal anisotropy favoured dislocation of the model lithosphere into kinematically independent blocks, creating a strain shadow within the central and proximal domains (Figs. 4.5a-4.5c).

4.3.4 Model D (α = 45°)

Early stages of deformation were characterised by partitioning of deformation into two north-south oriented rift graben in the distal domain and other two V-shaped rift basins bounded by N45°E oriented linear normal faults localised along the crustal anisotropies (Fig. 4.6a). These narrow structures have sinistral oblique-slip components, indicating that the weaker crust favoured dislocation of the model lithosphere into blocks with different displacement rates (See section 4.1), as in Model C (α = 30°) (Figs. 4.6a-4.6c).
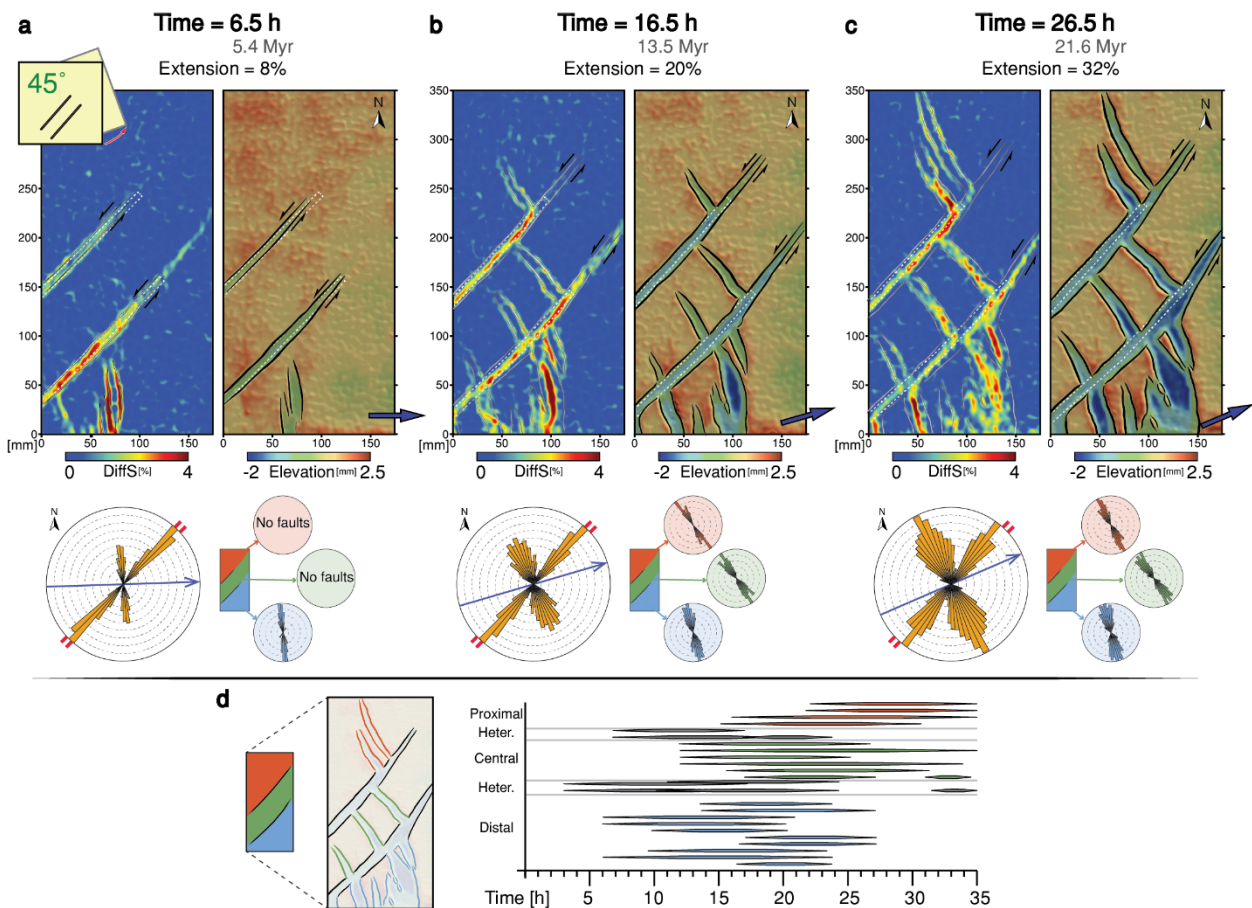
Figure 4.6 - Evolution of deformation for Model D with obliquity angle α = 45°, illustrated as in figures 4.3 and 4.4.

Boundary faults of the distal domain rift branches propagated northward, gradually changing their orientation as they propagated towards the southernmost linear anisotropy (Fig. 4.6a). A series of three

new rift branches with bounding faults trending ~N30°W formed in the central domain after 12 hours (~9.7 My) (Figs. 4.6b and 4.6d). These basins formed at slightly obtuse angles with respect to the extension direction, and at ~80° with respect to the weakness-related faults (Figs. 4.6b and 4.6e). The orientation of the central domain graben may be associated with a local modification of the stress field caused by horizontal displacement along the two linear anisotropies. This produced a zig-zag pattern and consequently resulted in a rhombic geometry (Figs. 4.6b-4.6c). Rift branches that developed in the central domain were laterally offset with respect to those formed early in the early formed distal domain, except for the westernmost graben (Fig. 4.6b).

Differential strain measurements indicate that strain along the oblique-slip fault zones propagated in a northeast direction (Figs. 4.6a-4.6c). Figure 4.6b shows that strain along the northernmost oblique-slip fault zone stopped propagating after ~16.5 hours (~13.4 My), when strain was relayed into the N30°W trending proximal domain rifts (Fig. 4.6b). Rift branches in the proximal domain developed with a right-lateral offset with respect to those in the central domain (Figs. 4.6b-4.6c). Orientation analysis of the proximal domain normal faults show a progressive rotation towards the north due to their proximity to the pole of rotation (Figs. 4.6c and 4.6e). Distal and central domain structures kept accommodating deformation during the final stages, but to a lesser extent than those in the proximal domain (Figs. 4.6c and 4.6e). The highest differential strain values during the late stages were detected at the intersection between the northward propagating central domain graben and the northernmost crustal anisotropy. These areas, in turn, coincide with greater fault throws and hence formed the deepest basins recorded in the experiment (Fig. 4.6c).

4.3.5 Model E (α = 60°)

Extension at early stages was predominantly accommodated by N-S trending faults that delimit two main rift branches that propagated northward, towards the pole of rotation (Fig. 4.7a). Differential strain measurements show minor localization along the crustal anisotropies, which results in short, N60°E oriented sinistral oblique normal faults (Fig. 4.7a). The northward propagation of the main rift branches was laterally deflected eastward by the presence of the anisotropies, as evidenced by the sinusoidal pattern of the differential strain field (Fig. 4.7a).

Most extension during the experiment was accommodated by N-S rift branches (Figs. 4.7a-4.7c). Maximum computed values of differential strain at early stages were detected in the western rift branch, but the faster northward propagation of the eastern rift indicates a progressive migration of deformation towards the moving plate (cf. Figs. 4.7a-4.7c). Advanced stages show distributed deformation in the distal domain, with low strains localised in the rift depression, indicative of activity on internal rift faults or hyperextension in the ductile layers of the lithosphere (e.g., Manatschal, 2004) (Fig. 4.7c). Oblique-slip extensional faults associated with the crustal anisotropies decreased their activity with ongoing deformation and became completely inactive after 23 hours (~18.6 My) (Fig. 4.7c).
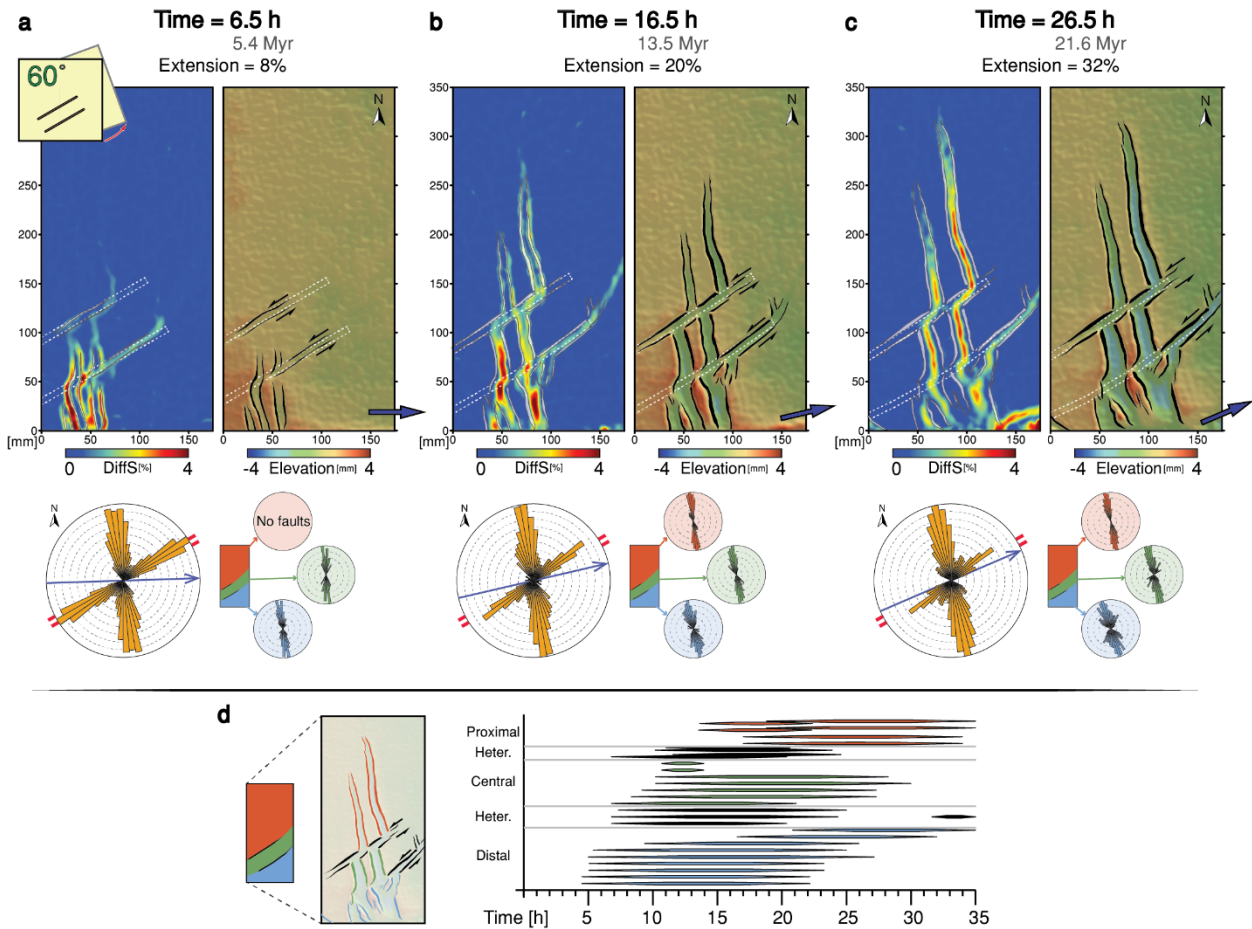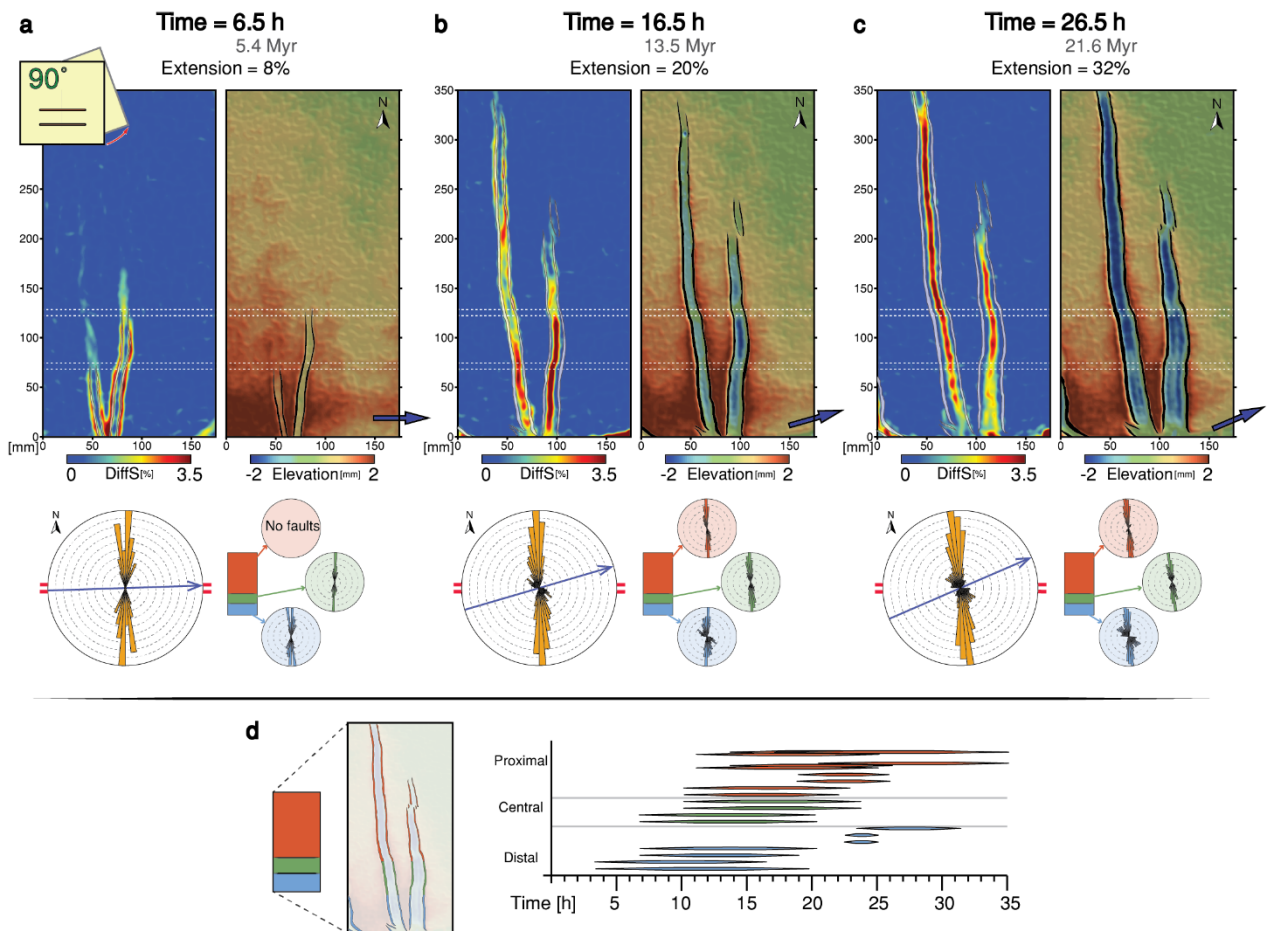
Figure 4.7 - Evolution of deformation for Model E with obliquity angle α = 60°, illustrated as in figures 4.3 and 4.4.

4.3.6 Model F (α = 90°)

Two extension-normal rift branches developed early in the experiment and propagated northward defining narrow V-shaped basins (Fig. 4.8a). The orientation of the bounding normal faults was not affected by the crustal anisotropies, but a pulsed northward progression of strain was detected in the computed differential strain field maps (Fig. 4.8a). A decrease in the amount of strain towards the north coincided with the location of the rift-perpendicular linear anisotropies (Fig. 4.8a). This suggests that deformation progression stalled in the proximity of the anisotropies and rift branches continued to propagate only after additional strain was accumulated (Figs. 4.8a-4.8b).

Early in the experiment the eastern rift branch displayed a more advanced spreading, having propagated beyond the southernmost linear weak area and subsequently slowing down in the proximity of the northern anisotropy (Fig. 4.8a). However, with ongoing deformation, the western branch grew faster and propagated northward beyond the eastern branch (Figs. 4.8a-4.8c), showing a similar progression to Model B (cf. Figs. 4.4 and 4.8).

Figure 4.8 - Evolution of deformation for Model F with obliquity angle α = 90°, illustrated as in figures 4.3 and 4.4.

Maximum computed strain values were located closer to the northern end of the model, indicating a progressive migration of deformation towards the pole of rotation (Fig. 4.8c). Differential strain measurements at the final stages do not exhibit compartmentalization of deformation, indicating that the propagation-inhibiting role of the crustal anisotropies was mostly active during the incipient rupture of the crust and not at later stages of rift deepening and propagation (cf. Figs. 4.8a-4.8c). Nevertheless, digital elevation maps display an along-axis variation in rift basin depth, with deeper sections located between the crustal anisotropies (Fig. 4.8c).

4.4 Discussion

4.4.1 Summary of results

The modelling results presented show how the presence and orientation of crustal anisotropies affects the propagation and evolution of continental rifts. The overall deformation pattern is broadly characterised by extensional structures that initiate at the southern end of the model and propagate northward towards the pole of rotation, in agreement with the general structural evolution previously

described for propagating rifts (Courtillot, 1982, 1980; Hey et al., 1980; Martin, 1984). Differences in the spatio-temporal evolution and rift architecture between experiments with similar rheological and kinematic initial conditions were solely dependent on the angle of obliquity of the crustal anisotropies, α (Fig. 4.9).

Extensional structures in models with α ≤ 30° (Models B, G, G2, C and C2) were strongly localised along the crustal anisotropies at early stages. This localisation is a result of the high angle between the anisotropies and the maximum instantaneous stretching direction and persisted throughout the experiment, although Model B (α = 0°) showed a wider distribution of deformation at advanced stages (Fig. 4.9 and 4.10). The overall fault development was greatly controlled by the linear weak sections; long, linear normal faults aligned with the anisotropies accommodated most of the extension, while only minor structures, trending approximately perpendicular to the extension direction, developed outside or beyond the linear weak areas. Displacement field evolutionary maps (Fig. 4.10) illustrate how the reactivation of the linear anisotropies as normal faults with a left-lateral component was easier when the obliquity angle was between 15° and 45°. This resulted in differential relative displacement between the distal and central domains of the experiments, which was maximum for Model C (α = 30°, clockwise) (Fig. 4.10).
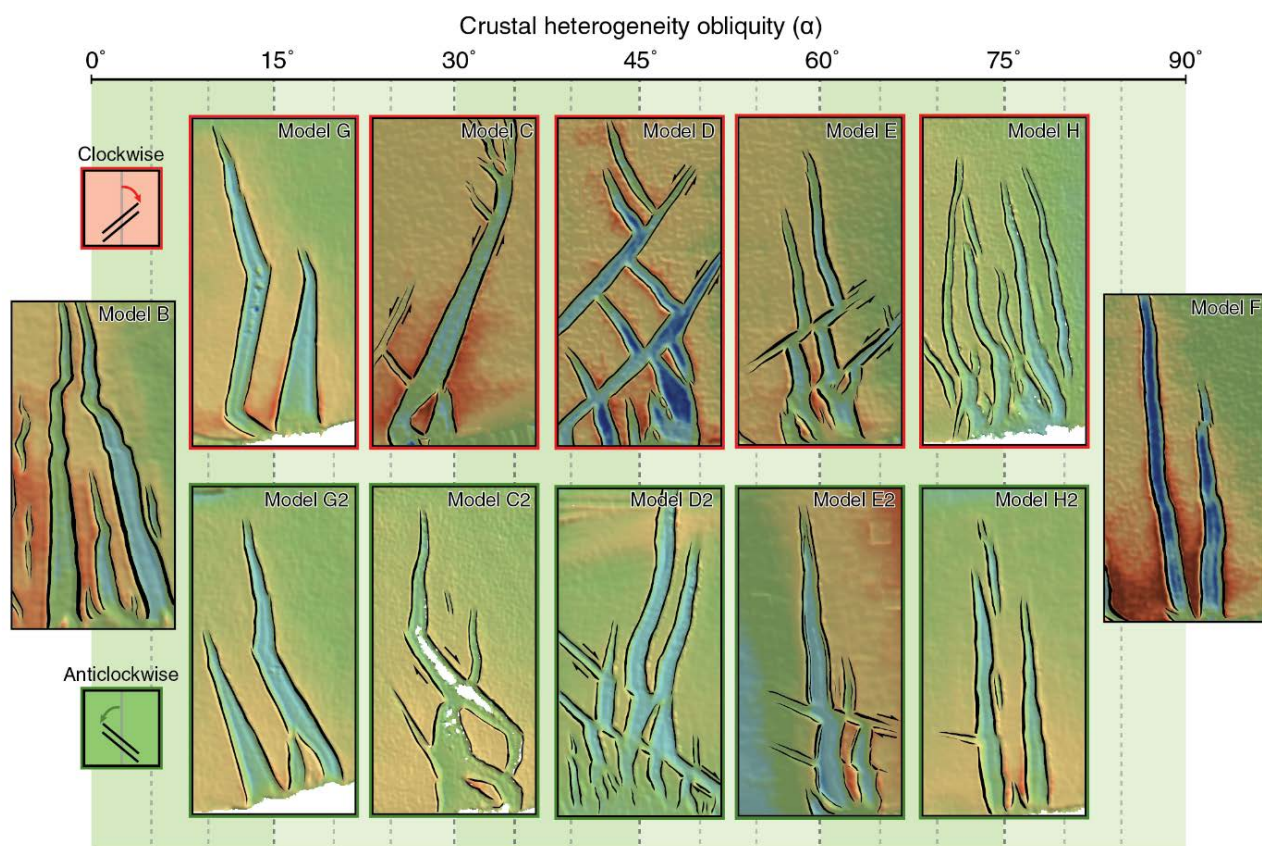
Figure 4.9 - Graphical summary of the analogue models arranged by the angle of obliquity of the crustal heterogeneities with respect to the general stretching direction, α. Line drawings of structures presented as an overlay to top-view DEMs. Comparison between clockwise and anticlockwise setting of the heterogeneities show close similarities in terms of fault pattern and final rift architecture.
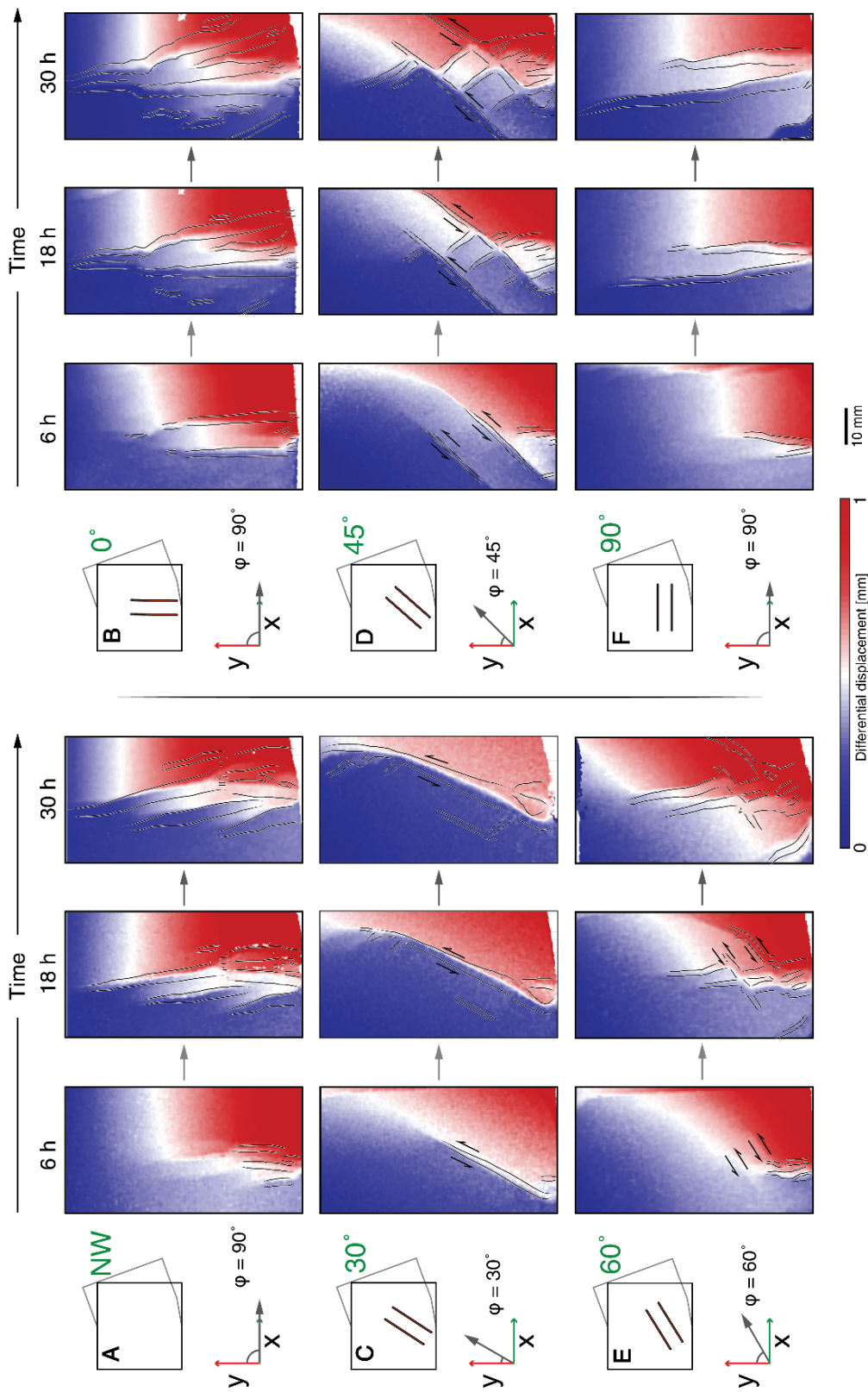
Figure 4.10 - Differential displacement for Models A to F over time. Shown field maps correspond to the displacement in a chosen direction, φ, as indicated in the bottom left panel for each model, which were calculated after decomposing absolute displacement values (see Extended Data). Colours represent the distance that the model surface has been displaced since the previous timeframe computed with the PIV, which was arbitrarily defined as 20 minutes (i.e. equivalent to ~0.3 Ma) for noise reduction and optimal visualisation (see Extended Data for details on deformation monitoring). Line drawings of interpreted structures are shown as semi-transparent black lines for reference.

Experiments with a linear anisotropy oriented between 30° and 60° (Models D, D2, E and E2) were characterised by complex interactions between the northward propagating normal faults and the crustal anisotropies. Localisation along the anisotropy was strongest at early stages, when normal fault sets with sinistral oblique-slip components developed, resulting in kinematic dislocation of the model lithosphere into discrete domains (Fig. 4.10). In both experiments, the oblique-slip activity gradually decreased with ongoing stretching and deformation was progressively transferred to extension-normal structures. This interaction resulted in rift branches that appear to have been laterally offset as they propagated northward across the anisotropies, resulting in rhombic fault-bounded domains (Figs. 4.9 and 4.10).

When α > 60° (Models H, H2 and F), the acute angle between the anisotropies and the stretching direction inhibited strain localisation and extension was almost entirely accommodated by N-S trending normal faults. The crustal anisotropies had minimal effects on fault trends during their northward propagation and induced minor lateral offsets (Figs. 4.9 and 4.10). A pulsed propagation of the extensional basins was observed only when the crustal heterogeneities were oriented parallel to the initial extension direction (Model F, Fig. 4.8). Deformation analyses show that strain accumulated in steps as it propagated along the main rift branches, and only penetrated through the pre-existing heterogeneities after a threshold strain was reached. This mechanism of propagation consequently led to deeper sections of the rifts in the vicinity of the crustal anisotropies.

4.4.2 Role of the position and orientation of heterogeneities

A complementary set of experiments was carried out with an anticlockwise orientation of the crustal heterogeneities and the same obliquity angles used above (Models C2, D2, E2, G2, H2, Table 4.2, Fig. 4.9). Similar first-order structural patterns and temporal evolutions of deformation were observed between experiments with the same angle of obliquity but opposite anisotropy orientation, with minor differences in the location of extensional faults outside the anisotropic linear zones (Fig. 4.9). While the position and relative orientation of the heterogeneities with respect to the stretching direction proves to have a significant impact, fault orientations and the influence of the crustal heterogeneities on the northward propagating rifts were comparable between experiments with clockwise and anticlockwise anisotropies.

Comparison between differential displacement field maps of selected clockwise (Models C, D and E) and anticlockwise (Models C2, D2 and E2) experiments provides insights on how the anisotropy orientation effects the sense of motion on oblique-slip fault zones (Fig. 4.11). Sinistral oblique-slip motion was detected early in the experiments when the linear anisotropies were oriented clockwise with respect to the rift propagation direction. Conversely, anticlockwise oriented linear anisotropies favoured dextral oblique-slip reactivation. The influence of the anisotropy orientation on the oblique-slip component of motion explains the differences observed in the lateral offsets of propagating rift branches between displaced domains (Fig. 4.9).
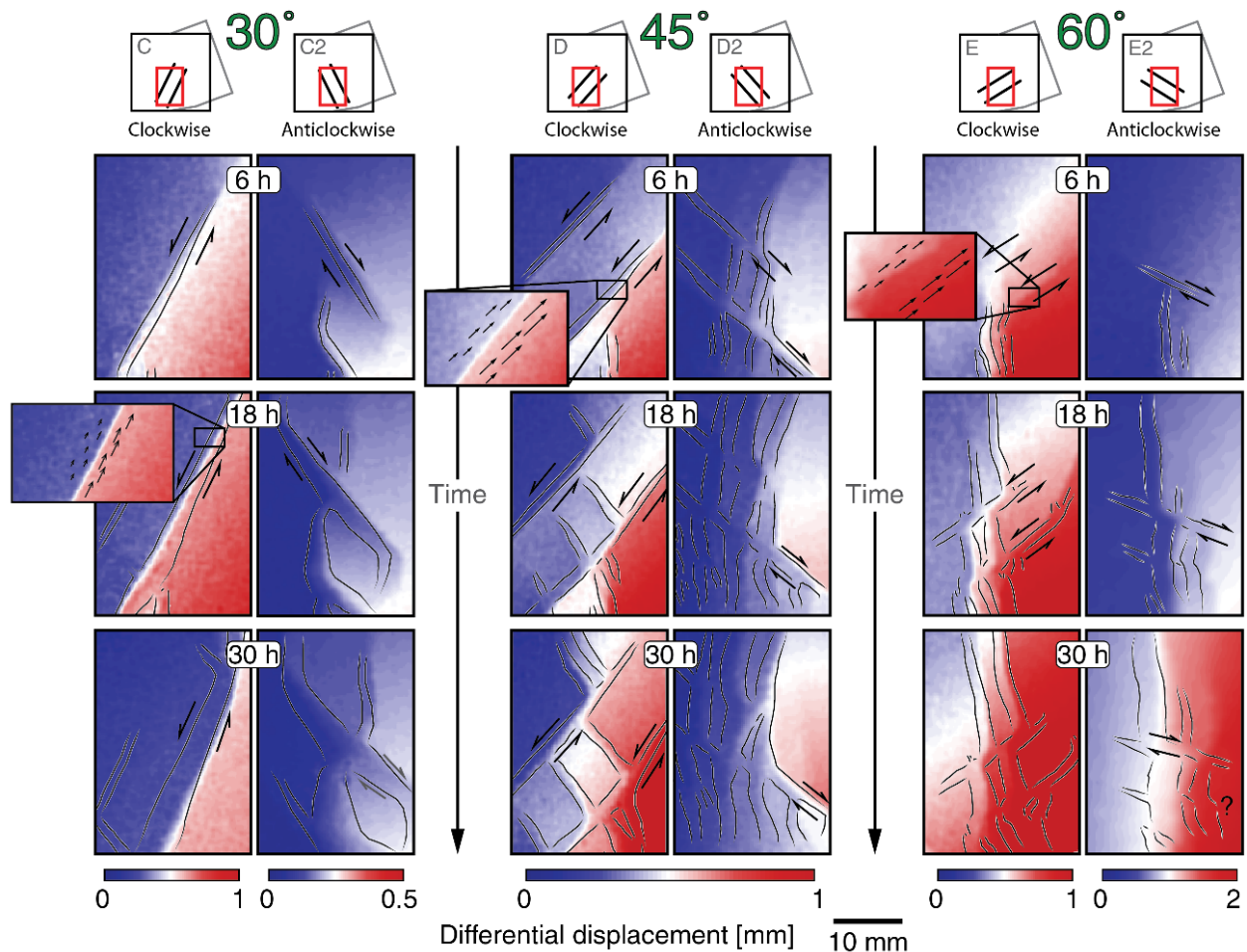
Figure 4.11 - Clockwise vs. anticlockwise comparison of differential displacement field maps for Models with α = 30° (C-C2), 45° (D-D2) and 60° (E-E2), computed and illustrated as in figure 4.10. Values correspond to the displacement parallel to the orientation of the heterogeneities (α) in order to highlight the sense of motion of the extensional structures. Small insets showing vector arrows are included to exemplify the relative amount of displacement between the different lithospheric blocks along the fault plane, from which the oblique-slip sense of motion along the crustal heterogeneities is inferred.

4.4.3 Natural examples

The experimental results can be compared to selected natural examples of continental rifts that have been affected by heterogeneous extensional stress fields and/or that experienced changes in extension direction over time. Due to the intrinsic complexity of natural rift systems, I cannot replicate all of the variables that control the evolution of continental rifts. However, I argue that our experiments provide first-order insights on the spatio-temporal evolution of propagating rifts. Here, I discuss comparisons between our experimental results and natural examples as a function of the angle of obliquity of the crustal anisotropies with respect to the extension-normal direction, α. For ease of visualization, some modelling results are mirrored and/or rotated in Figure 4.12 to compare with the natural prototypes.

4.4.3.1 Low obliquity (α ≤ 30°)

Tanganyika-Rukwa rift segments

The Tanganyika and Rukwa rift basins are located in the central segment of the eastern branch of the East African Rift System (EARS) (Fig. 4.12a). Present-day kinematics and recent fault activity is well constrained by geodetic, geophysical and focal mechanism data (e.g., Delvaux and Barth, 2010; Morley et al., 1992; Stamps et al., 2008), but the timing of events that led to the formation of these NW-SE oriented narrow basins remains controversial (Morley, 2010 and references therein). It is widely accepted that a series of NW-SE rift basins of Karoo age (Permo-Triassic) (Delvaux, 2001; Morley et al., 1992; Morley, 1999) played an important role in controlling the Oligocene to Present (Roberts et al., 2012) rifting of the Tanganyika-Rukwa area. The general direction of extension affecting the EARS is a contentious issue (Bellahsen et al., 2013 and references therein) (Fig. 4.12a), but recent studies support general E-W regional extension (Corti et al., 2007; Delvaux and Barth, 2010; Heidbach et al., 2010; Morley, 2010). Additionally, two-dimensional numerical simulations indicate that larger rifts may capture rigid cratons, which can lead to local rotations (Koehn et al., 2008). These rotations accommodate the orthogonal motion of larger plates and are consistent with the present-day anticlockwise rotation of the Victoria plate - containing the Tanzania craton - with respect to the Nubian plate (Calais et al., 2006; Koehn et al., 2008; Stamps et al., 2008) (Fig. 4.12a). The resultant obliquity between Karoo-age pre-existing discontinuities and the general direction of extension, in addition to the rotational component linked to the Victoria plate, makes the Tanganyika and Rukwa rifts a good analogue for the initial conditions of experiments with low obliquity (B, C, C2, G, G2, Figs. 4.9, 4.12a and Extended Data Figs. 4.2-4.4).

The Tanganyika-Rukwa rifts are narrow, deep basins bounded by a series of anomalously long, straight NW-SE trending faults that follow pre-existing heterogeneities (Corti et al., 2007; Morley et al., 1992; Ring, 1994) (Fig. 4.12b). Pure dip-slip motion characterised these main boundary faults at early stages (Delvaux, 2001; Foster and Jackson, 1998), indicating local stretching approximately perpendicular to the pre-existing heterogeneities (Fig. 4.12b). A similar behaviour was observed in our low obliquity experiments, which developed long, linear, dip-slip normal faults (Fig. 4.9 and Extended Data Figs. 4.2-4.4). The overall rift pattern in these models was reached at early stages and remained almost constant throughout the whole experiment (Figs. 4.4 and 4.5). This is also consistent with field observations in the Tunganyika-Rukwa rifts, which suggests that deformation pattern was relatively static since its initial formation (Morley, 2002).
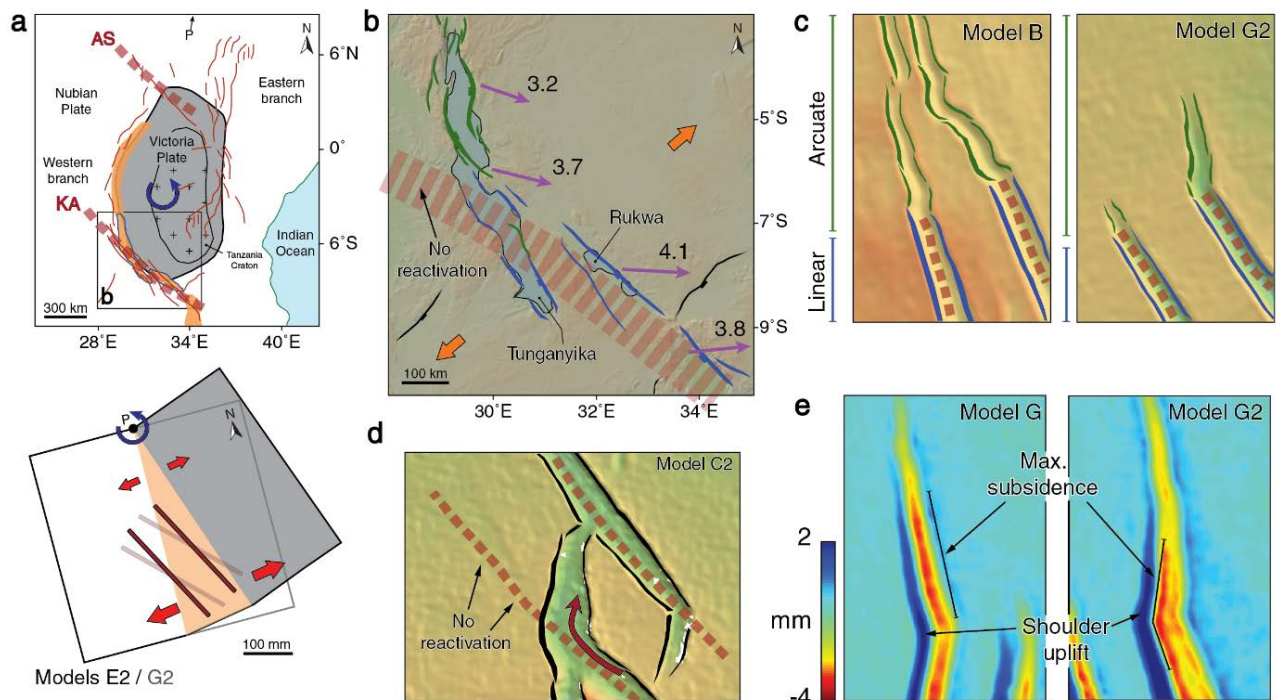
Figure 4.12 - Comparison with nature: Tanganyika-Rukwa rift segments. A. Cartoon illustration of the regional geological setting (top) and comparison with low obliquity models ($\alpha \leq 30°$) (bottom) Blue arrow indicates the sense of rotation of the moving plate (in grey). Red arrows illustrate the regional stretching direction. Model results are rotated 15° for comparison. B. Structural map of the Tanganyika-Rukwa rifts (after Morley et al., 1992). Orange arrows illustrate the inferred stretching direction at the moment of rift initiation (e.g., Ebinger et al., 1989) and purple arrows indicate Victoria-Nubia relative motion in mm/yr (Stamps et al., 2008). Red dashed lines indicate the location of the inferred pre-existing crustal weaknesses, inherited from a Karroo-age extensional tectonic stage. C. Top view DEMs of Model B and G2 showing the change in fault style from linear faults along the anisotropic area to short, arcuate faults beyond them. D. Example of a propagating rift branch ignoring a pre-existing heterogeneity, as interpreted in Central Lake Tanganyika. E. Subsidence/uplift maps of the timeframe 18-28 hours for models G and G2.

The deflection of the Tanganyika rift from a NW-SE direction to a more N-S orientation can be explained by the closer proximity of the northward propagating rift to the relative pole of rotation of the Victoria plate (Stamps et al., 2008) (Fig. 4.12a). All of our low obliquity experiments showed strong initial localisation along pre-existing heterogeneities, followed by later deflection of propagating rifts towards the pole of rotation (Figs. 4.4, 4.5 and 4.9). Models B, C2, G and G2 bear partial resemblance to this segment of the EAR. Only Lake Rukwa and the southern section of Lake Tanganyika were strongly influenced by pre-existing heterogeneities (Morley, 2010, 1999), which favoured the formation of long linear faults near the anisotropy but led to more sigmoidal or arcuate normal faults in the central and northern Lake Tanganyika areas (Fig. 4.12b). Similar observations were replicated in Models B and G2 (Fig. 4.12c). The development of these sigmoidal faults probably occurred synchronously with the northward propagation of the rift (Macgregor et al., 2017). Smaller scale discrete fabrics in the upper crust also contribute to this pattern, as shown by previous analogue models of fabric reactivation (Corti et al., 2007). Moreover, sediment thicknesses in the Rukwa rift appear to be less than in the more

extension-orthogonal central Tanganyika rift (Chorowicz, 2005; Corti et al., 2007; Misra and Mukherjee, 2015) (Fig. 4.12b). This is similar to the evolution of Models G and G2, in which the extensional basins that formed perpendicular to the stretching direction were deeper (Fig. 4.12e and Extended Data Figs. 4.2-4.3). The two heterogeneity-related rift branches accommodated most of the extension early in the experiments, but soon after deformation was transferred to a single rift branch with larger fault throw and therefore more accommodation space for sedimentation (Fig. 4.12c). The experimental evolution of deformation also indicates strong uplift of the western rift shoulders, which compares to the higher elevations in the western areas of Lake Tanganyika and Lake Rukwa (cf. Figs. 4.12b and 4.12e), which were probably aided by magma underplating (Morley et al., 1992).

A series of Pleistocene NE-SW trending extensional structures (e.g., Usangu rift and Lake Mweru) formed perpendicular to the main boundary faults of the Tanganyika-Rukwa rifts (Ebinger, 1989; Morley et al., 1992) (Fig. 4.12b). Field observations also suggest a relative change in the extension direction that reactivated earlier dip-slip faults as strike- and oblique-slip faults (Morley, 1999; Ring, 1994). The absence of normal faults with intermediate trends between the Tanganyika-Rukwa rifts and the Pleistocene NE-SW oriented extensional structures supports an abrupt change in the extension direction. Models B, C, C2, G, and G2 show a history of rift propagation that is partially analogous to the Oligocene-Pleistocene stages of the Tanganyika-Rukwa rifts. However, they do not explain the perpendicular structures that developed later, which implies a significant change in the extension direction that did not occur in our experiments. Such an abrupt change also explains dextral strike-slip reactivation of the main NW-SE trending faults (Ring, 1994). Since strain tends to keep accumulating in the same locations (Morley, 2002), the pre-Pleistocene normal faults acted as pre-existing heterogeneities that facilitated their reactivation under the new stretching regime. At the same time, our modelling results show that the left-lateral motion between domains was strongest when the weaknesses where favourably oriented (i.e. 30°- 45° clockwise, Fig. 4.11), and is consistent with a ~60° to 90° change in the extension direction (Delvaux et al., 1992; Ring et al., 1992; Versfelt and Rosendahl, 1989) (Fig. 4.12b).
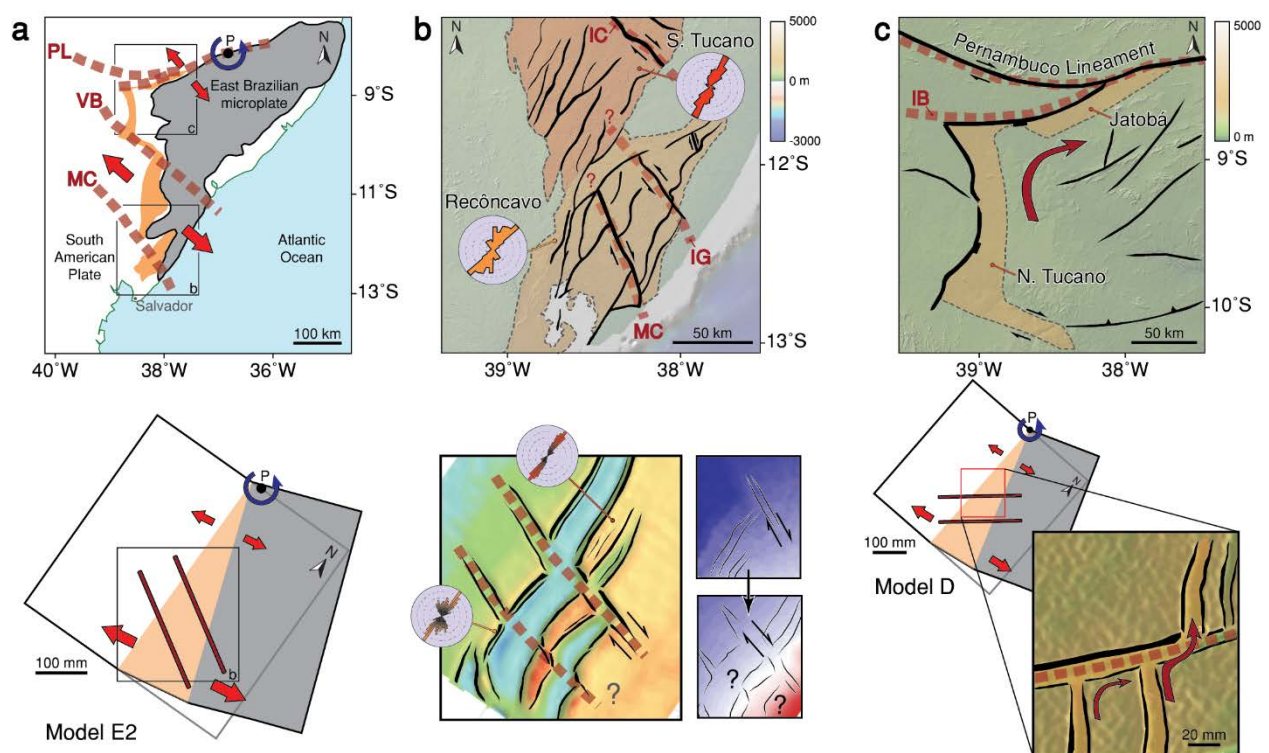
4.4.3.2 Intermediate obliquity (30° < α ≤ 60°)

Recôncavo-Tucano-Jatobá Basins

The Recôncavo-Tucano-Jatobá rift basins of Northeastern Brazil formed during the Neocomian during the opening of the South Atlantic Ocean (Heine et al., 2013; Milani and Davison, 1988). Previous studies (e.g., Darros de Matos, 2000, 1992; Milani and Davison, 1988) have shown that complex structural framework of these rift basins was strongly controlled by pre-existing crustal heterogeneities associated with E-W to NE-SW trending Pan-African shear zones (Magnavita, 1992; Milani, 1987; Fig. 4.13a). Several interpretations have proposed an anticlockwise rotation of the East Brazilian microplate (e.g., Milani and Davison, 1988; Szatmari and Milani, 1999) as a possible kinematic model to explain the spatio-temporal evolution of these basins, which opened from south to north (Fig. 4.13a). These conditions are comparable to experiments with intermediate anisotropy obliquity (Models D [α = 45°] and E [α = 60°]) (Fig. 4.13a). Fault trend analysis in the southernmost Recôncavo rift basin shows a dominant N 25° E oriented normal fault network and a secondary N 30° W trending strike-slip fault

group (Milani and Davison, 1988). The final architecture of Model E2 shows a very similar fault distribution both in terms of both geometry and sense of motion (Fig. 4.13b).

Differential strain measurements of experiments with α = 60° show a top-view sigmoidal strain pattern as rifts propagated across the crustal anisotropies (Fig. 4.7 and Extended Data Fig. 4.5), similar to the inferred deflecting role of pre-existing basement weaknesses in the Recôncavo rift (Milani and Davison, 1988). Such crustal anisotropies may have localised major transfer zones in the Recôncavo-Tucano-Jatobá system (Fig. 4.13b). Two of these shear zones dislocated the eastern section of the Recôncavo rift into three distinct compartments (Milani and Davison, 1988), similar to the displacement maps for our intermediate obliquity models (Fig. 4.11). The overall movement sense of reactivated shear zones and its change over time is difficult to determine in nature without corresponding kinematic indicators or crosscutting relationships. Analysing the evolution of laboratory experiments therefore provides insights into the complex rifting history of natural examples such as Northeastern Brazil.

Figure 4.13 - Comparison with nature: Recôncavo-Tucano-Jatobá basins. A. Cartoon illustration of the regional geological setting (top) and comparison with intermediate obliquity model E2 (α = 60°); (bottom) Blue arrow indicates the sense of rotation of the moving plate (in grey). Red arrows illustrate the regional stretching direction. Model results are rotated 35° for comparison. PL: Pernambuco Lineament, VB: Vaza Barris, MC: Mata-Catu. B. Structural map of the Recôncavo basin (after Milani and Davison, 1988) (top) and comparison with Model E2 (bottom). Red dashed lines indicate the location of the inferred pre-existing crustal weaknesses, associated to shear zones of Pan-African age. Rose diagrams show a good match between fault distribution in nature and in the model. MC: Mata-Catu, IT: Itaporanga, IC: Itapicuru. C. Structural map of the Jatobá basin (after Milani and Davison, 1988) and comparison with Model D (α = 45°). Example of propagating rift branch terminating abruptly against a linear crustal heterogeneity. IB: Ibimirim.

Field observations and differences in the throw of boundary faults support a dextral strike-slip motion on the NW section of the Mata-Catu transfer fault (Milani and Davison, 1988) (Fig. 4.13b). However, there are few kinematic constrains for its SE section. A sinistral sense of motion has been suggested, based on the present-day structural pattern (Milani and Davison, 1988). Our modelling provides additional constraints, since displacement field maps for model E2 ($\alpha = 60°$, anticlockwise) show a similar structural pattern to the southeastern end of the Mata-Catu fault (Fig. 4.13b). The model results indicate constant dextral oblique- and strike-slip motion on transfer zones in the northernmost sections of the experiment (Fig. 4.13b), as inferred for the Itapicuru, Itaporanga, and north of the Mata-Catu transfer zones (Milani and Davison, 1988). However, the distal domain shows more distributed deformation and a more complex evolution. At later stages in the experiment there is a local increase in displacement rates southwest of the southernmost crustal heterogeneity (Fig. 4.13b). A possible explanation for this is progressive rotation of the moving plate. While initially unfavourably oriented, the pre-existing weakness was eventually reactivated with a dextral sense of motion (Fig. 4.13b). At later stages, a shift in the relative orientation between the stretching direction and the heterogeneity orientation may have caused a reactivation with a sinistral sense of motion (Fig. 4.13b), which correlates well with observations in the eastern end of the Recôncavo rift (Milani and Davison, 1988).

The main boundary faults north of the Jatobá Graben terminate abruptly against the Ibimirim fault, which is associated with the major ENE-WSW trending Pernambuco Lineament (Fig. 4.13c). Similar behaviour is observed in Model D ($\alpha = 45°$). Rift propagation in the central domain halted when the northernmost crustal anisotropy was reached and strain was relayed onto the transfer zone (Fig. 4.6), as probably occurred in the Jatobá Graben-Ibimirim fault interaction zone (Milani and Davison, 1988). The North Tucano Graben has also been interpreted to cut through a basement weakness due to the latter's unfavourable orientation for reactivation (de Matos, 1992). This is analogous to models F ($\alpha = 90°$) and H ($\alpha = 75°$, anticlockwise), in which the crustal anisotropies did not affect the northward trend of rift propagation (Fig. 4.9).

The inherent complexity of the Northeastern Brazil rift system makes it difficult to test in a single analogue experiment. However, the intermediate to high obliquity between the general extension direction and the pre-existing basement structures makes it a good reference to compare with several experimental results (i.e. Models D, E, F and H). Detailed analysis of the experiments presented here provide plausible explanations for why planar basement weaknesses were either ignored or followed by the evolving rifts in the Recôncavo-Tucano-Jatobá system.
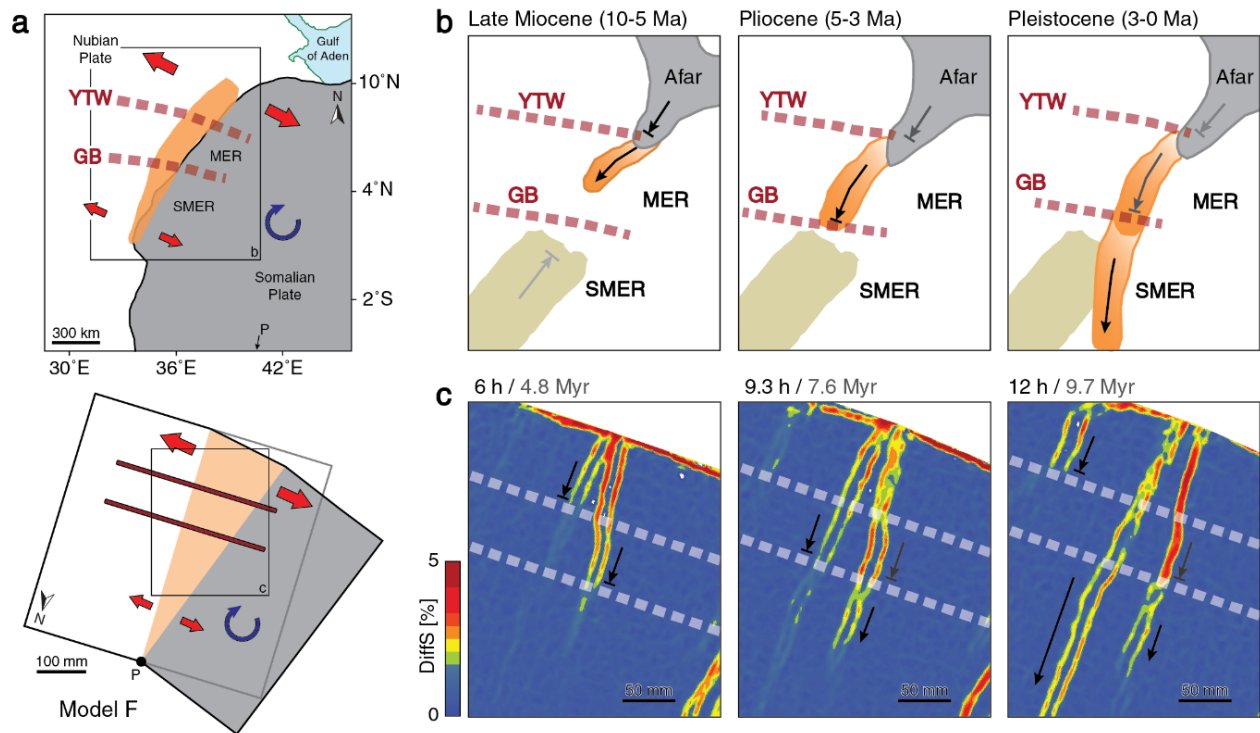
4.4.3.3 High obliquity ($\alpha > 60°$)

Main Ethiopian Rift

The NE-SW trending Main Ethiopian Rift (MER) is located between the Afar depression and the Kenya rift in the Eastern Branch of the East African Rift System (Fig. 4.14a). The intricate network of extensional faults and volcanic history of the MER reveal a complex tectono-magmatic evolution (e.g., Bonini et al., 2005; Corti, 2009; Ebinger et al., 2000). The role of two major lineaments in the evolution and propagation of the MER is of particular interest to this study.

The approximately E-W oriented Goba-Bonga (GB) and Yerer-Tullu Wellel (YTW) lineaments (Fig. 4.14a) are parallel to the general stretching direction (Abebe et al., 1998). The Somalian plate has been rotating clockwise with respect to the Nubian plate since the Middle Miocene (Bonini et al., 2005; Stamps et al., 2008) (Fig. 4.14a). This scenario is therefore analogous to the boundary conditions in model F (α = 90°) (Fig. 4.14a).

Figures 4.14 - **Comparison with nature: Main Ethiopian Rift (MER). A. Cartoon illustration of the regional geological setting (top) and comparison with high obliquity model F (α = 90°); (bottom) Blue arrow indicates the sense of rotation of the moving plate (in grey). Red arrows illustrate the regional stretching direction. Model results are mirrored and rotated ~160° for comparison. B. Schematic evolution of the main rift segments of the MER (after Bonini et al., 2005). C. Differential strain field map evolution for equivalent downscaled experimental timesteps, showing the hindering effect of the heterogeneities in rift propagation.**

Extensional structures developed in Southern Afar during the Middle Miocene formation of the Afar triple junction but did not propagate beyond the YTW lineament at that time (Bonini et al., 2005) (Fig. 4.14b). This is consistent with the evolution of Model F, in which propagation of initial rift-parallel structures appeared to slow down when they approached the first crustal anisotropy (Fig. 4.14c). Extensional deformation continued to propagate southwards beyond the YTW lineament and into the actual MER in the Late Miocene as a result of clockwise Somalian plate rotation (Bonini et al., 2005; Collet et al., 2000) (Fig. 4.14b). At this time, rift propagation was towards the SW, perpendicular to the general direction of extension, as observed in the Model F (Fig. 4.14c). It has been suggested that the presence of the YTW led to a minor right lateral offset of the rift segments (Corti, 2009; Keranen and Klemperer, 2008), which was also observed in Model F (Fig. 4.14c). Southwestward rift propagation was again hindered during the Pliocene by the transversal GB lineament, while the Southern MER (SMER) underwent a tectonic pause (Bonini et al., 2005) (Fig. 4.14b). The overall evolution of the MER shows a

good match with Model F, in which progressive rotational stretching resulted in the propagation of rift branches across transversal crustal anisotropies (see Figure 4.8 for complete evolution). While the anisotropies appear to have little influence in the orientation of the extensional structures (Fig. 4.12), they did play an important role stalling rift propagation, resulting in a pulsed rift history (e.g., Bosworth, 2015)., The final stages of the MER evolution during the Pleistocene were characterised by propagation of the rift across the GB lineament and subsequent reactivation of Early Miocene structures in the SMER (Bonini et al., 2005) (Fig. 4.14b).

The role of the GB lineament as a partial impediment to rift propagation can also be inferred from the SMER during the Early Miocene. Northward propagation of the SMER, associated with deformation in the Kenya Rift (Bonini et al., 2005), was temporarily halted when it reached the GB lineament. At this time, the SMER entered a tectonic hiatus and the onset of clockwise rotation of the Somalian Plate caused the southward development of the MER as described above (Fig. 4.14b). The development of locked zones has been identified in oceanic rifts (e.g., Courtillot, 1982; van Wijk and Blackman, 2005) but their origin in continental rifts remains poorly understood.

4.5 Conclusions

Kinematic rotation in three-dimensional laboratory experiments simulates realistic initial conditions for natural extensional settings with laterally heterogeneous stress fields. The use of a stereoscopic PIV system to monitor experiments provides key insights on the temporal evolution of rift development and propagation across crustal heterogeneities. The results illustrate how the orientation and obliquity of rheological heterogeneities in the crust have a strong influence on fault trends and lengths, the sense of movement on reactivated oblique-slip zones, and on the role crustal anisotropies play in dislocating the crust into kinematically independent blocks.

The experiments show that extension-normal and low obliquity heterogeneities ($\alpha \leq 30°$) favour the formation of anomalously long normal faults, which reach their near-final length early in the evolution of rifts in comparison to cases with a homogeneous lithosphere. Low to intermediate obliquity angles ($\sim15° \leq \alpha \leq 45°$) oriented clockwise with respect to the extension direction favour sinistral oblique-slip reactivation of linear anisotropies and subsequent dislocation of the crust into blocks with different displacement rates. Such dislocation is most effective and long lived when $\alpha = 30°$. Conversely, comparable obliquity angles with an anticlockwise orientation results in conditions that favour reactivation of heterogeneities as dip-slip or dextral oblique-slip normal faults. Nevertheless, the amount of oblique-slip or dip-slip deformation in all experiments varies over time and specific interpretations must be made for each particular scenario. Overall, our results demonstrate that the lateral sense of motion on faults is determined by the relative orientation of crustal anisotropies with respect to the stretching direction. Finally, both clockwise or anticlockwise orientated, very high obliquity crustal anisotropies ($\alpha > 60°$) have little influence on the trend of faults in spreading rifts. However, they may cause pulses in rift propagation, which results in along-axis variations in terms of subsidence rates, fault throws and depocentre depths.

4.6 Extended Data

Deformation and strain monitoring

Surface deformation was monitored with a stereoscopic particle image velocimetry (PIV) (Adam et al., 2005). Successive PIV photographs were taken at 2 min intervals during the experiments.

Following Molnar et al., (2017), I computed high-resolution displacement fields based on the strain tensor,

$$E_{ij} = \frac{\partial v_i}{\partial_j} \text{ with } i \in \{x, y, z\} \text{ and } j \in \{x, y, z\} \quad (4.1)$$

and calculated the gradient in the vector components i (x, y and z) along the j axis (x, y and z). I considered the 2-D strain matrix

$$\begin{vmatrix} E_{xx} & E_{xy} \\ E_{yx} & E_{yy} \end{vmatrix} \quad (4.2)$$

and defined the normal strain on surface, DiffS, as the largest eigenvalue of the matrix:

$$DiffS = \frac{(E_{xx} + E_{yy})}{2} + \sqrt{\left| \frac{(E_{xx} - E_{yy})^2}{4} + \frac{(E_{xy} - E_{yx})^2}{4} \right|} \quad (4.3)$$

I calculated differential data and then obtained cumulative data as the summation of the differential data. The time interval between the PIV images (2 min) sets the minimum increment possible to compute. However, due to the slow velocity at which the experiments are run, no discernible patterns are noticed when computing strain at such increments. In order to optimise the visualization and reduce noise, I chose a 10-image increment, or 20-minute differential time, which represents ~0.3 Myr in nature. Differential displacement fields (Figs. 4.10 and 4.11) were also computed with this time interval. I decomposed the absolute displacement field vectors into components parallel to the orientation of the heterogeneities (α), as exemplified in Extended Data Figure 4.1. I then compared the magnitude of the vectors at both sides of the oblique-slip faults (insets in Figs. 4.10 and 4.11) to infer the sense of motion.

Extended data figures
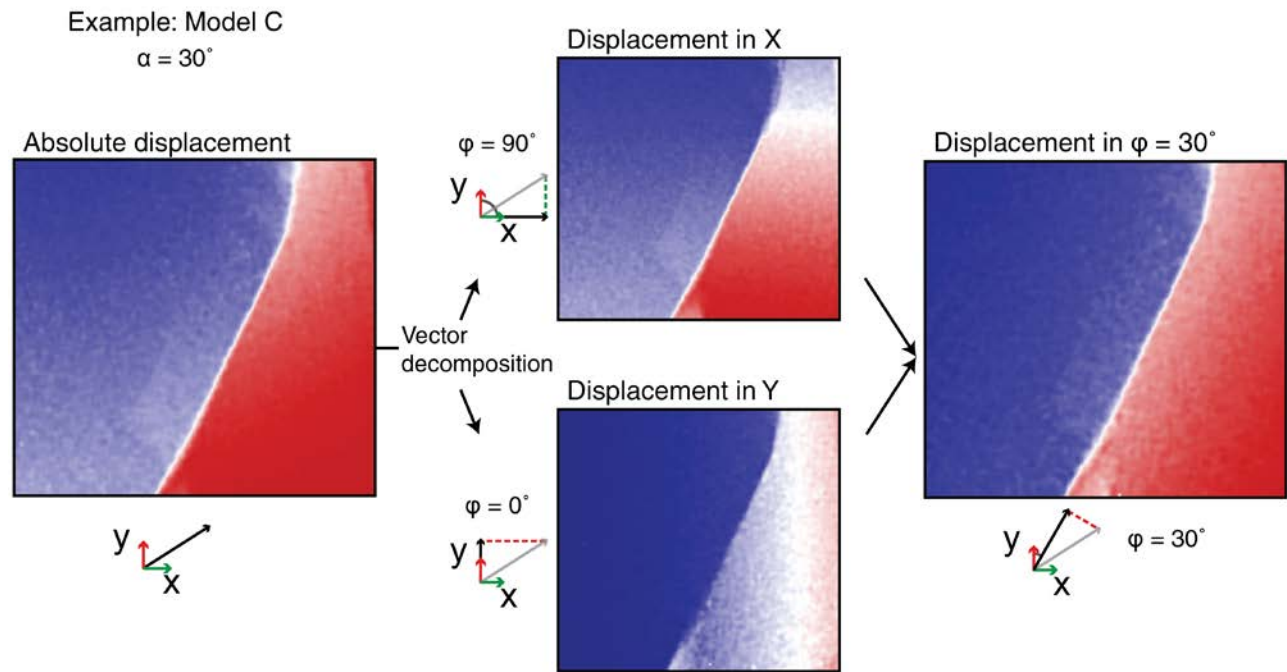
ED Figure 4.1 - Workflow and visual representation of differential displacement field maps calculations. In order to identify the sense of motion in the faulted areas, the absolute displacement field maps were decomposed into displacement in X and displacement Y. Employing simple trigonometry the displacement along the angle of orientation of the heterogeneities (Model C, $\alpha = 30°$ shown as an example) was calculated and used to quantify the sense of motion along both sides of the faulted area. A similar procedure was done for all experiments for the preparation of figures 4.10 and 4.11.
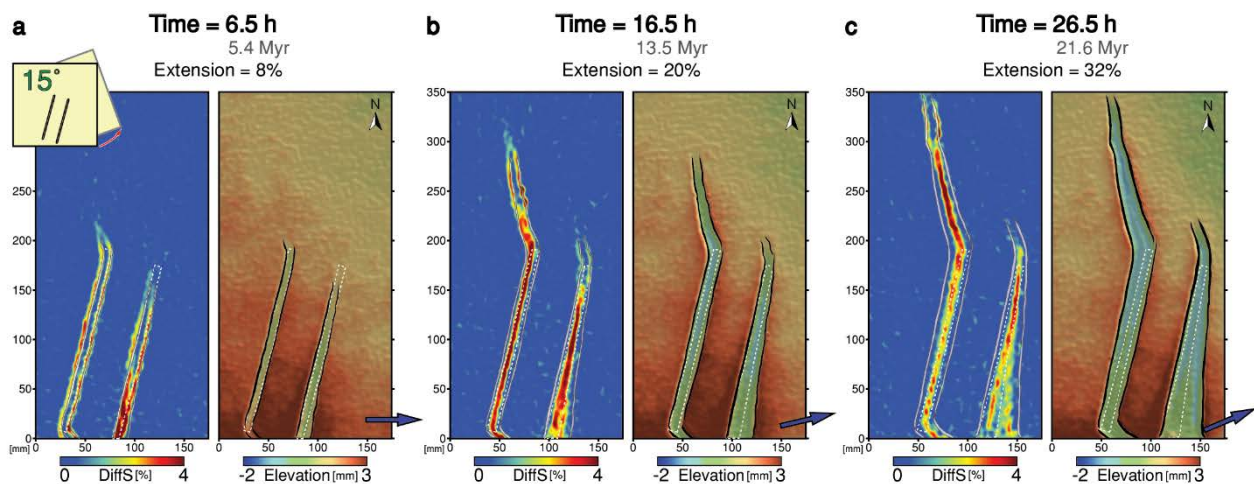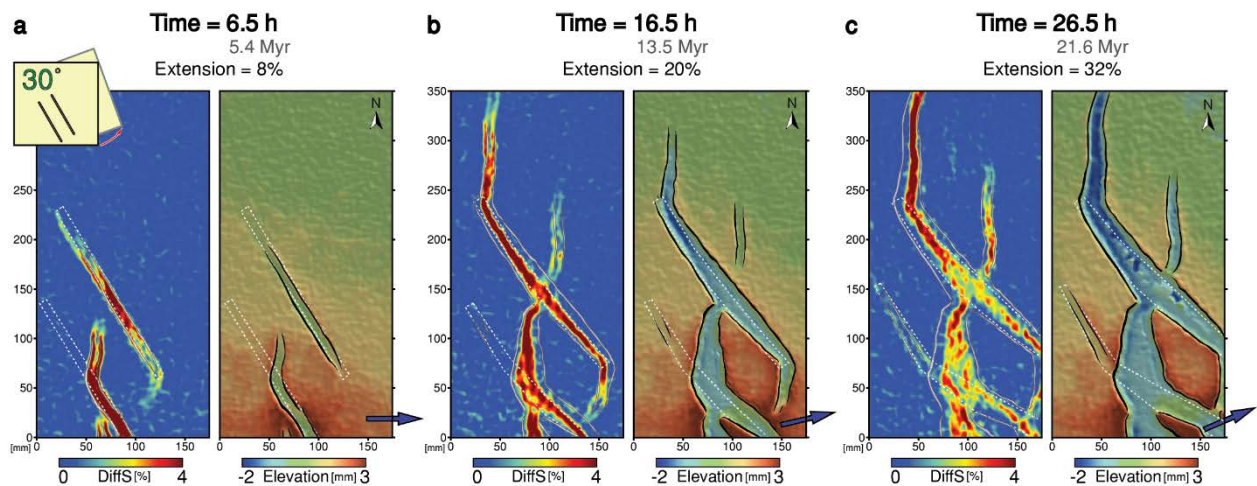

ED Figure 4.2 - Evolution of deformation for Model G with angle $\alpha = 15°$, oriented clockwise, illustrated as in figure 4.3. Location of the crustal heterogeneities is illustrated as a dashed white line in panels A, B and C.
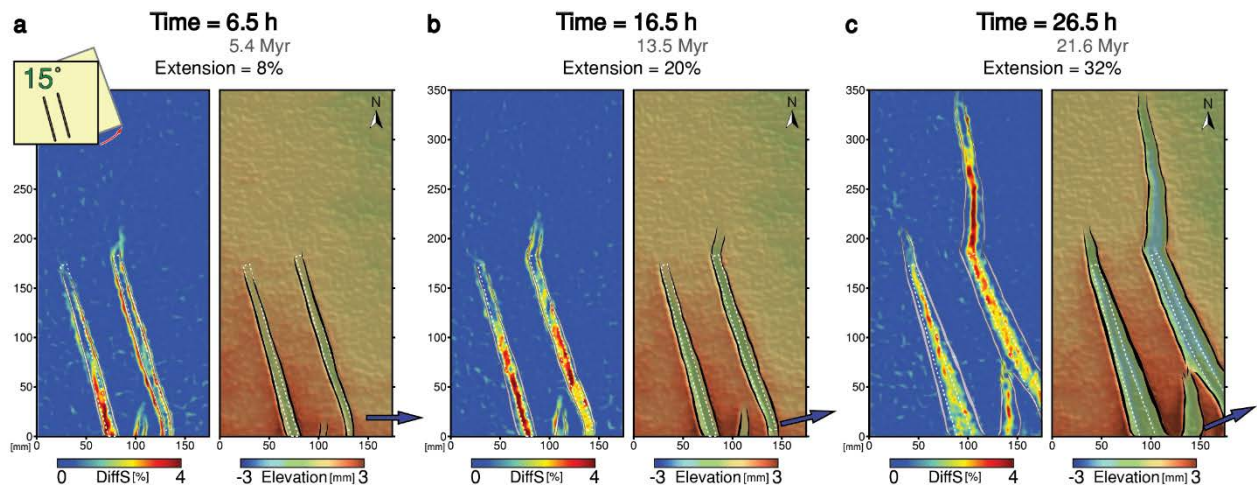
ED Figure 4.3 - Evolution of deformation for Model G2 with angle α = 15°, oriented anticlockwise, illustrated as in figure 4.3. Location of the crustal heterogeneities is illustrated as a dashed white line in panels A, B and C.

ED Figure 4.4 - Evolution of deformation for Model C2 with angle α = 30°, oriented anticlockwise, illustrated as in figure 4.3. Location of the crustal heterogeneities is illustrated as a dashed white line in panels A, B and C.
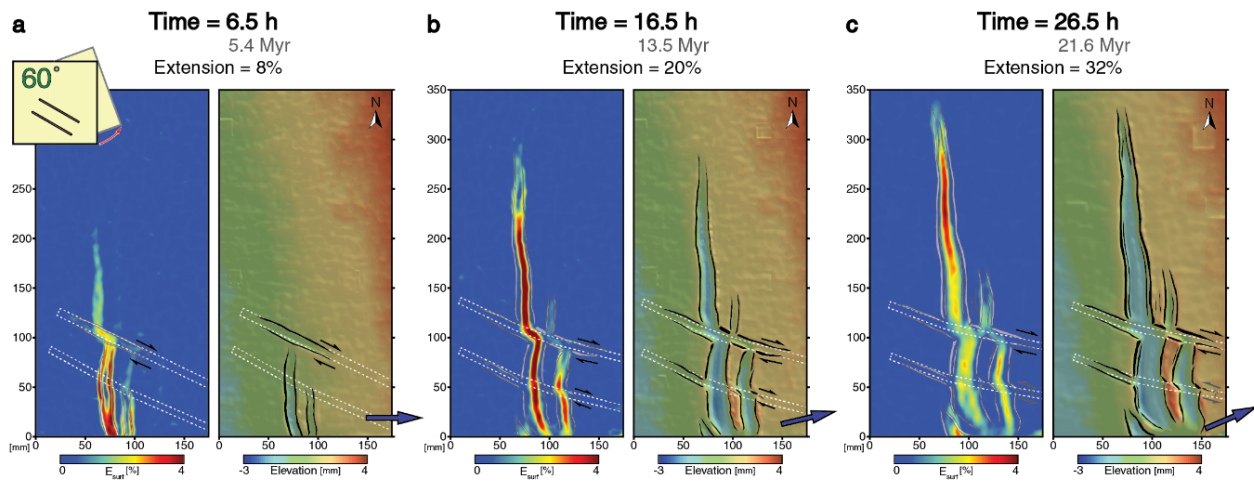
ED Figure 4.5 - Evolution of deformation for Model E2 with obliquity angle α = 60° and anticlockwise orientation, illustrated as in panel A of figure 4.3.

Chapter 5

# The Red Sea revisited: inferences from 3D analogue modelling of propagating rifts

Abstract

The Red Sea represents the best natural example to study the transition from continental rifting to ocean initiation. Numerous studies have shown that the pre-rifting conditions of the African and Arabian lithospheres were characterised by mantle and crustal heterogeneities. However, their influence on rift development and propagation remains uncertain. I use three-dimensional (3D) brittle-ductile analogue laboratory experiments with a rotational boundary condition to investigate the effect of three different configurations: (i) pre-existing rheological heterogeneities in the crust, (ii) in the lithospheric mantle, and (iii) in both. Comparison between experiments is used to define a hierarchy of influence, whereby crustal heterogeneities are outranked by lithospheric mantle heterogeneities. However, certain natural features can only be explained by the combined effects of both types of heterogeneities. Our experiments reproduce the geological history of the Red Sea and provide key insights on its deformation history in space and time. Our experimental results lend support to previous inferences on how pre-existing weak zones in the lithosphere have determined the present-day morphology of the Red Sea. When applied to other natural examples, our findings provide significant new insights on the role of crustal and lithospheric heterogeneities during continental rifting in general.

5.1 Introduction

How continental rifts evolve in space and time is one of the most enigmatic questions in tectonics and geodynamics. This is because it is a complex three-dimensional problem that is influenced by external boundary conditions, coupled with the presence of pre-existing heterogeneities in the continental crust. Continental rifts evolve via several key phases: (1) a stretching stage in which normal faults in the brittle upper crust accommodate most of extension; (2) a thinning mode in which deformation is transferred to the ductile lower crust and/or upper mantle; and (3) exhumation of the mantle, in magma-poor rifts, or voluminous basaltic magmatism, in magma-rich rifts, followed by the onset of seafloor spreading (e.g., Hill, 1991; Lavier and Manatschal, 2006). The Red Sea (Fig. 5.1) is the best example of where an active incipient ocean basin can be studied on Earth, since all the consecutive phases of rifting leading to break up and seafloor spreading are occurring simultaneously along the rift axis.
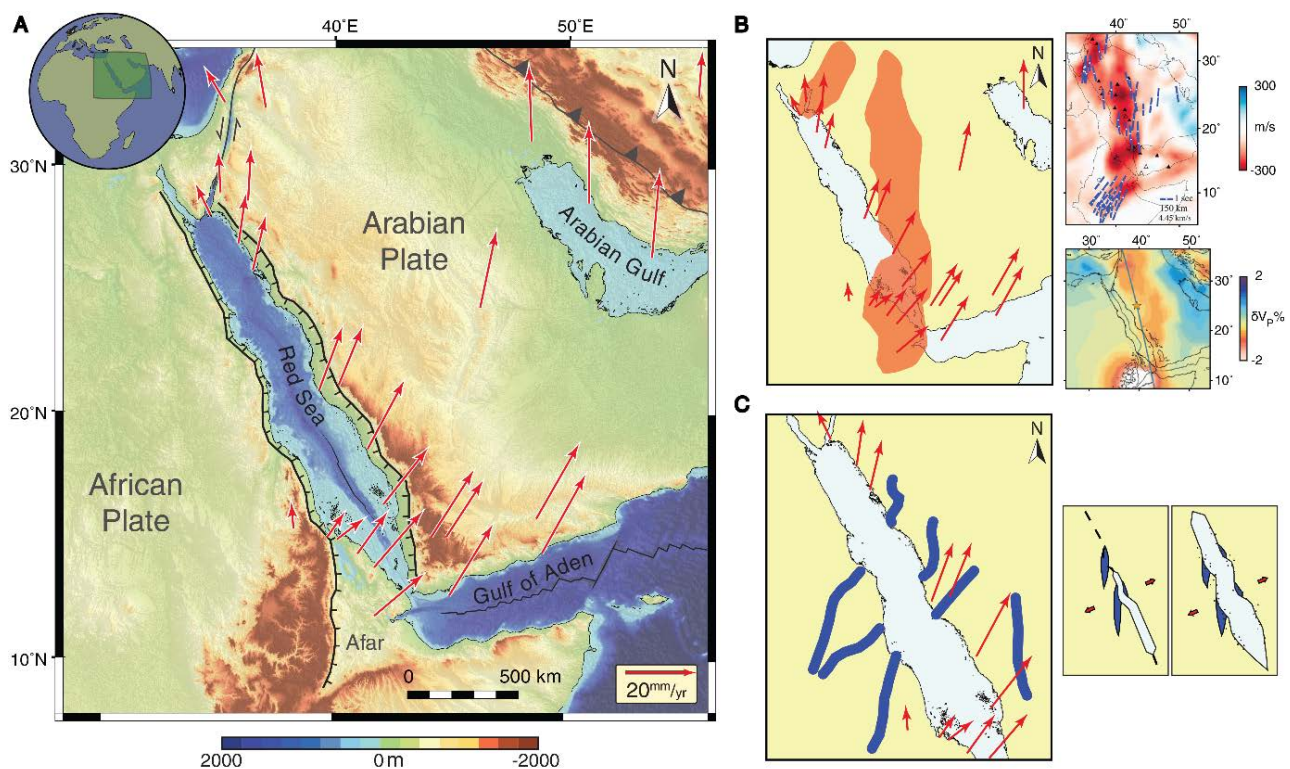
Figure 5.1 - Red Sea regional map and nature of pre-existing mechanical heterogeneities in the lithosphere. A. Bathymetric and topographic map of the Red Sea-Gulf of Aden rift system. GPS vectors (ArRajehi et al., 2010) indicate an anticlockwise rotation of Arabia with respect to Africa. B. Sketch drawing of the approximate location of the channelled Afar plume (after Chang et al., 2011) (left panel) and examples of tomographically imaged structure beneath the study area (Chang et al., 2011; Faccenna et al., 2013) (right panel). C. Sketch drawing indicating the location of Neoproterozoic suture and shear zones in the African and Arabian plates (after Johnson and Woldehaimanot, 2003) (left panel) and simplified cartoon interpretation of Dixon et al. (1987).

After more than 140 years of continuous scientific observation, starting with Suess' (1875) first expedition to the rift valleys of Africa, the general evolution of the Red Sea-Gulf of Aden rift system is well constrained (e.g., Bosworth et al., 2005). However, the influence of pre-existing vertical and lateral

variations in the mechanical properties of the lithosphere (Fig. 5.1) on the Cenozoic evolution of the Red Sea remains uncertain. These mechanical variations have been associated with Precambrian suture zones (Crane and Bonatti, 1987; Dixon et al., 1987), attenuated crust along the Mozambique Belt (Kazmin et al., 1978), or mantle plume channelling and thermal weakening (Chang et al., 2011; Ebinger and Sleep, 1998) (Fig. 5.1). Inherited structures from previous tectonic phases have been the focus of studies in both the Red Sea and other rift systems (e.g., Rhine graben [Michon and Merle, 2000], Rio Grande rift [Morgan et al, 1986], Main Ethiopian Rift [Abebe et al., 1998], Malawi rift [Ring et al., 1994]). Most of these studies provide strong local evidence for how earlier geological events controlled the localisation of rift-related structures and their evolution.

Scaled analogue laboratory modelling has made fundamental contributions to the simulation, analysis and understanding of the mechanisms of rifting (e.g., Benes and Davy, 1996; Corti et al., 2003; Vendeville et al., 1987). Laboratory experiments have been successful in replicating aspects such as the leading cause of separation of Arabia from Africa (Bellahsen et al., 2003), the origin of the Danakil Block (Molnar et al., 2018, [Chapter 3]; Souriot and Brun, 1992), the northward propagation of the Dead Sea rift (Mart and Dauteuil, 2000), fault reactivation in the Gulf of Suez (Bellahsen and Daniel, 2005) and oblique rifting in the Gulf of Aden (Autin et al., 2010, 2013). Although inherited structures have long been recognised as an important aspect of the tectonics of the Red Sea (e.g., Crane and Bonatti, 1987; Dixon et al., 1987; Ebinger, 1989; Johnson and Woldehaimanot, 2003), laboratory experiments that validate their inferred role as stress-guides, barriers to axial propagation or precursors to transform faults have not been carried out.

In this study, I employ laboratory experiments to test how different types of pre-existing rheological heterogeneities influence the evolution of deformation of the Red Sea rift and its overall morphology. I establish a hierarchy of controlling mechanical and kinematic influences on the rift geometry and the evolution of the Red Sea. Finally, I compare our results with the Red Sea rift and other natural examples and discuss the implications of our experiments for understanding how rifts propagate and interact with pre-existing rheological heterogeneities.

5.2 Tectonic setting

Early studies proposed that tensional forces induced by convection currents in the mantle were responsible for the opening of the Red Sea (Carey, 1958). Although many recent studies continue to support the key role of the Afar mantle plume, they suggest that it acted as a trigger rather than the main leading cause of the opening of the Red Sea-Gulf of Aden rift system (e.g., Buiter and Torsvik, 2014 and references therein). Conversely, it is generally agreed that far-field extension exerted by the slab pull of the Arabian plate subducting under the Eurasian plate acted as the dominant force that led to the formation of the Red Sea (e.g., Bellahsen et al., 2003). Therefore, the closure history of the Neotethys Ocean and the geodynamics of the Makran subduction zone (Fig. 5.2) played a major role in the opening of the Red Sea.
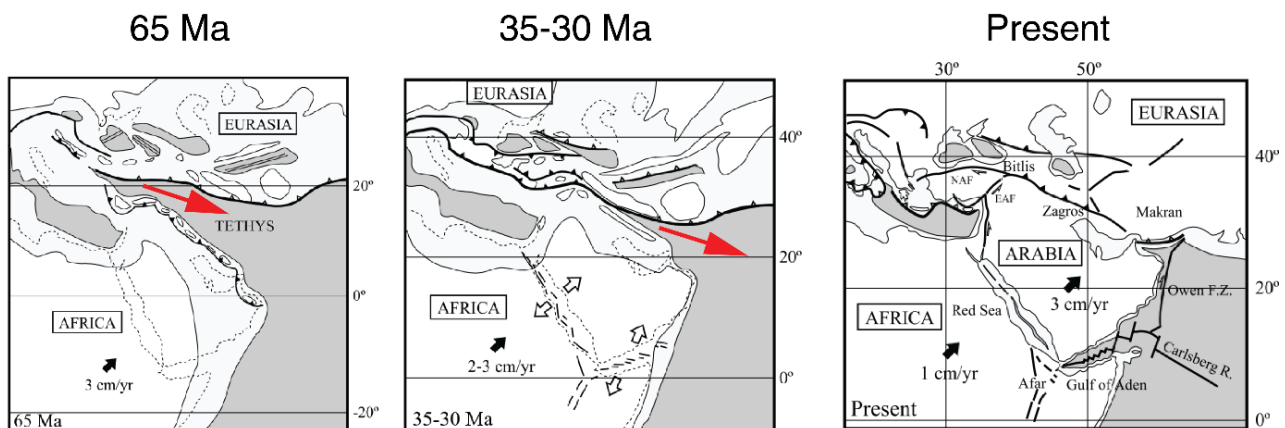
Figure 5.2 - Cartoon illustration of the Paleogene tectonic evolution of the Tethys Ocean (from Bellahsen et al., 2003). Red arrow indicates the direction in which the Tethys Ocean was consumed.

The Neotethys oceanic lithosphere was consumed from west to east in the Paleogene (Dercourt et al., 1986; 1993) (Fig. 5.2), such that continent-continent collision between the Arabian and Eurasian plates occurred first in the northwest and propagated south eastwards. Subduction of oceanic lithosphere is still active in the Makran subduction zone (Kazmi and Jan, 1997; Quittmeyer et al., 1984). The stronger slab pull force in the southeast resulted in an anticlockwise rotational motion of Arabia with respect to Eurasia, and it is considered to be the main driver for opening of the Red Sea (Bellahsen et al., 2003) (Fig. 5.3). McQuarrie et al. (2003) established that convergence between the Arabian and Eurasian plates has been approximately constant at 20-30 mm/yr since 56 Ma. ArRajehi et al. (2010) indicate that the motion of Arabia relative to Africa has increased by ~70% since 13 Ma. This acceleration coincides with a large-scale reorganisation event that involved the abandonment of the Gulf of Suez as an active rift after the collision of Arabia with Eurasia, resulting in the transfer of motion to the Aqaba-Levant transform fault (Fig. 5.3). Commensurate with this re-organisation was a switch in the external boundary forces with the rift shifting from approximately rift-normal movement to more oblique, and finally rotational extension that was established in the Middle Miocene (Bosworth et al., 2005; Ehrhardt et al., 2005) (Fig. 5.3). Estimates of Cenozoic rates of extension/compression can be compared to current extension rates. Present-day extension rates in the Northern Red Sea are ~7 mm/yr and in the Southern Red Sea they are ~16 mm/yr (ArRajehi et al., 2010; Chu and Gordon, 1998; McClusky et al., 2010; McQuarrie et al., 2003). It is established that the rotational component of Arabia Plate has been sustained over the last ~13-14 Ma (ArRajehi et al., 2010; McClusky et al., 2010).

The chronological evolution of the opening of the Red Sea remains controversial. Original studies using fission track data (Omar and Steckler, 1995) concluded that the rupture occurred synchronously along its length. The widespread intrusion of mafic dikes that occurred along the entire length of the rift during the Early Miocene supported this view (Sebai et al., 1991). Conversely, evidence for continental rift initiation in the southern Red Sea at ~27 Ma (Bosworth, 2005; Hughes et al., 1991) and in the Gulf of Suez at ~24 Ma suggests fast but diachronous rupture (Bosworth, 2005 and references therein). The south to north rupture is also supported by flow patterns of submarine salt glaciers mapped with new high-resolution bathymetric data (Augustin et al., 2014). It is now interpreted that the Red Sea opened diachronously from south to north, but at such high propagation rates that it is difficult to resolve in the geological record. Full oceanisation has not occurred in the far south of the

Red Sea, suggesting that sea-floor spreading is either propagating south or it is about to jump into the Afar Depression (Eagles et al., 2002).
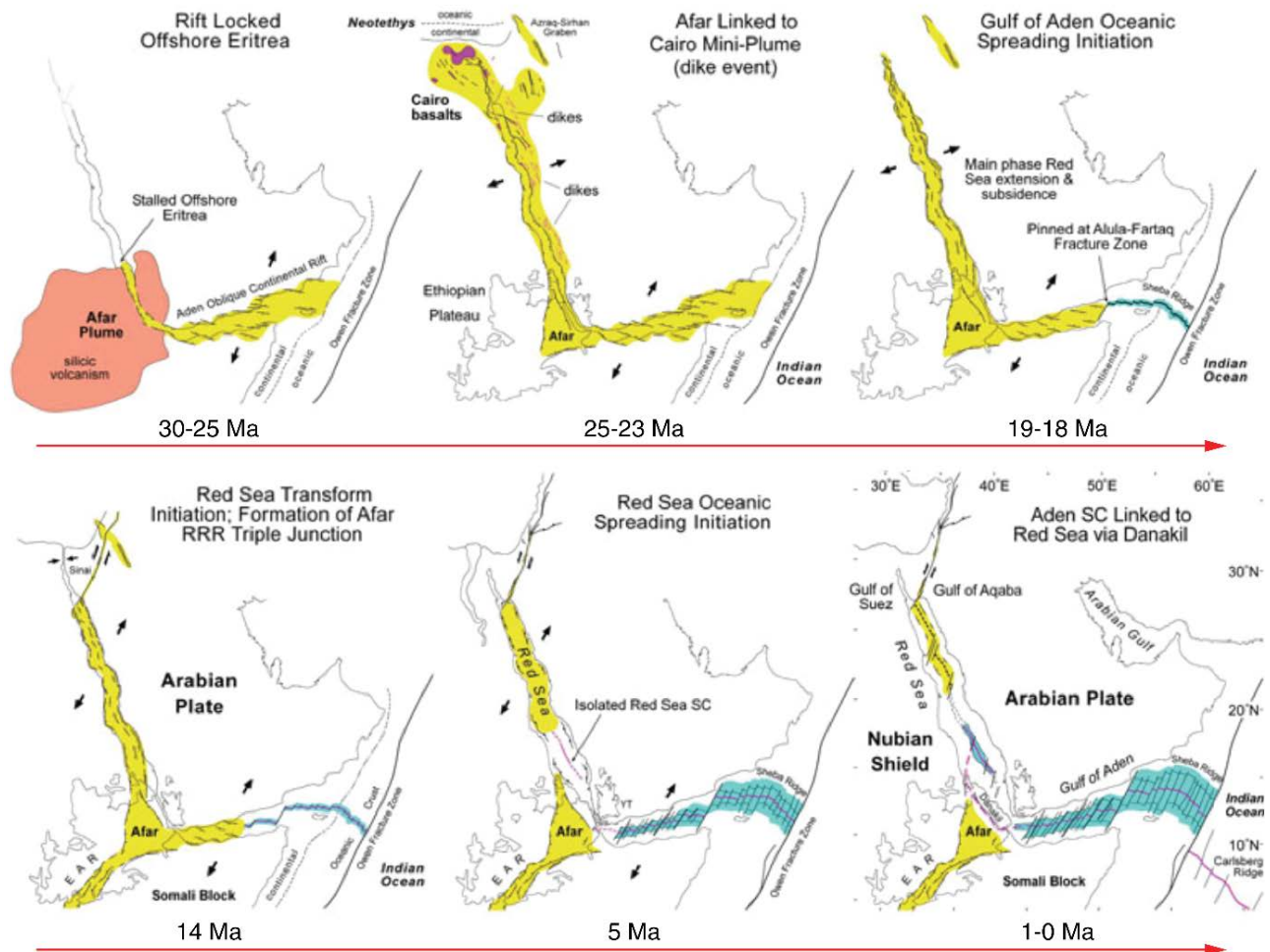
Figure 5.3 - Schematic evolutionary diagram showing stages from continental rifting, propagation and sea-floor spreading of the Red Sea-Gulf of Aden area (from Bosworth et al., 2015).

The presence of pre-existing variations in the rheological properties of the lithosphere along the Red Sea axis could have additionally hindered its northwestward propagation, acting as analogues to the 'locked zones' described first by Courtillot (1982). Bosworth (2015) suggested a hybrid mechanism, in which rifts could form by a combination of lateral propagation and instantaneous rupture along its axis. Despite different views on this matter, it is commonly interpreted that seafloor spreading began at ca. 5 Ma in the southern Red Sea (e.g., Axen et al., 2001; Joffe and Garfunkel, 1987; Pallister et al., 2010) and that the overall present day spreading of the Red Sea is characterised by northwest propagation (Fig. 5.3). However, recent evidence for episodic sea-floor spreading (Almalki et al., 2014) and for independent behaviour of spreading centres (Ligi et al., 2012) indicates that the geodynamics of the Red Sea are more complex than previously interpreted.

The leading causes of the characteristic morphology of the Red Sea, with its narrow shape bounded by perfectly matching sinusoidal rift escarpments (Figs. 5.1 and 5.3), are also uncertain. It is generally accepted that the general rift architecture and geometry of the Red Sea rift has been mainly controlled by the governing far-field stresses and relative plate motions throughout its entire tectonic history (e.g.,

Bosworth et al., 2005 and references therein) (Fig. 5.3). However, several lines of evidence point to a more complex explanation for the sinusoidal rift escarpments and basin geometry. Bonatti (1985) initially considered that pre-existing weak areas in the lithosphere were precursors to a large-offset oceanic transform. Dixon et al. (1987) interpreted a series of Neoproterozoic sutures as zones of lithospheric weakness that acted as stress guides, deflecting the northwestward propagation of the Red Sea. Crane and Bonatti (1987) similarly interpreted a series of paleo-shear zones as barriers to axial propagation. These NNE-SSW oriented morphotectonics features that intersect the Red Sea (Figs. 5.1 and 5.3) have been inferred from observations in foliated basement gneisses and are associated with the Panafrican orogeny (e.g., Khalil and McClay, 2009; Stern, 1981). Their influence has been reassessed by several studies, in which it was proposed that the pre-existing structures helped to localise normal faults on the African side of the rift (Kenea et al., 2001), or generated a pulsed rifting mode (Bosworth, 2015), or affected the distribution of asthenospheric upwellings (Ligi et al., 2012). Nevertheless, their influence on the evolution of the Red Sea-Gulf of Aden rift system is still unclear.

Several geophysical and seismic tomography studies support the idea of the channelling and northern flow of the Afar plume beneath Arabia (e.g., Chang et al., 2011; Faccenna et al., 2013; Hansen and Nyblade, 2013; Rolandone et al., 2013). This large-scale phenomenon potentially caused thermal weakening of the upper mantle. Since the channelling could have followed previously thinned sections in the lithosphere associated with approximately linear ancient rifts (Ebinger and Sleep, 1998), this weaker section of the upper mantle is sometimes regarded as an approximately linear feature (e.g., Chang et al., 2011; Molnar et al., 2017). The opening of the Red Sea therefore appears to be influenced by two different scales and depth extents of heterogeneities. By using three-dimensional (3D) analogue laboratory modelling, this study aims to evaluate the role of rheological heterogeneities in both the crust and the lithospheric mantle in order to improve our understanding of the structural and geodynamic evolution of the Red Sea.

5.3 Methods

I performed laboratory experiments following the approach of Molnar et al. (2017, [Chapters 2-4]). Our scaled 3D models consist of a three-layer, brittle-ductile model lithosphere that is constructed to sit within two U-shaped acrylic walls with internal dimensions of 44 x 44 cm (Fig. 5.4). A mixture of granular materials with a Mohr-Coulomb behaviour (e.g., Byerlee, 1978; Davy and Cobbold, 1991) was used to simulate the brittle upper crust and Polydimethylsiloxane (PDMS) was used to model the ductile lower crust. A mixture of PDMS, Plasticene® and hollow glass microspheres (e.g., Cruden et al., 2006; Molnar et al., 2017) was used to simulate the lithospheric mantle (Fig. 5.4). The 3-cm thick model lithosphere floats isostatically on a lower viscosity, higher density model asthenosphere simulated by a solution of Natrosol and sodium chloride in water (e.g., Boutelier et al., 2016; Davaille, 1999) contained within a 65 x 65 x 20 cm acrylic tank (Fig. 5.4). Some experiments incorporated a linear weak zone in the lithospheric mantle representing a lithospheric-scale heterogeneity, which was simulated by a lower viscosity PDMS-Plasticene mixture (Fig. 5.4). Discrete pre-existing crustal anisotropies were simulated by positioning cylindrical seeds of PDMS on top of the homogeneous lower crust (e.g., Le Calvez and Vendeville, 2002; Zwaan et al., 2015). These linear weak zones were incorporated to the models with

orientations chosen to match natural observations and are defined by the angle, α, between the extension-normal direction and the trend of the weakness (Fig. 5.4).
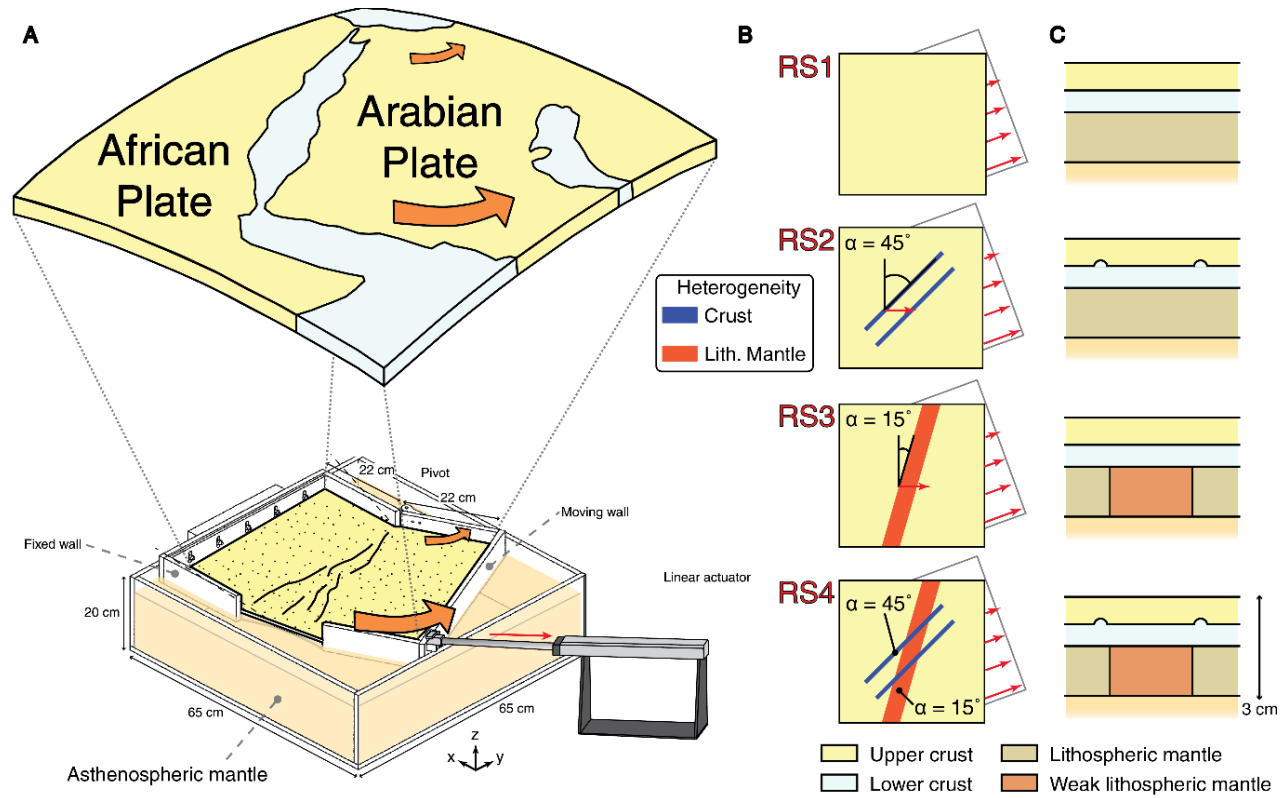
Figure 5.4 - Model setup and initial conditions. A. Drawing of the experimental setup (after Molnar et al., 2017) and comparison with the geodynamic setting of the African and Arabian plates. B. Top view graphical summary of the initial conditions of the models discussed in this study. C. Schematic cross sections corresponding to the initial rheological layering for each model shown in B.

The anticlockwise motion of Arabia with respect to Africa is recreated by imposing rotational extension on the model lithosphere about a fixed pivot point (proxy for Euler pole of rotation), located on the "north" side of the tank (Fig. 5.4). One wall is fixed to the side of the tank (hereafter referred to as the fixed plate; Fig. 5.4) and the other wall (hereafter referred to as the moving plate; Fig. 5.4) is pulled by a linear actuator at constant rates, with values approximately scaled to nature (e.g., ArRajehi et al., 2010; McClusky et al., 2010). Scaled lithospheric thicknesses were chosen from the results seismic refraction experiments in the region (Almakli et al., 2014; Gettings et al., 1986).

I adopted a model-to-nature length scale ratio of $L^* = L_m/L_n = 4 \times 10^{-7}$ (subscripts m and n refer to model and nature, respectively) such that a natural crustal thickness of 35 km is scaled down to 14 mm in the models. Considering a lower crust density of $\rho_n \approx 2760$ kg/m³ and a model upper crust density $\rho_m \approx 980$ kg/m³, a density scaling factor $\rho^* = \rho_m/\rho_n = 0.355$ km is defined. I set a viscosity scaling factor of $\eta^* = \eta_m/\eta_n = 2 \times 10^{-17}$ and since all the experiments were carried out in the normal field of gravity (1 g) the gravity scale ratio is $g^* = g_m/g_n = 1$. The time scaling factor is subsequently obtained from $t^* = \eta^*/\rho^* g^* L^* = t_m/t_p = 1.41 \times 10^{-10}$ such that 1 hour in the experiment corresponds to ~0.8 Ma in nature. A high-resolution particle imaging velocimetry (PIV) and digital photogrammetry monitoring system (e.g., Adam et al., 2005) was used to quantify surface strain and topography. An extensive description of the

experimental design, model construction, materials, scaling and deformation monitoring technique is presented in Molnar et al. (2017, [Chapter 2]).

5.4 Results

The main advantage of geodynamic modelling is that the effects of the controlling parameters can be isolated and quantified by performing different experiments with almost identical initial conditions and, in our case, by varying the type and obliquity of the pre-existing rheological heterogeneity. Accordingly, here I first summarise the evolution of deformation of previous experiments of rotational extension with (1) a homogeneous reference lithosphere, (2) two 45° trending linear crustal weaknesses, and (3) a 15° oriented linear weakness in the lithospheric mantle (Molnar et al., 2017, [Chapters 2 and 4]) (Fig. 5.4). I then present new experiments in which the pre-existing crustal and lithospheric mantle rheological heterogeneities are combined, and finally compare the results in detail to the evolution of the Red Sea.

5.4.1 Model RS1 (Homogeneous reference lithosphere)

Rotational extension in a homogeneous model lithosphere was initially accommodated by a series of symmetric rift basins trending sub-parallel to the stretching direction (Fig. 5.5a; 5 hours). The bounding normal faults of these narrow basins propagated laterally towards the pole of rotation and resulted in the classic V-shaped geometry of propagating continental rifts (e.g., Martin, 1984; Vink, 1982) (Fig. 5.5a; 10 hours). After 10 hours of rotational deformation, strain was gradually transferred to areas closer to the pole of rotation and two additional extension-normal rift branches formed in the centre of the model and propagated both north and south (Fig. 5.5a; 10 hours).

The overall rift architecture at this stage is already different with that inferred for the Red Sea. The general northward propagation of deformation in the models matches interpretations for the Red Sea, but the distribution of extensional structures was broader in the models than in the natural scenario (cf. Figs. 5.1 and 5.5a; 10 hours). Although the Red Sea rift basin is also wider in the south (e.g., Ghebreab, 1998; Fig. 5.1), extension is not accommodated by evenly spaced narrow rift basins as observed in model RS1 (Fig. 5.5a). In the experiment, rift boundary faults were always oriented perpendicular to the extension direction, while the sigmoidal shape of the main rift escarpments in the Red Sea indicate a different evolution. Extensional structures in the experiment continued to localise strain at more advanced stages of deformation, which resulted in the gradual deepening and widening of individual basins (Fig. 5.5a; 26 h). Additionally, the temporal evolution of differential strain (Chapter 4) indicates a north eastward migration of deformation, which also differs from the northwest propagation of deformation of the Red Sea (e.g., Augustin et al., 2014).
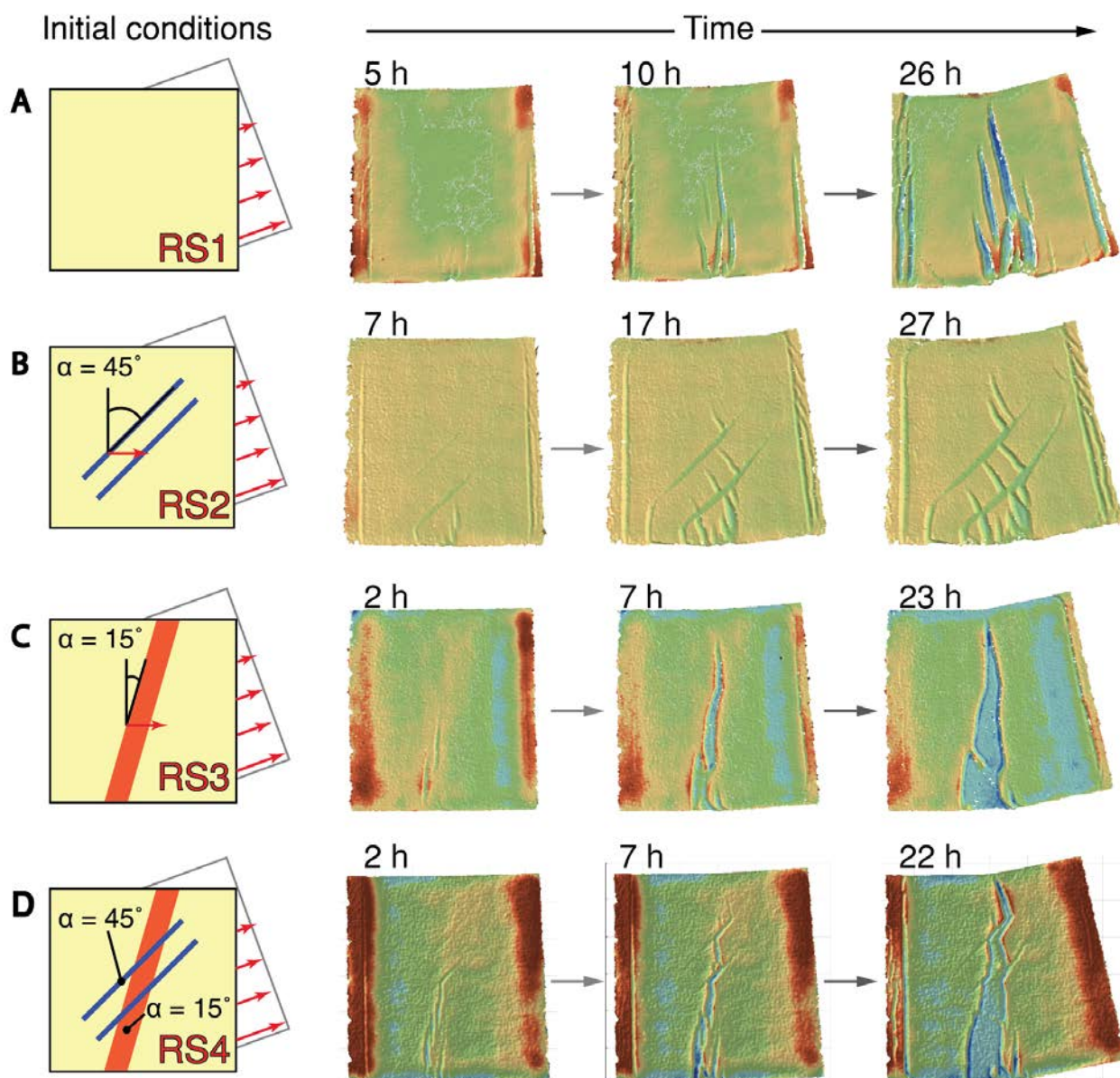
Figure 5.5 - Initial boundary conditions displaying the position and obliquity of the linear heterogeneities and summary evolutionary diagram showing top-view digital elevation models of experiments with (A) reference homogeneous lithosphere, (B) 45° oriented crustal weaknesses, (C) 15° trending linear weak lithospheric mantle, and (D) combined presence of crustal and lithospheric mantle heterogeneities.

5.4.2 Model RS2 (Crustal heterogeneities with α = 45°)

The inclusion of two N45°E oriented crustal heterogeneities resulted in the partitioning of deformation into a series of extension-normal narrow rift basins - similar to those observed at early stages in model RS1 - and long, linear extensional faults in the vicinity of the weaknesses (Fig. 5.5b). Analysis of differential displacement field maps of the experiment (Chapter 4) indicate a component of sinistral oblique-slip on the heterogeneity-related structures, which is consistent with the sense of motion inferred during reactivation of the main Neoproterozoic suture zones that transverse the Red

Sea (e.g., Dixon et al., 1987; Johnson and Woldehaimanot, 2003). However, the extent of extensional structures in the experiment was similar in width to that observed in model RS1 and therefore does not bear a good resemblance to the Red Sea (cf. Figs. 5.1, 5.4a and 5.4b).

Ongoing rotational stretching of the model lithosphere was characterised by an overall northward propagation of deformation, with a complex interaction between a group of north-south trending rift basins and the SE-NW narrow basins that developed above the crustal weaknesses (Fig. 5.5b). This produced a zig-zag pattern and consequently resulted in a rhombic geometry in which the deepest rift sections were detected at the intersection between the northward propagating grabens and the northernmost crustal anisotropy (Molnar et al. [2018], [Chapter 4]). The final rift architecture of model RS2 is substantially different to the structural pattern of the Red Sea, as highlighted by the development of several extensional structures in a wide area in the model rather than a single main rupture zone in nature (cf. Figs. 5.1 and 5.5b at 27 hours).

5.4.3 Model RS3 (Lithospheric mantle heterogeneity with α = 15°)

The presence of a linear weak lithospheric mantle in this experiment resulted in a significantly different evolution of deformation in comparison to models RS1 and RS2. Early stages were characterised by the development of two narrow north-south oriented rift basins within the weak area (Fig. 5.5c) that delimited an intra-rift horst (e.g., Molnar et al., 2017; Zwaan et al., 2015). These elongated basins adopted a V-shaped geometry and later propagated northward rapidly by a process of unzipping, similar to that interpreted for the Red Sea (e.g., Augustin et al., 2014; Molnar et al., 2017; Omar and Steckler, 1995; Fig. 5.5c). In the experiment it took ~5 hours between the detection of a crustal rupture at the southern end (Fig. 5.5c; 2 hours) and the point when the propagating rift tip reached the northernmost region of the model (Fig. 5.5c; 7 hours). This scales to ~4 Ma in nature, which is in good agreement with the aforementioned difference of ~3 Ma between the timing of rifting in the southern and northern Red Sea.

A remarkable first-order structural and kinematic similarity was previously noted by Molnar et al., (2018, [Chapter 3]) between the model intra-rift horst in this experiment and the Danakil block in the southern Red Sea. The overall evolution of deformation in model RS3 bears a strong resemblance to the spatio-temporal evolution of the Red Sea rift. However, no strike- or oblique-slip reactivation of pre-existing structures in the crust was observed, and the main rift escarpments in the experiment are more linear than those observed in the African and Arabian borders of the Red Sea (cf. Figs. 5.1 and 5.5c).
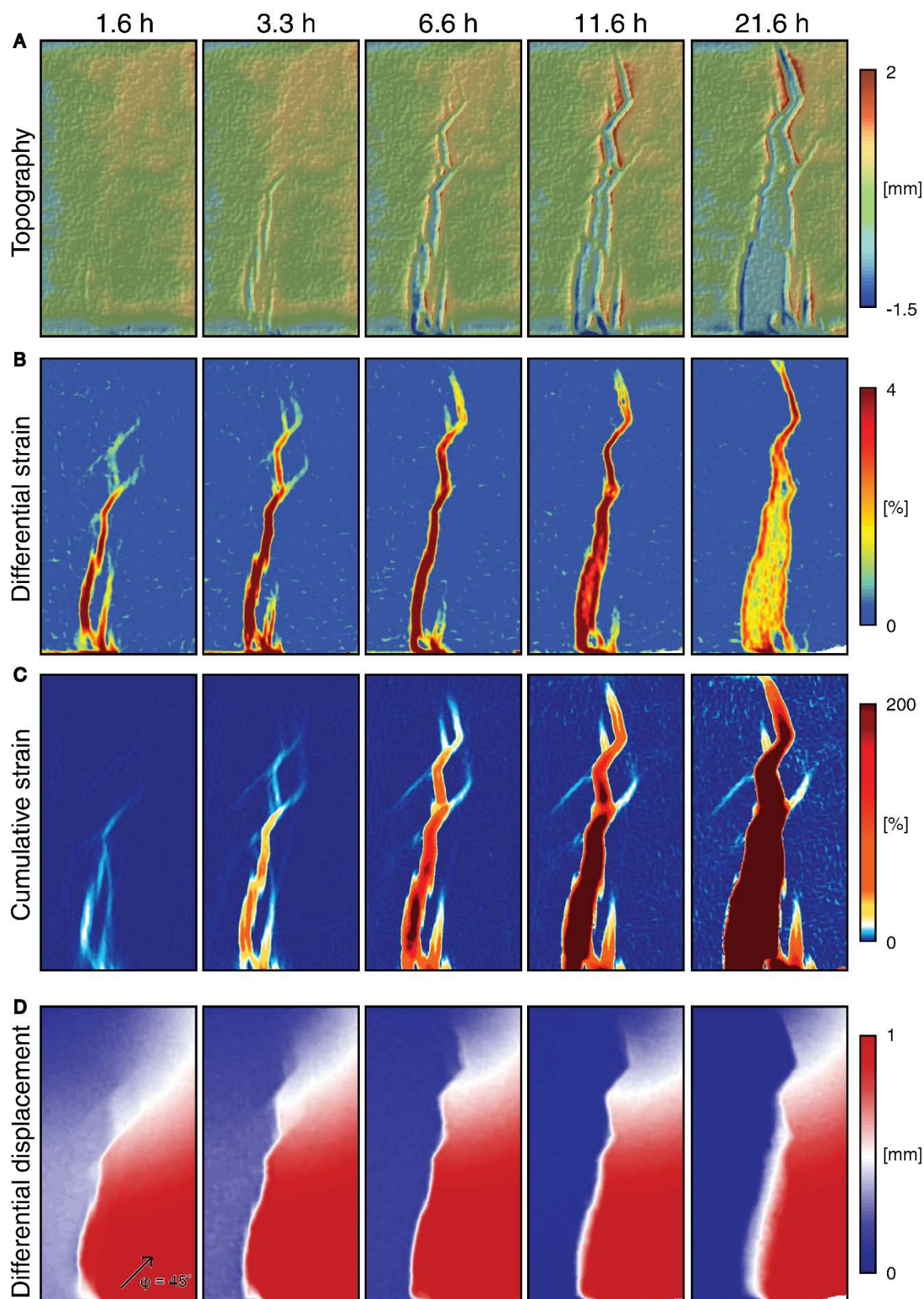
Figure 5.6 - Evolution of deformation for Model RS4. A. Digital elevation models showing top-view surface topography. B. Differential normal strain field maps. C. Cumulative normal strain field maps. D. Differential displacement.

5.4.4 Model RS4 (Combined crustal and mantle heterogeneities)

Early stages of deformation were characterised by a narrow rift basin bounded by approximately north-south oriented normal faults in the southern end of the model (Fig. 5.5a). At this stage, short SE-NW trending extensional faults also developed along the southernmost crustal heterogeneity, in the centre of the model (Fig. 5.6a; 1.6 hours). Differential strain measurements show how extension was partitioned into extension-normal oriented compartments within the lithospheric mantle weakness, similar to model RS3, and along the crustal heterogeneities, similar to model RS2 (Fig. 5.6b; 3.3 hours). Differential displacement field maps at these stages allowed the detection of a jump in displacement rates between the southern and northern sections of the crustal heterogeneities (Fig. 5.6d; 3.3 hours). The expression of this jump is a relatively abrupt northwestward decrease in displacement rates across the central section of the crustal weaknesses. Analysis of displacement vectors indicate an oblique-slip sinistral sense of motion for the reactivation of the crustal weaknesses (Fig. 5.6d; 1.6 hours).

Progressive lithospheric stretching was accompanied by the along-axis nucleation of the early-developed compartments and by the rapid propagation of the resulting narrow rift towards the pole of rotation (Fig. 5.6a; 6.6 hours). The time difference in the experiment between crustal rupture in the southern and northern ends of the model is similar to that calculated for model RS3 and is also consistent with the inferred geological evolution of the Red Sea (Bosworth et al., 2005 and references therein). The rotational boundary condition partially prevented the nucleation of the compartments in the southern section, favouring the formation of an intra-rift segment that started rotating anticlockwise, similar to model RS3 (Fig. 5.6a; 6.6 hours). Although this intra-rift segment in the experiment was later fragmented into minor blocks (Fig. 5.5a; 21.6 hours), the spatio-temporal evolution of its initial stages resembles interpretations given for the Danakil block in the southern Red Sea (e.g., Collet et al., 2000; McClusky et al., 2010; Molnar et al., 2018; [Chapter 3]).

When the propagating rift tip reached the pre-existing crustal heterogeneities in the centre of the model, the main rupture zone aligned with the heterogeneity. The propagation of the rift in this part of the experiment resulted in a "zig-zag" unzipping mechanism (Fig. 5.6a; 6.6 hours). The resulting narrow rift geometry with sigmoidal boundary faults is strikingly similar to the present-day rift morphology of the Red Sea (cf. Figs. 5.1 and 5.6a; 21.6 hours). Differential strain measurements from intermediate to late stages of deformation in the experiment show that no more strain was localised along the crustal weaknesses on either side of the main rift (Fig. 5.6a; 6.6-21.6 hours). This suggests that the oblique- or strike-slip reactivation of pre-existing crustal structures is strongest at early stages of deformation and that it is superseded by strain localisation within the weak lithospheric mantle. Differences in the total strain accumulated along the different rheological heterogeneities after 21.6 hours support this observation (Fig. 5.6c; 21.6 hours). Differential displacement rate measurements provide additional insights into the temporal variations of the oblique- and or strike-slip kinematics. Comparison between early (1.6 hours) and late (21.6 hours) stages of deformation in Figure 5.6d shows that a linear step in displacement rates occurred along both crustal heterogeneities during the initial stages. This variation in displacement rates became diffuse in the southern heterogeneity at later stages but an abrupt jump was still observed in the northernmost heterogeneity. This phenomenon is related to the proximity of the northernmost heterogeneity to the pole of rotation and it may highlight the key

role of the Aqaba-Levant transform fault during the Cenozoic rift evolution of the Red Sea (e.g., Bosworth et al., 2005).

5.5 Discussion

5.5.1 Hierarchy of controlling factors

Comparison between experiments with different initial conditions allowed me to identify the first-order effects of pre-existing rheological heterogeneities in an extending lithosphere. Structural evolution in the reference experiment with a homogeneous lithosphere evolved as evenly spaced subparallel V-shaped basins that covered a wide area in the southern end of the model and propagated toward the pole of rotation. This was the only experiment with an approximately symmetric rift pattern (Fig. 5.5a).

The presence of linear weak areas in the crust prior to continental rifting favoured the development of normal faults near the weaknesses, producing an early partitioning of deformation. However, because the difference in mechanical strength between the crustal weaknesses and the surrounding normal lithosphere was not sufficiently large to localise all the deformation, extension was equally accommodated by both extension-normal structures and heterogeneity-related structures throughout the entire experiment. This resulted in a series of rift basins with variable orientations that covered an area of similar width to that in the reference experiment. Crustal heterogeneities have a strong influence on fault orientation but do not favour the development of narrow rift basins (Fig. 5.5b).

The incorporation of a linear weakness in the lithospheric mantle resulted in significant differences in the overall rift morphology with respect to previous experiments. The resulting rift basin had a slightly sigmoidal shape and developed almost entirely within the weak zone. Linear weaknesses in the lithospheric mantle strongly localise deformation from early stages onwards and favour the development of narrow, rapidly-propagating rifts that advance toward the pole of rotation (Fig. 5.5c).

Deformation evolution for the case where both crustal and lithospheric mantle heterogeneities are present can be partially described as a summation of the mechanisms of continental rifting discussed above. Short-term reactivation of the crustal heterogeneities was coeval with localisation of deformation along the lithospheric mantle weakness at early stages. However, early formed domains of strain partitioning later localised entirely along compartments positioned within the weak lithospheric mantle. From this stage onward, localisation of deformation along the pre-existing crustal structures was practically non-existent and the rift developed as a narrow and fast-propagating basin (Figs. 5.5d and 5.6). The sigmoidal shape of the main border faults shows the best match to the rift architecture of the Red Sea.

Our experimental results have established the following hierarchy of factors that control the characteristics of rifting. The presence of a weak zone in the lithospheric mantle layer is the first-order control on the overall mechanical behaviour of extending lithosphere, rift architecture and style of rifting. The presence of crustal heterogeneities has a second-order effect, which influences variations in fault trends along the rift axis. Additionally, rotational kinematic boundary conditions played a

significant role since all experiments were characterised by an overall northward progression of deformation, whereby strain was progressively transferred along the rift axis towards the pole of rotation. By contrast, orthogonal or oblique extension with identical rheological internal conditions is expected to concentrate strain along the rift axis synchronously (cf. Bellahsen and Daniel, 2005; Bonini et al., 1997; McClay and White, 1995), with increased localisation in regions with a lower integrated lithospheric strength. This hierarchy is valid from a mechanical point of view, and it based on the assumption that other important parameters in nature such as temperature effects on the rheology of the lithosphere, plume impingement or magmatic additions, which are not recreated explicitly in our models, do not vary significantly over time.

5.5.2 Comparison with natural examples

5.5.2.1 The Red Sea

The opening of the Red Sea is comparable to model RS4 (Fig. 5.7). Several studies have demonstrated that the Arabian plate is moving to the northeast about a pole of rotation located within the Mediterranean coastline of Egypt (e.g., Chu and Gordon, 1998; McClusky and Mahmoud, 2003; Sella et al., 2002). This motion has been sustained over the last ~13-14 Ma (ArRajehi et al., 2010; McClusky et al., 2010). The extensional strain exerted on the Arabia/Africa boundary creates a strong displacement gradient that increases towards the southeast (Fig. 5.7). Model RS4 can be compared to nature by comparing GPS vectors (McClusky et al., 2010) with experimental velocity vectors (Figs. 5.7a-b). Apart from the kinematics, our models are also analogous to the Red Sea region because they incorporated mechanical weaknesses in both the crust and lithospheric mantle, which have been proposed to have controlled the history of continental rifting and rift propagation (e.g., Crane and Bonatti, 1987; Dixon et al., 1987). Despite the simplifications in our analogue experiments, the deformation evolution of the Red Sea is strikingly similar to model RS4 (Fig. 5.7).
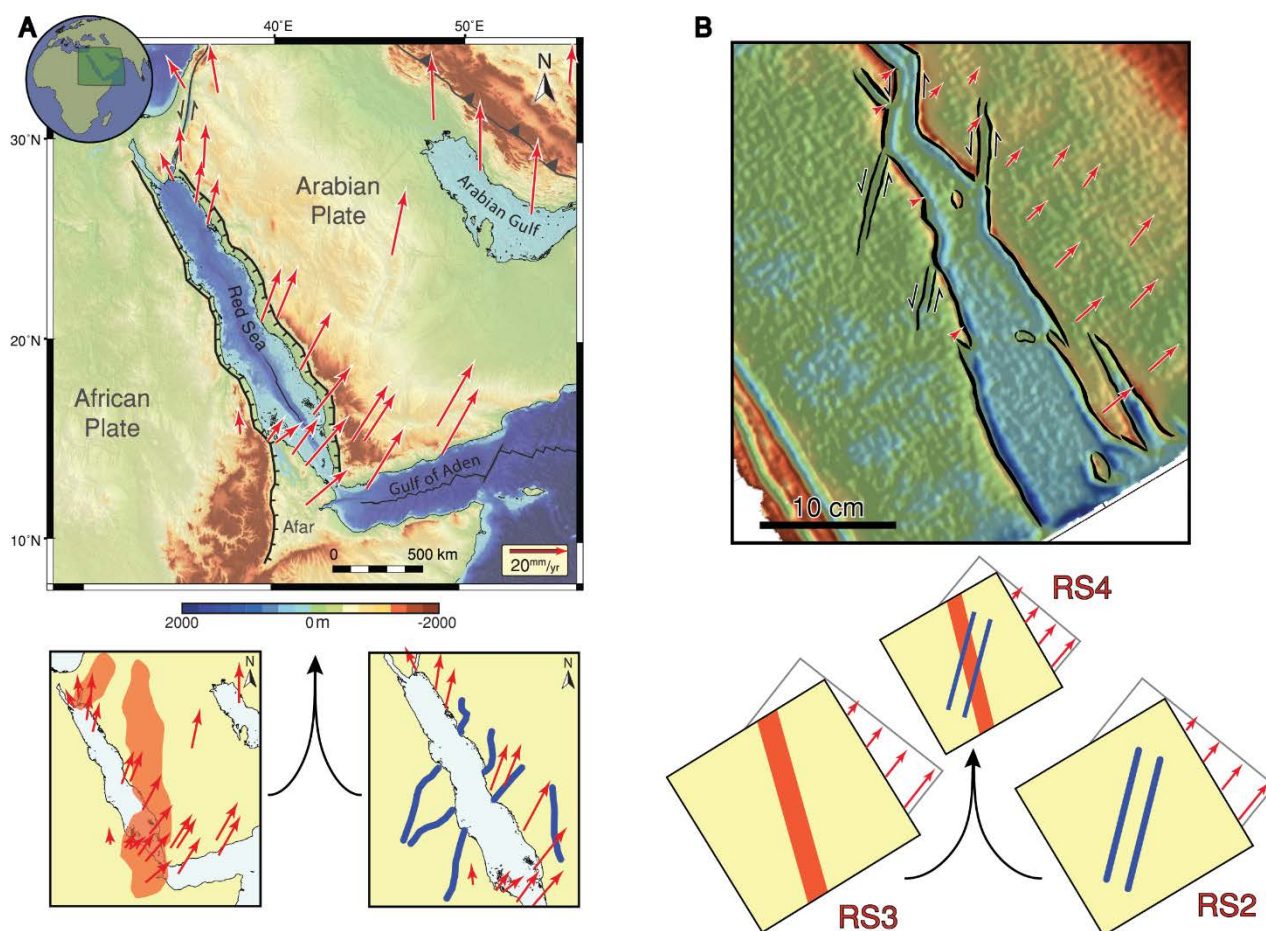
Figure 5.7 - **Comparison of the Red Sea with Model RS4. A. Bathymetric and topographic map of the Red Sea-Gulf of Aden rift system illustrated as in Figure 5.1. Bottom panels show sketch drawings indicating the inferred location of lithospheric mantle (left) and crustal (right) heterogeneities. B. Digital elevation model showing top-view surface topography of Model RS4.**

Continental rifting initiated in the southern Red Sea between about ~30 and 25 Ma (Bosworth et al., 2005 and references within), although there is no consensus on the precise age due to variations between dating methodologies (e.g., Berggren et al., 1995; Bunter and Abdel Magid, 1989; Hughes and Filatoff, 1995; Plaziat et al., 1998). The initial stages of deformation in the Red Sea were characterised by roughly north-south trending compartments that were separated by accommodation zones (Bosworth, 1994; Jarrige et al., 1990), exactly as observed in Model RS4 (Fig. 5.6a; 3.3 h). This phase was followed by an episode of very rapid rift propagation, reaching the northernmost section of the experiments after ~4 hours, which scales up to ~3.2 Ma. This duration is within the estimated time range between the onset of rift initiation in the southern Red Sea (~30-25 Ma; Bosworth et al., 2005) and in the Gulf of Suez (≤ 23 Ma; Hughes and Beydoun, 1992). Widespread dike intrusion between 25-23 Ma (e.g., Sebai et al., 1991) support the idea of essentially simultaneous rifting along the entire axis of the Red Sea. Based on the geological record, it is impossible to discern if the rifting initiation in the Red Sea was synchronous along its margins or if it propagated northward (Bosworth, 2015).

Differential and cumulative strain measurements in Model RS4 indicate segmentation of deformation into two elongated compartments that delimited an intra-rift block (Figs. 5.6a-b-c; 3.3 hours). Similar to the behaviour in Model RS3, this intra-rift block later evolved as isolated continental

block that rotated anticlockwise around an independent pole of rotation (Fig. 5.5c-d). This also resembles the formation and evolution of the Danakil block in the southern Red Sea, which was initially bounded by the Danakil depression to the west and by the main Red Sea rift to the east (Molnar et al., 2017). While in model RS4 the intra-rift block collapsed shortly after rotation was initiated (Fig. 5.6a; 11.6 hours), the first-order evolution of deformation is in good agreement with natural observations. I suggest that the localisation of deformation into compartments and the wider distribution of deformation in the southern Red Sea is associated with a weaker section of the lithospheric mantle, in turn possibly linked to the northward channelling of the Afar plume (Chang et al., 2011; Courtillot et al., 1999; Faccenna et al., 2013; Molnar et al., 2017).

Rift branches nucleated to form a single V-shaped propagating rift after 6.6 hours in Model RS4 (Fig. 5.6a; 6.6 hours), and rift propagation was substantively affected by the pre-existing crustal heterogeneities. Ziegler and Cloetingh (2004) concluded that abandoned crustal weaknesses such as rifts can be reactivated under new extensional stresses because crustal-scale faults permanently weaken the lithosphere. Lyakhovsky et al. (2012) also indicated that fractured rocks have a long-term effect that significantly pre-conditions the locus of rifting at later stages. In Model RS4, the reactivation of pre-existing crustal structures was strongest at early stages (Fig. 5.6b; 1.6-3.3 hours) and they were later abandoned when strain was transferred to the northward propagating rift. I therefore infer that the presence of pre-existing crustal structures was a key condition that contributed to forming the characteristic sigmoidal pattern of the Red Sea escarpments. This also implies that escarpment geometries can be used to predict the location of zones of crustal weakness in modern and ancient rifts.

After 6.6 hours the northernmost rift tip in Model RS4 had bifurcated into two V-shaped secondary rift branches. By 11.6 hours the westernmost branch stopped propagating northward and extension in this area was accommodated entirely by the easternmost branch. Similarly, in the Red Sea, at around 14-11 Ma, the Gulf of Suez was abandoned as an active rift and extension in the northern Red Sea was accommodated by the Aqaba-Levant transform fault (Bosworth et al., 2005). No significant changes were observed in the rift morphology in Model RS4 after 11.6 hours. Previous comparisons of analogue models with the Red Sea (Molnar et al., 2017) showed a good match, but failed to explain the deflections of the main boundary faults observed in nature. The incorporation of pre-existing crustal heterogeneities into the experiments, in addition to a linear weak lithospheric mantle and a strong rotational kinematic, demonstrates that these are the three main mechanical and kinematic conditions underlying the spatio-temporal evolution and present day morphology of the Red Sea.

5.5.2.2 Fragmentation of Gondwana

The opening of the Western Indian Ocean during the Late Jurassic developed as a result of the rotational motion of Africa with respect to East Gondwana, with a pole of rotation located approximately in the Falkland plateau (Reeves et al., 2016; Fig. 5.8a). The pre-rift conditions are not well constrained, but the interpreted spatio-temporal evolution of this natural example is very similar to Model RS4. An initially narrow rift propagated towards the pole of rotation, resulting in rift segments that were alternatively oriented perpendicular and oblique to the extension direction, defining a 'zig-zag' propagation pattern (Fig. 5.8a). Evidence of propagation of deformation away from the main rift and into the continents is manifested by a series of failed rifts (e.g., Anza rift; Fig. 5.8a) and massive

dyke swarms (e.g., Okavango dyke swarm; Fig. 5.8a) (Reeves et al., 2016) and are analogous to observations in our experiments. In the central section of the Model RS4, a fragment of continental lithosphere became stranded within the main rift in proximity to a pre-existing crustal heterogeneity (Fig. 5.8a, bottom panel). The mechanism of formation of this continental fragment could be an analogue for the enigmatic origin of the Beira High, which was stranded offshore Mozambique (Fig. 5.8a, top panel).
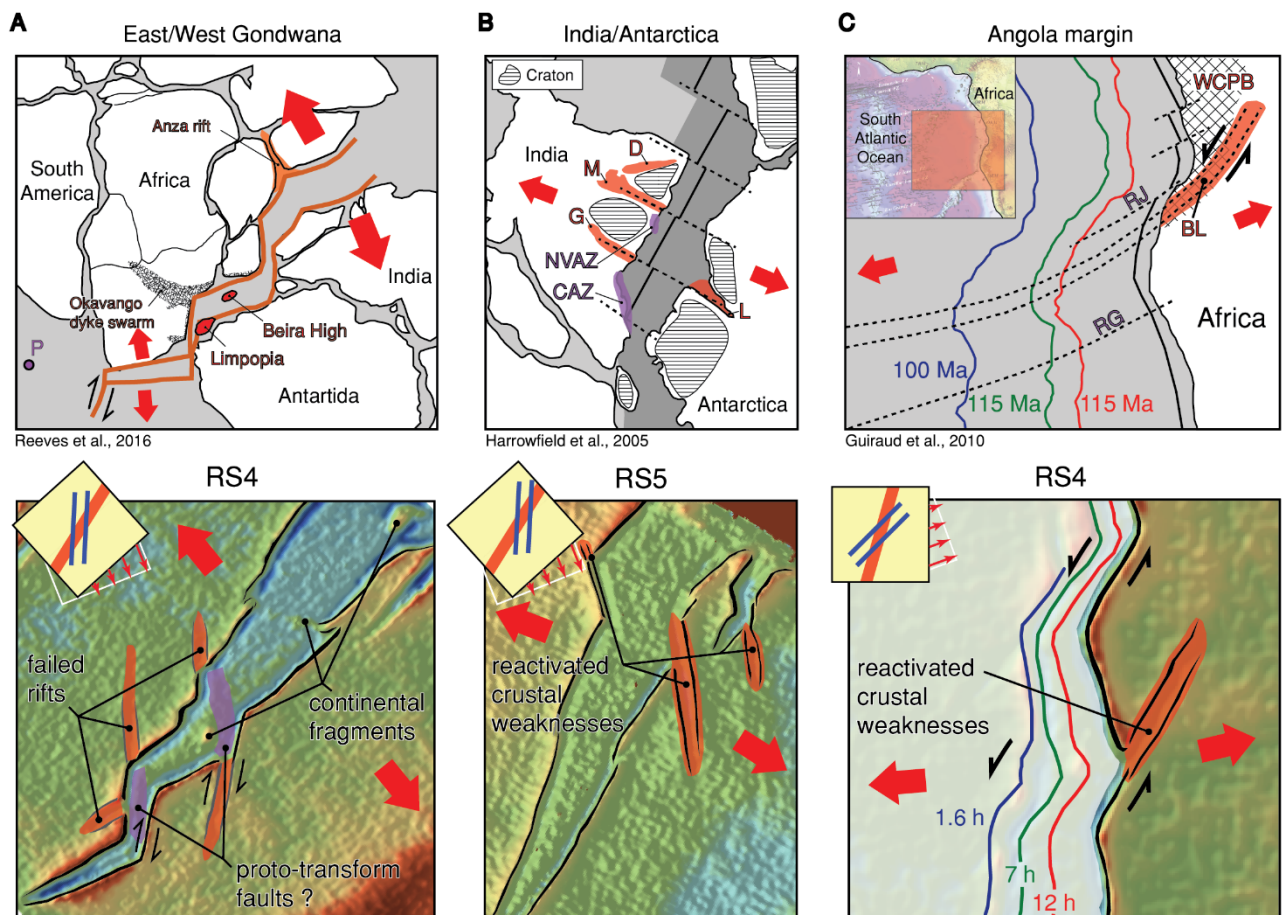
Figure 5.8 - Comparison of natural examples (top panel) with model results (bottom panel). A. East/West Gondwana fragmentation. B. India/Antarctica separation. D = Damodar, M = Mahanadi, G = Godavari, NVAZ = North Vizag accommodation zone, CAZ = Coromandal accommodation zone, L = Lambert. Red arrows indicate approximate direction of extension. C. Angola margin, South Atlantic Ocean. RG = Rio Grande transform zone, RJ = Rio de Janeiro transform zone, BL = Benguela-Lucapa fracture zone, WCPB = West Congolian Panafrican Belt.

The subsequent fragmentation of East Gondwana into India, Antarctica and Australia also presents similar characteristics to the evolution of the experiments presented in this study (e.g., Harrowfield et al., 2005; Veevers, 2009; Fig. 5.8b). An additional experiment (Model RS5, Extended Data Fig. 5.1) was carried out with similar initial conditions to RS4, but with the crustal heterogeneities located further south, away from the pole of rotation (Extended Data Fig. 5.1). This favoured early strain localisation in the areas where the rheological heterogeneities were superimposed and resulted in a similar 'zig-zag' pattern to Model RS4 (Extended Data Fig. 5.1). Crustal heterogeneities oriented at high-angles to the rifts were also partially reactivated into the adjacent continents as narrow extensional basins (Fig. 5.8b),

resembling the failed arms of triple junctions. Similarly, it has been interpreted that the coal-bearing narrow rifts of East India and Antarctica (Damodar, Mahanadi and Godavari valleys, Lambert graben) exploited crustal anisotropies in a similar manner to that observed in Model RS5 (Harrowfield et al., 2005). Whether these anisotropies were precursors to oceanic transform faults or not is also still discussed (e.g., Veevers, 2009). Additionally, the continental margins of East India contain segments that are both orthogonal (e.g., Krishna-Godavari and Mahanadi rift zones) and oblique (e.g., Coromandal and North Vizag accommodation zones) to the inferred direction of extension (Sinha et al., 2016) (Fig. 5.8b). Finally, the formation of isolated continental fragments and microcontinents at these margins, as inferred from the analogue experiments, has similarly been suggested for the Late Jurassic break-up of Gondwana (e.g., Gaina et al., 2007, 2003; Sinha et al., 2016). However, the evolution was probably more complex in nature since the Africa-Antarctica spreading centre was propagating eastward at the same time as the westward propagation of the Australia-India spreading centre (Sinha et al., 2016).

The opening of the South Atlantic Ocean during the Early Cretaceous shows partial similarities with the fragmentation of East Gondwana. The Euler pole of rotation for South America/Africa was located in the Arctic Ocean (Nurnberg and Müller, 1991) and continental break up consequently developed by a classical "unzipping" mechanism by propagating from south to north. The West African passive margins are relevant to the experiments presented here because numerous studies have shown that variably oriented, pre-existing rift basins and Panafrican mobile belts (e.g., Antobreh et al., 2009; Guiraud et al., 2010; Mbina Mounguengui and Guiraud, 2009) controlled the onset of rifting and continental break-up (Fig. 5.8c). Guiraud et al. (2010) distinguished two types of segments across the margin in a similar way to those observed in the east Indian margin (Fig. 5.8b): transform margins, which are aligned with major oceanic fracture zones and are in turn oblique to the general direction of extension; and orthogonal-rifted margins that lie between the aforementioned segments (Fig. 5.8c). Model RS4 resembles this setting and provides some insights on the West African passive margins. The West Congolian Panafrican Belt (WCPB) is a relict Neoproterozoic continental rift that may have exerted a first-order control in the localisation of deformation during the opening of the South Atlantic Ocean, as inferred from Model RS4. Alternatively, sections with pre-existing crustal heterogeneities in the interior of the African continent were partially reactivated (e.g., Kwanza horst) and the associated transform segment had a left-lateral sense of motion in both Model RS4 and nature (Fig. 5.8c). In the Angola margin, these sections evolved into major oceanic transform faults (Rio de Janeiro/Benguela/Lucapa fracture zones and Ascension fracture zone; Fig. 5.8c), supporting the previously suggested link between pre-existing lithospheric weaknesses and transform faults (e.g., Behn and Lin, 2000; Cochran and Martinez, 1988; Gerya, 2012).

5.6 Conclusion

I presented three-dimensional analogue experiments of propagating rifts that provide insights on continental rifting and break-up processes in space and time. Comparison between models with different kinds of pre-existing rheological heterogeneities allowed me to define how they both independently and jointly influence the lateral growth of continental rifts. Furthermore, I have defined a hierarchy of influence for different pre-existing rheological heterogeneities. Weaknesses in the

lithospheric mantle exert a first-order control and localise deformation throughout the entire rifting process, while crustal weaknesses exert a second-order influence. However, certain features observed in nature require a combination of both types of heterogeneities.

The Red Sea represents the best natural laboratory to compare with our experimental results because it is a juvenile basin with well constrained tectonic boundary conditions, it preserves several phases of rifting, and it is associated with linear mantle and crustal heterogeneities that intersect the rift. Our results suggest that the distinctive narrow shape of the Red Sea and the observed variations in the trend of rift escarpments is a consequence of the superimposed weaknesses in both the lithospheric mantle and the crust, as well as the strong rotational kinematic component that characterises the motion of the Arabian plate. Application to other natural examples, such as the break-up of Gondwana and the south Atlantic demonstrates that comprehending the influence of internal and boundary conditions prior to continental rifting is fundamental to understand the evolution of continental rifting, break-up and the onset of sea-floor spreading.

5.7 Extended Data
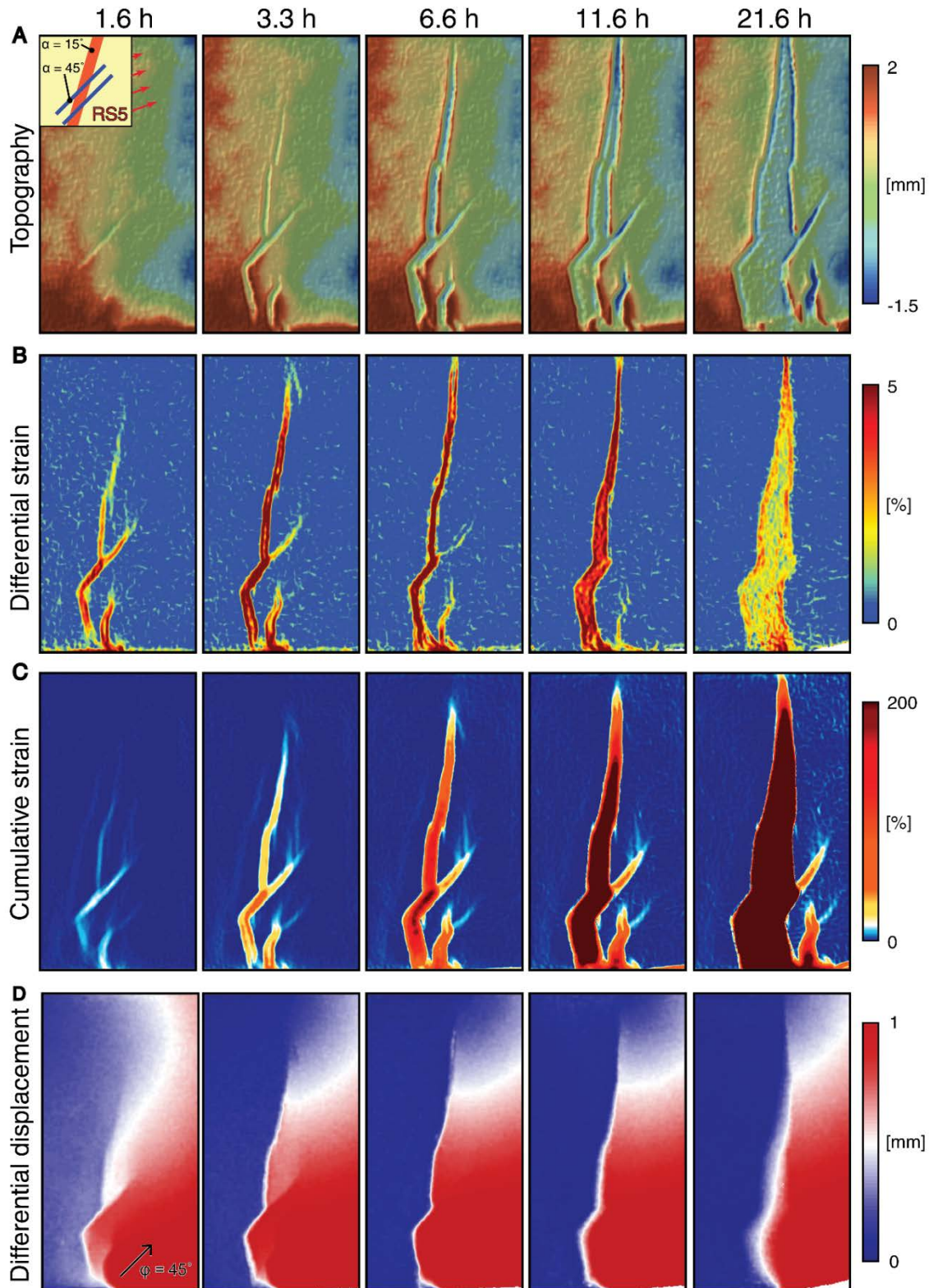
ED Figure 5.1 - Evolution of deformation of Model RS5. A. Digital elevation models showing top-view surface topography. Top left inset indicates initial location of the pre-existing heterogeneities, illustrated as in Figure 5.4. B. Differential normal strain field maps. C. Cumulative normal strain field maps. D. Differential displacement.

Chapter 6

Discussion

6.1 Introduction

This thesis presents new insights on the spatio-temporal evolution of continental rifts using a novel analogue modelling setup and a high-resolution deformation monitoring technique. The research specifically focused on simulating extensional settings with a kinematic rotational component and investigated how the resulting propagating rifts interact with different kinds of pre-existing rheological heterogeneities. This final chapter summarises the main findings and conclusions of the previous chapters, covering the aims of the project and addressing the first-order questions presented in Chapter 1:

- Can I characterise the overall temporal and spatial evolution of deformation in large-scale propagating rifts?

- Do rifts always propagate towards a pole of rotation during rotational rifting?

- How is extension accommodated in the presence of a linear weak zone in the lithospheric mantle? And how do crustal heterogeneities influence rift morphology?

- Do lithospheric weaknesses contribute to the development of microcontinents during rifting?

I additionally discuss the implications of the modelling results for understanding complex structural patterns in continental rifts and make suggestions for further research.

6.1.1 Rotational deformation of a homogeneous lithosphere (Chapters 2-5)

The effects of including pre-existing rheological heterogeneities in the lithosphere can only be fully characterised by comparing all of the experimental results with a reference experiment with a homogenous lithosphere (i.e. no pre-existing rheological heterogeneity). The reference experiments were used in all the chapters as point of comparison, and also provided additional key insights on rift propagation.

The extension gradient imposed on the models produced, in all cases, extension-orthogonal normal faults that were initially distal to the pole of rotation, which subsequently linked up and evolved to V-shaped basins with tips that propagated towards the north. Progressive deformation led to along-axis lateral growth of the rift basins, while strain was simultaneously transferred to the rift depressions. At a more regional scale, extensional features that developed at later stages were located closer to the pole of rotation and propagated both south and north. During the final stages of the experiments, structures originally formed in the southern and western parts of the model lithosphere became extinct and strain was transferred towards the moving plate, in the direction of the extensional far field stress (imposed by the linear actuator), causing lithospheric thinning. These findings have important implications for understanding complex fault patterns and interactions in ancient and modern rifts because mapping geological structures usually only provides a snapshot of the entire tectonic evolution. Although it is often difficult to infer the temporal evolution of the fault network if the field, these modelling results

provide a framework for interpretation of extensional tectonic settings influenced by gradients in the direction and magnitude of extension.

6.1.2 Role of linear weak lithospheric mantle (Chapter 2)

Pre-existing structures in the lithosphere are common in many divergent tectonic settings. These structures range from lateral variations in lithospheric thickness that perturb mantle flow (e.g., Ebinger and Sleep, 1998), weaknesses within the upper mantle caused by activity of mantle plumes or hot spots (Corti, 2008), mantle penetrating shear zones characterised by reduced grain size (Heron et al., 2016), or inherited mechanical anisotropies with lattice preferred orientation of olivine crystals (Tommasi and Vauchez, 2001). I specifically tested the effect of a pre-existing linear weak lithospheric mantle on the propagation of rotational rifts. Their influence of such heterogeneities is described as a function of the angle of obliquity of the linear weakness, as follows.

Low obliquity (0° < α < 45°): the classical 'unzipping' style of rifting (Omar and Steckler, 1995) was observed in the presence of a linear weakness oriented with a low angle with respect to the propagation direction. Rifts initially developed as short, extension-orthogonal grabens located within the weak zone, which accommodated the bulk of the extensional strain, and then connected and propagated without obstruction towards the pole of rotation. Depending on the angle of obliquity and position of the heterogeneity, some rift branches were deflected from the main rupture zone to become aborted when they penetrated through the boundary between weak and normal lithosphere, resulting in abandoned rift basins and delimiting intra-rift horsts (see section 6.1.3).

Moderate/high obliquity (45° ≤ α < 60°): strong strain partitioning was observed from early stages when a linear weak lithospheric mantle transects the propagating rift at a moderate to high obliquity. Deformation is subdivided into (1) extension-normal V-shaped basins that propagated toward the pole of rotation, reminiscent to the early stages of the reference experiments, and (2) rift grabens that were aligned at intermediate angles between the direction of extension and the linear weakness, which grew with progressive deformation in a similar fashion to the compartments developed in the early stages of experiments with low obliquity. Deformation was relayed from the extension-normal structures into the rift basins within the weak zone at later stages. Ultimately, all active extension was accommodated in these areas, with rift branches propagating both south and north.

6.1.3 Microcontinent formation (Chapter 3)

The three-dimensional analogue models presented in Chapter 3 support the hypothesis that rotational extensional kinematics, in the presence of a linear, lithospheric-scale weakness are two important conditions involved in the formation of microcontinental fragments. Detailed analysis of an eleven-experiment series showed similar evolutionary steps to those described for cases of low obliquity in Chapter 2, in which intra-rift horsts were repeatedly developed during the early stages of continental rifting. I consistently observed how these elongated continental slivers spalled away from rifted margins, demonstrating that the proposed initial conditions are sufficient for the formation of incipient microcontinents. Additional kinematic and thermo-mechanical variables that characterise later

stages of this process determine whether this fragment evolves to become a microcontinent *sensu stricto* (Scrutton, 1976) or remains connected via unbroken continental lithosphere to a passive margin as an outer high (e.g., Schuepbach and Vail, 1980), continental ribbon (e.g., Lister et al., 1986) or marginal plateau (Mercier de Lepinay 2016 and references therein). Novel analogue models are presented in this chapter to define a tectonic framework for, and significant insights on mechanisms of microcontinent formation.

6.1.4 Role of linear crustal heterogeneities (Chapter 4)

Crustal heterogeneities are also a common feature in extensional settings, often associated with previous tectonic phases, comprising a range of structures from pre-existing basement faults (e.g., Wilson et al., 2010) to suture zones (e.g., Stern and Johnson, 2010), volcano-tectonic linear structures (e.g., Abebe et al., 1998) and orogenic belts (e.g., Vauchez et al., 1997), among others. These inherited structures are often juxtaposed against other discontinuities such that the role they play in the evolution of deformation is challenging to infer from the geological record. In this chapter I independently tested an additional type of pre-existing condition by restricting rheological heterogeneities to the crust. As with the experiments with mantle lithosphere heterogeneities, I summarise the spatio-temporal evolution of deformation based on the angle of obliquity and relative orientation below.

Rift-parallel to low obliquity (α ≤ ~15°): extension-orthogonal heterogeneities in the crust rapidly localised deformation at early stages. Their presence favoured the formation of long linear faults that quickly reached near-final lengths (viz., constant length model, e.g., Morley, 2002), which facilitated rapid transfer of strain to areas closer to the pole of rotation. When heterogeneities were oriented clockwise at low angles (0° < α ≤ 15°), a slightly left-lateral oblique-slip deformation characterised normal faults associated with the heterogeneity, as opposed to the pure dip-slip faulting observed for heterogeneities oriented anticlockwise or perpendicular to the extension direction. However, the relative orientation with respect to the rift axis (clockwise vs. anticlockwise) did not affect the spatio-temporal structural evolution and the rift architecture was approximately mirrored.

Low to intermediate obliquity (~15° < α < 45°): these experiments showed the most dissimilar evolution of deformation as a function of their relative orientation with respect to the direction of rift propagation. A clockwise orientation favoured the formation of long linear faults at early stages and rapid propagation of deformation through the linear weak area. A similar evolution to the rift-parallel and low-obliquity cases was observed, with the addition of a strong left-lateral reactivation of the pre-existing discontinuities. When the heterogeneities were oriented anticlockwise, normal faults associated with the weak areas developed as dip-slip faults and extension-normal structures advanced from the opening side towards the pole of rotation, cutting across the linear heterogeneities. This behaviour resulted in a zig-zag pattern and block dislocation, comparable to the evolution of intermediate to high obliquity angle experiments.

Intermediate to high obliquity (45° ≤ α ≤ 60°): a complex rhombic (or zig-zag) interplay between heterogeneity-related faults and extension-normal structures resulted from intermediate- to high-angle pre-existing heterogeneities in the crust. The relative orientation of the pre-existing features was a major controlling factor in the type of faulting observed during lithospheric extension. A clockwise

orientation favoured sinistral oblique- and strike-slip faulting while an anticlockwise orientation resulted in dextral oblique- and strike-slip deformation. Lateral motion detected in the vicinity of the heterogeneities created a partial dislocation of the crust into blocks that were displaced at different rates. This represents the most challenging scenario for interpreting the spatio-temporal evolution of deformation from geological and geophysical evidence because the resulting zig-zag pattern is very similar to the structural of rifts that have been affected by two phases of extension, each with considerably different stretching directions.

High to rift-perpendicular obliquity (~60° < α ≤ 90°): when the heterogeneities transected propagating rifts at very high angles, the orientation of horizontally propagating normal faults was not affected and showed extension-normal trends throughout the whole experiment. Minor lateral rift offsets were observed as they propagated across the discontinuities. Additionally, differential strain measurements showed a partial stalling of propagation in the vicinity of the pre-existing rheological heterogeneities.

6.1.5 Combined presence of mantle and crustal heterogeneities in the lithosphere (Chapter 5)

Experiments from previous chapters were further evaluated and additional models with new initial conditions were run to investigate the hierarchical control of pre-existing linear weaknesses in the crust and lithospheric mantle. The role of a rotational kinematic boundary condition was also re-addressed.

The presence of a linear zone of weak lithospheric mantle always exerts a first-order influence on the style of rifting and on the temporal evolution of deformation. Extension was initially accommodated in structures that formed within the lithospheric mantle weak zone and did not propagate into normal lithosphere until the final stages of deformation. Crustal heterogeneities had a second-order influence. When they were the only type of weakness present, deformation was distributed within a region that was as wide as in the reference experiment, but the fault trends were strongly controlled by the heterogeneities. When both types of rheological heterogeneities were present, the overall evolution was a summation of their individual effects. Strong localisation at early stages along the weak lithospheric mantle zone developed simultaneously with the development of extensional faults parallel to the crustal heterogeneities. This was followed by a progressive abandonment of the crustal heterogeneity-related structures and the propagation of a V-shaped rift towards the pole of rotation, caused by the imposed rotational boundary condition. The presence of both crustal and lithospheric mantle heterogeneities appears to be the only combination that explains the distinctive morphology of the Red Sea. A similar scenario may also be relevant to major break-up processes during the fragmentation of Gondwana.

6.2 Implications of the research

6.2.1 Implications for continental rifting and break-up

The development and propagation of rifts is a consequence of the relative motion of diverging plates around a pole of rotation. Although many major continental break up events in Earth's history are known to have involved relative rotation between plates, most geodynamic modelling has focused on rifting in which the relative plate motion is orthogonal or oblique. This assumption of a translational rather than rotational motion does not simulate lateral variations in stress or strain within large regions undergoing continental extension. Consequently, our experiments are novel in that they incorporate a three-dimensional relative motion of lithospheric plates and additionally include linear heterogeneities of diverse nature and orientation.

Many publications have focussed on studying the nature of so-called heterogeneities, their classification, identification, and roles they play during continental rifting. This thesis provides a comprehensive review of how variably oriented, linear mechanical weaknesses in the lithosphere may influence the first-order evolution of propagating rifts in space and time. Close similarities to numerous examples of ancient and modern rifts validate the outcomes of our simplified experiments. I anticipate these results will provide a starting point for more sophisticated geodynamic investigations of continental break up by rotational rifting, and a new structural and tectonic framework for the interpretation of major continental fragmentation events, including the formation of microcontinents in the geological record.

6.2.2 Implications for microcontinent formation

The origin of microcontinents and isolated continental fragments has been commonly associated with processes that follow the final stages of continental break-up, such as ridge jumps or interactions with hot spots. Our scaled analogue experiments show for the first time that rotational rifting and vertical and lateral variations in the properties of the lithosphere can result in microcontinent formation.

The results presented here demonstrate that the separation of microcontinents from passive margins occurs during continental rifting and before the onset of sea-floor spreading, which is a significant breakthrough in understanding microcontinent formation. In these cases, pre-existing lithospheric weaknesses exert a first order control on where and when microcontinents form, providing an important element for reconstruction of Earth's tectonic history. This finding specifies a geological framework to explain the location and distribution of microcontinents preserved within the Earth's crust, such as the Danakil block in the southern Red Sea, isolated continental fragments, ridges and plateaus offshore western Australia, the Jan Mayen microcontinent, the Cukchi Borderlands, the Limpopia and Beira fragments and Mauritia in the Indian Ocean, Sri Lanka, and many others.

6.2.3 Implications for mineral and energy resource exploration

Rift zones and passive margins are known to host large petroleum and gas reservoirs and ore deposits around the world. Despite an ever-increasing amount of surface and subsurface data – with constantly improving resolution - understanding the temporal evolution of complex fault patterns is still challenging. This thesis provides detailed information on the time dependence of deformation localization patterns, fault development, linkage and compartmentalisation during rifting. The resulting comprehension of the mechanical behaviour of the extending lithosphere will result in critical insights on kinematic and dynamic processes within extensional sedimentary basins (e.g., trap formation, migration and accumulation in petroleum geology), which will impact our ability to target resources.

6.3 Suggestions for future research

The modelling results outlined in this thesis provide a framework for understanding the controlling role of pre-existing rheological and kinematic conditions in the evolution of rifts, with direct application to natural examples such as the Red Sea, the Tyrrhenian Sea, selected segments of the East African Rift, rift basins from Northeastern Brazil and the fragmentation of Gondwana. However, the evolution of extensional tectonic settings in nature is exceedingly complex and additional aspects should to be tested to fully establish the hierarchy of the factors that control rift evolution. These aspects include:

Strong areas in the lithosphere: this study focused on how propagating continental rifts are affected by transversal weak sections of lithosphere. However, it is widely known that cratonic areas are rheologically stronger (e.g., Courtillot, 1982; Morley, 1999; Ziegler and Cloetingh, 2004) and should therefore contribute to strain localisation and the overall evolution of deformation. While a number of studies have investigated this aspect by means of analogue modelling with orthogonal kinematic boundary conditions (e.g., Corti et al 2011; Ding et al., 2016) and rotational (e.g., Benes et al., 1996; Sun et al 2009), most of them have been designed for a specific scenario in nature. Taking a systematic or generic approach, further modelling investigating the first-order role of stronger lithospheric domains on propagating rifts will provide important insights on the role of cratonic blocks during regional extension (i.e. Courtillot's [1982] 'locked zones').

Sedimentation: our models did not incorporate the effects of sedimentation, which is a variable that is achievable in analogue experiments with the appropriate laboratory setup and deformation monitoring equipment (e.g., Corti et al., 2011, 2010; McClay and White, 1995; Zwaan et al., 2017b). Although previous studies have suggested that syn-rift sedimentation may cause a switch from wide to narrow rifting mode (Bialas and Buck, 2009; Lizarralde et al., 2007) or may delay continental break-up (Martín-Barajas et al., 2013), no 3D modelling has been presented to support these theories. Alternatively, novel 3D analogue models presented by Zwaan et al. (2017b) have indicated that although syn-rift sedimentation does not have a first-order influence on the evolution of continental rifts, sedimentation becomes more influential on a longer timescale. Testing variable rates of sediment infill across different time-scales may help to further understand such complex processes. However, the issue of sediment infill is very challenging to simulate accurately since sedimentation in analogue models is commonly done by uniformly sifting an additional layer of the granular material used for

modelling the upper crust, while sediment infill in nature occurs via complex system tracts (e.g., Presser, 1993).

Variable rates of extension: since the 1980s and 1990s, the role of the rate of extension has been shown to exert a major control on the style of rifting (e.g., Kusznir and Park, 1987). Recent work has also suggested an abrupt change in extension rates during the rifting to drifting transition (Brune et al., 2016). This fundamental factor should be addressed in future modelling in order to understand how the evolution of deformation in rotational extensional settings is affected by variable rates of extension that either: 1) remain constant throughout the entire rifting process or that 2) naturally change over time during the extensional phase. However, the inclusion of realistic strain-rate dependent, elasto-visco-plastic rheologies is beyond the capability of current experimental modelling techniques, as discussed below.

Elasto-visco-plastic and temperature-dependent materials: the rheology of the lithosphere and asthenosphere is inherently complex and its simulation in scaled analogue experiments is challenging. Significant advances have occurred since early thermomechanical models of sea-floor spreading (e.g., Oldenburg and Brune, 1972), as demonstrated in more recent sophisticated thermo-mechanical laboratory set-ups recreating geothermal gradients (e.g., Boutelier and Oncken, 2011). Cross-disciplinary efforts between analogue modellers and materials engineers could bridge the remaining gap and eventually introduce new analogue materials capable of simulating the creation of new oceanic crust during ocean initiation in the laboratory. This would contribute to the poorly-understood role of the accretion of oceanic lithosphere in transferring stress during the transition from continental break up to ocean initiation.

Numerical modelling: laboratory experimental methods are well suited for modelling lithospheric extension with rotational boundary conditions because such kinematic behaviour cannot currently be simulated using numerical methods. Numerical simulations of oblique extension (e.g., Brune, 2014), bi-directional extension of a single plate (e.g., Gerya and Burov, 2017), rift propagation (e.g., Koopman et al., 2014; Mondy et al., 2018; van Wijk and Blackman, 2005) have been successfully carried out. Nonetheless, most used numerical codes are only capable of modelling Cartesian domains, in which the reproduction of pure rotations is currently not possible. Future efforts in computational geodynamics should be directed to address this limitation. In this context, it is anticipated that the work presented in this thesis will provide a starting point for more sophisticated future geodynamic investigations of continental break up by rotational rifting.

References

Abebe, T., Mazzarini, F., Innocenti, F., Manetti, P., 1998. The Yerer-Tullu Wellel volcanotectonic lineament: A transtensional structure in central Ethiopia and the associated magmatic activity. J. African Earth Sci. 26, 135–150. doi:10.1016/S0899-5362(97)00141-3

Abera, R., van Wijk, J., Axen, G., 2016. Formation of continental fragments: The Tamayo Bank, Gulf of California, Mexico. Geology 44, 595–598. doi:10.1130/G38123.1

Acocella, V., 2014. Structural control on magmatism along divergent and convergent plate boundaries: Overview, model, problems. Earth-Science Rev. 136, 226–288. doi:10.1016/j.earscirev.2014.05.006

Acocella, V., Faccenna, C., Funiciello, R., Rossetti, F., 1999. Sand-box modelling of basement-controlled transfer zones in extensional domains. Terra Nov. 11, 149–156. doi:10.1046/j.1365-3121.1999.00238.x

Adam, J., Klinkmüller, M., Schreurs, G., Wieneke, B. 2013. Quantitative 3D strain analysis in analogue experiments simulating tectonic deformation: Integration of X-ray computed tomo- graphy and digital volume correlation techniques. J. Struct. Geol. 55, 127- 149.

Adam, J., Urai, J.L., Wieneke, B., Oncken, O., Pfeiffer, K., Kukowski, N., Lohrmann, J., Hoth, S., van der Zee, W., Schmatz, J., 2005. Shear localisation and strain distribution during tectonic faulting—new insights from granular-flow experiments and high-resolution optical image correlation techniques. J. Struct. Geol. 27, 283–301. doi:10.1016/j.jsg.2004.08.008

Agostini, A., Corti, G., Zeoli, A., Mulugeta, G., 2009. Evolution, pattern, and partitioning of deformation during oblique continental rifting: Inferences from lithospheric-scale centrifuge models. Geochemistry, Geophys. Geosystems 10. doi:10.1029/2009GC002676

Allemand, P., Brun, J.-P., Davy, P., Van Den Driessche, J., 1989. Symétrie et asymétrie des rifts et mécanismes d'amincissement de la lithosphère. Bull. la Société géologique Fr. 3, 445–451. doi:10.2113/gssgfbull.V.3.445

Allen, P., Allen, J. 2005. Basin Analysis. Principles and Applications. Blackwell, Oxford.

Allen, P. A., Allen, J. R., 2013. Basin analysis: Principles and application to petroleum play assessment. Wiley-Blackwell (Eds.), 632 pp.

Allken, V., Huismans, R., Thieulot, C., 2011. Three-dimensional numerical modeling of upper crustal extensional systems. J. Geophys. Res. 116, B10409. doi:10.1029/2011JB008319

Allken, V., Huismans, R.S., Thieulot, C., 2012. Factors controlling the mode of rift interaction in brittle-ductile coupled systems: A 3D numerical study. Geochemistry, Geophys. Geosystems 13, 1–18. doi:10.1029/2012GC004077

Almalki, K.A., Betts, P.G., Ailleres, L., 2015. The Red Sea – 50 years of geological and geophysical research. Earth-Science Rev. doi:10.1016/j.earscirev.2015.05.002

Almalki, K.A., Betts, P.G., Ailleres, L., 2014. Episodic sea-floor spreading in the Southern Red Sea. Tectonophysics 617, 140–149. doi:10.1016/j.tecto.2014.01.030

Amato, A., Alessandrini, B., Cimini, G., Frepoli, A., Selvaggi, G., 1993. Active and remnant subducted slabs beneath Italy: evidence from seismic tomography and seismicity, Ann. di Geofisica, 26

Angelier J., 1985. Extension and rifting: the Zeit region, Gulf of Suez. J. Struct. Geol. 7, 605–612.

Antobreh, A.A., Faleide, J.I., Tsikalas, F., Planke, S., 2009. Rift-shear architecture and tectonic development of the Ghana margin deduced from multichannel seismic reflection and potential field data. Mar. Petrol. Geol. 26, 345–368.

Applegate, B., Shor, A.N., 1994. The northern Mid-Atlantic and Reykjanes Ridges: Spreading center morphology between 55°500N and 63°000N. J. Geophys. Res., 99, 17.935-17.956.

Armijo, R., Tapponnier, P., Mercier, J., 1986. Quaternary extension in southern Tibet: field observations and tectonic implications. J. Geophys. Res. 91, 13 803–13 872.

Armitage, J.J., Collier, J.S., Minshull, T.A., 2010. The importance of rift history for volcanic margin formation. Nature 465, 913–917. doi:10.1038/nature09063

ArRajehi, A., McClusky, S., Reilinger, R., Daoud, M., Alchalbi, A., Ergintav, S., Gomez, F., Sholan, J., Bou-Rabee, F., Ogubazghi, G., Haileab, B., Fisseha, S., Asfaw, L., Mahmoud, S., Rayan, A., Bendick, R., Kogan, L., 2010. Geodetic constraints on present-day motion of the Arabian Plate: Implications for Red Sea and Gulf of Aden rifting. Tectonics 29, TC3011. doi:10.1029/2009TC002482

Artemjev, M. E., Artyushkov, E.V., 1971. Structure and isostasy of the Baikal Rift and the mechanism of rifting, J. Geophys. Res., 76, 1197-1211.

Artyushkov, E.V., 1973. Stresses in the lithosphere caused by crustal thickness inhomogeneities. J. Geophys. Res. 78, 7675–7708.

Artyushkov, E. V., 1983. Geodynamics, 312 pp., Elsevier, Amsterdam.

Arzi, A.A., 1978. Critical phenomena in the rheology of partially melted rocks. Tectonophysics 44, 173–184.

Atwater, T., 1970. Implications of Plate Tectonics for the Cenozoic Tectonic Evolution of Western North America. Geol. Soc. Am. Bull. 81, 3513–3536.

Audet, P., Bürgmann, R., 2011. Dominant role of tectonic inheritance in supercontinent cycles. Nat. Geosci. 4, 184–187. doi:10.1038/ngeo1080

Augustin, N., Devey, C.W., van der Zwan, F.M., Feldens, P., Tominaga, M., Bantan, R.A., Kwasnitschka, T., 2014. The rifting to spreading transition in the Red Sea. Earth Planet. Sci. Lett. 395, 217–230. doi:10.1016/j.epsl.2014.03.047

Autin, J., Bellahsen, N., Husson, L., Beslier, M., Leroy, S., D'Acremont, E., 2010. Analog models of oblique rifting in a cold lithosphere. Tectonics 29, TC6016. doi:10.1029/2010TC002671

Autin, J., Bellahsen, N., Leroy, S., Husson, L., Beslier, M.O., D'Acremont, E., 2013. The role of structural inheritance in oblique rifting: Insights from analogue models and application to the Gulf of Aden. Tectonophysics 607, 51–64. doi:10.1016/j.tecto.2013.05.041

Axen, G., Lam, P., Grove, M., Stockli, D., Hassanzadeh, J., 2001. Exhumation of the west-central Alborz Mountains, Iran, Caspian subsidence, and collision-related tectonics. Geology 29, 559–562. doi:10.1130/0091-7613(2001)029<0559:EOTWCA>2.0.CO;2

Barbier, F., Duverge, J., le Pichon, X., 1986. Structure profonde de la marge Nord-Gascogne. Implications sur le mechanisme de rifting et de formation de la marge continentale. Bull. Cent. Rech. Explor. Prod. Elf-Aquitaine 10, 105-121.

References

Bastow, I.D., Nyblade, A.A., Stuart, G.W., Rooney, T.O., Benoit, M.H., 2008. Upper mantle seismic structure beneath the Ethiopian hot spot: Rifting at the edge of the African low-velocity anomaly. Geochemistry, Geophys. Geosystems 9. doi:10.1029/2008GC002107

Bastow, I.D., Stuart, G.W., Kendall, J.M., Ebinger, C.J., 2005. Upper-mantle seismic structure in a region of incipient continental breakup: Northern Ethiopian rift. Geophys. J. Int. 162, 479–493. doi:10.1111/j.1365-246X.2005.02666.x

Beaumont, C., Ings, S. J., 2012. Effect of depleted continental lithosphere counterflow and inherited crustal weakness on rifting of the continental lithosphere: General results. J. Geophys. Res. 117 (B8), B08407. doi:10.1029/2012JB009203

Begg, G.C., Griffin,W.L.,Natapov, I.M., O'Reilly, S.Y., Grand, S.P., O'Neil, C.J., Hronsky, J.M.A., Poudjom-Djomani, Y.H., Swain, C.J., Deen, T., Bowden, P., 2009. The lithospheric architecture of Africa: seismic tomography, mantle petrology, and tectonic evolution. Geosphere 5, 23–50.

Behn, M.D., Lin, J., 2000. Segmentation in gravity and magnetic anomalies along the U.S. East Coast passive margin: implications for incipient structure of the oceanic litho- sphere. J. Geophys. Res. 105, 25769

Behn, M., Lin, J., Zuber, M., 2002. A continuum mechanics model for normal faulting using a strain-rate softening rheology: Implications for thermal and rheological controls on continental and oceanic rifting. Earth Planet. Sci. Lett. 202, 725–740. doi:10.1016/S0012-821X(02)00792-6

Behrend, F., 1918. Die Stratigraphie des oestlichen Zentralafrika. Beitr Geol Erforsch Dtsch Schutzgebiet 15: 1-146

Bellahsen, N., Daniel, J., 2005. Fault reactivation control on normal fault growth : An experimental study. J. Struct. Geol. 27, 769-780. doi:10.1016/j.jsg.2004.12.003

Bellahsen, N., Faccenna, C., Funiciello, F., Daniel, J.M., Jolivet, L., 2003. Why did Arabia separate from Africa? Insights from 3-D laboratory experiments. Earth Planet. Sci. Lett. 216, 365–381. doi:10.1016/S0012-821X(03)00516-8

Bellahsen, N., Leroy, S., Autin, J., Razin, P., d'Acremont, E., Sloan, H., Pik, R., Ahmed, A., Khanbari, K., 2013. Pre-existing oblique transfer zones and transfer/transform relationships in continental margins: New insights from the southeastern Gulf of Aden, Socotra Island, Yemen. Tectonophysics 607, 32–50. doi:10.1016/j.tecto.2013.07.036

Ben-Avraham, Z., Katsman, R., 2015. The formation of graben morphology in the Dead Sea Fault, and its implications. Geophys. Res. Lett. 42, 6989–6996. doi:10.1002/2015GL065111

Benes, V., 1995. Rift propagation into a continental margin: tectonic study of the western Woodlark Basin and physical analogue modelling. University of Toronto.

Benes, V., Davy, P., 1996. Modes of continental lithospheric extension: experimental verification of strain localization processes. Tectonophysics 254, 69–87. doi:10.1016/0040-1951(95)00076-3

Benes, V., Scott, S., 1996. Oblique rifting in the Havre Trough and its propagation into the continental margin of New Zealand: Comparison with analogue experiments. Mar. Geophys. Res. 18, 189–201. doi:10.1007/BF00286077

Benes, V., Scott, S.D., Binns, R.A., 1994. Tectonics of rift propagation into a continental margin: Western Woodlark Basin, Papua New Guinea. J. Geophys. Res. 99, 4439–4455.

Beniest, A., Koptev, A., Burov, E., 2017. Numerical models for continental break-up: Implications for the South Atlantic. Earth Planet. Sci. Lett. 461, 176–189. doi:10.1016/j.epsl.2016.12.034

Benoit, M.H., Nyblade, A.A., Pasyanos, M.E., 2006. Crustal thinning between the Ethiopian and East African plateaus from modeling Rayleigh wave dispersion. Geophys. Res. Lett. 33, 1–5. doi:10.1029/2006GL025687

Bercovici, D., Ricard, Y., 2014. Plate tectonics, damage and inheritance. Nature 508, 513–6. doi:10.1038/nature13072

Berggren, W.A., Kent, D.V., Aubry, M.-E, Hardenbol, J. (Eds.), 1995. Geochronology, Time scales and Global Stratigraphic Correlation. SEPM Spec. Publ. 54.

Bialas, R. W., Buck., W. R., 2009. How sediment promotes narrow rifting: Applications to the Gulf of California. Tectonics, 28, TC4014. doi: 10.1029/2008TC002394

Biddle, K.T., Christie-Blick, N., 1985. Glossary e strike-slip deformation, basin formation, and sedimentation. In: Biddle, K.T., Christie-Blick, N. (Eds.), Strike-slip Deformation, Basin Formation, and Sedimentation. Society of Economic Mineralogists, 375-386. Special Publication 37.

Birch, F., 1954. The present state of geothermal investigations, Geophysics, 19, 645-659.

Bonatti, E., 1985. Punctiform initiation of seafloor spreading in the Red Sea during transition from a continental to an oceanic rift. Nature 316, 33–37.

Bonatti, E., Seyler, M., Channell, J., Giraudeau, J., Mascle, G., 1990. Peridotites drilled from the Tyrhenian Sea, ODP Leg 107 107.

Bonini, M., Corti, G., Innocenti, F., Manetti, P., Mazzarini, F., Abebe, T., Pecskay, Z., 2005. Evolution of the Main Ethiopian Rift in the frame of Afar and Kenya rifts propagation. Tectonics 24, 1–21. doi:10.1029/2004TC001680

Bonini, M., Souriot, T., Boccaletti, M., Brun, J.P., 1997. Successive orthogonal and oblique extension episodes in a rift zone: Laboratory experiments with application to the Ethipian Rift. Tectonics 16, 347–362.

Bosworth, W., 1994. A model for the three-dimensional evolution of continental rift basins, north-east Africa. Geology of Northeast Africa (Part 2), Geologische Rundschau, Springer 83, 671–688.

Bosworth, W., 2015. Geological Evolution of the Red Sea: Historical Background, Review and Synthesis. doi:10.1007/978-3-662-45201-1

Bosworth, W., 1985. Geometry of propagating continental rifts. Nature 316, 625–627. doi:10.1038/316625a0

Bosworth, W., 1987. Off-axis volcanism in the Gregory rift, east Africa: implications for models of continental rifting, Geology, 15, 397-400

Bosworth, W., Huchon, P., McClay, K., 2005. The Red Sea and Gulf of Aden Basins. J. African Earth Sci. 43, 334–378. doi:10.1016/j.jafrearsci.2005.07.020

Bott, M.H.P., Kusznir, N.J., 1979. Stress distributions associated with compensated plateau uplift structures with application to the continental splitting mechanism. Geophys. J. R. Astron. Soc. 56, 451–459. doi:10.1111/j.1365-246X.1979.tb00177.x

Boutelier, D., Chemenda, A., Jorand, C., 2002. Thermo-mechanical laboratory modelling of continental subduction : first experiments. J. Virtual Explor. 6, 61–65. doi:10.1016/j.epsl.2004.02.013

Boutelier, D., Cruden, A., 2013. Slab rollback rate and trench curvature controlled by arc deformation. Geology 41, 911–914. doi:10.1130/G34338.1

References

Boutelier, D., Oncken, O., 2011. 3-D thermo-mechanical laboratory modeling of plate-tectonics: modeling scheme, technique and first experiments. Solid Earth 2, 35–51. doi:10.5194/se-2-35-2011

Boutelier, D., Saumur, B., Cruden, A.R., 2016. Density and visco-elasticity of Natrosol 250 HH solutions for experimental tectonics. J. Struct. Geol. 1–38. doi:10.1016/j.jsg.2016.03.001

Boutelier, D., Schrank, C., Cruden, A., 2008. Power-law viscous materials for analogue experiments: New data on the rheology of highly-filled silicone polymers. J. Struct. Geol. 30, 341–353. doi:10.1016/j.jsg.2007.10.009

Braun, J., Thieulot, C., Fullsack, P., DeKool, M., Beaumont, C., Huismans, R.S., 2008. DOUAR: A new three-dimensional creeping flow numerical model for the solution of geological problems. Physics of the Earth and Planetary Interiors 171, 76-91.

Brun, J.P., 1999. Narrow rifts versus wide rifts : inferences for the mechanics of rifting from laboratory experiments 695–712.

Brun, J., Choukroune, P., 1983. Normal faulting, block tilting, and décollement in a stretched crust. Tectonics, 2(4), 345–356.

Brune, S., 2014. Evolution of stress and fault patterns in oblique rift systems: 3D numerical lithospheric-scale experiments from rift to breakup. Geochemistry, Geophys. Geosystems 3392–3415. doi:10.1002/2014GC005446

Brune, S., Autin, J., 2013. The rift to break-up evolution of the Gulf of Aden: Insights from 3D numerical lithospheric-scale modelling. Tectonophysics 607, 65–79. doi:10.1016/j.tecto.2013.06.029

Brune, S., Corti, G., Ranalli, G., 2017. Controls of inherited lithospheric heterogeneity on rift linkage: Numerical and analogue models of interaction between the Kenyan and Ethiopian rifts across the Turkana depression. Tectonics. doi:10.1002/2017TC004739

Brune, S., Heine, C., Clift, P.D., Pérez-Gussinyé, M., 2016a. Rifted margin architecture and crustal rheology: Reviewing Iberia-Newfoundland, central South Atlantic, and South China sea. Mar. Pet. Geol. doi:10.1016/j.marpetgeo.2016.10.018

Brune, S., Heine, C., Pérez-Gussinyé, M., Sobolev, S. V, 2014. Rift migration explains continental margin asymmetry and crustal hyper-extension. Nat. Commun. 5, 4014. doi:10.1038/ncomms5014

Brune, S., Popov, A., Sobolev, S., 2013. Quantifying the thermo-mechanical impact of plume arrival on continental break-up. Tectonophysics 604, 51–59. doi:10.1016/j.tecto.2013.02.009

Brune, S., Popov, A., Sobolev, S., 2012. Modeling suggests that oblique extension facilitates rifting and continental break-up. J. Geophys. Res. Solid Earth 117, 1–17. doi:10.1029/2011JB008860

Brune, S., Williams, S.E., Butterworth, N.P., Müller, R.D., 2016b. Abrupt plate accelerations shape rifted continental margins. Nature 536, 1–4. doi:10.1038/nature18319

Buck, W. R., 1988. Flexural rotation of normal faults. Tectonics, 7, 959–973.

Buck, W.R., 1991. Modes of continental lithospheric extension. J. Geophys. Res. 96, 20161. doi:10.1029/91JB01485

Buckingham, E., 1914. On physically similar systems; illustrations of the use of dimensional equations, Phys. Rev., 4, 345–376.

Bunter M. A. G., Abdel Magid A. E. M., 1989. The Sudanese Red Sea; New developments in stratigraphy and petroleum-geological evolution. J. Pet. Geol. 12, 145–166.

Buiter, S.J.H., Torsvik, T.H., 2014. A review of Wilson Cycle plate margins: A role for mantle plumes in continental break-up along sutures? Gondwana Res. 26, 627–653. doi:10.1016/j.gr.2014.02.007

Burchfield, B.C., Stewart, J.H., 1966. "pull-apart" origin of the central segment of Death Valley, California. Bull. Geol. Soc. Am. 77, 439–442. doi:10.1130/0016-7606(1966)77[439:POOTCS]2.0.CO;2

Burke, K., Dewey, J.., 1974. Two plates in Afric during the Cretaceous? Nature 249, 313–316. doi:10.1038/249313a0

Burke, K., Dewey, J.F., 1973. Plume-Generated Triple Junctions: Key Indicators in Applying Plate Tectonics to Old Rocks. J. Geol. 81, 406–433. doi:10.1086/627882

Burke, K., Whiteman, A.J., 1973. Uplift, rifting and the break-up of Africa. In: Tarling, D.H., Runcorn, S.K. (Eds.), Implications of Continental Drift to the Earth Sciences. Academic Press, New York, 735–755.

Burov, E., Cloetingh, S., 1997. Erosion and rift dynamics: New thermomechanical aspects of post-rift evolution of extensional basins, Earth Planet. Sci. Lett., 150, 7–26, doi:10.1016/S0012-821X(97)00069-1

Burov, E., Gerya, T., 2014. Asymmetric three-dimensional topography over mantle plumes. Nature 513, 85–89. doi:10.1038/nature13703

Buttinelli, M., Scrocca, D., De Rita, D., Quattrocchi, F., 2014. Modes of stepwise eastward migration of the northern Tyrrhenian Sea back-arc extension: Evidences from the northern Latium offshore (Italy). Tectonics 33, 187–206. doi:10.1002/2013TC003365

Byerlee, J., 1978. Friction of Rocks 116.

Calais, E., Ebinger, C., Hartnady, C., Nocquet, J.M., 2006. Kinematics of the East African Rift from GPS and earthquake slip vector data. Geol. Soc. Spec. Publ. 9–22.

Campbell, W.. 2003. Introduction to Geomagnetic Fields. Cambridge: Cambridge University Press. doi:10.1017/CBO9781139165136

Cappelletti, A., Tsikalas, F., Nestola, Y., Cavozzi, C., Argnani, A., Meda, M., Salvi, F., 2013. Impact of lithospheric heterogeneities on continental rifting evolution: Constraints from analogue modelling on South Atlantic margins. Tectonophysics 608, 30–50. doi:10.1016/j.tecto.2013.09.026

Carey, S.W., 1958. Continental Drift – a symposium. University of Hobart, 375 pp.

Chang, S.J., Merino, M., Van der Lee, S., Stein, S., Stein, C.A., 2011. Mantle flow beneath Arabia offset from the opening Red Sea. Geophys. Res. Lett. 38, 1–5. doi:10.1029/2010GL045852

Chapman, D. S., Rybach L., 1985. Heat flow anomalies and their interpretation, J. Geodyn., 4, 3-37.

Chen, L., Zhang, Z., Song, H., Li, F., Franke, D., 2013. Numerical modeling of extensional sedimentary basin formation with MATLAB: Application to the northern margin of the South China Sea. Comput. Geosci. 51, 153–165. doi:10.1016/j.cageo.2012.07.014

Chen, Z., Schellart, W.P., Strak, V., Duarte, J.C., 2016. Does subduction-induced mantle flow drive backarc extension? Earth Planet. Sci. Lett. 441, 200–210. doi:10.1016/j.epsl.2016.02.027

Chenin, P., Beaumont, C., 2013. Influence of offset weak zones on the development of rift basins: Activation and abandonment during continental extension and breakup, J. Geophys. Res., 118, 1– 23, doi:10.1002/jgrb.50138

Chery, J., Lucazeau, F., Daignieres, M., Vilotte, J.P., 1989. Strain localization in rift zones (case of thermally softened lithosphere): a finite element approach, Bull. Soc. geol. Fr., 3, 437-443.

References

Childs, C., Holdsworth, R.E., Jackson, C.A.-L., Manzocchi, T.,Walsh, J.J., Yielding, G. (Eds.) The Geom- etry and Growth of Normal Faults. Geological Society, London, Special Publications, 439. First published online August 17, 2016, doi:10.1144/ SP439.16

Choi, E., Lavier, L., Gurnis, M., 2008. Thermomechanics of mid-ocean ridge segmentation. Phys. Earth Planet. Inter. 171, 374–386. doi:10.1016/j.pepi.2008.08.010

Chorowicz, J., 2005. The East African rift system. J. African Earth Sci. 43, 379–410. doi:10.1016/j.jafrearsci.2005.07.019

Chorowicz, J., Sorlien, C., 1992. Oblique extensional tectonics in the Malawi Rift, Africa, Geol. Soc. Am. Bull., 104, 1015-1023

Chu, D., Gordon, R., 1998. Current plate motions across the Red Sea. Geophys. J. Int. 135, 313–328. doi:10.1046/j.1365-246X.1998.00658.x

Clifton, A.E., Schlische, R.W., Withjack, M.O., Ackermann, R. V., 2000. Influence of rift obliquity on fault-population systematics: Results of experimental clay models. J. Struct. Geol. 22, 1491–1509. doi:10.1016/S0191-8141(00)00043-2

Cloos, H., 1930. Kunstliche Gebirge, Natur Mus., Frankf., Part 2, 258-269.

Cochran, J., Martinez, F., 1988. Evidence from the northern Red Sea on the transition from continental to oceanic rifting. Tectonophysics, 153, 25–53, doi: 10.1016/0040-1951(88)90006-6

Cochran, J.R., 1981. The Gulf of Aden: structure and evolution of a young ocean basin and continental basin. J. Geophys. Res. 86 (1), 263–287.

Cochran, J.R., 1982. The magnetic quiet zone in the eastern Gulf of Aden: implacations for the early development of the continental margin. Geophys. J. R. Astron. Soc. 68, 171–201.

Coleman, R.G., Hadley, D.G., Fleck, R.G., Hedge, C.T., Danato, M.M., 1979. The Miocene Tihama–Asir ophiolite and its bearing on the opening of the Red Sea, evolution and mineralization of the Arabian–Nubian Shield. Inst. Appl. Geol. Bull. 3, 173–186.

Coney, P. J., 1980. Cordilleran metamorphic core complexes: An overview, in Crittenden, M. D., Jr., et al.(Eds.), Cordilleran metamorphic core complexes: Geological Society of America Memoir 153, 7–134.

Collet, B., Taud, H., Parrot, J.F., Bonavia, F., Chorowicz, J., 2000. A new kinematic approach for the Danakil block using a Digital Elevation Model representation. Tectonophysics 316, 343–357. doi:10.1016/S0040-1951(99)00263-2

Corti, G., 2012. Evolution and characteristics of continental rifting: Analog modeling-inspired view and comparison with examples from the East African Rift System. Tectonophysics 522–523, 1–33. doi:10.1016/j.tecto.2011.06.010

Corti, G., 2009. Continental rift evolution: From rift initiation to incipient break-up in the Main Ethiopian Rift, East Africa. Earth-Science Rev. 96, 1–53. doi:10.1016/j.earscirev.2009.06.005

Corti, G., 2008. Control of rift obliquity on the evolution and segmentation of the main Ethiopian rift. Nat. Geosci. 1, 258–262. doi:10.1038/ngeo160

Corti, G., Bonini, M., Conticelli, S., Innocenti, F., Manetti, P., Sokoutis, D., 2003. Analogue modelling of continental extension: A review focused on the relations between the patterns of deformation and the presence of magma. Earth-Science Rev. 63, 169–247. doi:10.1016/S0012-8252(03)00035-7

Corti, G., Calignano, E., Petit, C., Sani, F., 2011. Controls of lithospheric structure and plate kinematics on rift architecture and evolution: An experimental modeling of the Baikal rift. Tectonics 30, 1–16. doi:10.1029/2011TC002871

Corti, G., Ranalli, G., Agostini, A., Sokoutis, D., 2013. Inward migration of faulting during continental rifting: Effects of pre-existing lithospheric structure and extension rate. Tectonophysics 594, 137–148. doi:10.1016/j.tecto.2013.03.028

Corti, G., Ranalli, G., Mulugeta, G., Agostini, A., Sani, F., Zugu, A., 2010. Control of the rheological structure of the lithosphere on the inward migration of tectonic activity during continental rifting. Tectonophysics 490, 165–172. doi:10.1016/j.tecto.2010.05.004

Corti, G., van Wijk, J., Cloetingh, S., Morley, C.K., 2007. Tectonic inheritance and continental rift architecture: Numerical and analogue models of the East African Rift system. Tectonics 26, 1–13. doi:10.1029/2006TC002086

Courtillot, V.E., 1982. Propagating rifts and continental breakup. Tectonics 1, 239–250.

Courtillot, V.E., 1980. Opening of the Gulf of Aden and Afar by progressive tearing. Phys. Earth Planet. Inter. 21, 343–350. doi:10.1016/0031-9201(80)90137-5

Courtillot, V., Cisowski, S., 1987. The Cretaceous-Tertiary boundary events: External or Internal causes? EOS, 68, 193-200.

Courtillot, V.E., Jaupart, C., Manighetti, I., Tapponnier, P., Besse, J., 1999. On causal links between flood basalts and continental breakup. Earth Planet. Sci. Lett. 166, 177–195. doi:10.1016/S0012-821X(98)00282-9

Crane, K., Bonatti, E., 1987. The role of fracture zones during early Red Sea rifting: structural analysis using Space Shuttle radar and LANDSAT imagery. J. Geol. Soc. London. 144, 407–420. doi:10.1144/gsjgs.144.3.0407

Crider, J.G., Pollard, D.D., 1998. Fault linkage: three-dimensional mechanical interaction between echelon normal faults. J. Geoph. Res. 103 (24), 373–393.

Crossley, R., 1984. Controls of sedimentation in the Malawi Rift Valley, Central Africa. Sedimentary Geology 40, 33–50.

Cruden, A., Nasseri, M., Pysklywec, R., 2006. Surface topography and internal strain variation in wide hot orogens from three-dimensional analogue and two-dimensional numerical vice models. Geol. Soc. Spec. Publ. 253, 79–104. doi:10.1144/GSL.SP.2006.253.01.04

Darros de Matos, R.M., 2000. Tectonic evolution of the equatorial South Atlantic. In: Mohriak, W., Taiwani, M. (Eds.), Atlantic Rifts and ContinentalMargins. Geophysical Monograph Series 115, 331-354.

Darros de Matos, R., 1992. The northeast brazilian rift system. Tectonics 11, 766–791.

Dauteuil, O., Bourgeois, O., Mauduit, T., 2002. Lithosphere strength controls oceanic transform zone structure : insights from analogue models. Geophys. J. Int. 150, 706–714.

Dauteuil, O., Brun, J.P., 1993. Oblique rifting in a slow-spreading ridge. Nature 361, 145–148. doi:10.1038/361145a0

Davaille, A., 1999. Two-layer thermal convection in miscible viscous fluids. J. Fluid Mech. 379, 223–253. doi:10.1017/S0022112098003322

Davaille, A., Girard, F., Le Bars, M., 2002. How to anchor hotspots in a convecting mantle? Earth Planet. Sci. Lett. 203, 621–634. doi:10.1016/S0012-821X(02)00897-X

References

Davaille, A., Le Bars, M., Carbonne, C., 2003. Thermal convection in a heterogeneous mantle. Comptes Rendus Geosci. 335, 141–156. doi:10.1016/S1631-0713(03)00003-8

Davis, D., Suppe, J., Dahlen, A., 1983. Mechanics of fold-and-thrust belts and accretionary wedges. J. Geoph. Res. 88. 1153-1172.

Davy, P., Cobbold, P., 1991. Experiments on shortening of a 4-layer model of the continental lithosphere. Tectonophysics 188, 1–25.

de Beaumont, E., 1847. Note sur les systèmes de montagnes les plus anciens de l'Europe, Bull. Soc. Geol. Fr., 4, 864-991.

de Beaumont, E., 1827. Observations géologiques, Ann. Mines, 2, 5-82.

Delvaux, D., 2001. Tectonic and palaeostress evolution of the Tanganyika-Rukwa-Malawi rift segment, East African Rift System. Peri-Tethys Mem. 6 Peri-Tethyan Rift. Basins Passiv. Margins 545–567.

Delvaux, D., Barth, A., 2010. African stress pattern from formal inversion of focal mechanism data. Tectonophysics 482, 105–128. doi:10.1016/j.tecto.2009.05.009

Delvaux, D., Levi, K., Kajara, R., Sarota, J., 1992. Cenozoic Paleostress and Kinematic Evolution of the Rukwa - North Malawi Rift Valley (East African Rift System). Bull. Centres Rech. Explor. -Prod. Elf Aquitaine 16, 383–406.

Dercourt, J., Ricou, L. E., Vrielynck, B., 1993. Atlas Tethys Palaeoenvironmental Maps, 307 pp., Gauthier-Villars, Paris.

Dercourt, J., Zonenshain, L. P., Ricou, L.-E., 1986. Geological evolution of the Tethys belt from the Atlantic to the Pamir since the Lias, Tectonophysics, 123, 241–315.

Desa, M.A., Ismaiel, M., Suresh, Y., Krishna, K.S., 2018. Oblique strike-slip motion off the Southeastern Continental Margin of India: Implication for the separation of Sri Lanka from India. J. Asian Earth Sci. 156, 111–121. doi:10.1016/j.jseaes.2018.01.015

Detrick, R.S., Von Herzen, R.P., Parsons, B., Sandwell, D., Dougherty, M., 1986. Heat flow observations on the bermuda rise and thermal models of midplate swells. J. Geophys. Res. 91, 3701–3723.

Ding, W., Li, J., 2016. Propagated rifting in the Southwest Sub-basin, South China Sea: Insights from analogue modelling. J. Geodyn. doi:10.1016/j.jog.2016.02.004

Dixon, T., Stern, R., Hussein, I., 1987. Control of Red Sea rift geometry by Precambrian structures. Tectonics 6, 551–571.

Dooley, T., Schreurs, G., 2012. Analogue modeling of intraplate strike-slip tectonics: A review and new experimental results. Tectonophysics 574,1–71

Duarte, J., Schellart, W.P., Cruden, A., 2014. Rheology of petrolatum–paraffin oil mixtures: Applications to analogue modelling of geological processes. J. Struct. Geol. 63, 1–11. doi:10.1016/j.jsg.2014.02.004

Dubinin, E.P., Grokholsky, A.L., Makushkina, A.I., 2018. Physical modeling of the formation conditions of microcontinents and continental marginal plateaus. Izv. Phys. Solid Earth 54, 66–78. doi:10.1134/S1069351318010056

Duffy, O.B., Nixon, C.W., Bell, R.E., Jackson, C.A.-L., Gawthorpe, R.L., Sanderson, D.J., Whipp, P.S., 2017. The topology of evolving rift fault networks: Single-phase vs multi-phase rifts. J. Struct. Geol. INPRESS. doi:10.1016/j.jsg.2017.02.001

Dunbar, J.A., Sawyer, D.S., 1996. Three-dimensional dynamical model of continental rift propagation and margin plateau formation. J. Geophys. Res. Earth 101, 27845–27863. doi:10.1029/96jb01231

Eagles, G., Gloaguen, R., Ebinger, C., 2002. Kinematics of the Danakil microplate. Earth Planet. Sci. Lett. 203, 607–620. doi:10.1016/S0012-821X(02)00916-0

Ebinger, C.J., 1989. Tectonic development of the western branch of the East African rift system. Geol. Soc. Am. Bull. 101, 885–903. doi:10.1130/0016-7606(1989)101<0885

Ebinger, C.J., Sleep, N.H., 1998. Cenozoic magmatism throughout east Africa resulting from impact of a single plume. Nature 395, 788–791.

Ebinger, C.J., Yemane, T., Harding, D.J., Tesfaye, S., Kelley, S., Rex, D.C., 2000. Rift deflection, migration, and propagation: Linkage of the Ethiopian and Eastern rifts, Africa. Bull. Geol. Soc. Am. 112, 163–176. doi:10.1130/0016-7606(2000)112<163:RDMAPL>2.0.CO;2

Ehrhardt, A., Hübscher, C., Ben-Avraham, Z., Gajewski, D., 2005. Seismic study of pull-apart-induced sedimentation and deformation in the Northern Gulf of Aqaba (Elat). Tectonophysics 396, 59–79. doi:10.1016/j.tecto.2004.10.011

Engdahl, E.R., van der Hilst, R., Buland, R., 1998. Global teleseismic earthquake relocation with improved travel times and procedures for depth determination. Bulletin of the Seismological Society of America 88, 722-743.

England, P., 1983. Constraints on extension of continental lithosphere. J. Geophys. Res. 88, 1145. doi:10.1029/JB088iB02p01145

Escher, B. G., Kuenen, H., 1929. Experiments in connection with salt domes, Leid. Geol. Meded. 3, 151-182.

Faccenna, C., Becker, T.W., Jolivet, L., Keskin, M., 2013. Mantle convection in the Middle East: Reconciling Afar plume, Arabia collision and Aegean trench rollback. Earth Planet. Sci. Lett.

Faccenna, C., Becker, T.W., Lucente, F.P., Jolivet, L., Rossetti, F., 2001. History of subduction and and back arc extension in the central Mediterranean. Geophys. J. Int. 145, 809–820.

Faccenna, C., Davy, P., Brun, J.-P., Funiciello, R., Giardini, D., Mattei, M., Nalpas, T., 1996. The dynamics of back-arc extension: an experimental approach to the opening of the Tyrrhenian Sea. Geophys. J. Int. 126, 781–795. doi:10.1111/j.1365-246X.1996.tb04702.x

Faccenna, C., Mattei, M., Funiciello, R., Jolivet, L., 1997. Styles of back-arc extension in the Central Mediterranean. Terra Nov. 9, 126–130. doi:10.1046/j.1365-3121.1997.d01-12.x

Farrington, R.J., Stegman, D.R., Moresi, L.N., Sandiford, M., May, D.A., 2010. Interactions of 3D mantle flow and continental lithosphere near passive margins. Tectonophysics 483, 20–28. doi:10.1016/j.tecto.2009.10.008

Feng, B.X., Amponsah, P.O., Martin, R., Ganne, J., Jessell, M.W., 2015. 3-D numerical modelling of the influence of pre-existing faults and boundary conditions on the distribution of deformation: example of North-Western Ghana. Precambrian Res. doi:10.1016/j.precamres.2015.06.006

Finch, E., Gawthorpe, R., 2017. Growth and Interaction of Normal Faults and Fault Network Evolution in Rifts: Insights from Three Dimensional Discrete Element Modelling. Geol. Soc. Spec. Publ.

Finckh, L., 1912. Die jungvulkanischen Gesteine des Kiwusee-Gebietes. Wiss Ergeb Dtsch Zentral-Afrika-Expedition: 1907-1908, 1, 1-44.

References

Fletcher, R.C., Hudec, M.R., Watson, I.A., 1995. Salt glacier and composite sediment-salt glacier models for the emplacement and early burial of allochthonous salt sheets, in Jackson, M.P.A., Roberts, D.G., and Snelson, S. (Eds.), Salt Tectonics: A Global Perspective: American Association of Petroleum Geologists Memoir 65, 77–108.

Fletcher, R., Kusznir, N., Roberts, A., Hunsdale, R., 2013. The formation of a failed continental breakup basin: The Cenozoic development of the Faroe-Shetland Basin. Basin Res. 25, 532–553. doi:10.1111/bre.12015

Fossen, H., 2010, Structural Geology: Cambridge University Press, Cambridge, 463 pp.

Fossen, H., Rotevatn, A., 2016. Fault linkage and relay structures in extensional settings-A review. Earth-Science Rev. 154, 14–28. doi:10.1016/j.earscirev.2015.11.014

Foster, A., Jackson, J., 1998. Focal mechanism solutions of large African earthquakes: Implications for rheology and kinematics: Geoph. J. Int. 134, 422–448.

Freund, R., Merzer, A., 1976. Anisotropic Origin of Transform Faults, Science.

Funiciello, F., Faccenna, C., Heuret, a., Lallemand, S., Di Giuseppe, E., Becker, T.W., 2008. Trench migration, net rotation and slab-mantle coupling. Earth Planet. Sci. Lett. 271, 233–240. doi:10.1016/j.epsl.2008.04.006

Furlong, K.P., Fountain, D.M., 1986. Continental crustal underplating: thermal considerations and seismic–petrologic consequences. J. Geoph. Res. 91, 8285–8294.

Gac, S., Geoffroy, L., 2009. 3D Thermo-mechanical modelling of a stretched continental lithosphere containing localized low-viscosity anomalies (the soft-point theory of plate break-up). Tectonophysics 468, 158–168. doi:10.1016/j.tecto.2008.05.011

Gaina, C., Müller, R.D., Brown, B.J., Ishihara, T., 2003. Microcontinent formation around Australia. Spec. Pap. 372 Evol. Dyn. Aust. Plate 372, 405–416. doi:10.1130/0-8137-2372-8.405

Gaina, C., Müller, R.D., Brown, B., Ishihara, T., Ivanov, S., 2007. Breakup and early seafloor spreading between India and Antarctica. Geoph. J. Int. 170, 151–169.

Galland, O., Bertelsen, H.S., Guldstrand, F., Girod, L., Johannessen, R.F., Bjugger, F., Burchardt, S., Mair, K., 2016. Application of open-source photogrammetric software MicMac for monitoring surface deformation in laboratory models. J. Geophys. Res. Solid Earth 121, 2852–2872. doi:10.1002/2015JB012564

Gawthorpe, R. L. and Hurst, J. M., 1993. Transfer zones in extensional basins: their structural style and influence on drainage development and stratigraphy, J. Geol. Soc., 150, 1137–1152. doi:10.1144/gsjgs.150.6.1137

Gerya, T., 2013. Initiation of Transform Faults at Rifted Continental Margins : 3D Petrological – Thermomechanical Modeling and Comparison to the Woodlark Basin. Petrology 21, 550–560. doi:10.1134/S0869591113060039

Gerya, T., 2013. Three-dimensional thermomechanical modeling of oceanic spreading initiation and evolution. Phys. Earth Planet. Inter. 214, 35–52. doi:10.1016/j.pepi.2012.10.007

Gerya, T., 2012. Origin and models of oceanic transform faults. Tectonophysics 522–523, 34–54. doi:10.1016/j.tecto.2011.07.006

Gerya, T., 2010. Dynamical instability produces transform faults at mid-ocean ridges. Science (80-.). 329, 1047–50. doi:10.1126/science.1191349

Gerya, T., Burov, E., 2017. Nucleation and evolution of ridge-ridge-ridge triple junctions: Thermomechanical model and geometrical theory. Tectonophysics. doi:10.1016/j.tecto.2017.10.020

Gerya, T.V., Yuen, D.A., 2007. Robust characteristics method for modelling multiphase visco-elasto-plastic thermo-mechanical problems. Physics of the Earth and Planetary Interiors 163, 83-105.

Gettings, M.E., Blank, H.R., Mooney, W.D., Healey, G.H., 1986. Crustal structure of southwestern Saudi Arabia. J. Geophys. Res. 91, 6491–6512.

Ghebreab, W., 1998. Tectonics of the Red Sea reassessed. Earth-Science Rev. 44, 1–44.

Gibbs, A. D., 1984. Structural evolution of extensional basin margins. J. Geol. Soc. 141, 609–620

Goes, S., Govers, Vacher, P., 2000. Shallow mantle temperatures under Europe from P and S wavetomography, J. Geophys. Res., 105, 11.153–11.169.

Goetze, C., Evans, B., 1979. Stress and temperature in the bend- ing lithosphere as constrained by experimental rock mechan- ics, Geophys. J. Roy. Astr. S., 59, 463–478, doi:10.1016/0148- 9062(80)91167-5.

Goguel, J., 1952. Traité de Tectonique.Masson, Paris. Translated by Thalmann, H. E. (1962). In: Tectonics, Freeman, San Francisco.

Green, W. V, Achauer, U., Meyer, R.P., 1991. A three-dimensional seismic image of the crust and upper mantle beneath the Kenya rift . Nature 354, 199–203. doi:10.1038/354199a0

Gregg, P., Behn, M., Lin, J., Grove, T., 2009. Melt generation, crystallization, and extraction beneath segmented oceanic transform faults. J. Geophys. Res. 114, B11102. doi:10.1029/2008JB006100

Gregory, J.W., 1921. The Rift Valleys and Geology of East Africa. Seely Service, London, 479 pp.

Gregory, J.W., 1894. Contributions to the physical geography of British East Africa. Geogr. J. Lond. 4, 290-315

Gudlaugsson, S.T., Gunnarsson, K., Sand, M., Skogseid, J., 1988. Tectonic and volcanic events at the Jan Mayen Ridge microcontinent. Geol. Soc. London, Spec. Publ. 39, 85–93. doi:10.1144/GSL.SP.1988.039.01.09

Gueydan, F., Précigout, J., 2013. Modes of continental rifting as a function of ductile strain localization in the lithospheric mantle: Tectonophysics. doi: 10.1016/j.tecto.2013.11.029

Gueydan, F., Morency, C., Brun, J.-P., 2008. Continental rifting as a function of lithosphere mantle strength: Tectonophysics, 460, no. 1-4, p. 83-93, doi:10.1016/j.tecto.2008.08.012

Guiraud, M., Buta-Neto, A., Quesne, D., 2010. Segmentation and differential post-rift uplift at the Angola margin as recorded by the transform-rifted Benguela and oblique-to-orthogonal-rifted Kwanza basins. Mar. Pet. Geol. 27, 1040–1068. doi:10.1016/j.marpetgeo.2010.01.017

Gupta, S., Cowie, P.A., Dawers, N.H., Underhill, J.R., 1998. A mechanism to explain rift-basin subsidence and stratigraphic patterns through fault-array evolution. Geology 26, 595-598.

Haggerty, S.E., 1979. The aeromagnetic mineralogy of igneous rocks. Can. J. Earth Sci. Vol 16, 1281–1293. doi:10.1139/e79-112

Hall, J., 1812. Account of a series of experiments, shewing the effects of compression in modifying the action of heat. Trans. R. Soc. Edin. 6, 71–185.

Hall, J., 1815. On the vertical position and convolution of certain strata, and their relation with granite. Trans R. Soc. Edin. 7, 79–108.

Hall, S. A., 1989. Magnetic evidence for the nature of the crust beneath the southern Red Sea, J. Geophys. Res., 94(B9), 12267–12279, doi:10.1029/JB094iB09p12267.

References

Hamilton, W., 1987. Crustal extension in the Basin and Range Province, southwestern United States. In: Coward, M.P., Dewey, J.F.., Hancock, P.L. (Eds.), Continental Extensional Tectonics, 28. Geol. Soc. London Spec. Pub, 155–176.

Hansen, S.E., Nyblade, A.A., 2013. The deep seismic structure of the Ethiopia/Afar hotspot and the African superplume. Geophys. J. Int. 194, 118–124. doi:10.1093/gji/ggt116

Hansen, S.E., Nyblade, A.A., Benoit, M.H., 2012. Mantle structure beneath Africa and Arabia from adaptively parameterized P-wave tomography: Implications for the origin of Cenozoic Afro-Arabian tectonism. Earth Planet. Sci. Lett. 319–320, 23–34. doi:10.1016/j.epsl.2011.12.023

Harrowfield, M., Holdgate, G.R., Wilson, C.J.L., McLoughlin, S., 2005. Tectonic significance of the Lambert graben, East Antarctica: Reconstructing the Gondwanan rift. Geology 33, 197–200. doi:10.1130/G21081.1

Healy, J. H., Mooney, W. D., Blank, H. R., Gettings, M. E., Kohler, W. M., Lamson, R. J., Leone, L. E., 1982. Saudi Arabian Seismic deep-refraction profile: final project report. US Geological Survey, Open File Report, 02–37(IR-436)

Heezen, B.C., Tharp, M., 1965. Tectonic Fabric of the Atlantic and Indian Oceans and Continental Drift. Philos. Trans. R. Soc. A Math. Phys. Eng. Sci. 258, 90–106. doi:10.1098/rsta.1965.0024

Heidbach, O., Tingay, M., Barth, A., Reinecker, J., Kurfeß, D., Müller, B., 2010. Global crustal stress pattern based on the World Stress Map database release 2008. Tectonophysics 482, 3–15. doi:10.1016/j.tecto.2009.07.023

Heine, C., Brune, S., 2014. Oblique rifting of the equatorial atlantic: Why there is no saharan atlantic ocean. Geology 42, 211–214. doi:10.1130/G35082.1

Heine, C., Zoethout, J., Muller, R.D., 2013. Kinematics of the South Atlantic rift. Solid Earth 4, 215–253. doi:10.5194/se-4-215-2013

Hennig, E., 1916. Die Fauna des deutsh-ostrafrikanischen Urgonfazies. Z Dtsch Geol Ges 68A:441-476

Henza, A.A., Withjack, M.O., Schlische, R.W., 2010. Normal-fault development during two phases of non-coaxial extension: An experimental study. J. Struct. Geol. 32, 1656–1667. doi:10.1016/j.jsg.2009.07.007

Herbert, J.W., Cooke, M.L., Souloumiac, P., Madden, E.H., Mary, B.C.L., Maillot, B., 2015. The work of fault growth in laboratory sandbox experiments. Earth Planet. Sci. Lett. 432, 95–102. doi:10.1016/j.epsl.2015.09.046

Heron, P.J., Pysklywec, R.N., Stephenson, R., 2016. Lasting mantle scars lead to perennial plate tectonics. Nat. Commun. 7, 11834. doi:10.1038/ncomms11834

Herzberg, C.T., Fyfe, W.S., Carr, M.J., 1983. Density constraints on the formation of the continental Moho and crust. Contrib. to Mineral. Petrol. 84, 1–5. doi:10.1007/BF01132324

Hess, H.H., 1962. History of the Ocean Basins. Petrologic Studies – A Volume in Honour of A.F. Buddington. Memoir Geological Society of America, 55, 599–620.

Hey, R., 1977. A new class of "pseudofaults" and their bearing on plate tectonics: a propagating rift model. Earth Planet. Sci. Lett. 37, 321–325.

Hey, R., Duennebier, F.K., Morgan, W.J., 1980. Propagating rifts on midocean ridges. J. Geophys. Res. Solid Earth 85, 3647–3658. doi:10.1029/JB085iB07p03647

Hey, R., Martinez, F., Höskuldsson, Á., Benediktsdóttir, Á., 2010. Propagating rift model for the V-shaped ridges south of Iceland. Geochemistry, Geophys. Geosystems 11. doi:10.1029/2009GC002865

Hieronymus, C., 2004. Control on seafloor spreading geometries by stress- and strain-induced lithospheric weakening. Earth Planet. Sci. Lett. 222, 177–189. doi:10.1016/j.epsl.2004.02.022

Hill, R.I., 1991. Starting plumes and continental break-up. Earth Planet. Sci. Lett. doi:10.1016/0012-821X(91)90218-7

Hill, R.I., Campbell, H., Davies, G.F., Griffiths, R.W., 1992. Mantle plumes and continental tectonics. Science 256, 186–192.

Hinz, K., 1981. A hypothesis of terrestrial catastrophes: wedges of very thick oceanward dipping reflectors beneath passive continental margins: their origin and environmental significance. Geologisches Jahrbuch, Reihe E Geophysik, 3–28.

Holdsworth, R.E., Butler, C.A., Roberts, A.M., 1997. The recognition of reactivation during continental deformation. J. Geol. Soc. London. 154, 73–78. doi:10.1144/gsjgs.154.1.0073

Holmes, A., 1928. Radioactivity and earth movements. Trans. Geol. Soc. Glasg. 18 (3). 559–608.

Hooke, R.L., 1972. Geomorphic Evidence for Late-Wisconsin and Holocene Tectonic Deformation, Death Valley, California. Geol. Soc. Am. Bull. 83, 2073–2098.

Hooke, R.L., 1968. Steady-state relationships on arid-region alluvial fans in closed basins. Am. J. Sci. 266, 609–629.

Hubbert, M.K., 1937. Theory of scalale models as applied to the study of geologic structures. Geol. Soc. Am. Bull. 48, 1459–1520. doi:10.1130/GSAB-48-1459

Hubbert, M. King, 1951. Mechanical basis for certain familiar geologic structures, Bull. Geol. Soc. Am., 62, 355-372.

Huet, B., Le Pourhiet, L., Labrousse, L., Burov, E., Jolivet, L., 2011. Post-orogenic extension and metamorphic core complexes in a heterogeneous crust: the role of crustal layering inherited from collision. application to the cyclades (aegean domain). Geophys. J. Int. 184 (2), 611-625.

Hughes, G.W., Beydoun, Z.R., 1992. The Red Sea- Gulf of Aden: Biostratigraphy, lithostratigraphy and palaeoenvironments. J. Petr. Geol. 15, 135-156.

Hughes G. W., Filatoff, J., 1995. New biostratigraphic constraints on Saudi Arabian Red Sea pre- and syn-rift sequences. In: Al-Husseini MI (Ed.) Middle east petroleum geosciences, Geo'94, vol 2. Gulf PetroLink, Bahrain, 517–528

Hughes, G. W., Varol, O., Beydoun, Z. R., 1991. Evidence for middle Oligocene rifting of the Gulf of Aden and for late Oligocene rifting of the southern Red Sea, Mar. Pet. Geol., 8, 354–358, doi:10.1016/0264-8172 (91)90088-I

Huismans, R., Beaumont, C., 2011. Depth-dependent extension, two-stage breakup and cratonic underplating at rifted margins. Nature 473, 74–78. doi:10.1038/nature09988

Huismans, R., Beaumont, C., 2014. Rifted continental margins: The case for depth-dependent extension. Earth Planet. Sci. Lett. 407, 148–162. doi:10.1016/j.epsl.2014.09.032

Huismans, R., Beaumont, C., 2003. Symmetric and asymmetric litho- spheric extension: relative effects of frictional-plastic and viscous strain softening. J. Geophys. Res. 108, 2496.

Huismans, R.S., Podladchikov, Y.Y., Cloetingh, S., 2001. Transition from passive to active rifting: Relative importance of asthenospheric doming and passive extension of the lithosphere. J. Geophys. Res. Solid Earth 106, 11271–11291. doi:10.1029/2000JB900424

References

Illsley-Kemp, F., Keir, D., Bull, J.M., Gernon, T.M., Ebinger, C., Ayele, A., Hammond, J.O.S., Kendall, J.M., Goitom, B., Belachew, M., 2017. Seismicity during continental breakup in the Red Sea rift of Northern Afar.

Jackson, J., McKenzie, D., 1983. The geometrical evolution of normal fault systems. J. Struct. Geol. 5, 471-482.

Jacoby, W.R., 1976. Paraffin model experiment of plate tectonics. Tectonophysics 35, 103–113. doi:10.1016/0040-1951(76)90031-7

Jammes, S., Lavier, L., Manatschal, G., 2010. Extreme crustal thinning in the Bay of Biscay and the Western Pyrenees: From observations to modeling. Geochem. Geophys. Geosystems 11, 830-832. doi: 10.1029/2010GC003218

Jarrige, J.-J., Ott d'Estevou, P., Burollet, P.F., Montenat, C., Prat, P., Richert, J.-P., Thiriet, J.-P., 1990. The multistage tectonic evolution of the Gulf of Suez and Northern Red Sea continental rift from field observations. Tectonics 9, 441–465.

Jaupart, C., Mareschal, J.C., 1999. The thermal structure and thickness of continental roots. Dev. Geotecton. 24, 93–114. doi:10.1016/S0419-0254(99)80007-X

Jeanniot, L., Kusznir, N., Mohn, G., Manatschal, G., Cowie, L., 2016. Constraining lithosphere deformation modes during continental breakup for the Iberia-Newfoundland conjugate rifted margins. Tectonophysics 680, 28–49. doi:10.1016/j.tecto.2016.05.006

Joffe, S., Garfunkel, Z., 1987. Plate kinematics of the circum Red Sea - a re-evaluation. Tectonophysics 141, 5–22.

Johnson, P.R., Woldehaimanot, B., 2003. Development of the Arabian-Nubian Shield: perspectives on accretion and deformation in the northern East African Orogen and the assembly of Gondwana. Geol. Soc. Spec. Publ. 206, 289–325. doi:10.1144/GSL.SP.2003.206.01.15

Johnston, C., 1844. Travels in southern Abyssinia through the country of Adal to the Kingdom of Shoa. Madden, London, 492 pp

Kampunzu, A. B., Lubala, R. T. (Eds.), 1991. Magmatism in Extensional Structural Settings. The Phanerozoic African Plate. Xxviii + 639 pp. Berlin, Heidelberg, New York, London, Paris, Tokyo, Hong Kong: Springer-Verlag.

Karato, J., 1993, Importance of anelasticity in the interpretation of seismic tomography: Geophysical Research Letters, 20, 1623–1626.

Katz, R., Ragnarsson, R., Bodenschatz, E., 2005. Tectonic microplates in a wax model of sea-floor spreading. New J. Phys. 7, 37. doi:10.1088/1367-2630/7/1/037

Kazmi, A.H., Jan, M.Q., 1997. Geology and Tectonics of Pakistan, Graphic Publishers, Karachi, 554 pp.

Kazmin, V., Shifferaw, A., Balcha, T., 1978. The Ethiopian basement: Stratigraphy and possible manner of evolution. Geol. Rundschau 67, 531–546. doi:10.1007/BF01802803

Keep, M., McClay, K.R., 1997. Analogue modelling of multiphase rift systems. Tectonophysics 273, 239–270. doi:10.1016/S0040-1951(96)00272-7

Keranen, K., Klemperer, S.L., 2008. Discontinuous and diachronous evolution of the Main Ethiopian Rift: Implications for development of continental rifts. Earth Planet. Sci. Lett. 265, 96–111. doi:10.1016/j.epsl.2007.09.038

Khain, V. Y., 1992. The role of rifting in the evolution of the Earth's crust. Tectonophyiscs 215, 1-7.

Kirby, S.H., 1983. Rheology of the lithosphere. Rev. Geophys. Space Phys. 21 (6), 1458–1487

Koehn, D., Aanyu, K., Haines, S., Sachau, T., 2008. Rift nucleation, rift propagation and the creation of basement micro-plates within active rifts 458, 105–116. doi:10.1016/j.tecto.2007.10.003

Kohlstedt, D.L., Evans, B., Mackwell, S.J., 1995. Strength of the lithosphere: Constraints imposed by laboratory experiments. J. Geophys. Res.: Solid Earth 100 (B9), 17587-17602. doi: 10.1029/95JB01460

Koopmann, H., Brune, S., Franke, D., Breuer, S., 2014. Linking rift propagation barriers to excess magmatism at volcanic rifted margins. Geology 42, 1071–1074. doi:10.1130/G36085.1

Koptev, A., Calais, E., Burov, E., Leroy, S., Gerya, T., 2015. Dual continental rift systems generated by plume–lithosphere interaction. Nat. Geosci. 8. doi:10.1038/ngeo2401

Korme, T., Acocella, V., Abebe, B., 2004. The Role of Pre-existing Structures in the Origin, Propagation and Architecture of Faults in the Main Ethiopian Rift. Gondwana Res. 7, 467–479. doi:10.1016/S1342-937X(05)70798-X

Kreemer, C., Klein, E., Shen, Z.-K., Wang, M., Estey, L., Wier, S., Boler, F., 2014. A geodetic platemotion and Global Strain Rate Model. Geochemistry, Geophys. Geosystems 130. doi:10.1002/2014GC005407.Received

Krenkel, E., 1924, Der Syrische Bogen. Zentralbl. Mineral. 9, 274-281.

Kusznir, N.J., Karner, G.D., 2007. Continental lithospheric thinning and breakup in response to upwelling divergent mantle flow: application to the Woodlark, Newfoundland and Iberia margins. Geol. Soc. London, Spec. Publ. 282, 389–419. doi:10.1144/SP282.16

Kusznir, N.J., Marsden, G., Egan, S.S., 1991. A flexural-cantilever simple-shear/pure shear model of continental lithosphere extension: applications to the Jeanne d'Arc basin, Grand Banks and Viking Graben, North Sea. In: Roberts, A.M., Yielding, G., Freeman, B. (Eds.), The Geometry of Normal Faults, 56, Geol. Soc. London, 41–60.

Kusznir, N.J., Park, R.G., 1987. The extensional strength of the continental lithosphere: its dependence on geothermal gradient, and crustal composition and thickness. Geol. Soc. Spec. Publ. 28, 35–52. doi:10.1144/GSL.SP.1987.028.01.04

Larsen, P.-H., 1988. Relay structures in a lower Permian basement-involved extension system, East Greenland. J. Struct. Geol. 10, 3–8. doi:10.1016/0191- 8141(88)90122-8.

Lavier, L., Manatschal, G., 2006. A mechanism to thin the continental lithosphere at magma-poor margins. Nature 440, 324–328. doi:10.1038/nature04608

Le Calvez, J. H., Vendeville, B. C., 1996. 3-D fault interaction in experimental models of normal-fault relays: Geological Society of America, South-Central Section Meeting, Program and Abstracts, 28, no. 1, 49.

Le Calvez, J.H., Vendeville, B.C., 2002. Experimental designs to model along-strike fault interaction. J. Virtual Explor. 7, 7–24. doi:10.3809/jvirtex.2002.00043

Le Pichon, X., Francheteau, J. and Bonnin, J., 1973. Plate Tectonics. Elsevier, Amsterdam, 302 pp.

Le Pourhiet, L., Huet, B., May, D.A., Labrousse, L., Jolivet, L., 2012. Kinematic interpretation of the 3D shapes of metamorphic core complexes. Geochemistry, Geophys. Geosystems 13, 1–17. doi:10.1029/2012GC004271

Le Pourhiet, L., Huet, B., Traoré, N., 2014. Links between long-term and short-term rheology of the lithosphere: Insights from strike-slip fault modelling. Tectonophysics 631, 146–159. doi:10.1016/j.tecto.2014.06.034

References

Le Pourhiet, L., May, D.A., Huille, L., Watremez, L., Leroy, S., 2017. A Genetic Link Between Transform and Hyper-Extended Margins. Earth Planet. Sci. Lett. 465, 184–192. doi:10.1016/j.epsl.2017.02.043

Leeder, M.R., Gawthorpe, R.L., 1987. Sedimentary models for extensional tilt- block/half graben basins. In: Coward, M.P., Dewey, J.F., Hancock, P.L. (Eds.), Continental Extensional Tectonics. Geol. Soc. Lond. Spec. Publ. 28, 139–152

Liao, J., Gerya, T., 2014. From continental rifting to seafloor spreading: Insight from 3D thermo-mechanical modelling. Gondwana Res. doi:10.1016/j.gr.2014.11.004

Ligi, M., Bonatti, E., Bortoluzzi, G., Cipriani, A., Cocchi, L., Caratori Tontini, F., Carminati, E., Ottolini, L., Schettino, A., 2012. Birth of an ocean in the Red Sea: Initial pangs. Geochemistry, Geophys. Geosystems 13, Q0809. doi:10.1029/2012GC004155

Lillie, R. J. 1999. Whole Earth Geophysics. An Introductory Textbook for Geologists and Geophysicists. Prentice-Hall, Upper Saddle River, NJ.

Lilies, J.H., Greiner, G., 1978. Rhinegraben and the Alpine system: Geological Society of America Bulletin, 89, 770-782.

Lister, G.S., Etheridge, M.A., Symonds, P.A., 1986. Detachment faulting and the evolution of passive continental margins. Geology 14, 246–250. doi:10.1130/0091-7613(1986)14<246:DFATEO>2.0.CO

Lizarralde, D., Axen, G.J., Brown, H.E., Fletcher, J.M., González-Fernández, A., Harding, A.J., Holbrook, W.S., Kent, G.M., Paramo, P., Sutherland, F., Umhoefer, P.J., 2007. Variation in styles of rifting in the Gulf of California. Nature 448:466–469. doi:10. 1038/nature06035.

Lowrie, W., 2007. Fundamentals of Geophysics. Cambridge: Cambridge University Press. doi:10.1017/CBO9780511807107

Lyakhovsky, V., Segev, A., Schattner, U., Weinberger, R., 2012. Deformation and seismicity associated with continental rift zones propagating toward continental margins. Geochemistry, Geophys. Geosystems 13, 1–21. doi:10.1029/2011GC003927

Macgregor, D., Argent, J., Sansom, P., 2017. Introduction to the thematic set : Tectonics and petroleum systems of East Africa.

Magnavita, L.P., 1992. Geometry and kinematics of the Recôncavo-Tucano-Jatobá Rift, NE Brazil. PhD Thesis.

Malavieille, J., Taboada, A., 1991. Kinematic model for basin and range extension, Geology, 19, 555-558.

Malinverno, A., Ryan, W.B.F., 1986. Extension in the Tyrrhenian Sea and shortening in the Apennines as result of arc migration driven by sinking of the lithosphere 5, 227–245.

Malvern Instruments Limited, 2012. Understanding yield stress measurements, white paper.

Manatschal, G., 2004. New models for evolution of magma-poor rifted margins based on a review of data and concepts from West Iberia and the Alps. Int. J. Earth Sci. 93, 432–466. doi:10.1007/s00531-004-0394-7

Manatschal, G., Lavier, L., Chenin, P., 2015. The role of inheritance in structuring hyperextended rift systems: Some considerations based on observations and numerical modelling. Gondwana Res. 27, 140–164. doi:10.1016/j.gr.2014.08.006

Marotta, A.M., Roda, M., Conte, K., Spalla, M.I., 2016. Thermo-mechanical numerical model of the transition from continental rifting to oceanic spreading: the case study of the Alpine Tethys. Geol. Mag. 155, 1–30. doi:10.1017/S0016756816000856

Marques, F., Cobbold, P., Lourenço, N., 2007. Physical models of rifting and transform faulting, due to ridge push in a wedge-shaped oceanic lithosphere. Tectonophysics 443, 37–52. doi:10.1016/j.tecto.2007.07.002

Mart, Y., Dauteuil, O., 2000. Analogue experiments of propagation of oblique rifts. Tectonophysics 316, 121–132.

Martin, A.K., 1984. Propagating rifts: crustal extension during continental rifting. Tectonics 3, 611–617. doi:10.1029/TC003i006p00611

Martín-Barajas, A., González-Escobar M., Fletcher J. M., Pacheco M., Oskin M., Dorsey R., 2013. Thick deltaic sedimentation and detachment faulting delay the onset of continental rupture in the Northern Gulf of California: Analysis of seismic reflection profiles, Tectonics, 32, 1294–1311, doi:10.1002/tect.20063

Martins-Neto, M.A., Catuneanu, O., 2009. Rift sequence stratigraphy. Mar. Pet. Geol. 27, 247–253. doi:10.1016/j.marpetgeo.2009.08.001

Mattei, M., Kissel, C., Funiciello, R., 1996. No tectonic rotation of the Tuscan Tyrrhenian margin (Italy) since late Messinian. J. Geophys. Res. B Solid Earth 101, 2835–2845. doi:10.1029/95JB02398

Mbina Mounguengui, M., Guiraud,M., 2009. Neocomian to early Aptian syn-rift evolution of the normal to oblique-rifted North Gabon Margin (Interior and N'Komi Basins). Marine and Petroleum Geology 26:1000–1017. doi:10.1016/j. marpetgeo.2008.11.001

McClay, K., 1976. The rheology of plasticine, Tectonophysics 33, T7-T15.

McClay, K., White, M., 1995. Analogue modelling of orthogonal and oblique rifting. Mar. Pet. Geol. 12, 137–151.

McClusky, S., Mahmoud, S., 2003. GPS contraints on Africa and Arabi plate motions 126–138.

McClusky, S., Reilinger, R., Ogubazghi, G., Amleson, A., Healeb, B., Vernant, P., Sholan, J., Fisseha, S., Asfaw, L., Bendick, R., Kogan, L., 2010. Kinematics of the southern Red Sea-Afar Triple Junction and implications for plate dynamics. Geophys. Res. Lett. 37, L05301. doi:10.1029/2009GL041127

McDermott, K., Reston, T., 2015. To see, or not to see? Rifted margin extension. Geology 43, 967–970. doi:10.1130/G36982.1

McKenzie, D., 1978. Some remarks on the development of sedimentary basins. Earth Planet. Sci. Lett. 40, 25–32. doi:10.1016/0012-821X(78)90071-7

McKenzie, D., Weiss, N., 1975. Speculations on the Thermal and Tectonic History of the Earth. Geophys. J. R. Astron. Soc. 42, 131–174. doi:10.1111/j.1365-246X.1975.tb05855.x

McKenzie, D.P., Sclater, J.G., 1971. The Evolution of the Indian Ocean. Geophys. J. R. Astron. Soc. 25, 437–528. doi:10.1038/scientificamerican0573-62

McQuarrie, N., Stock, J.M., Verdel, C., Wernicke, B.P., 2003. Cenozoic evolution of Neotethys and implications for the causes of plate motions. Geophys. Res. Lett. 30, 2036. doi:10.1029/2003GL017992

Mercier de Lepinay, M., Loncke, L., Basile, C., Roest, W.R., Patriat, M., Maillard, A., De Clarens, P., 2016. Transform continental margins - Part 2: A worldwide review. Tectonophysics 693, 96–115. doi:10.1016/j.tecto.2016.05.038

References

Metcalfe, I., 1988. Origin and assembly of south-east Asian continental terranes. Geol. Soc. London, Spec. Publ. 37, 101–118. doi:10.1144/GSL.SP.1988.037.01.08

Michon, L., Merle, O., 2000. Crustal structures of the Rhinegraben and the Massif Central grabens: An experimental approach. Tectonics, 19, no. 5, 896–904, doi: 10.1029/2000TC900015

Milani, E. J., 1987. Aspectos da evolução tectônica das bacias do Recôncavo, e Tucano Sul, Bahia, Brasil (Tese de mestrado na Universidade Federal de Ouro Preto, 1985): Boletim Técnico da Petrobras, Seção Exploração de Petróleo, 18, 1–61.

Milani, E.J., Davison, I., 1988. Basement control and transfer tectonics in the Reconcavo-Tucano-Jatoba rift, Northeast Brazil. Tectonophysics 154. doi:10.1016/0040-1951(88)90227-2

Milia, A., Torrente, M.M., 2015. Tectono-stratigraphic signature of a rapid multistage subsiding rift basin in the Tyrrhenian-Apennine hinge zone (Italy): A possible interaction of upper plate with subducting slab. J. Geodyn. 86, 42–60. doi:10.1016/j.jog.2015.02.005

Milia, A., Torrente, M.M., Massa, B., Iannace, P., 2013. Progressive changes in rifting directions in the Campania margin (Italy): New constrains for the Tyrrhenian Sea opening. Glob. Planet. Change 109, 3–17. doi:10.1016/j.gloplacha.2013.07.003

Milia, A., Torrente, M.M., Tesauro, M., 2016. From stretching to mantle exhumation in a triangular backarc basin (Vavilov basin, Tyrrhenian Sea, Western Mediterranean). Tectonophysics. doi:10.1016/j.tecto.2016.10.017

Misra, A.A., Mukherjee, S., 2015. Tectonic Inheritance in Continental Rifts and Passive Margins. doi:10.1007/978-3-319-20576-2

Nicolas E. Molnar, Alexander R. Cruden, Peter G. Betts, 2018. Unzipping continents and the birth of microcontinents. Geology 46(5), 451–454. doi: https://doi.org/10.1130/G40021.1

Molnar, N.E., Cruden, A.R., Betts, P.G., 2017. Interactions between propagating rotational rifts and linear rheological heterogeneities: Insights from three-dimensional laboratory experiments. Tectonics 36, 420–443. doi:10.1002/2016TC004447

Molnar, P., Tapponnier, P., 1975. Cenozoic tectonics of Asia: Effects of a Continental Collision. Science (80-.). 189, 419–426.

Mondy, L.S., Rey, P.F., Duclaux, G., Moresi, L., 2018. The role of asthenospheric flow during rift propagation and breakup. Geology 46, 1–4.

Montelli, R., Nolet, G., Dahlen, F.A., Masters, G., 2006. A catalogue of deep mantle plumes: new results from finite-frequency tomography. Geochem. Geophys. Geosyst. 7 (11). doi:10.1029/2006GC001248.

Montelli, R., Nolet, G., Dahlen, F.A., Masters, G., Engdahl, E.R., Hung, S.H., 2004. Finite-frequency tomography reveals a variety of plume in the mantle. Science 303, 338–343.

Mooney, W., Gettings, M., Blank, H., Healy, J., 1985a. Saudi Arabian seismic-refraction profile: a traveltime interpretation of crustal and upper mantle structure. Tectonics 111, 173–246.

Mooney, W., Gettings, M., Blank, H., Healy, J., 1985b. Saudi Arabian seismic-refraction profile: a traveltime interpretation of crustal and upper mantle structure. Tectonophysics 111, 173–246.

Moresi, L., Betts, P.G., Miller, M.S., Cayley, R.A., 2014. Dynamics of continental accretion. Nature 508, 245–248. doi:10.1038/nature13033

Moresi, L., Quenette, S., Lemiale, V., Mériaux, C., Appelbe, B., Mühlhaus, H.B., 2007. Computational approaches to studying non-linear dynamics of the crust and mantle. Phys. Earth Planet. Inter. 163, 69–82. doi:10.1016/j.pepi.2007.06.009

Morgan, P., 1982. Heat flow in rift zones, In: Palmason, G. (Ed.) Continental and Oceanic Rifts. Am. Geophys. Union Geodyn. Ser. 8, 107-22.

Morgan, P., Seager, W.R., Golombek, M.P., 1986. Cenozoic thermal, mechanical and tectonic evolution of the Rio Grande Rift. J. Geophys. Res. 91, 6263. doi:10.1029/JB091iB06p06263

Morley, C.K., 2010. Stress re-orientation along zones of weak fabrics in rifts: An explanation for pure extension in "oblique" rift segments? Earth Planet. Sci. Lett. 297, 667–673. doi:10.1016/j.epsl.2010.07.022

Morley, C.K., 2002. Evolution of large normal faults: Evidence from seismic reflection data. Am. Assoc. Pet. Geol. Bull. 86, 961–978. doi:10.1306/61eedbfc-173e-11d7-8645000102c1865d

Morley, K., 1999. Influence of Preexisting Fabrics on Rift Structure 151–160.

Morley, C. K., 1988. Variable extension in Lake Tanganyika, Tectonics, 7, 785–801.

Morley, C.K., Cunningham, S.M., Harper, R.M., Wescott, W.A., 1992. Geology and Geophysics of the Rukwa Rift, East-Africa. Tectonics 11, 69–81.

Morley, C.K., Nelson, R.A., Patton, T.L., Munn, S.G., 1990. Transfer zones in the East African Rift System and their relevance to hydrocarbon exploration in rifts. American Association of Petroleum Geologists Bulletin 74, 1234–1253.

Müller, R.D., Gaina, C., Roest, W.R., Hansen, D.L., 2001. A recipe for microcontinent formation. Geology 29, 203–206. doi:10.1130/0091-7613(2001)029<0203:ARFMF>2.0.CO;2

Müller, R.D., Seton, M., Zahirovic, S., Williams, S.E., Matthews, K.J., Wright, N.M., Shephard, G.E., Maloney, K.T., Barnett-moore, N., Bower, D.J., Cannon, J.S., 2016. Ocean basin evolution and global-scale reorganization events since Pangea breakup. Annu. Rev. Earth Planet. Sci. Lett. 44, 107–138. doi:10.1146/annurev-earth-060115-012211

Nabighian, M.N., Ander, M.E., Grauch, V.J.S., Hansen, R.O., LaFehr, T.R., Li, Y., Pearson, W.C., Peirce, J.W., Phillips, J.D., Ruder, M.E., 2005. Historical development of the gravity method in exploration. Geophysics 70, 63ND. doi:10.1190/1.2133785

Nagel, T.J., Buck, W.R., 2004. Symmetric alternative to asymmetric rifting models. Geology, 32, 937-940.

Naliboff, J., Buiter, S.J.H., 2015. Rift reactivation and migration during multiphase extension. Earth Planet. Sci. Lett. 421, 58–67. doi:10.1016/j.epsl.2015.03.050

Naliboff, J.B., Buiter, S.J.H., Péron-Pinvidic, G., Osmundsen, P.T., Tetreault, J., 2017. Complex fault interaction controls continental rifting. Nat. Commun. 8. doi:10.1038/s41467-017-00904-x

Nemčok, M., Sinha, S.T., Dore, A.G., Lundin, E.R., Mascle, J., Rybar, S., 2016. Mechanisms of microcontinent release associated with wrenching-involved continental break-up; a review. Geol. Soc. London, Spec. Publ. 431, 323–359. doi:10.1144/SP431.14

Nemčok, M., Stuart, C., Rosendahl, B.R., Welker, C., Smith, S., Sheya, C., Sinha, S.T., Choudhuri, M., Allen, R., Reeves, C., Sharma, S.P., Venkatraman, S., Sinha, N., 2013. Continental break-up mechanism; lessons from intermediate- and fast-extension settings. Geol. Soc. Spec. Publ. 373–401.

References

Nestola, Y., Storti, F., Bedogni, E., Cavozzi, C., 2013. Shape evolution and finite deformation pattern in analog experiments of lithosphere necking. Geophys. Res. Lett. 40, 5052–5057. doi:10.1002/grl.50978

Nestola, Y., Storti, F., Cavozzi, C., 2015. Strain rate-dependent lithosphere rifting and necking architectures in analog experiments. J. Geophys. Res. Solid Earth 584–594. doi:10.1002/2014JB011623.Received

Nettleton, L. L., 1934. Fluid mechanics of salt domes, Bull. Am. Ass. Petrol. Geol., 18, 1175-1204.

Nettleton, L. L., 1943. Recent experimental and geophysical evidence of mechanics of salt-dome formation, Bull. Am. Ass. Petrol. Geol., 27, 51-63

Neumann, E.-R., Ramberg, I.B., 1977. Petrology and Geochemistry of Continental Rifts.

Nür, A., Ron, H., Scotti, O., 1986. Fault mechanics and the kinematics of block rotations. Geology 14, 746–749. doi:10.1130/0091-7613(1986)14<746:FMATKO>2.0.CO;2

Nürnberg, D., Müller, R. D., 1991. The tectonic evolution of the South Atlantic from Late Jurassic to present. Tectonophysics, 191, 27-53.

O'Bryan, J., Cohen, R., Gilliland, W., 1975. Experimental Origin of Transform Faults and Straight Spreading-Center Segments. GSA Bull. 86, 793–796. doi:10.1130/0016-7606(1975)86<793

Oldenburg, D., Brune, J., 1975. An Explanation for the Orthogonality of Ocean Ridges and Transform Faults. J. Geophys. Res. 80, 2575–2585.

Oldenburg, D., Brune, J., 1972. Ridge transform fault spreading pattern in freezing wax. Science (80-.). 178, 301–304.

Omar, G., Steckler, M.S., 1995. Fission Track Evidence on the Initial Rifting of the Red Sea : Two Pulses , No Propagation. Science (80-.). 270, 1341–1344.

Pallister, J., McCausland, W.., Jónsson, S., Lu, Z., Zahran, H., Hadidy, S.E., Aburukbah, A., Stewart, I., Lundgren, P., White, R., Moufti, M., 2010. Broad accommodation of rift-related extension recorded by dyke intrusion in Saudi Arabia. Nat. Geosci. 3, 705–712. doi:10.1038/ngeo966

Panien, M., Schreurs, G., Pfiffner, A., 2005. Sandbox experiments on basin inversion: testing the influence of basin orientation and basin fill. J. Struct. Geol. 27, 433-445. doi:10.1016/j.jsg.2004.11.001

Patacca, E., Sartori, R., Scandone, P., 1990. Tyrrhenian basin and Apenninic Arcs: kinematic relations since Late Tortonian times. Mem. Soc. Geol. It 45, 425–451. doi:10.1007/978-94-011-2016-6_7

Peacock, D.C.P., Knipe, R.J., Sanderson, D.J., 2000. Glossary of normal faults. J. Struct. Geol. 22, 291-305.

Peacock, D.C.P., Nixon, C.W., Rotevatn, A., Sanderson, D.J., Zuluaga, L.F., 2016. Glossary of fault and other fracture networks. J. Struct. Geol. 92, 12–29. doi:10.1016/j.jsg.2016.09.008

Peacock, D.C.P., Sanderson, D.J., 1991. Displacements, segment linkage and relay ramps ramps in normal fault zones. J. Struct. Geol. 13, 721-733.

Pérez-Gussinyé, M., Morgan, J.P., Reston, T.J., Ranero, C.R., 2006. The rift to drift transition at non-volcanic margins: Insights from numerical modelling. Earth Planet. Sci. Lett. 244, 458–473. doi:10.1016/j.epsl.2006.01.059

Peron-Pinvidic, G., Manatschal, G., 2010. From microcontinents to extensional allochthons: witnesses of how continents rift and break apart? Pet. Geosci. 16, 189–197. doi:10.1144/1354-079309-903

Petersen, K.D., Armitage, J.J., Nielsen, S.B., Thybo, H., 2015. Mantle temperature as a control on the time scale of thermal evolution of extensional basins. Earth Planet. Sci. Lett. 409, 61–70. doi:10.1016/j.epsl.2014.10.043

Petrunin, A. G., Sobolev, S. V., 2008. Three-dimensional numerical models of the evolution of pull-apart basins, Phys. Earth Planet. Inter., 171, 387–399.

Philippon, M., Corti, G., Sani, F., 2014. Evolution, distribution, and characteristics of rifting in southern Ethiopia. Tectonics 1–24. doi:10.1002/2013TC003430.

Phillips, J.D., Ross, D.A., 1970. Continuous seismic reflection profiles in the Red Sea: Philosophical Transactions of the Royal Society of London, ser. A, 267, 143–152.

Pigram, C.J., Davies, H.L., 1987. Terranes and the accretion history of the New Guinea orogen. BMR J. Aust. Geol. Geophys. 10, 193–211.

Pitman, W.C., Talwani, M., 1972. Sea-floor spreading in the North Atlantic. Geol. Soc. America Bull., 83, 619-646.

Pitman, W.C., Andrews, J.A., 1985. Subsidence and thermal history of small pull-apart basins, in Strike-slip Deformation, Basin Formation, and Sedimentation, edited by K.T. Biddle and N. Christie-Blick, Spec. Publ. Soc. Econ. Paleontol. Mineral., 37, 45-49.

Plaziat, J.C., Montenat, C., Barrier, P., Janin, M.C., Orszag-Sperber, F., Philobbos, E., 1998. Stratigraphy of the Egyptian syn-rift deposits: correlations between axial and peripheral sequences of the north- western Red Sea and Gulf of Suez and their relations with tectonics and eustasy. In: Purser BH, Bosence DWJ (Eds.) Sedimentation and Tectonics in Rift Basins—Red Sea—Gulf of Aden. Chapman and Hall, London, 211–222

Pollack, H.N., Hurter, S.J., Johnson, J.R., 1993. Heat flow from the Earth's interior: Analysis of the global data set. Rev. Geophys. 31, 267. doi:10.1029/93RG01249

Price, N.J., Cosgrove, J.W., 1990. Analysis of Geological Structures. Cambridge Uni- versity Press, Cambridge.

Prosser, S., 1991. Tectonicsystems tracts: their recognition and significance in basin analysis. In: Williams, G.D. and Dobb, A., convenors, Tectonics and Seismic Sequence Stratigraphy. Meeting of TSG/Petroleum Group of the Geoloqical Society of London, London.

Prosser, S., 1993. Rift-related linked depositional systems and their seismic expression. Geol. Soc. London, Spec. Publ. 71, 35–66. doi:10.1144/GSL.SP.1993.071.01.03

Pushcharovsky, Y.M., 2013. Microcontinents in the Atlantic Ocean. Geotectonics 47, 241–250. doi:10.1134/S0016852113040067

Pysklywec, R., Cruden, A., 2004. Coupled crust-mantle dynamics and intraplate tectonics: Two-dimensional numerical and three-dimensional analogue modeling. Geochemistry, Geophys. Geosystems 5, Q10003. doi:10.1029/2004GC000748

Quittmeyer, R.C., Kafka, A.L., Armbruster, J.G., 1984. Focal mechanisms and depths of earthquakes in central Pakistan: a tectonic interpretation. J. Geophys. Res. 89, 2459-2470.

Ragnarsson, R., Ford, J., Santangelo, C., Bodenschatz, E., 1996. Rifts in Spreading Wax Layers. Phys. Rev. Lett. 76, 3456–3459. doi:10.1103/PhysRevLett.76.3456

Ramberg, H., 1967. Model Experimentation of the Effect of Gravity on Tectonic Processes. Geophys. J. R. Astron. Soc. 14, 307–329. doi:10.1111/j.1365-246X.1967.tb06247.x

References

Ramsay, J., Huber M., 1987. The techniques of the modern structural geology 1, Strain Analysis, 650 pp., Academic, London.

Ranalli, G., 2001. Experimental tectonics: From Sir James Hall to the present. J. Geodyn. 32, 65–76. doi:10.1016/S0264-3707(01)00023-0

Ranalli, G., 1995. Rheology of the Earth. Chapman & Hall, London, UK, 413 pp.

Ranalli, G., 1982. Robert Hooke and the Huttonian theory. J. Geol. 90, 319–325.

Ranalli, G., Murphy, D.C., 1987. Rheological stratification of the lithosphere. Tectonophysics 132 (4), 281–295.

Ranero, C.R., Pérez-Gussinyé, M., 2010. Sequential faulting explains the asymmetry and extension discrepancy of conjugate margins. Nature 468, 294–299. doi:10.1038/nature09520

Reck, H., 1914. Oldoinyo L'Engai, ein tatiger Vulkan im Gebiete der Deutsch-Ostafrikanischen Bruchstufe. Branca-Festschrrift. Bornträger, Leipzig, 373-409

Reeves, C. V., Teasdale, J.P., Mahanjane, E.S., 2016. Insight into the Eastern Margin of Africa from a new tectonic model of the Indian Ocean. Geol. Soc. London, Spec. Publ. 431, 299–322. doi:10.1144/SP431.12

Riller, U., Cruden, A.R., Boutelier, D., Schrank, C.E., 2012. The causes of sinuous crustal-scale deformation patterns in hot orogens: Evidence from scaled analogue experiments and the southern Central Andes. J. Struct. Geol. 37, 65–74. doi:10.1016/j.jsg.2012.02.002

Ring, U., 1994. The influence of preexisting structure on the evolution of the Cenozoic Malawi rift (East African rift system) 13, 313–326.

Ring, U., Betzler, C., Delvaux, D., 1992. Normal vs. strike-slip faulting during rift development in East Africa: The Malawi rift. Geology 20, 1015–1018. doi:10.1130/0091-7613(1992)020<1015:NVSSFD>2.3.CO;2

Ritsema, J., Allen, R., 2003. The elusive mantle plume, Earth Planet. Sci. Lett., 207, 1–12.

Ritsema, J., Van Heijst, H.J., Woodhouse, J.H., 1999. Complex Shear Wave Velocity Structure Imaged Beneath Africa and Iceland. Science (80-.). 286, 1925–1928. doi:10.1126/science.286.5446.1925

Roberts, E.M., Stevens, N.J., O'Connor, P.M., Dirks, P.H.G.M., Gottfried, M.D., Clyde, W.C., Armstrong, R.A., Kemp, A.I.S., Hemming, S., 2012. Initiation of the western branch of the East African Rift coeval with the eastern branch. Nat. Geosci. 5, 289–294. doi:10.1038/ngeo1432

Roberts, A., Yielding, G., 1994. Continental extensional tectonics, in Continental Deformation, edited by P.L. Hancock, Pergamon, New York, 233-250.

Robin, C., Colantoni, P., Gennesseaux, M., Rehault, J.P., 1987. Vavilov seamount: A mildly alkaline Quaternary volcano in the Tyrrhenian Basin. Mar. Geol. 78, 125–136. doi:10.1016/0025-3227(87)90071-5

Rolandone, F., Jaupart, C., Mareschal, J.C., Garipy, C., Bienfait, G., Carbonne, C., Lapointe, R., 2002. Surface heat flow, crustal temperatures and mantle heat flow in the Proterozoic Trans-Hudson Orogen, Canadian Shield. J. Geophys. Res. 107 (B12), 2341. doi:10.1029/2001JB000698

Rolandone, F., Lucazeau, F., Leroy, S., Mareschal, J.C., Jorand, R., Goutorbe, B., Bouquerel, H., 2013. New heat flow measurements in Oman and the thermal state of the Arabian Shield and Platform. Tectonophysics 589, 77–89. doi:10.1016/j.tecto.2012.12.034

Rosenbaum, G., Lister, G.S., 2004. Neogene and Quaternary rollback evolution of the Tyrrhenian Sea, the Apennines, and the Sicilian Maghrebides. Tectonics 23, 1–17. doi:10.1029/2003TC001518

Rosendahl, B.R., 1987. Architecture of continental rifts with special reference to East Africa. Annu. Rev. Earth Planet. Sci. Lett. 15, 445–503.

Rosendahl, B. R., Reynolds, D., Lorber, P., Burgess, C., McGill, J., Scott, D., Lambiase J. Derksen, S., 1986. Structural expressions of rifting: lessons from Lake Tanganyika. In: Sedimentation in the East African Rifts (Eds L. E. Frostick et al.), Spec. Publ. Geol. Soc. London No. 25, 29-43.

Royden, L., Keen, C.E., 1980. Rifting processes and thermal evolution of the continental margin of eastern Canada determined from subsidence curves. Earth Planet. Sci. Lett., 51, 343-361.

Ruppel, C., 1995. Extensional processes in continental lithosphere. J. Geophys. Res. Solid Earth 100, 24187–24215. doi:10.1029/95JB02955

Schellart, W.P., 2011. Rheology and density of glucose syrup and honey: Determining their suitability for usage in analogue and fluid dynamic models of geological processes. J. Struct. Geol. 33, 1079–1088. doi:10.1016/j.jsg.2011.03.013

Schellart, W.P., 2008. Kinematics and flow patterns in deep mantle and upper mantle subduction models: Influence of the mantle depth and slab to mantle viscosity ratio. Geochemistry, Geophys. Geosystems 9. doi:10.1029/2007GC001656

Schellart, W.P., 2000. Shear test results for cohesion and friction coefficients for different granular materials: Scaling implications for their usage in analogue modelling. Tectonophysics 324, 1–16. doi:10.1016/S0040-1951(00)00111-6

Schellart, W.P., Jessell, M., Lister, G., 2003. Asymmetric deformation in the backarc region of the Kuril arc, northwest Pacific: New insights from analogue modeling. Tectonics 22, 1047. doi:10.1029/2002TC001473

Schlagenhauf, A., Manighetti, I., Malavieille, J., Dominguez, S., 2008. Incremental growth of normal faults: Insights from a laser-equipped analog experiment. Earth Planet. Sci. Lett. 273, 299–311. doi:10.1016/j.epsl.2008.06.042

Schlische, R.W., Olsen, P.E., 1990. Quantitative Filling Model for Continental Extensional Basins with Applications to Early Mesozoic Rifts of Eastern North America. J. Geol. 98, 135–155. doi:10.1086/629390

Scholz, C. H., 1990. The Mechanics of Earthquakes and Faulting, 439 pp., Cambridge Univ. Press, New York.

Schöpfer, M.P.J., Zulauf, G., 2002. Strain-dependent rheology and the memory of plasticine. Tectonophysics 354, 85–99. doi:10.1016/S0040-1951(02)00292-5

Schrank, C., Cruden, A., 2010. Compaction control of topography and fault network structure along strike-slip faults in sedimentary basins. J. Struct. Geol. 32, 184–191. doi:10.1016/j.jsg.2009.11.003

Schrank, C.E., Boutelier, D.A., Cruden, A.R., 2008. The analogue shear zone: From rheology to associated geometry. J. Struct. Geol. 30, 177–193. doi:10.1016/j.jsg.2007.11.002

Schreurs, G., 1994. Experiments on strike-slip faulting and block rotation. Geology 22(6), 567–570.

Schreurs, G., Buiter, S.J.H., Boutelier, D., Corti, G., Costa, E., Cruden, A., Daniel, J.-M., Hoth, S., Koyi, H., Kukowski, N., Lohrmann, J., Ravaglia, A., Schlische, R.W., Withjack, M.O., Yamada, Y., Cavozzi, C., DelVentisette, C., Elder Brady, J., Hoffmann-Rothe, A., Mengus, J.-M., Montanari, D., and Nilforoushan, F., 2006, Analogue benchmarks of shortening and extension experiments, Geological Society, London, Special Publications 253, 1-27. doi: 10.1144/GSL.SP.2006.2/53.01.01

References

Schuepbach, M.A., Vail, P.R., 1980. Evolution of outer highs on divergent continental margins. In, Continental Tectonics — studies in geophysics. US National Academy of Science, Washington D.C., 50-61

Schultz, R.A., Fossen, H., 2008. Terminology for structural discontinuities. Am. Assoc. Pet. Geol. Bull. 92, 853-867.

Scrutton, R.A., 1976. Microcontinents and their significance. Geodyn. Prog. Prospect. 5, 177–189.

Sebai, A., Zumbo, V., Féraud, G., Bertrand, H., Hussain, A.G., Giannérini G., Campredon, R., 1991. 40Ar/39Ar dating of alkaline and tholeiitic magmatism of Saudi Arabia related to the early Red Sea rifting. Earth Planet. Sci. Lett. 104, 473-487.

Sella, G.F., Dixon, T.H., Mao, A., 2002. REVEL: A model for Recent plate velocities from space geodesy. J. Geophys. Res. 107, 2081. doi:10.1029/2000JB000033

Sengör, A.M.C., Burke, K., 1978. Relative timing of rifting and volcanism on Earth and its tectonic implications. Geophys. Res. Lett. 5, 419–421.

Sengör, A.M.C., Dewey, J.F., 1990. Terranology: Vice or Virtue? Philos. Trans. R. Soc. A Math. Phys. Eng. Sci. 331, 457–477.

Sengör, A.M.C., Natal'in, B.A., Burtman, V.S., 1993. Evolution of the Altaid tectonic collage and Paleozoic crustal growth in Eurasia. Nature 366, 461–464.

Seton, M., Müller, R.D., Zahirovic, S., Gaina, C., Torsvik, T., Shephard, G., Talsma, A., Gurnis, M., Turner, M., Maus, S., Chandler, M., 2012. Global continental and ocean basin reconstructions since 200Ma. Earth-Science Rev. 113, 212–270. doi:10.1016/j.earscirev.2012.03.002

Sharp, I. R., Gawthorpe, R. L., Underhill, J. R., Gupta, S., 2000. Fault-propagation folding in extensional settings: Examples of structural style and synrift sedimentary response from the Suez rift, Sinai, Egypt. Geological Society of America Bulletin, 112, 1877–1899, doi:10.1130/0016- 7606(2000)112<1877:FPFIES>2.0.CO;2

Sharples, W., Moresi, L.-N., Jadamec, M. A, Revote, J., 2015. Styles of Rifting and Fault Spacing in Numerical Models of Crustal Extension. J. Geophys. Res. Solid Earth 4379-4404. doi:10.1002/2014JB011813

Shemenda, A., Grocholsky, A., 1994. Physical modeling of slow seafloor spreading. J. Geophys. Res. 99, 9137–9153.

Shih, J., Molnar, P., 1975. Analysis and Implications of the Sequence of Ridge Jumps That Eliminated the Surveyor Transform Fault. J. Geophys. Res. 80, 4815–4822.

Sichler, B., 1980. La biellette danakile: un modèle pour l'évolution géodynamique de l'Afar. Bull. la société géologique Fr. 22, 925–933.

Simmons, N. A., S. C. Myers, Johannesson, G., 2011. Global-scale P wave tomography optimized for prediction of teleseismic and regional travel times for Middle East events: 2. Tomographic inversion, J. Geophys. Res. Solid Earth., 116(B4), B04305, doi:10.1029/2010JB007969

Sims, D., Ferrill, D.A., Stamatakos, J.A., 1999. Role of a ductile decollement in the development of pull-apart basins; experimental results and natural examples. J. Struct. Geol. 21, 533–554.

Sinha, S.T., Nemčok, M., Choudhuri, M., Sinha, N., Rao Pundarika, D., 2016. The role of break-up localization in microcontinent separation along a strike-slip margin : the East India – Elan Bank case study. Geol. Soc. London, Spec. Publ. 431, 95–123. doi:10.1144/SP431.5

Sleep, N.H., 1971. Thermal Effects of the Formation of Atlantic Continental Margins by Continental Break up. Geophys. J. R. Astron. Soc. 24, 325–350.

Sloss, L.L., 1963. Sequences in the cratonic interior of north America. Bull. Geol. Soc. Am. 74, 93–114. doi:10.1130/0016-7606(1963)74[93:SITCIO]2.0.CO;2

Smith, M., Mosley, P., 1993. Crustal heterogeneity and basement influence on the development of the Kenya rift, East Africa 12, 591–606.

Sokoutis, D., Corti, G., Bonini, M., Brun, J.P., Cloetingh, S., Mauduit, T., Manetti, P., 2007. Modelling the extension of heterogeneous hot lithosphere. Tectonophysics 444, 63–79. doi:10.1016/j.tecto.2007.08.012

Souriot, T., Brun, J.P., 1992. Faulting and block rotation in the Afar triangle, East Africa: the Danakil "crank-arm' model. Geology 20, 911–914. doi:10.1130/0091-7613(1992)020<0911:FABRIT>2.3.CO;2

Stamps, D.S., Calais, E., Saria, E., Hartnady, C., Nocquet, J.M., Ebinger, C.J., Fernandes, R.M., 2008. A kinematic model for the East African Rift. Geophys. Res. Lett. 35, 1–6. doi:10.1029/2007GL032781

Steckler, M.S., Berthelot, F., Lyberis, N., Le Pichon, X., 1988. Subsidence in the Gulf of Suez: implications for rifting and plate kinematics. Tectonophysics 153, 249–270

Steckler, M.S., ten Brink, U.S., 1986. Lithospheric strenght variations as a control on new plate boundaries: examples from the northern Red Sea region. Earth Planet. Sci. Lett. 79, 120–132.

Stern, R.J., 1981. Petrogenesis and tectonic setting of Late Precambrian ensimatic volcanic rocks, Central Eastern Desert of Egypt. Precam-brian Research 16, 195–230.

Stern, R.J., Johnson, P., 2010. Continental lithosphere of the Arabian Plate: A geologic, petrologic, and geophysical synthesis. Earth-Science Rev. 101, 29–67. doi:10.1016/j.earscirev.2010.01.002

Suess, E., 1891. Die Brüche des östlichen Africa. In: Beitrage zur Geologischen Kenntnis des östlichen Africa, Denkschriften Kaiserlichen Akademie der Wissenschaftliche Klasse, Wien 50, 555–556.

Suess, E., 1875. Die Entstehung der Alpen. W. Braunmüller Wien, 168 pp

Sun, Z., Zhong, Z., Keep, M., Zhou, D., Cai, D., Li, X., Wu, S., Jiang, J., 2009. 3D analogue modeling of the South China Sea: A discussion on breakup pattern. J. Asian Earth Sci. 34, 544–556. doi:10.1016/j.jseaes.2008.09.002

Svartman Dias, A.E., Lavier, L.L., Hayman, N.W., 2015, Conjugate rifted margins width and asymmetry: The interplay between lithospheric strength and thermomechanical processes: J. Geophys. Res.: Solid Earth, 120, no. 12, 2015JB012074, doi: 10.1002/2015JB012074.

Szatmari, P., Milani, E.J., 1999. Microplate rotation in northeast Brazil during South Atlantic rifting: Analogies with the Sinai microplate. Geology 27, 1115–1118. doi:10.1130/0091-7613(1999)027<1115:MRINBD>2.3.CO;2

ten Grotenhuis, S., Piazolo, S., Passchier, C., Bons, P., 2002. Are polymers suitable rock analogs? Tectonophysics 350, 35-47

Tentler, T., Acocella, V., 2010. How does the initial configuration of oceanic ridge segments affect their interaction? Insights from analogue models. J. Geophys. Res. 115, B01401. doi:10.1029/2008JB006269

Theunissen, K., Klerkx, J., Melnikov, A., Mruma, A., 1996. Mechanisms of inheritance of rift faulting in the western branch of the East African Rift, Tanzania. Tectonics 15 (4), 776–790

Thomas, W.A., Astini, R.A., 1996. Argentine Precordillera: A Traveler from the Quachita Embayment of North America Laurentia. Science. 273, 752–757.

References

Tillman, F., Benz, H., Priestley, K., Okubo, P., 2001. P-wave velocity structure of the uppermost mantle beneath Hawaii from travel time tomography, Geophys. J. Int., 146, 594–606.

Tommasi, A., Vauchez, A., 2001. Continental rifting parallel to ancient collisional belts: An effect of the mechanical anisotropy of the lithospheric mantle. Earth Planet. Sci. Lett. 185, 199–210. doi:10.1016/S0012-821X(00)00350-2

Torsvik, T.H., Amundsen, H., Hartz, E.H., Corfu, F., Kusznir, N., Gaina, C., Doubrovine, P. V., Steinberger, B., Ashwal, L.D., Jamtveit, B., 2013. A Precambrian microcontinent in the Indian Ocean. Nat. Geosci. 6, 1–5. doi:10.1038/ngeo1736

Tron, V., Brun, J.P., 1991. Experiments on oblique rifting in brittle-ductile systems. Tectonophysics 188, 71–84.

Turcotte, D., 1974. Are transform faults thermal contraction cracks? J. Geophys. Res. 79, 2573–2577. doi:10.1029/JB079i017p02573

Twiss, R.J., Moores, E.M., 1992. Structural Geology. Freeman, New York.

Uhligh, C., 1912. Beitraege zur Kenntnis der Geologie und Petrographie Ostrafrikas: I. Ueberblick ueber den Aufbau Ostrafrikas zwischen dem Victoriasee und der Kueste des Indischen Ozeans, besonders laengs der Uganda-Eisenbahn. Zentralbl Mineral Geol Palaont, 559-568

Uhligh, C., 1909. Die Ostrafrikanische Bruchstufe und die angrenzenden Gebiete zwischen den Seen Magad und Lawa ja Mwerie, sowie dem West-Guss der Meru. Mitt dtsch Schutzgebiet Suppl 2, 63 pp

Umhoefer, P.J., Stone, K.A., 1996. Description and kinematics of the southeast Loreto basin fault array, Baja California Sur, México: A positive field test of oblique-rift models: J. Struct. Geol. 18, 595–614.

Vail, P.R., Mitchum, R.M., Todd, R.G., Widmier, J.M., Thompson, S., Sangree, J.B., Bubb, J.N. Hatlelid, W.G., 1977. Seismic stratigraphy and global changes of sea-level. In: Payton, C.E. (Ed.) Seismic Stratigraphy — Applications to Hydrocarbon Exploration. AAPG Memoir, 26, 49–212

van der Meer, F., 2012. Remote-sensing image analysis and geostatistics. Int. J. Remote Sens. 33, 5644–5676. doi:10.1080/01431161.2012.666363

van Wijk, J., 2005. Role of weak zone orientation in continental lithosphere extension. Geophys. Res. Lett. 32, L02303. doi:10.1029/2004GL022192

van Wijk, J., Cloetingh, S., 2002. Basin migration caused by slow lithospheric extension. Earth Planet. Sci. Lett. 198, 275–288.

van Wijk, J.W., Blackman, D.K., 2005. Dynamics of continental rift propagation: The end-member modes. Earth Planet. Sci. Lett. 229, 247–258. doi:10.1016/j.epsl.2004.10.039

Vauchez, A., Barruol, G., Tommasi, A., 1997. Why do continents break-up parallel to ancient orogenic belts? Terra Nov. 9, 62–66. doi:10.1111/j.1365-3121.1997.tb00003.x

Vauchez, A., Tommasi, A., Barruol, G., 1998. Rheological heterogeneity, mechanical anisotropy and deformation of the continental lithosphere. Tectonophysics 296, 61–86. doi:10.1016/S0040-1951(98)00137-1

Veevers, J.J., 2009. Palinspastic (pre-rift and -drift) fit of India and conjugate Antarctica and geological connections across the suture. Gondwana Res. 16, 90–108. doi:10.1016/j.gr.2009.02.007

Vendeville, B., Cobbold, P.R., Davy, P., Choukroune, P., Brun, J.P., 1987. Physical models of extensional tectonics at various scales. Geol. Soc. London, Spec. Publ. 28, 95–107. doi:10.1144/GSL.SP.1987.028.01.08

Versfelt, J., Rosendahl, B.R., 1989. Relationships between pre-rift structure and rift architecture in Lakes Tanganyika and Malawi, East Africa. Nature. doi:10.1038/337354a0

Vine, F., 1966. Spreading of the Ocean Floor: New Evidence. Science 154, 1405–1415.

Vink, G.E., 1982. Continental rifting and the implications for Plate Tectonics Reconstructions B13, 10677–10688.

Vink, G.E., Morgan, W.J., Zhao, W.-L., 1984. Preferential rifting of continents: A source of displaced terranes. J. Geophys. Res. 89, 10072–10076. doi:10.1029/JB089iB12p10072

Walsh, J.J., Watterson, J., 1991. Geometric and kinematic coherence and scale effects in normal fault systems. In: Roberts, A.M., Yielding, G., Freeman, B. (Eds.), The Geometry of Normal Faults, 193-203. Geological Society Special Publication 56.

Watremez, L., Burov, E., D'Acremont, E., Leroy, S., Huet, B., Le Pourhiet, L., Bellahsen, N., 2013. Buoyancy and localizing properties of continental mantle lithosphere: Insights from thermomechanical models of the eastern Gulf of Aden. Geochemistry, Geophys. Geosystems 14, 2800–2817. doi:10.1002/ggge.20179

Watterson, J., 1986. Fault dimensions, displacements and growth. Pure and Applied Geophysics 124 (1–2), 365–373

Weijermars, R., 1986. Flow behaviour and physical chemistry of bouncing putties and related polymers in view of tectonic laboratory applications. Tectonophysics 124, 325–358. doi:10.1016/0040-1951(86)90208-8

Weissel, J. K, Hayes, D. E., 1972. Magnetic anomalies in the Southeast Indian Ocean: Antarctic Oceanology 11: The Australian-New Zealand Sector, ed. D. E. Hayes, Antarctic Research Series, 19, Am. Gcopltys. On., 145-196.

Wernicke, B., 1985. Uniform-sense normal simple shear of the continental lithosphere. Can. J. Earth Sci. 22, 108–125. doi:10.1139/e85-009

Wernicke, B., 1981. Low-angle normal faults in the Basin and Range Province: nappe tectonics in an extending orogen. Nature 291, 645–648.

Wernicke, B., Burchfield, B.C., 1982. Models of extensional tectonics. J. Struct. Geol., 4, 105-115

White, N., 1994. An inverse method for determining lithospheric strain rate variation on geological timescales. Earth Planet. Sci. Lett. 122, 351–371. doi:10.1016/0012-821X(94)90008-6

White, N., 1993. Recovery of srain rate variation from inversion of subsidence data. Nature 366, 461–464.

White, R., McKenzie, D., 1989. Magmatism at rift zones: The generation of volcanic continental margins and flood basalts. J. Geophys. Res. 94, 7685. doi:10.1029/JB094iB06p07685

Whittaker, J.M., Williams, S.E., Halpin, J.A., Wild, T.J., Stilwell, J.D., Jourdan, F., Daczko, N.R., 2016. Eastern Indian Ocean microcontinent formation driven by plate motion changes. Earth Planet. Sci. Lett. 1, 1–10. doi:10.1016/j.epsl.2016.09.019

Will, T.M., Frimmel, H.E., 2017. Where does a continent prefer to break up? Some lessons from the South Atlantic margins. Gondwana Res. doi:10.1016/j.gr.2017.04.014

Willemse, E. J. M., 1997. Segmented normal faults: correspondence between three-dimensional mechanical models and field data: J. Geophys. Res. 102, 675- 692.

References

Williams, S.E., Whittaker, J.M., Granot, R., Müller, D.R., 2013. Early India-Australia spreading history revealed by newly detected Mesozoic magnetic anomalies in the Perth Abyssal Plain. J. Geophys. Res. Solid Earth 118, 3275–3284. doi:10.1002/jgrb.50239

Willis, B., 1893. The mechanism of Appalachian structure. U. S. Geol. Surv. Ann. Rep. 13 (2), 211–282.

Wilson, R.W., Holdsworth, R.E., Wild, L.E., McCaffrey, K.J.W., England, R.W., Imber, J., Strachan, R.A., 2010. Basement-influenced rifting and basin development: a reappraisal of post-Caledonian faulting patterns from the North Coast Transfer Zone, Scotland. Cont. Tectonics Mt. Build. Leg. Peach Horne 335, 795–826. doi:10.1144/SP335.32

Wilson, T., 1966. Did the Atlantic close and then re-open? Nature 211, 676–681.

Withjack, M., Jamison, W.R., 1986. Deformation produced by oblique rifting. Tectonophysics 126, 99–124.

Wosnitza, E.M., Hofmann, R., Behrmann, J.H., 2001. New apparatus for thermomechanical analogue modelling. GSA Bull.

Wu, B., Conrad, C.P., Heuret, a., Lithgow-Bertelloni, C., Lallemand, S., 2008. Reconciling strong slab pull and weak plate bending: The plate motion constraint on the strength of mantle slabs. Earth Planet. Sci. Lett. 272, 412–421. doi:10.1016/j.epsl.2008.05.009

Wu, G., Lavier, L.L., Choi, E., 2015. Modes of continental extension in a crustal wedge. Earth Planet. Sci. Lett. 421, 89–97. doi:10.1016/j.epsl.2015.04.005

Xie, X., Heller, P.L., 2009. Plate tectonics and basin subsidence history. Bull. Geol. Soc. Am. 121, 55–64.

Zeyen, H., Volker, F., Wehrle, V., Fuchs, K., Sobolev, S., Altherr, R., 1997. Styles of continental rifting: crust-mantle detachment and mantle plumes. Tectonophysics 278, 329–352. doi:10.1016/S0040-1951(97)00111-X

Ziegler, P.A., Cloetingh, S., 2004. Dynamic processes controlling evolution of rifted basins. Earth-Science Rev. 64, 1–50. doi:10.1016/S0012-8252(03)00041-2

Zorin, Y. A., 1981. The Baikal rift: An example of the intrusion of asthenospheric material into the lithosphere as the cause of disruption of lithospheric plates, Tectonophysics, 73, 91–104.

Zulauf, J., Zulauf, G., 2004. Rheology of plasticine used as rock analogue: The impact of temperature, composition and strain. J. Struct. Geol. 26, 725–737. doi:10.1016/j.jsg.2003.07.005

Zulauf, G., Zulauf, J., Hastreiter, P., Tomandl, B., 2003. A deformation apparatus for three-dimensional coaxial deformation and its application to rheologically stratified analogue material. J. Struct. Geol. 25, 469-480.

Zwaan, F., Schreurs, G., 2017a. How oblique extension and structural inheritance influence rift segment interaction: Insights from 4D analog models. Interpretation 5, SD119-SD138. doi:10.1190/INT-2016-0063.1

Zwaan, F., Schreurs, G., Adam, J., 2017b. Effects of sedimentation on rift segment and transfer zone evolution in orthogonal and oblique extension settings: Insights from analogue models analysed with 4D X-ray computed tomography and digital volume correlation techniques. Glob. Planet. Change c. doi:10.1016/j.gloplacha.2017.11.002

Zwaan, F., Schreurs, G., Naliboff, J., Buiter, S.J.H., 2015. Insights into the effects of oblique extension on continental rift interaction from 3D analogue and numerical models. Tectonophysics 693, 239–260. doi:10.1016/j.tecto.2016.02.036
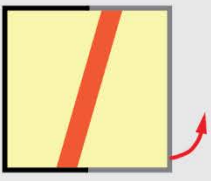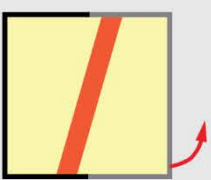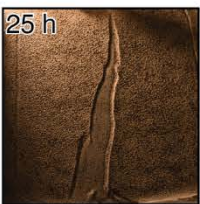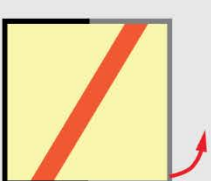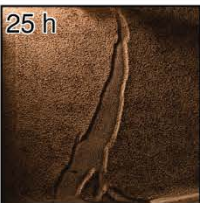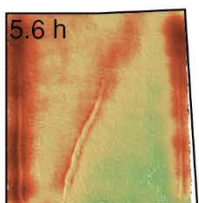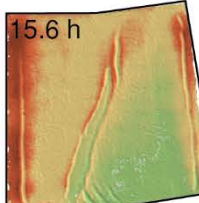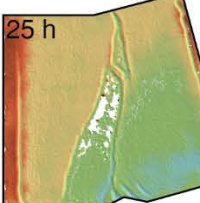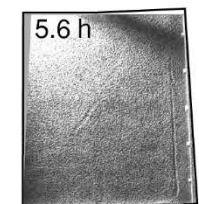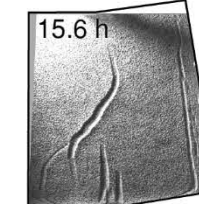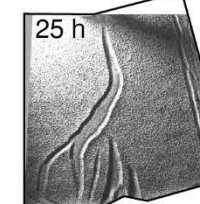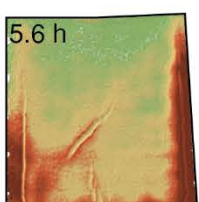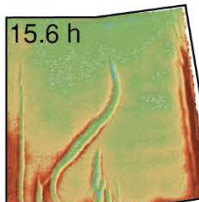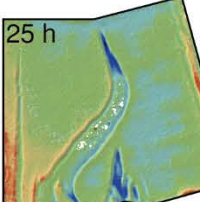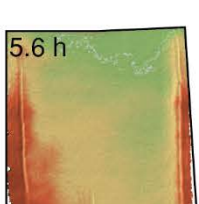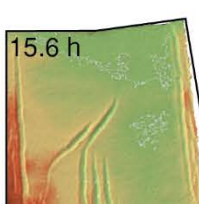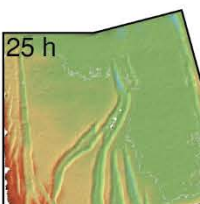
Appendix A

Evolutionary diagrams of all experiments performed
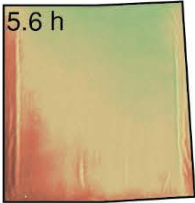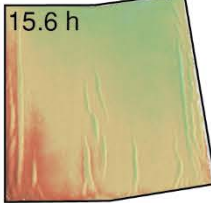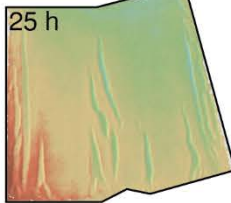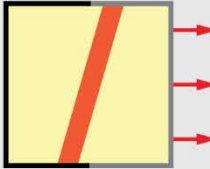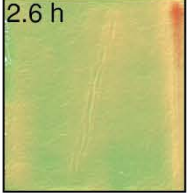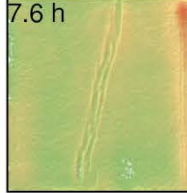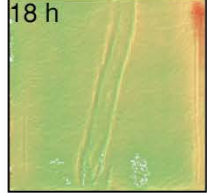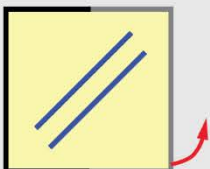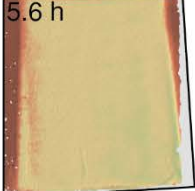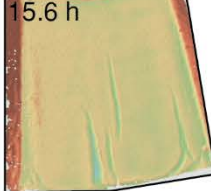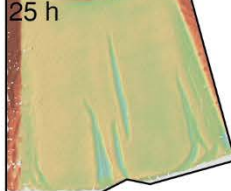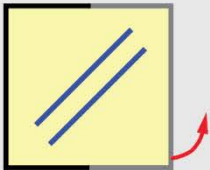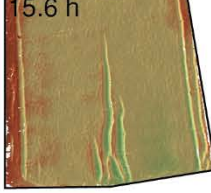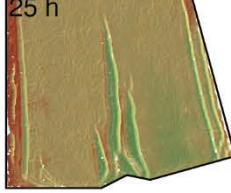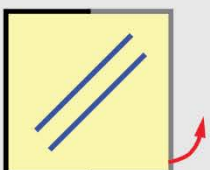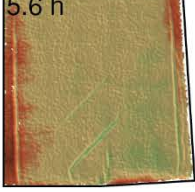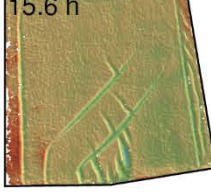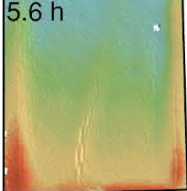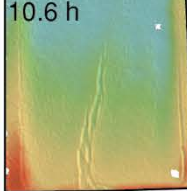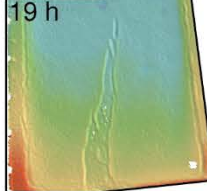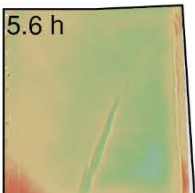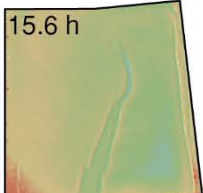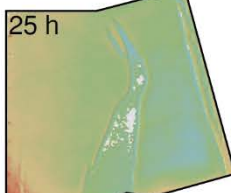
Appendix

Exp. #	Initial conditions	Early	Intermediate	Late

Exp. #	Initial conditions	Early	Intermediate	Late

Exp. #	Initial conditions	Early	Intermediate	Late
22		5.6 h	15.6 h	25 h
23		2.6 h	7.6 h	18 h
24		5.6 h	15.6 h	25 h
25		5.6 h	15.6 h	25 h
26		5.6 h	15.6 h	25 h
27		5.6 h	10.6 h	19 h
28		5.6 h	15.6 h	25 h

Exp. #	Initial conditions	Early	Intermediate	Late
29		5.6 h	15.6 h	25 h
30		5.6 h	15.6 h	25 h
31		1.6 h	6.6 h	21 h
32		5.6 h	15.6 h	25 h
33		5.6 h	15.6 h	25 h
34		5.6 h	15.6 h	25 h
35		2 h	7 h	22 h

Exp. #	Initial conditions	Early	Intermediate	Late
36		6.5 h	16.5 h	21.6 h
37		5.6 h	15.6 h	25 h
38		6.5 h	16.5 h	21.6 h
39		6.5 h	16.5 h	21.6 h
40		5.6 h	15.6 h	23 h
41		6.5 h	16.5 h	21.6 h
42		5.6 h	15.6 h	25 h

Exp. #	Initial conditions	Early	Intermediate	Late
43		5.6 h	15.6 h	25 h
44		5.6 h	15.6 h	25 h
45		6.5 h	16.5 h	21.6 h

Appendix

Appendix B

Extensional apparatus design

Appendix

Appendix B - Table of contents

Extensional apparatus design plans

3D PDF Files and animation movies

Orthogonal extension \ Rotational extension \ 15° Oblique extension \ 30° Oblique extension \

45° Oblique extension \ 60° Oblique extension

 https://figshare.com/s/0d36e967bc4fce9396c2

All the design plans, 3D PDFs and animation movies presented in this appendix have been produced by Brett Williams from Monash University Instrumentation Facility.
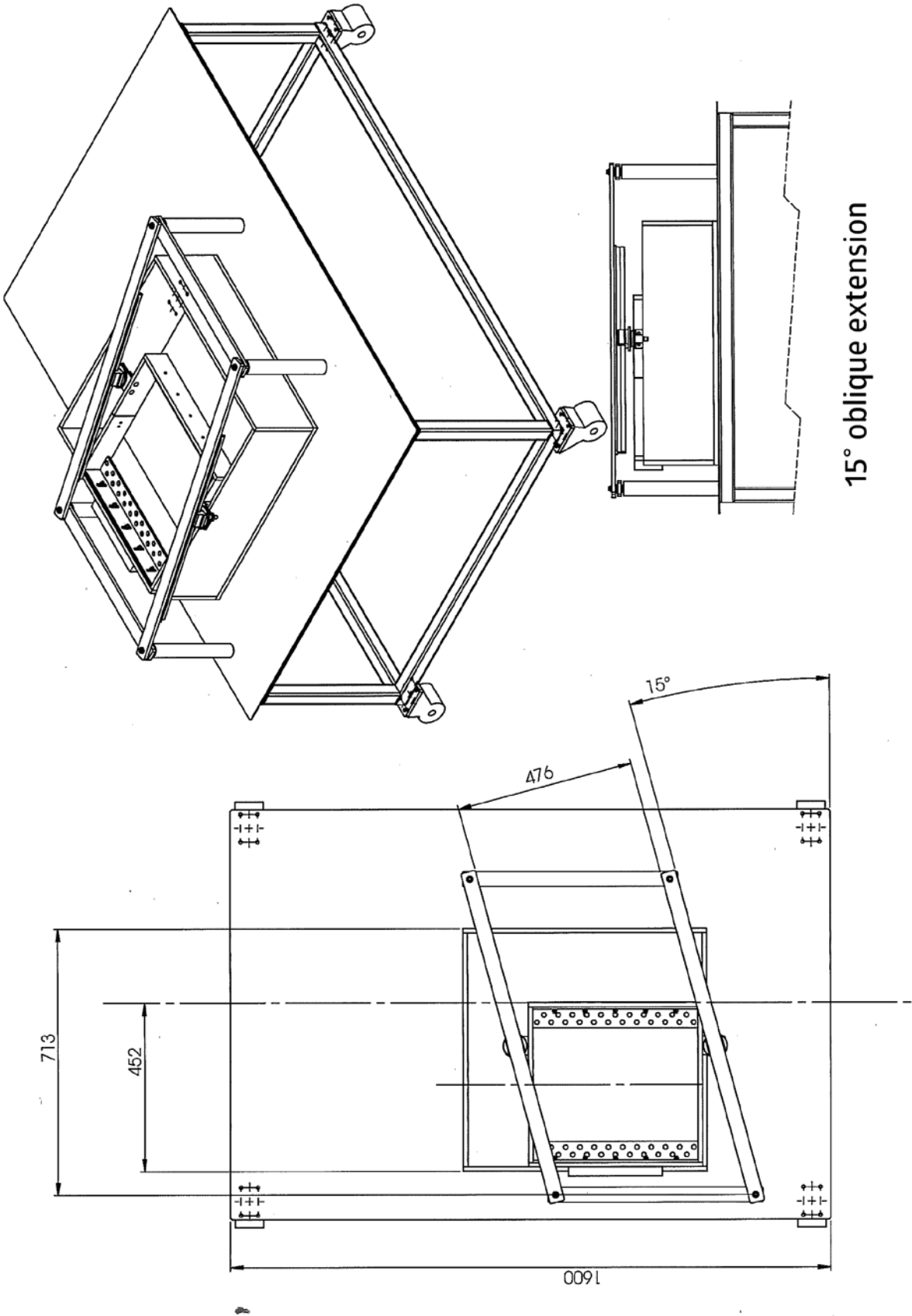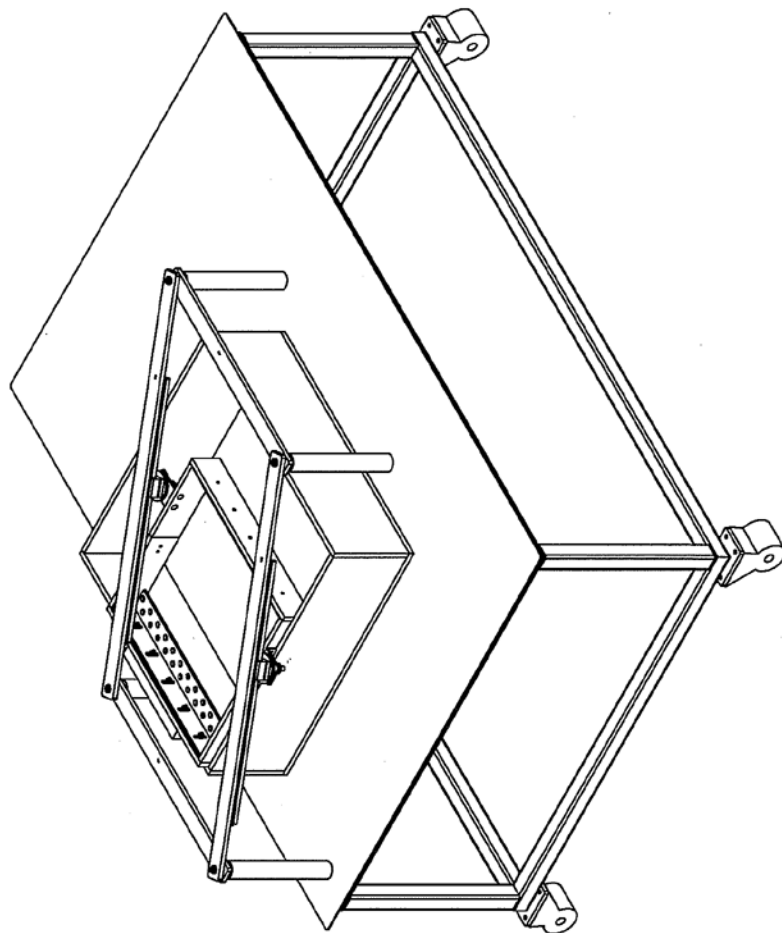
Plexiglass tank

650

626

626

650

12

200

12

Table

1600

1100

630

1142

Rotational extension

650

626

452

650

626

102

60

39°

238

24.5°

200

225

Orthogonal extension

15° oblique extension

15°

476

713

452

1600

30° oblique extension

30°

37,5

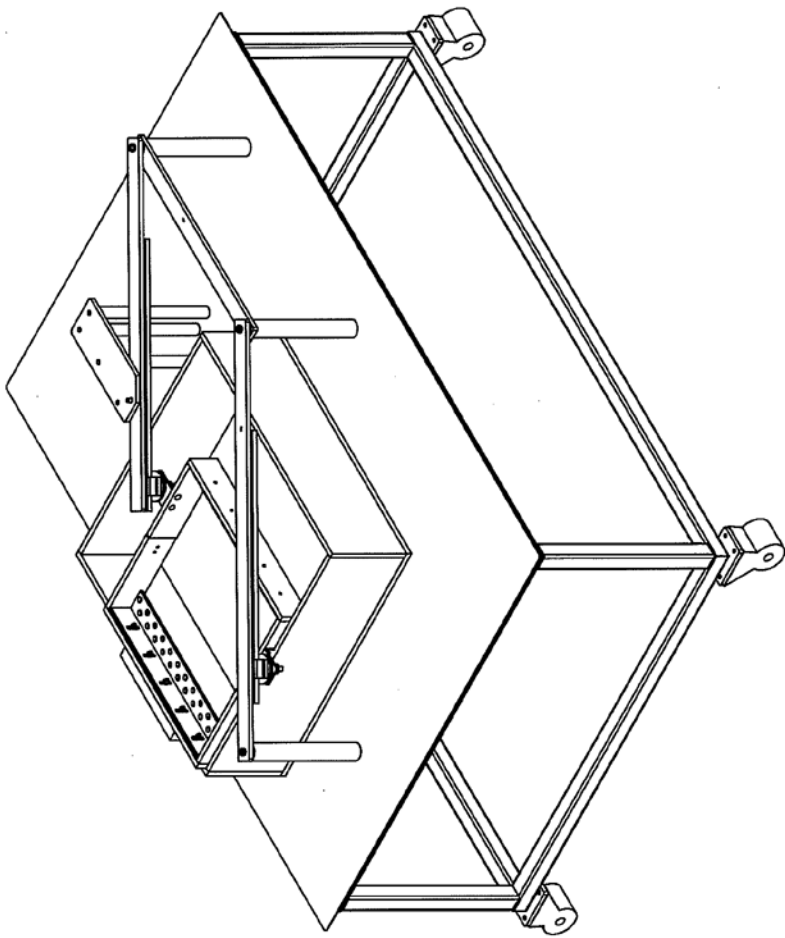45° oblique extension

45°

755

60° oblique extension

60°

755
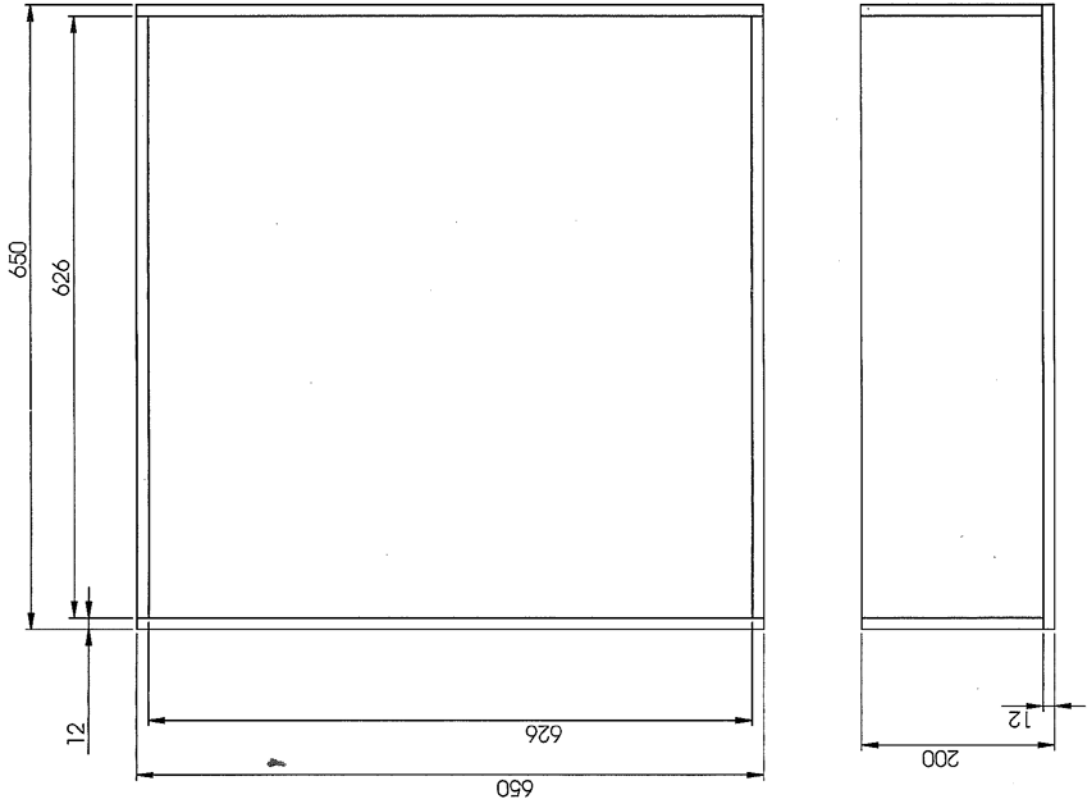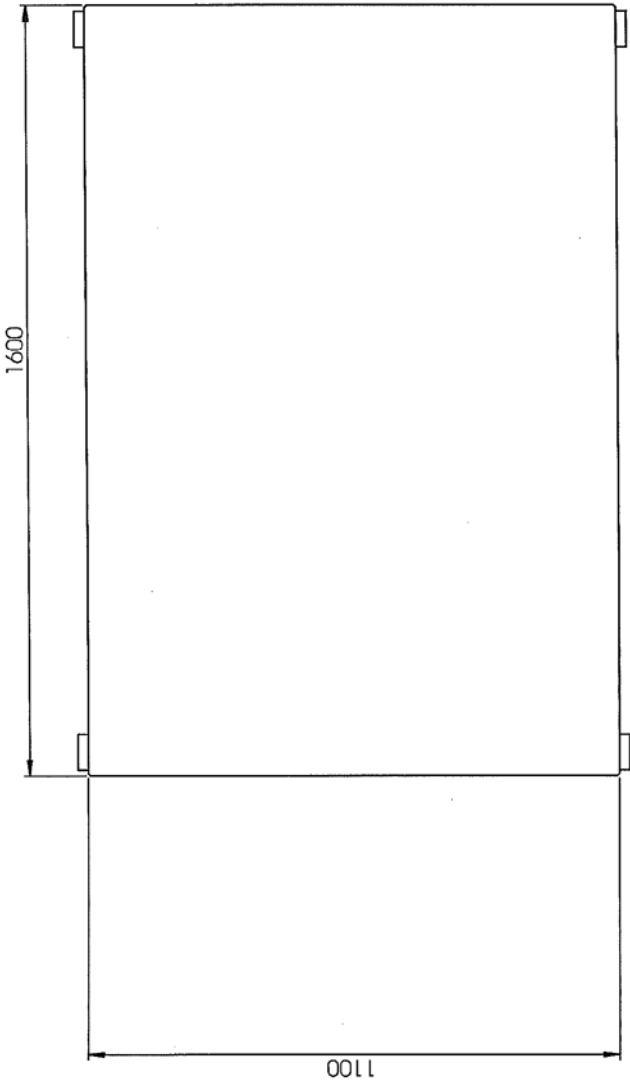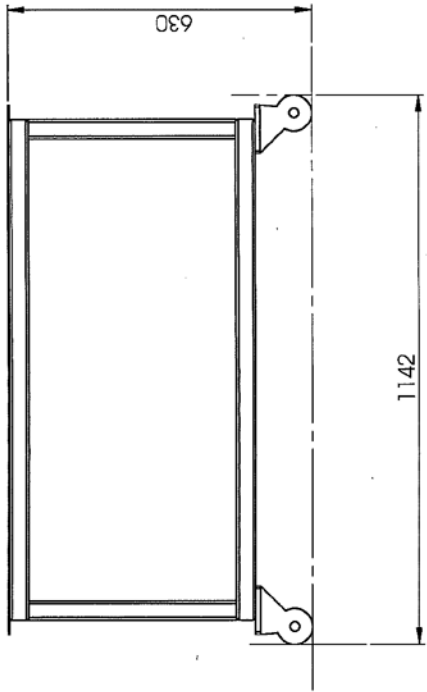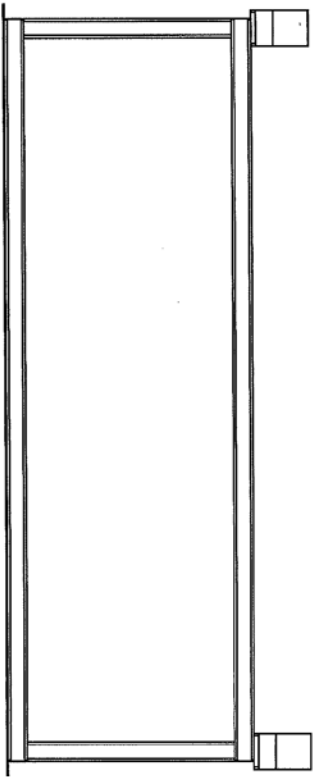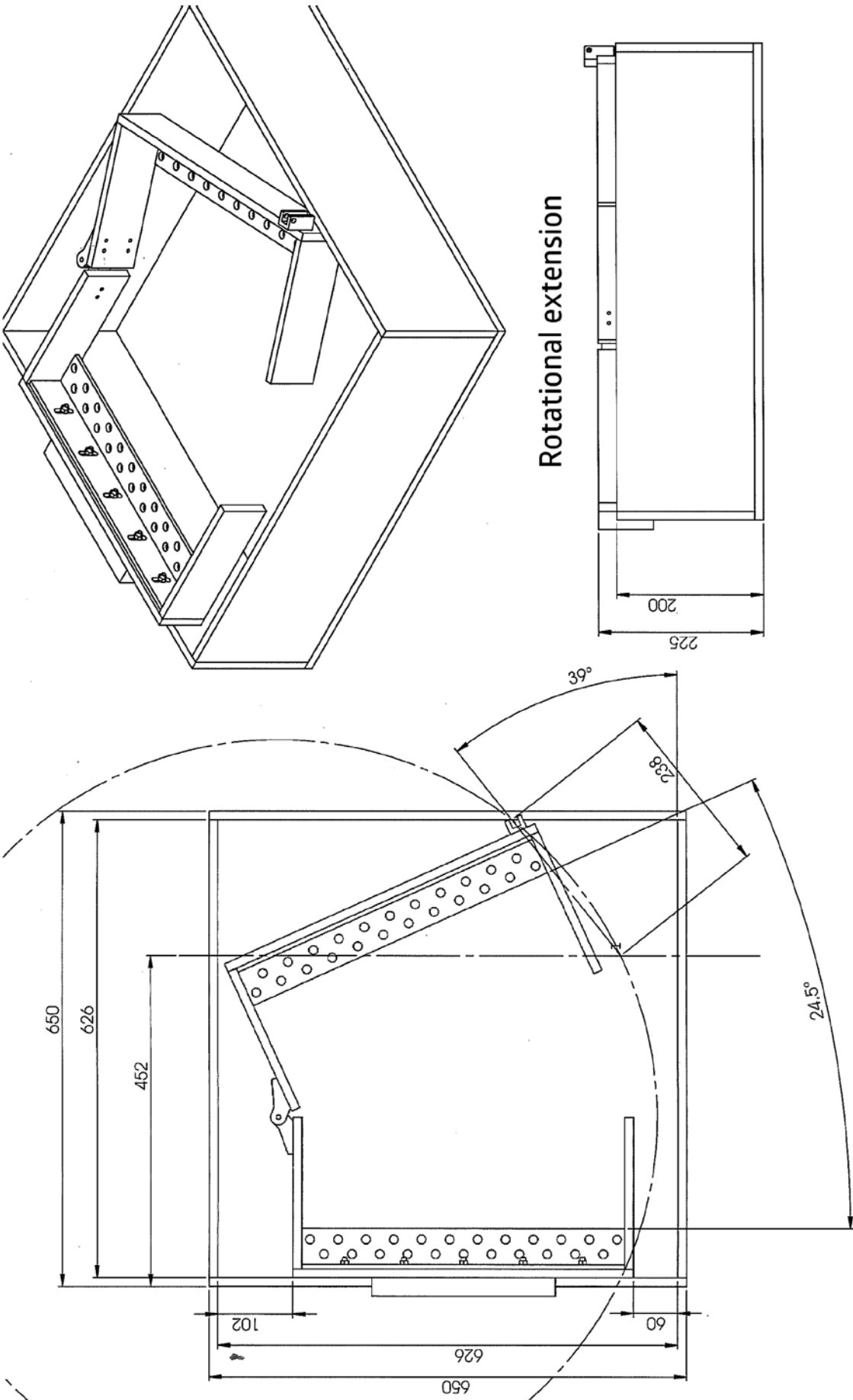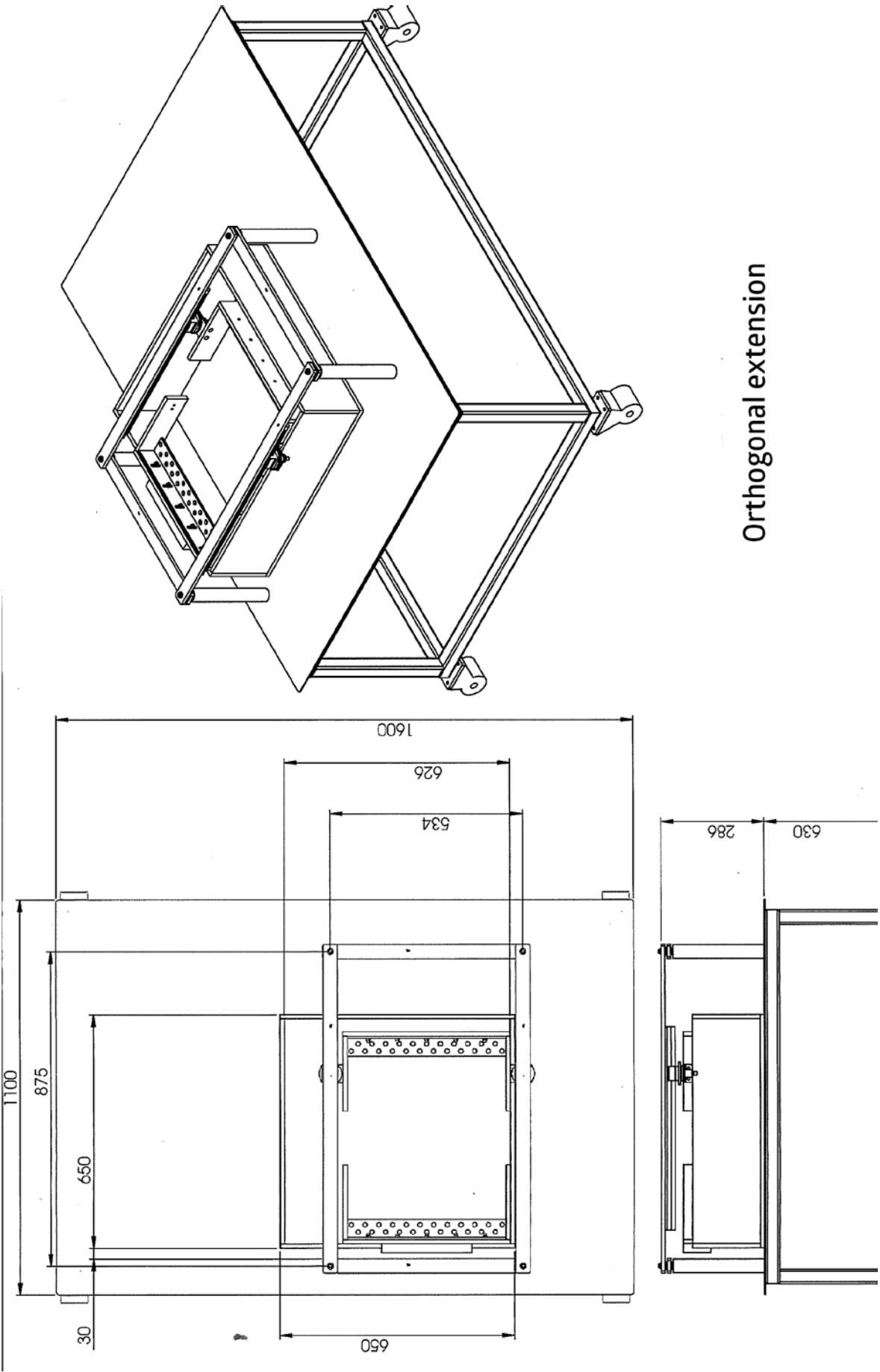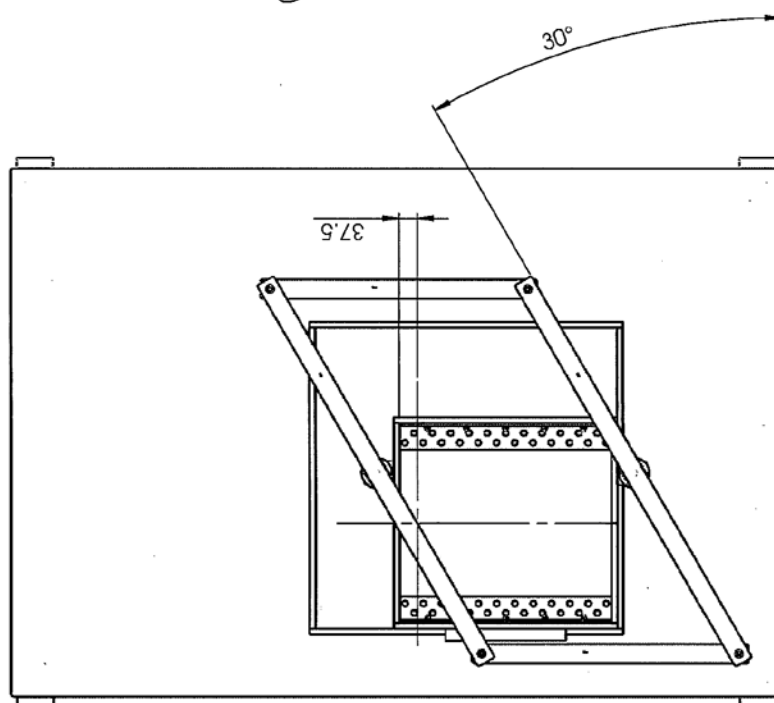
Appendix
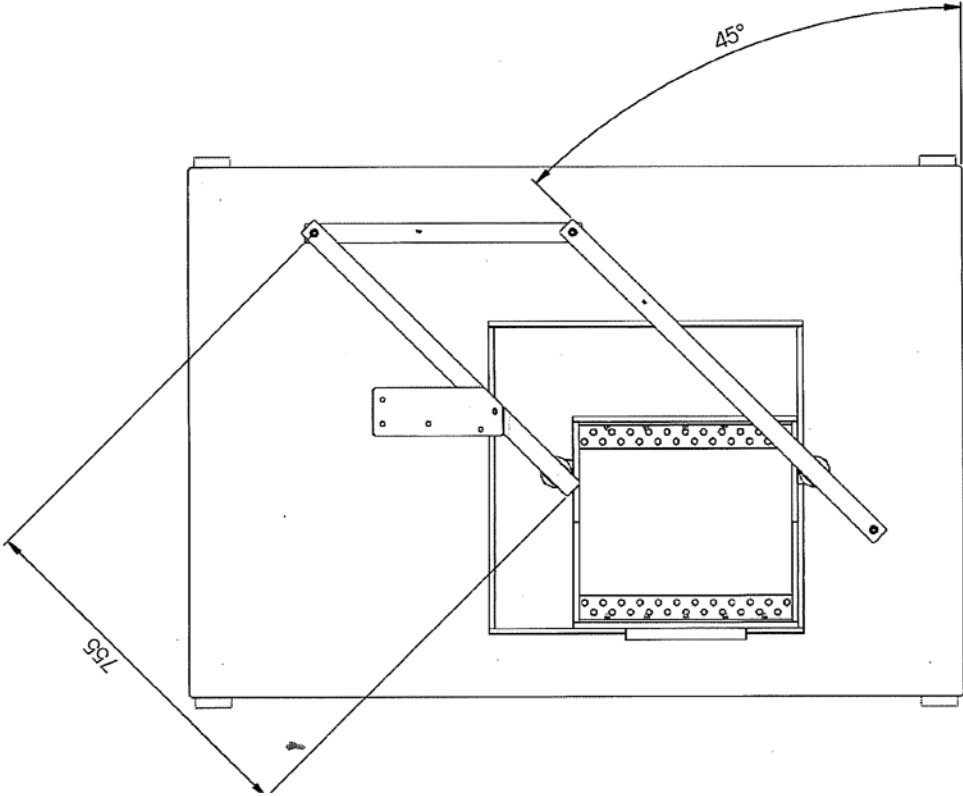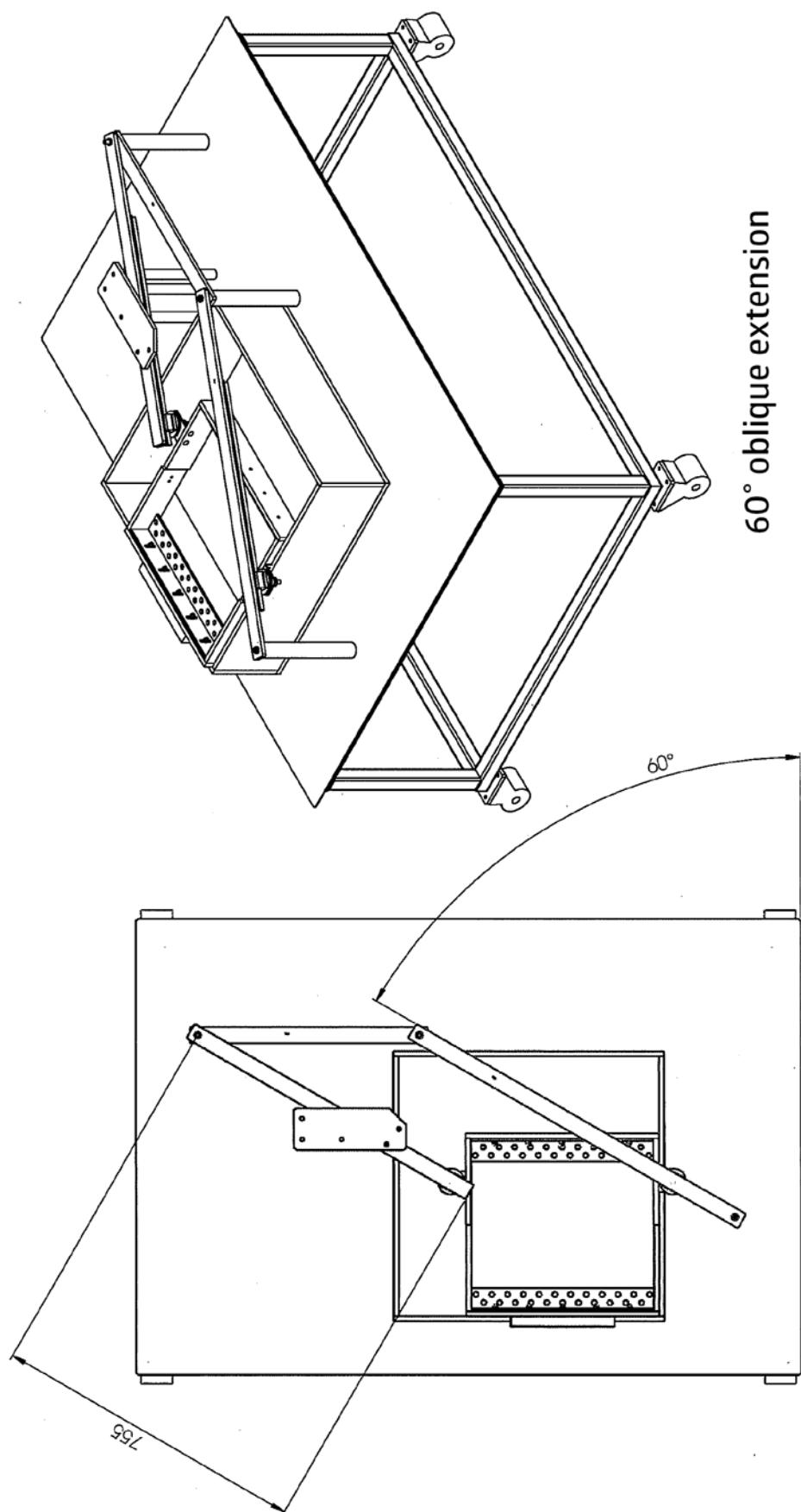
Appendix C

Extended Data movie files for Chapter 2

Appendix

Deformation evolution of the experiments discussed in Chapter 2 are shown in Extended Data Movies 1 to 5. Extended Data Movies 6 to 10 show repeated experiments with the same boundary conditions. Plan view visualization in terms of elevation, incremental strain and cumulative strain, as illustrated in figures 2.5 to 2.9. Areas that turn white in the center of the models denote sections in which significant stretching causes the dark-colored sand grains sifted on the surface that serve as passive markers (See Deformation monitoring and analysis) to reach a distance that is bigger than the PIV search windows overlap, representing the complete rupture of the model upper crust.

Extended Data Movie 1. Deformation evolution of Experiment 8: reference experiment (i.e., no linear weakness zone).

Extended Data Movie 2. Deformation evolution of Experiment 11: low obliquity (α = 15°) linear weakness zone.

Extended Data Movie 3. Deformation evolution of Experiment 18: low obliquity (α = 30°) linear weakness zone.

Extended Data Movie 4. Deformation evolution of Experiment 20: moderate obliquity (α = 45°) linear weakness zone.

Extended Data Movie 5. Deformation evolution of Experiment 21: high obliquity (α = 60°) linear weakness zone.

Extended Data Movie 6. Comparison of deformation evolution; Experiment 8 and Experiment 22.

Extended Data Movie 7. Comparison of deformation evolution; Experiment 11 and Experiment 16

Extended Data Movie 8. Comparison of deformation evolution; Experiment 18 and Experiment 17.

Extended Data Movie 9. Comparison of deformation evolution; Experiment 20 and Experiment 19.

Extended Data Movie 10. Comparison of deformation evolution; Experiment 21 and Experiment 12.

All extended data movie files have been uploaded to Figshare and can be accessed through the following hyperlink:

https://figshare.com/s/c67023735d52835ec3a6